Alma Mater Studiorum
Università di Bologna

Dottorato di ricerca in

SCIENZE FARMACEUTICHE

Ciclo **XXII**

Settore scientifico-disciplinare di afferenza: **CHIM/06**

Title of Dissertation

SUPRAMOLECULAR FUNCTIONAL ASSEMBLIES WITH PHOTO OR CHEMICAL ADDRESSABILITY

Dissertation presented by

Dr. Paolo Neviani

Coordinatore Dottorato

Prof. Maurizio Recanatini

Relatore

Prof. Gian Piero Spada

Esame finale anno 2010

ABSTRACT

Supramolecular self-assembly represents a key technology for the spontaneous construction of nanoarchitectures and for the fabrication of materials with enhanced physical and chemical properties. In addition, a significant asset of supramolecular self-assemblies rests on their reversible formation, thanks to the kinetic lability of their non-covalent interactions. This dynamic nature can be exploited for the development of "self-healing" and "smart" materials towards the tuning of their functional properties upon various external factors. One particular intriguing objective in the field is to reach a high level of control over the shape and size of the supramolecular architectures, in order to produce well-defined functional nanostructures by rational design. In this direction, many investigations have been pursued toward the construction of self-assembled objects from numerous low-molecular weight scaffolds, for instance by exploiting multiple directional hydrogen-bonding interactions. In particular, nucleobases have been used as supramolecular synthons as a result of their efficiency to code for non-covalent interaction motifs. Among nucleobases, guanine represents the most versatile one, because of its different H-bond donor and acceptor sites which display self-complementary patterns of interactions. Interestingly, and depending on the environmental conditions, guanosine derivatives can form various types of structures.

Most of the supramolecular architectures reported in this Thesis from guanosine derivatives require the presence of a cation which stabilizes, via dipole-ion interactions, the macrocyclic G-quartet that can, in turn, stack in columnar G-quadruplex arrangements. In addition, in absence of cations, guanosine can polymerize via hydrogen bonding to give a variety of supramolecular networks including linear ribbons. This complex supramolecular behavior confers to the guanine-guanine interactions their upper interest among all the homonucleobases studied. They have been subjected to intense investigations in various areas ranging from structural biology and medicinal chemistry – guanine-rich sequences are abundant in telomeric ends of chromosomes and promoter regions of DNA, and are capable of forming G-quartet based structures– to material science and nanotechnology.

- *Thesis Organization*

This Thesis, organized into five Chapters, describes mainly some recent advances in the form and function provided by self-assembly of guanine based systems. More generally, Chapter 4 will focus on the construction of supramolecular self-assemblies whose self-assembling process and self-assembled architectures can be controlled by light as external stimulus.

Chapter 1 will describe some of the many recent studies of G-quartets in the general area of nanoscience. Natural G- quadruplexes can be useful motifs to build new structures and biomaterials such as self-assembled nanomachines, biosensors, therapeutic aptamer and catalysts. In **Chapters 2-4** it is pointed out the core concept held in this PhD Thesis, i.e. the supramolecular organization of lipophilic guanosine derivatives with photo or chemical addressability. **Chapter 2** will mainly focus on the use of cation-templated guanosine derivatives as a potential scaffold for designing functional materials with tailored physical properties, showing a new way to control the bottom-up realization of well-defined nanoarchitectures. In section **2.6.7**, the self-assembly properties of compound **28a** may be considered an example of open-shell moieties ordered by a supramolecular guanosine architecture showing a new (magnetic) property. **Chapter 3** will report on ribbon-like structures, supramolecular architectures formed by guanosine derivatives that may be of interest for the fabrication of molecular nanowires within the framework of future molecular electronic applications. In section **3.4** we investigate the supramolecular polymerizations of derivatives dG **1** and G **30** by light scattering technique and TEM experiments. The obtained data reveal the presence of several levels of organization due to the hierarchical self-assembly of the guanosine units in ribbons that in turn aggregate in fibrillar or lamellar soft structures. The elucidation of these structures furnishes an explanation to the physical behaviour of guanosine units which display organogelator properties. **Chapter 4** will describe photoresponsive self-assembling systems. Numerous research examples have demonstrated that the use of photochromic molecules in supramolecular self-assemblies is the most reasonable method to noninvasively manipulate their degree of aggregation and supramolecular architectures. In section **4.4** we report on the photocontrolled self-assembly of modified guanosine nucleobase ***E*-42**: by the introduction of a photoactive moiety at C8 it is possible to operate a photocontrol over the self-assembly of the molecule, where the existence of G-quartets can be alternately switched on and off. In section **4.5** we focus on the use of

cyclodextrins as photoresponsive host-guest assemblies: αCD–azobenzene conjugates **47-48** (section **4.5.3**) are synthesized in order to obtain a photoresponsive system exhibiting a fine photocontrollable degree of aggregation and self-assembled architecture. Finally, **Chapter 5** contains the experimental protocols used for the research described in **Chapters 2-4**.

TABLE OF CONTENTS

Chapter 1. The G-Quartet in Nanoscience

A great deal of the material in this Chapter is published in :

- Kaucher, M. S.; Harrell Jr., W. A.; Davis, J. T. in *Quadruplex Nucleic Acids*, Neidle, S.; Balasubramanian, S. (Ed.), Royal Society of Chemistry, Cambridge, U.K., **2006**, Chapter 10.

'Nature that fram'd us of four elements,
Warring within our breasts for regiment,
Doth teach us all to have aspiring minds:
Our souls, whose faculties can comprehend
The wondrous Architecture of the world……'
Christopher Marlowe (1564–1593), *Conquests of Tamburlaine*

1.1 Introduction

Self-assembly is central to many processes in biology and chemistry. The G-quartet, a hydrogen-bonded macrocycle formed upon the cation-templated self-association of guanosine analogs, was first identified in the early 1960s as the basic building block for hydrogels formed by 5'-GMP. Since those early days, many different nucleosides, oligonucleotides and synthetic derivatives have been shown to form a rich array of G-quadruplex structures. This Chapter summarizes some of the many recent studies of G-quartets in the general area of nanoscience.

1.2 What is Supramolecular Chemistry?[1]

As a distinct area, supramolecular chemistry dates back to the late 1960s, although early examples of supramolecular systems can be found at the beginning of modern-day chemistry, for example, the discovery of chlorine clathrate hydrate, the inclusion of chlorine within a solid water lattice, by Sir Humphrey Davy in 1810.

So, *what is supramolecular chemistry*? It has been described as 'chemistry beyond the molecule', whereby a 'supermolecule' is a species that is held together by non-covalent interactions between two or more covalent molecules or ions. It can also be described as 'lego™ chemistry' in which each lego™ brick represents a molecular building block and these blocks are held together by intermolecular interactions (bonds), of a reversible nature, to form a supramolecular aggregate. These intermolecular bonds include electrostatic interactions, hydrogen bonding, π–π interactions, dispersion

interactions and hydrophobic or solvophobic effects. Supramolecular chemistry is a multidisciplinary field which impinges on various other disciplines, such as the traditional areas of organic and inorganic chemistry, needed to synthesise the precursors for a supermolecule, physical chemistry, to understand the properties of supramolecular systems and computational modelling to understand complex supramolecular behaviour. A great deal of biological chemistry involves supramolecular concepts and in addition a degree of technical knowledge is required in order to apply supramolecular systems to the real world, such as the development of *nanotechnological* devices. Supramolecular chemistry can be split into two broad categories, *host–guest chemistry* (see **4.5**) and *self-assembly*. The difference between these two areas is a question of size and shape. If one molecule is significantly larger than another and can wrap around it then it is termed the 'host' and the smaller molecule is its 'guest', which becomes enveloped by the host (Figure 1.1a). One definition of hosts and guests was given by Donald Cram, who said '*The host component is defined as an organic molecule or ion whose binding sites converge in the complex…The guest component is any molecule or ion whose binding sites diverge in the complex'.*[2] A *binding site* is a region of the host or guest that is of the correct size, geometry and chemical nature to interact with the other species. Thus, in Figure 1.1a the covalently synthesised host has four binding sites that converge on a central guest binding pocket. Host–guest complexes include biological systems, such as enzymes and their substrates, with enzymes being the host and the substrates the guest. In terms of coordination chemistry, metal–ligand complexes can be thought of as host–guest species, where large (often macrocyclic) ligands act as hosts for metal cations. If the host possesses a permanent molecular cavity containing specific guest binding sites, then it will generally act as a host both in solution and in the solid state and there is a reasonable likelihood that the solution and solid state structures will be similar to one another. On the other hand, the class of solid state *inclusion compounds* only exhibit host–guest behaviour as crystalline solids since the guest is bound within a cavity that is formed as a result of a hole in the packing of the host lattice. Such compounds are generally termed *clathrates* from the Greek *klethra*, meaning 'bars' (Figure 1.1b). Where there is no significant difference in size and no species is acting as a host for another, the non-covalent joining of two or more species is termed *self-assembly*. Strictly, self-assembly is an equilibrium between two or more molecular components to produce an aggregate with a structure that is dependent only on the *information* contained within the chemical building blocks

(Figure 1.1c). This process is usually spontaneous but may be influenced by solvation or templation effects or in the case of solids by the nucleation and crystallisation processes.

Nature itself is full of supramolecular systems, for example, deoxyribonucleic acid (DNA) is made up from two strands which self-assemble *via* hydrogen bonds and aromatic stacking interactions to form the famous double helical structure. The inspiration for many supramolecular species designed and developed by chemists has come from biological systems.

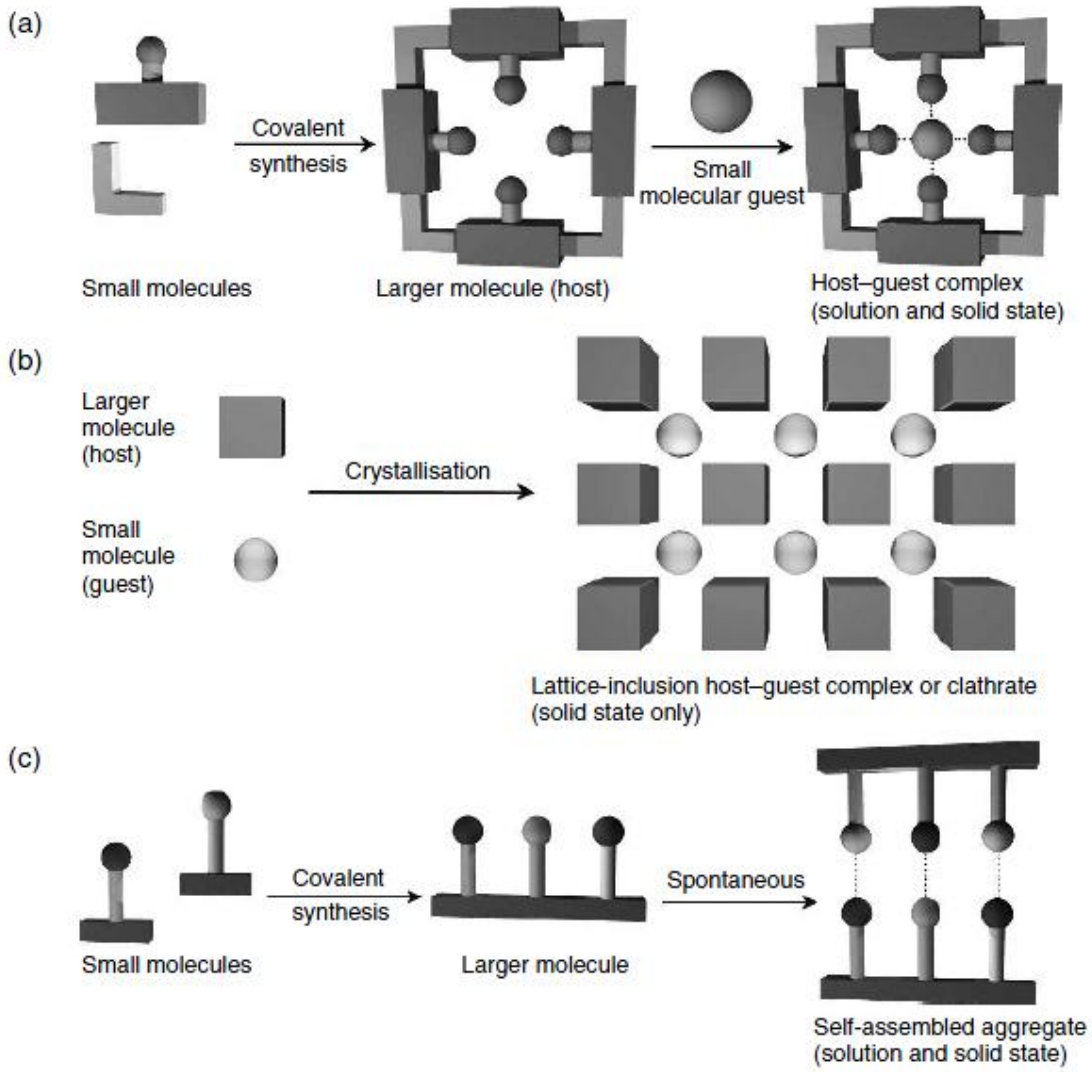

Figure 1.1. The development of a supramolecular system from molecular building blocks (binding sites represented by circles): (a) host–guest complexation; (b) lattice inclusion; (c) self-assembly between complementary molecules. (From reference 1)

1.3 Self-Assembly

Self-assembly is a powerful tool for the preparation of assemblies of well-defined (nano)architecture and for obtaining materials with tailored physicochemical properties (in particular, electronic and optical properties).[3] This approach has been used to obtain different materials, for example, gels, liquid crystals and discrete assemblies, with potential broad practical applications. A great effort has been devoted to the investigation of self-organised architectures from functional dye (and other low-molecular-weight) scaffolds[4,5] based on directional, multiple hydrogen-bonding interactions. As mentioned before, one valuable feature of supramolecular self-assembly is its dynamic nature, due to the reversibility of the non-covalent interactions. This dynamic nature leads to the preparation of functional materials, the physical properties of which can be tuned and controlled by external stimulii, for example, light.[5]

1.4 Guanosine is a Building Block for Diverse Assemblies

As mentioned before nature's use of a simple genetic code to enable life's complex functions is an inspiration for supramolecular chemistry, in fact DNA nucleobases carry the key information utilizing a variety of cooperative and non-covalent interactions. One versatile multiple hydrogen-bonding unit is represented by guanosine.

Nucleobases are well known for their ability to form complementary hydrogen bonds with their base pairs (Figure 1.2). These hydrogen bonds, on the Watson-Crick edge, are essential in holding DNA duplexes together.[6] Although all nucleobases can form additional hydrogen bonds through their Hoogsteen edges, guanine is well-known for its ability to self-associate.[7]

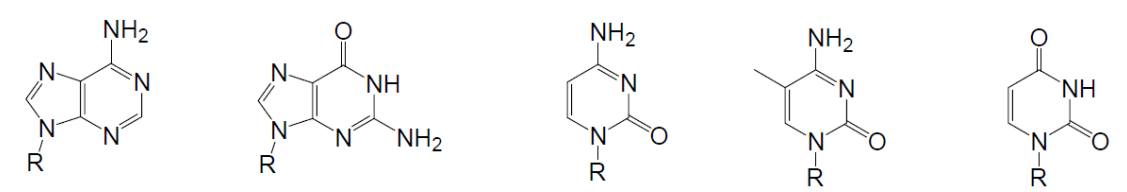

Figure 1.2. Natural nucleobases

Guanine **2** contains both a Watson-Crick edge and a Hoogsteen edge (Figure 1.3).[6] Moreover, the Watson-Crick edge has two hydrogen bond donors that can hydrogen bond with the two hydrogen bond acceptors on the Hoogsteen edge. With this series that are possible for hydrogen bonds, there are several different structures of self-associated guanine (Figure 1.4).

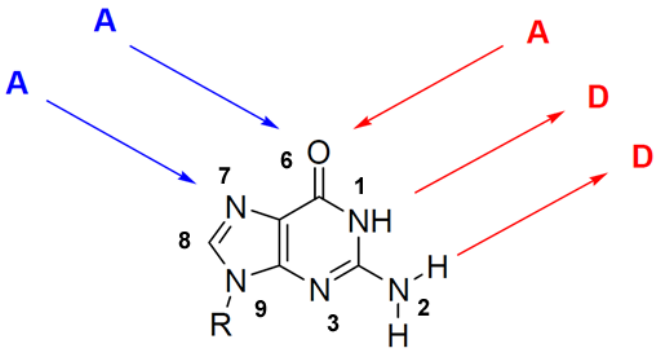

Figure 1.3. Depiction of the Waston-Crick (red arrows) and Hoogsteen (blue arrows) edges of guanine **2**.

Not including dimers, there are two long polymeric or ribbon structures that guanine can form (see Chapter 3).[7-9] The first structure is a ribbon with an overall dipole (Figure 1.4a), while the other ribbon has no dipole (Figure 1.4b). Although ribbons with no dipoles are favored, ribbons with dipoles are observed particularly when R is a large group. Figure 1.4c shows a third self-assembled structure that guanine can form: a cyclic self-assembled structure. This cyclic structure, the G-quartet, is typically favored in the presence of cations, since cations stabilize the electrostatically negative regions of the central oxygens of the G-quartet. The sugar moiety typically associated with the guanine base also has a large impact on the structure formed by guanine derivatives.[8,10,11]

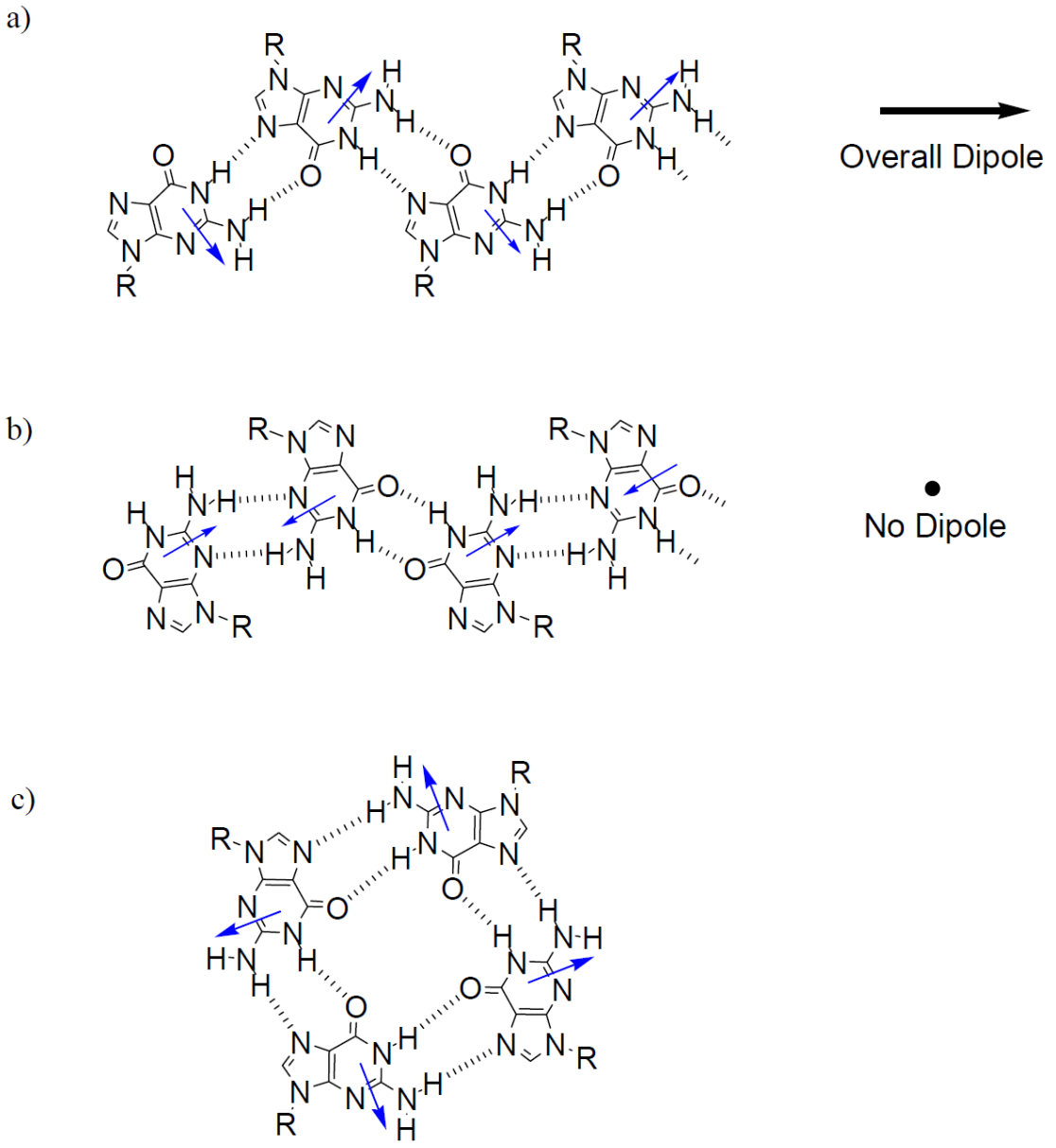

Figure 1.4. Self-assembled structures of guanine: a) ribbon with a dipole, b) ribbon with no dipole, and c) cyclic tetramer (G-quartet).

1.5 Guanosine Forms Self-Assembled Cyclic Structures – G-Quartets

The G-quartet was first identified in 1962 as the basic building block for formation of hydrogels by 5'-GMP **6**.[12] Gellert and colleagues used fiber diffraction data to propose that a square planar G-quartet was formed by eight intermolecular hydrogen bonds between the Hoogsteen and Watson-Crick edges of neighboring nucleobases (Figure 1.4c). Shortly after, polyguanylic acid was also found to form multistranded

helical coils.[13] It was also observed that hydrogels were not formed at basic pH. The smaller G-quartet assemblies in basic conditions could be studied by NMR spectroscopy.[14] It was later shown that alkali metals (Na^+ and K^+) stabilized these G-quartets. Coordination to the four inward directed carbonyl oxygens by alkali metal ions enabled the G-quartets to be stacked into G-quadruplexes. Pinnavaia and colleagues found that 5'-GMP **6** forms diastereomeric G_8-K^+ octamers by sandwiching two G-quartets with eight inward directed carbonyl oxygens coordinated to a central cation.[15] More recently, Wu and colleagues used a combination of data from diffusion NMR and dynamic light scattering measurements to determine the size of nanostructures formed by sodium 5'-GMP **6** at pH 8 (Figure 1.5).[16] Wu's group identified two major species in solution: stacked 5'-GMP monomers and stacked G-quartets. For 5'-GMP concentrations in the 18-34 wt % range, the structures had an average length between 8 and 30 nm, corresponding to a cylinder composed of 24-87 stacked G-quartets. The impressive length of G-quadruplexes formed from 5'-GMP **6** in water underscores the highly cooperative participation of hydrogen bond, ion-dipole, π–π stacking and cation–dipole interactions and causes, at a sufficiently high concentration, the self-correlation of the columns to generate liquid-crystalline phases.

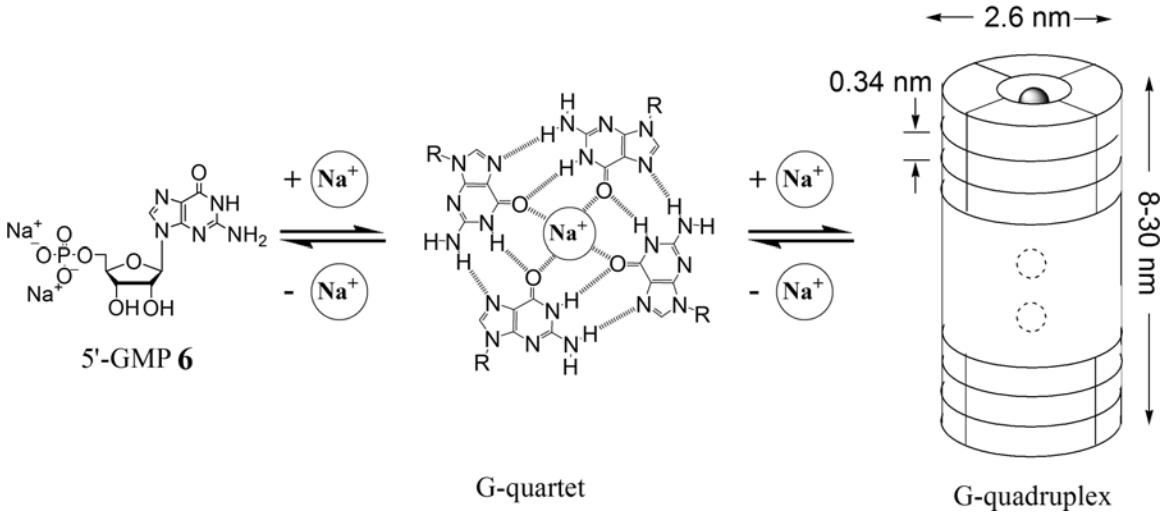

Figure 1.5. Depiction of the G-quadruplex cylinder formed by the self-assembly of 5'-GMP **6**. (From reference 16)

1.6 DNA G-Quadruplex Structures

Interest in the structural arrangements of G-quartet-based systems dates back to early 1990s by the identification that guanine-rich sequences are abundant in telomeric ends of chromosomes and promoter regions of DNA, and are capable of forming G-quartet-based structures, the G-quadruplexes, in vitro.[17] Since those days, thousands of reports have been published on the biological relevance of G-quartet formation and on the structural investigation of the arrangements of G-quadruplexes.[18]

1.6.1 G-rich DNA and RNA regions form G-quadruplex structures

Both DNA and RNA have been found to fold into G-quadruplex structures. These tertiary structures of the folded DNA and RNA molecules can be either unimolecular, bimolecular, or a tetraplex (Figure 1.6).[19-22] The biological importance of these DNA and RNA G-quadruplex structures have come under increased attention, in particular with regard to telomeric DNA and nucleic acid aptamers.[19-22]

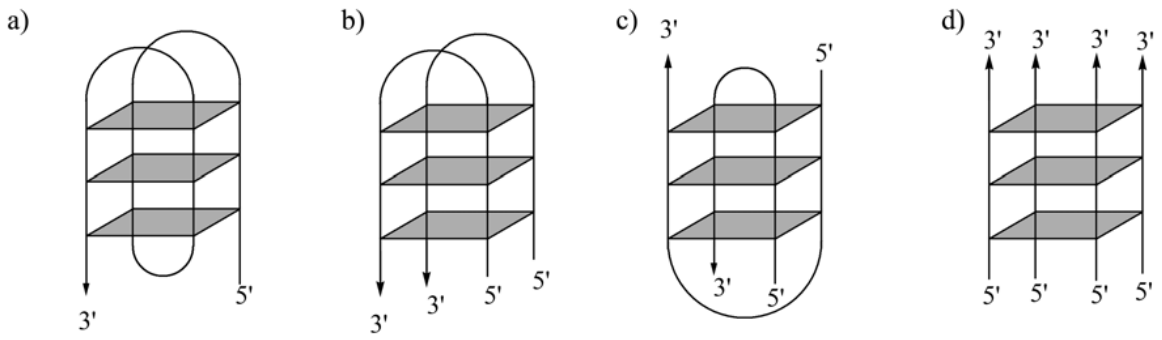

Figure 1.6. Examples of nucleic acid G-quadruplexes: a) unimolecular, b) edgewise loop bimolecular, c) diagonal loop bimolecular, and d) parallel tetraplex. Gray rectangles represent G-quartets, while the lines represent the phosphate backbone.

Telomeric DNA is a G-rich region at the end of DNA strands. In healthy cells, telomeric DNA slowly decays, which eventually leads to cell death.[19, 23-27]

In tumorous cells, telomeric DNA is extended through the action of the telomerase enzyme, thus allowing the tumorous cell life to be prolonged.[28] Telomeres are single-stranded DNA substrates for telomerase enzymes.[19-22] Since these G-rich ends of DNA can form G-quadruplexes (Figure 1.7) and stop telomerase from extending the DNA, G-quadruplex stabilizing molecules are potentially valuable anticancer drugs.[29-36] These

telomerase inhibitors recognize the face, edge, loop, or groove of the G-quadruplex (Figure 1.8).[29-36]

Furthermore DNA and RNA aptamers are nucleic acid species that fold into tertiary structures that can bind to specific targets such as small molecules.[37] One of the more studied G-rich aptamers is the thrombin binding aptamer. The thrombin binding aptamer (TBA) is a 15-residue DNA oligonucleotide with the sequence d(5'-GGTTGGTGTGGTTGG-3') that binds with high affinity and selectivity to the protease thrombin.[38]

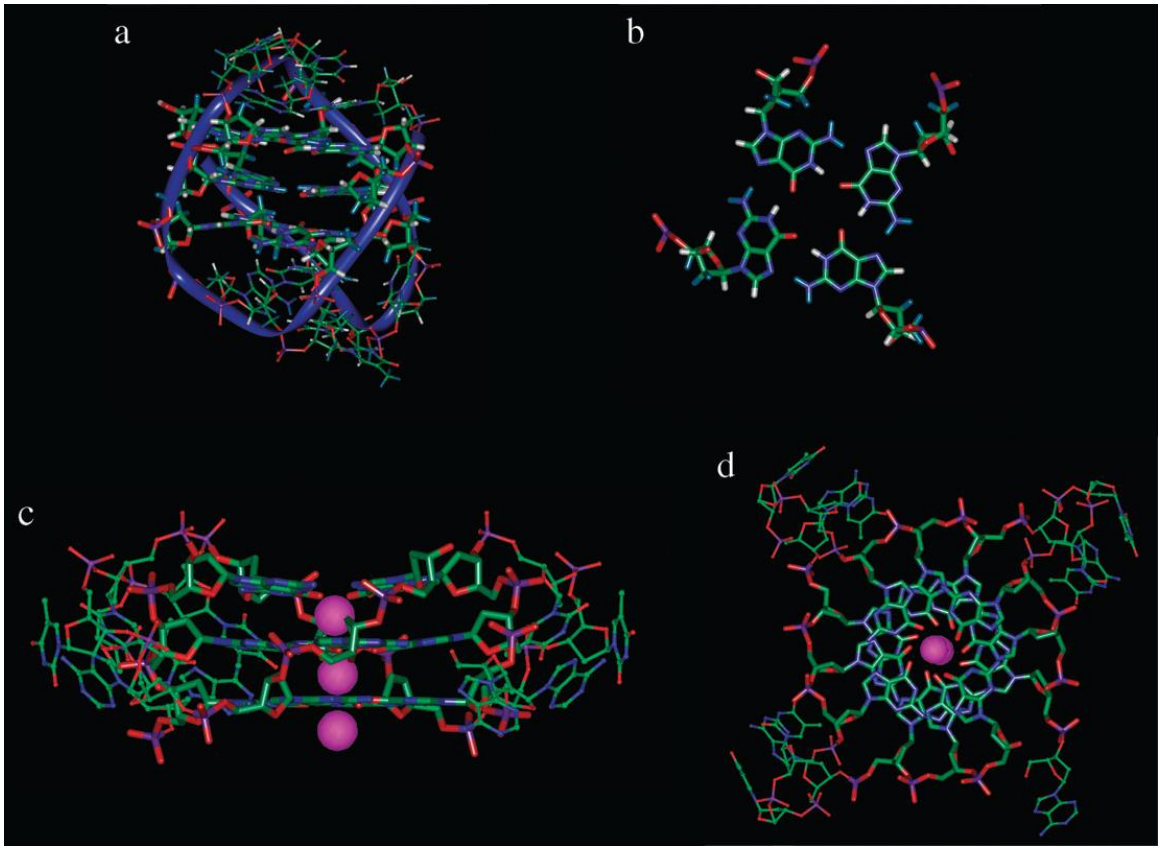

Figure 1.7. (a) Side view of the antiparallel human telomeric G-quadruplex structure solved by Wang and Patel using NMR spectroscopy, from PDB (Protein Data Bank) entry 143D. (b) Detailed view of the central G-quartet from PDB entry 143D. (c) Side view of the parallel human telomeric G-quadruplex structure solved by Parkinson, Lee and Neidle using X-ray crystallography, from PDB entry 1KF1. (d) Top view of the parallel structure from PDB entry 1KF1. In all cases, guanines are shown as cylinders, other bases as balls and sticks. Potassium ions are shown in magenta. (From reference 18e)

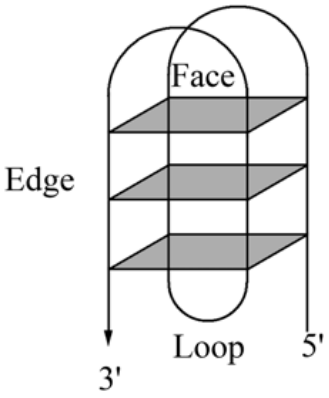

Figure 1.8. Examples of binding sites that are targeted by telomerase inhibitors.

Nanomolar concentrations of this DNA aptamer can inhibit formation of the fibrin clots that result from thrombin activation. Shortly after its discovery, the groups of Bolton and Feigon used NMR spectroscopy to determine TBA's solution structure in the presence of K^+.[39,40] The single-stranded d (5'-GGTTGGTGTGGTTGG-3') can form a unimolecular G-quadruplex that is shaped like a chair, with two stacked G-quartets connected by two TT loops and a central 3-base TGT loop (Figure 1.9). Potassium cation is essential for the templation and stabilization of the chair-type G-quadruplex by TBA, and both solution NMR spectroscopy and mass spectrometry have shown that the TBA G-quadruplex has a pronounced selectivity for coordination of K^+ over Na^+.[40,41] An x-ray crystal structure of a thrombin-TBA complex confirmed TBA's chair-like structure and suggested that this G-quadruplex DNA bound to the fibrinogen exosite, an anion binding location distinct from the protease's active site.[42] Later experiments have shown that thrombin has 2 distinct binding epitopes that recognize different G-quadruplex ligands.[43]

By using thrombin mutants, competitive binding assays and chemical cross-linking, Tasset and colleagues confirmed that the 15-mer TBA binds to the fibrinogen exosite, whereas another 29-mer oligonucleotide, one that folds into a different G-quadruplex topology, binds tightly to thrombin's heparin-binding exosite. A number of thrombin biosensors have been developed based on the simultaneous use of these 2 distinct G-quadruplex recognition sites. Although the TBA aptamer originally gained notoriety for its potential as a therapeutic anti-thrombolytic agent, this oligonucleotide has also been important in the supramolecular chemistry of G-quadruplexes. As described in more detailed below, the TBA sequence has served as the primary model for the development of a range of sensors and nanomachines.

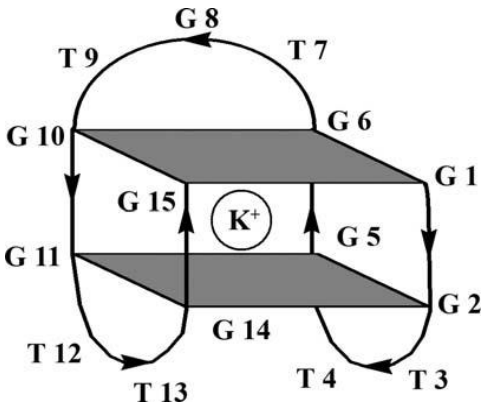

Figure 1.9. Schematic of the thrombin binding aptamer (TBA).

1.7 Biosensors and Nanostructures Based on DNA G-Quadruplex Structures

1.7.1 Potassium ion sensors

As described earlier, TBA, a 15-mer oligonucleotide, folds into stable G-quadruplexes under well-defined conditions. TBA has been exploited to develop optical and electronic sensors, for analytes ranging from K^+ ion to proteins to nucleic acids based on this facet. The use of the TBA sequence as the basis for a biosensor is nicely demonstrated in a recent study by Takenaka's group.[44] They used a modified TBA as a fluorescent indicator for detecting K^+ in water. Attachment of pyrene groups to the 5' and 3'-ends of the DNA gave a probe coined "PSO-py" for potassium sensing oligonucleotide-pyrene. This PSO-py is a promising sensor for the real-time detection of K^+ in biological and environmental samples. One challenge in developing an optical K^+ sensor is achieving selectivity in the presence of high Na^+ concentrations. Another challenge is to obtain a fast response that allows for real-time monitoring of the cation. PSO-py used the excimer formation from π-stacked pyrenes to signal K^+ binding. In the absence of K^+, PSO-py is primarily unfolded and provides little excimer emission. In the presence of K^+, the 5' and 3' ends of the folded DNA stack pyrenes in a face-to-face geometry to give a new excimer band (Figure 1.10). Importantly, the presence of other cations gave little interference as only K^+ binds with high-affinity to the TBA G-quadruplex. The fluorescence spectrum of PSO-py in the absence of K^+ showed a weak monomer emission at 390 nm. Addition of K^+ gave a strong excimer band at 480 nm,

accompanied by quenching of monomer emission. Changes in excimer fluorescence indicated that the K^+ and Na^+ complexes of PSO-py had dissociation constants (Kd) of 7.33 and 272 mM, respectively. This K^+/Na^+ selectivity coefficient of 37 for PSO-py is higher than for many other previous K^+ sensors. Independent CD measurements of PSOpy, in the presence and absence of K^+, confirmed that the excimer fluorescence corresponded to a structural shift from a random coil to a chair-like G-quadruplex. The dynamics of the fluorescence response for the PSO-py/K^+ system also showed a short response time (within seconds) upon variation in ion concentration. Moreover, this dynamic excimer fluorescence was both reversible and reproducible. The PSO-py oligonucleotide, well suited for real-time monitoring of K^+ in water, is representative of a range of bioprobes that have been rationally designed by using knowledge of G-quadruplex structure and properties.

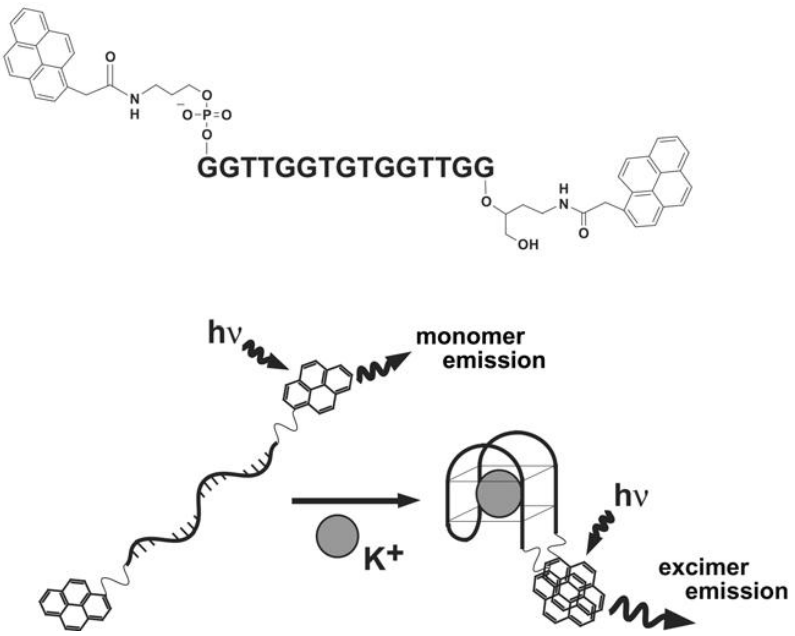

Figure 1.10. Chemical structure of the PSO-py and the expected G-quadruplex induced by K^+ binding. Pyrene excimer emission occurs in the presence of K^+ (From reference 44)

The PSO-py oligonucleotide, which uses excimer emission as an optical signal, is actually a second-generation sensor. Takenaka's prototype, described in 2002, was a modified DNA oligonucleotide that underwent efficient fluorescence resonance energy transfer (FRET) upon folding into an intramolecular G-quadruplex.[45] This original PSO

with the sequence d (5'-GGGTTAGGGTTAGGGTTAGGG-3') had a 6-carboxyfluorescein donor group attached to its 5'- end and a rhodamine acceptor linked to the 3'-terminus. When folded into a G-quadruplex, the 2 chromophores are located close enough together to undergo efficient energy transfer **(**Figure 1.11). Importantly, G-quadruplex formation by this PSO, as measured by FRET, was again highly selective for K^+ over Na^+.

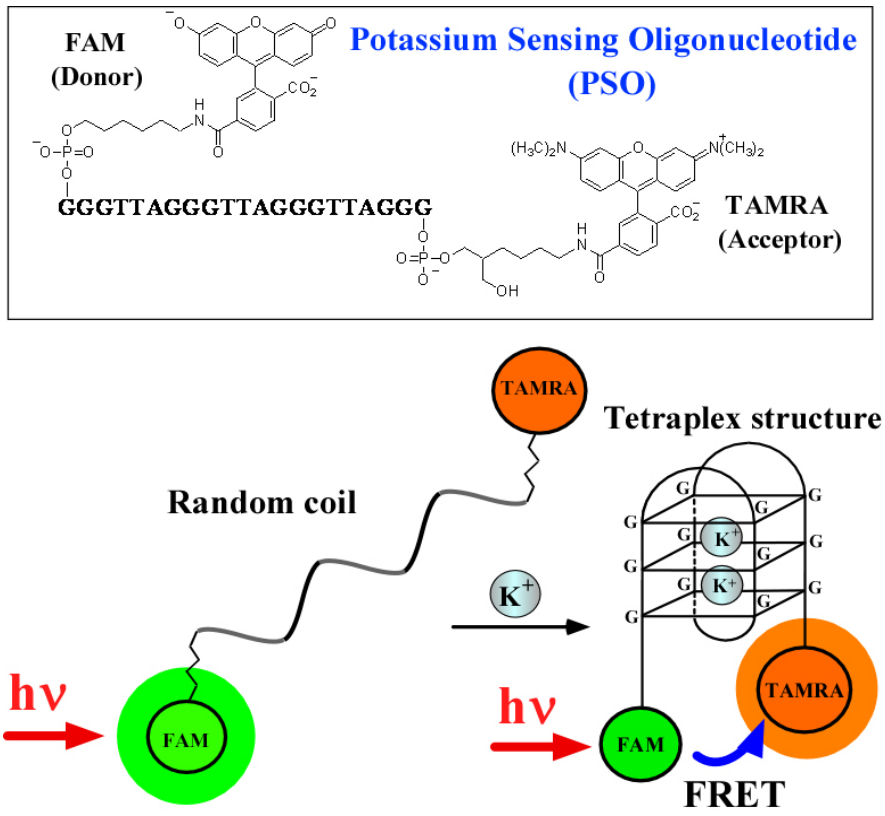

Figure 1.11. Chemical structure of the PSO and the expected G-quadruplex induced by K^+ binding. In this case FRET occurs in the presence of K^+. (From reference 45)

Ho and Leclerc described another interesting method for the optical detection of K^+, based on formation of colored complexes between a cationic polythiophene and negatively charged DNA (Figure 1.12).[46,47] Because of changes in the conformation of its conjugated backbone, this flexible polymer senses different DNA topologies. Ho and Leclerc showed that this polythiophene distinguishes the single-stranded and G-quadruplex forms of TBA, enabling the polymer to be used as a selective probe for K^+, since that specific ion is required for folding TBA. This simple "staining" method for detection of the TBA G-quadruplex (or for any species that templates or stabilizes G-quadruplex structure) has the obvious advantage that it does not require chemical labeling

of the DNA. Ho and Leclerc have also shown that their method is useful for the selective and sensitive (femtomolar range) measurement of the thrombin protein and for the highly enantioselective detection of L-adenosine.[46] Leclerc's biosensor strategy should also be ideal for identification of small molecules that bind to the G-quadruplex, thus providing a new method for screening potential anti-telomerase drugs.

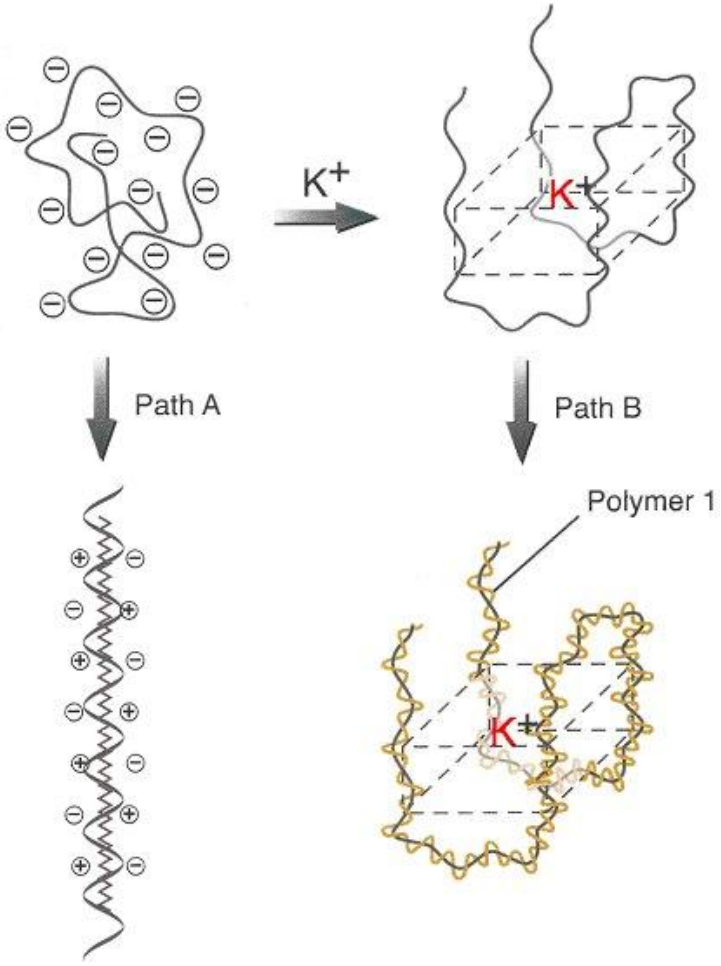

Figure 1.12. An optical K^+ sensor based on a complex formed between G-quadruplex DNA and a conjugated cationic polymer. (From reference 46)

Wang and co-workers recently developed a related polymer-based assay for K^+ detection that benefits from the sensitivity that is available from the FRET process. In their case, energy transfer was observed from a cationic conjugated polymer to a TBA oligonucleotide labeled at its 5'-end with a fluorescein acceptor. Notably, they observed a significant increase in emission at 518 nm for the polymer-labeled TBA complex only when in the presence of relatively low concentrations of K^+. The magnitude of the FRET signal, which has a $1/r^6$ dependence on the distance between donor and acceptor, was

attributed to the stronger electrostatic interactions that hold the cationic polymer closer to the compact and charge-dense G-quadruplex form of the TBA (Figure 1.13). In this way, K^+ ion was readily detected in water at low concentrations, even when other monovalent and divalent cations were present in excess.[48]

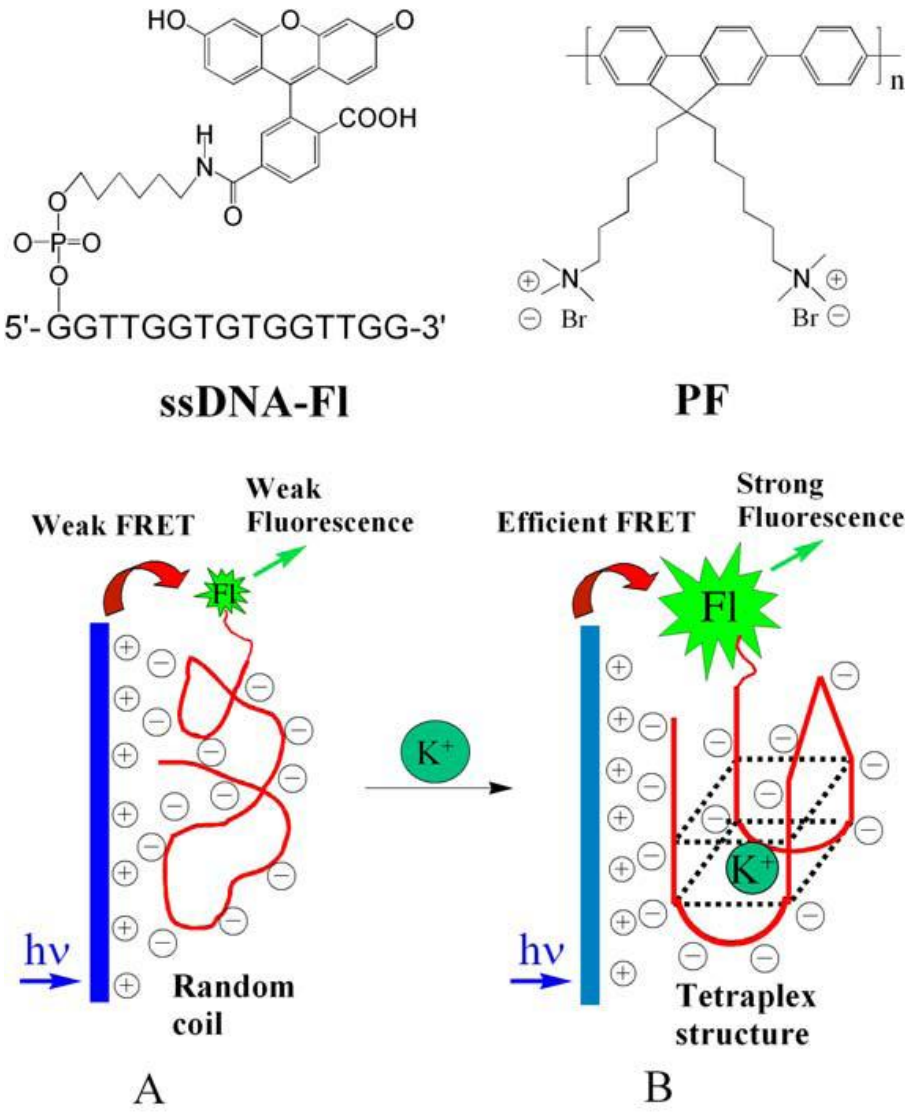

Figure 1.13. Schematic representation of an optical K^+ sensor based on G-quadruplex-polymer interactions that lead to FRET. (From reference 48)

1.7.2 G-quadruplexes as optical sensors for proteins

In 1998, Hieftje and colleagues described the first example of a protein sensor formed by the TBA sequence.[49] They prepared a DNA conjugate that had the TBA labeled at its 5'-end with fluorescein and modified at its 3'-end by an amino siloxane

linker, enabling covalent attachment of the oligonucleotide to a glass surface (Figure 1.14). Once the modified DNA had been tethered to glass they used evanescent-wave-induced detection of fluorescence anisotropy to detect the specific binding of thrombin in solution to the immobilized TBA ligand. The resulting protein-DNA complex, being much larger than the DNA probe showed a significant change in its rotational diffusion rate, as detected by the change in fluorescence anisotropy. The change in fluorescence anisotropy was specific to both the TBA and the protein analyte. Thus, scrambled DNA sequences that don't form G-quadruplexes did not show any enhanced fluorescence anisotropy. Likewise, serine proteases other than thrombin did not bind to the fluorescein-labeled TBA. This TBA biosensor was sensitive and rapid, as it could detect as little as 0.7 amol of thrombin over a dynamic range of 3 orders of magnitude (from nanomolar to micromolar) in less than 10 minutes.

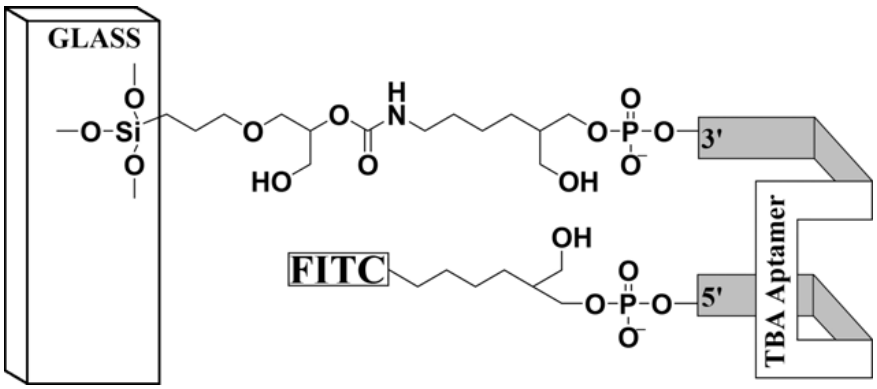

Figure 1.14. A fluorescein modified DNA oligonucleotide that functions as biosensor for thrombin. (From reference 49)

Lee and Walt used a related strategy to build a thrombin biosensor by covalent attachment of the TBA sequence to silica microspheres.[50] They then used a fiber optic device to detect the binding of fluorescein-labeled thrombin to these glass beads. They also developed a more practical assay that involved the competitive binding and displacement of fluorescein-labeled thrombin by unlabeled protein. Despite the need for specialized equipment this paper described an assay for thrombin in solution that was highly selective, rapid and reproducible. In 2001 Stanton and colleagues described the use of "aptamer beacons" for the direct detection of thrombin binding.[51] They chemically synthesized an oligonucleotide that contained the TBA sequence embedded within a longer DNA strand that was designed to form a stem-loop structure in the absence of thrombin. This DNA oligonucleotide contained a fluorescein chromophore at its 5'-end

and a quencher group at its 3'-end. Thus, when the oligonucleotide was in its stem-loop conformation the 5'-fluorescein was quenched by the nearby 3'-DABCYL unit. Addition of thrombin shifted the DNA's conformational equilibrium from the stem-loop structure to a folded G-quadruplex, causing an increase in the chromophore-quencher distance and a fluorescence enhancement (Figure 1.15). The authors stressed that this method for thrombin detection could, in principle, be applied to other nucleic acid aptamers by simply embedding the protein binding sequence within an unproductive stem-loop structure that contained juxtaposed fluorescent label and quencher. Binding of the target protein should shift the conformational equilibrium and stabilize the aptamer's structure, resulting in fluorescence enhancement as the fluorophore-quencher separation changes. They envisioned using this strategy to make biosensors for proteomics applications using high-throughput, automated selection techniques.

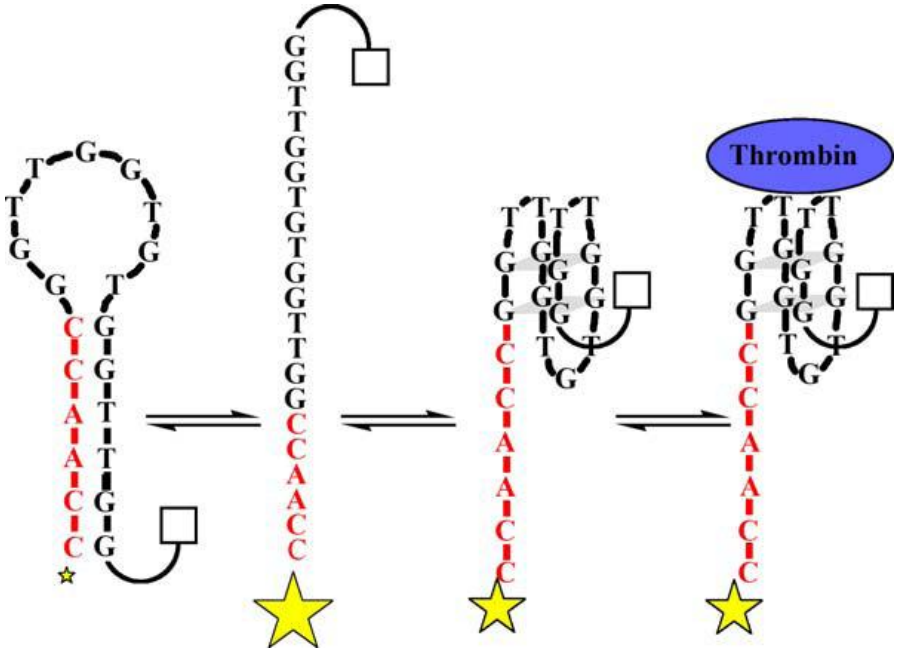

Figure 1.15. A protein biosensor based on the "aptamer beacon" strategy. Thrombin shifts the DNA's conformational equilibrium to G-quadruplex and produces an increase in fluorescence as the donor-quencher groups get farther apart, compared to the stem-loop structure. (From reference 51)

Tan and colleagues also used the aptamer beacon strategy to develop real time sensing of thrombin.[52,53] In addition to using fluorescence quenching, they also used both FRET and excimer strategies that allowed for significant fluorescence enhancement upon formation of a DNA-thrombin complex. Their aptamer beacon design involved labeling

the 5'-end of a 15-mer with an energy acceptor, 6-FAM, and the 3'-end with a coumarin group as an energy donor. (Figure 1.16) This modified 15-mer tended to favor a random coil conformation in low salt and the absence of thrombin, whereas the equilibrium was shifted to the folded TBA G-quadruplex in the presence of thrombin. This conformational change resulted in a significant enhancement in the fluorescence signal for 6-FAM as the chromophores came closer together in the folded state. These assays were highly sensitive giving a detection limit of 112 ± 9 pM for thrombin.

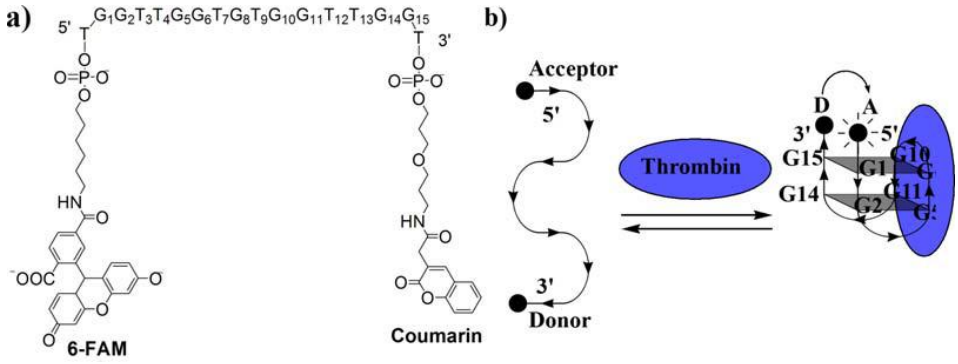

Figure 1.16. Structure of a) acceptor-donor TBA and b) schematic showing FRET upon binding of thrombin to TBA. (From reference 52)

In 2003, Nutiu and Li described a strategy for the preparation of fluorescent sensors based on their use of so-called "Structure-Switching Signaling Aptamers".[54,55] These DNA aptamers work by undergoing a major structural change from duplex DNA to a DNA-target complex. The starting duplex is formed between a DNA strand that contains the aptamer sequence and 2 shorter oligonucleotides; one of the shorter oligonucleotides contains a fluorophore and the other short strand contains a quencher. In the absence of the thrombin target the aptamer strand binds to the short oligonucleotide containing the quencher, bringing it into proximity to the fluorophore and causing maximum quenching. Upon addition of the thrombin protein, the aptamer sequence releases the short oligonucleotide containing the bound quencher, resulting in a strong fluorescence enhancement. (Figure 1.17)

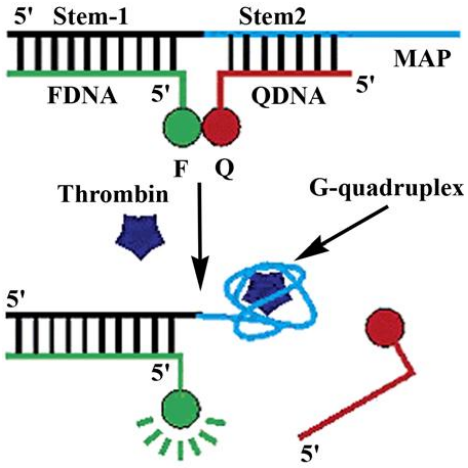

Figure 1.17. The Structure-Switching Signaling Aptamer. A DNA duplex composed of three strands of DNA places a fluorophore (F) close to a quencher group (Q). Upon addition of thrombin, the QDNA piece is released, and the fluorescence increases. (From reference 55)

In 2005, Heyduk and Heyduk took advantage of the fact that thrombin has 2 different DNA binding epitopes to facilitate the simultaneous co-association of 2 different aptamers.[56] Each aptamer was outfitted with a flexible linker region and a DNA sequence that would allow DNA duplex formation and enable simultaneous FRET enhancement. In the absence of the thrombin analyte the 2 DNA strands don't associate because the complementary binding region is too short. However, when both sequences are bound to thrombin the increased entropy favors duplex formation and subsequent FRET enhancement (Figure 1.18).

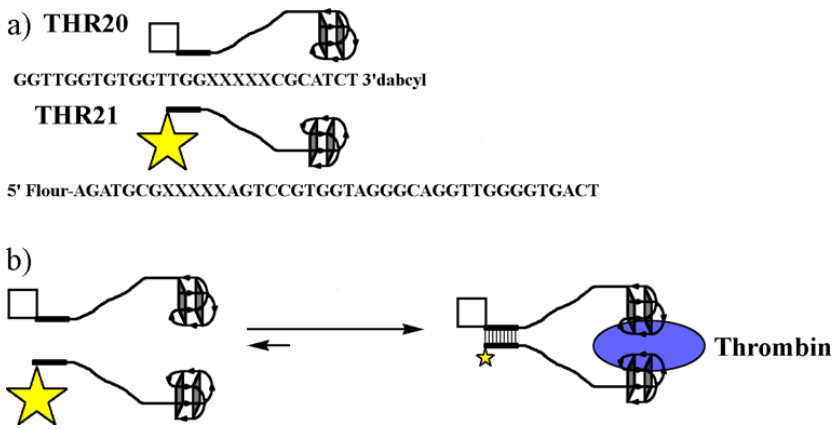

Figure 1.18. a) Detection of thrombin by binding 2 different G-quadruplexes at different epitope binding sites. b) Association of the 2 strands of DNA on the thrombin surface leads to fluorescence quenching. (From reference 56)

Willner and colleagues used thrombin's 2 binding epitopes to design an ingenuous method for the optical detection of thrombin.[57] Willner's group used gold nanoparticles functionalized with thiolated aptamers to enable the amplified detection of thrombin both in solution and on glass surfaces (Figure 1.19).[58,59] Reaction of the functionalized Au nanoparticles with thrombin in solution led to significant aggregation, since thrombin's two binding epitopes enabled crosslinking of the Au nanoparticles. Addition of thrombin led to a significant decrease in the plasmon absorbance for the Au nanoparticles. The isolated precipitates were resuspended in solution containing a CTAB surfactant and then used to seed nanoparticle growth using HAuCl4 and NADH. This catalytic growth of the nanoparticles was monitored by the gold's increased Plasmon absorbance at 530 nm. Furthermore, the enlarged nanoparticles showed a red-shifted absorbance at 650 nm that was proposed to originate from a coupled plasmon exciton due to contacts between enlarged Au nanoparticles. These solution protocols for Au nanoparticle growth were also adapted to enable the optical sensing of thrombin on glass. A TBA oligonucleotide containing a siloxane unit was covalently attached to a glass surface and thrombin was bound to the resulting monolayer. The Au nanoparticles containing the thiolated TBA were then allowed to bind to thrombin through the second epitope site. Catalytic growth of the bound Au nanoparticles was then carried out in the presence of HAuCl4, CTAB, and NADH. Both absorbance spectra and QCM measurements confirmed that the thrombin could be detected in a concentration dependant fashion. SEM images also showed that the Au nanoparticles came in contact with each other, entirely consistent with the presence of the interparticle absorbance band at 650 nm.

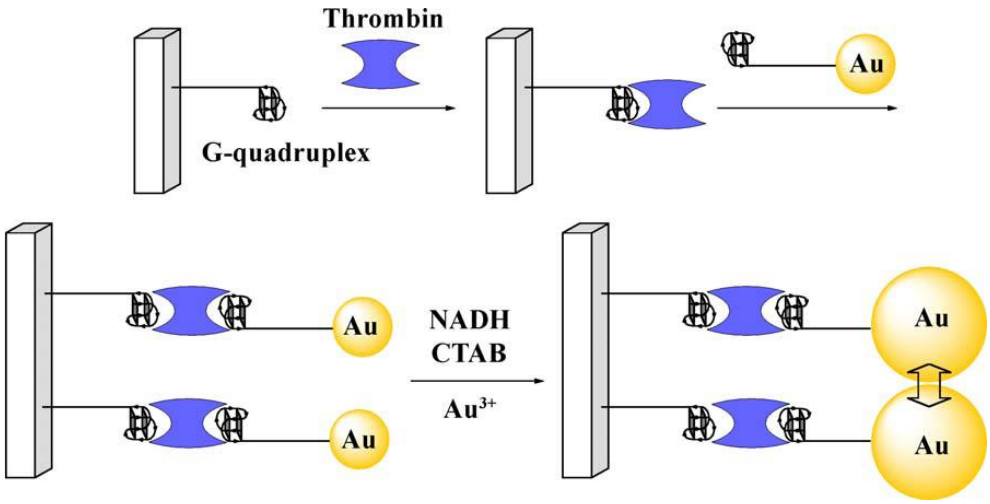

Figure 1.19. Amplified detection of thrombin based on enlargement of Au nanoparticles. (From reference 57)

1.7.3 G-quadruplexes in the electrochemical detection of proteins

In the past few years a new direction in TBA-based biosensors has been the development of methods for the electrochemical detection of thrombin. Some of the reported advantages of these electrochemical biosensors are their potential to provide high sensitivity, fast response times, low costs, easy fabrication, and the possibility for miniaturization. Ikebukoru and colleagues were the first to report on a TBA based electrochemical sensor.[60] Like others, they took advantage of thrombin's two separate binding sites. Fabrication of the device involved immobilizing a thiolated TBA sequence onto a gold electrode. A second oligonucleotide that can fold into a G-quadruplex structure was covalently modified at its 3'-end with the enzyme glucose dehydrogenase (GDH). Addition of thrombin to this solution resulted in formation of a sandwich structure wherein the GDH was brought close to the gold electrode. Oxidation of glucose by the immobilized GDH enzyme resulted in a measurable electrical current (Figure 1.20). No current was detected in the absence of thrombin, demonstrating that the GDH needs to be close to the Au electrode. Using this electrochemical detection device, thrombin at concentrations as low as 1 uM could be detected.

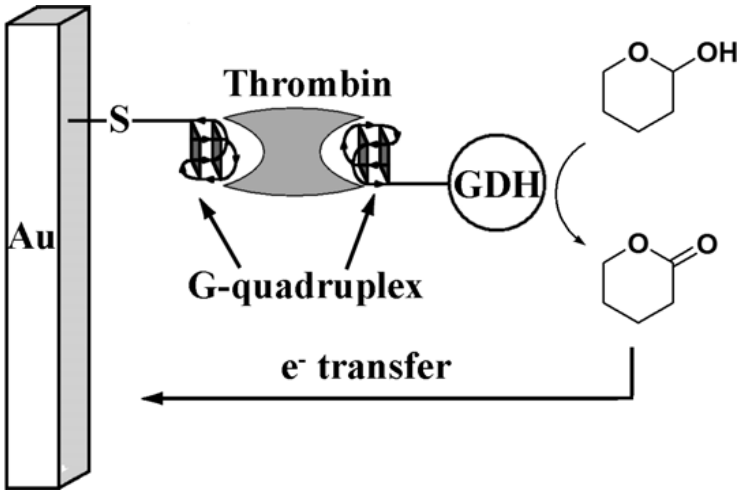

Figure 1.20. Electrochemical detection of thrombin through the coupled oxidation of glucose by glucose dehydrogenase. (From reference 60)

In the last year a flurry of papers from the groups of Hianik, Plaxco, Lee and O'Sullivan have appeared describing a variety of approaches for the electrochemical detection of thrombin.[61-65] Plaxco and colleagues used a 5'-thiolated DNA oligonucleotide containing both the TBA sequence and an electrochemically active group (methylene blue) attached to the 3'-end of the DNA.[62] This modified DNA oligonucleotide was attached via its thiol tether to the gold electrode. In the absence of thrombin the DNA adopts a conformation such that the electroactive methylene blue label can bind to the gold surface and enable electron transfer with the electrode. However, binding of thrombin by the folded TBA sequence results in a conformational change that turns off electron transfer between the 3'-methylene blue label and the gold electrode. Presumably the aptamer's conformational change significantly increases the electron-tunneling distance between the electrode and the electroactive label. This particular sensor, used to measure thrombin in blood serum, demonstrated excellent dynamic range of 10-700 nM and outstanding sensitivity, such that thrombin at 10-100 nM concentrations could be measured from blood plasma (Figure 1.21a). Radi and O'Sullivan recently described a similar approach wherein they attached a thiolated TBA sequence containing a redox-active ferrocene group to a gold electrode.[65] A bifunctional 15-base TBA derivative with a ferrocene group and a thiol at its respective 5' and 3' termini was prepared. After anchoring this electroactive aptamer to a gold electrode the rest of the gold surface was coated with 2-mercaptoethanol to form a mixed monolayer. Cyclic voltammetry (CV), differential pulse voltammetry (DPV), and electrochemical impedance spectroscopy (EIS) were used to characterize this DNA- modified electrode. The modified electrode gave a

voltammetric signal due to the redox reaction of the TBA's ferrocene group. The increase in signal intensity upon binding thrombin to the TBA sensor was attributed to a conformational transition from random coil to the folded G-quadruplex (Figure 1.21b). In this "signal-on" system, which contrasts to Plaxco's "signal-off" system,[62] the authors noted an increased electrochemical signal upon binding thrombin. They suggested that the short length of their DNA tether resulted in a conformational change that brings the ferrocene label closer to the electrode surface and increases electron transfer. This "signal-on" electrochemical biosensor was used for the detection of thrombin without the need for any special reagents. The sensor had nanomolar detection limit for its target and showed little interference from nonspecific proteins. The aptasensor could be easily regenerated and reused 25 times without any loss in detection sensitivity.[63]

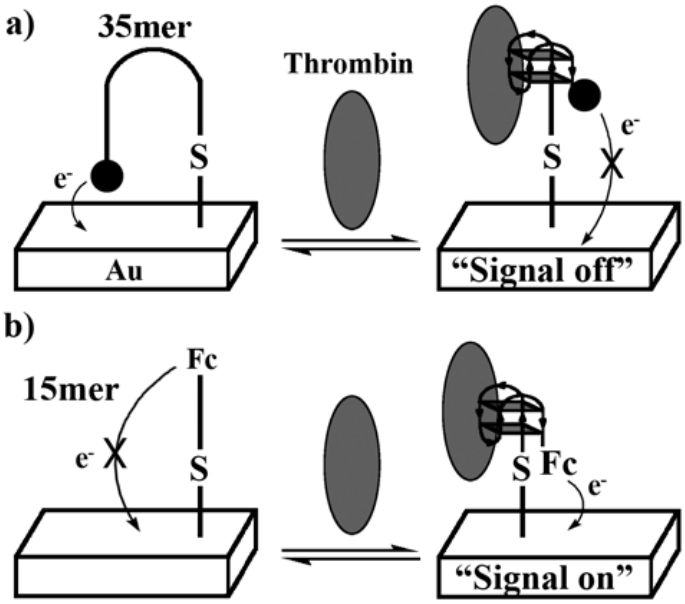

Figure 1.21. Electrochemical biosensors for the detection of thrombin a) "signal-off system" described for a 35mer oligonucleotide containing the TBA sequence and b) "signal-on" system. (From reference 62,65)

1.7.4 Biosensors for nucleic acids

DNA can also be optically detected using TBA-thrombin interactions.[66-68] Fan and colleagues used an electrochemical version of the "molecular beacon" approach to detect DNA hybridization by measuring the electrochemical signal that accompanied a conformational change in the sensor.[68] Their strategy involved attaching a ferrocene tag to a thiolated TBA sequence within a stem-loop DNA structure, followed by subsequent

attachment of the labeled DNA to a gold electrode. Hybridization of this sensor with a complementary DNA sequence then triggered a conformational change in this surface-confined TBA sensor, which led to a corresponding change in the electron tunneling distance between the Au electrode and the ferrocene label. Using cyclic voltammetry, target DNA concentrations as low as 10 pM could be measured using this sensor. In an elegant approach toward DNA detection, Willner and colleagues introduced the use of "catalytic beacons".[66-67] Their method is illustrated in Figure 1.22. The thrombin protein was covalently modified with an oligonucleotide containing the TBA sequence.[67] In the absence of a complementary DNA strand the appended TBA sequence folds into a G-quadruplex and blocks the enzyme's active site. Addition of a complementary DNA strand unfolds the G-quadruplex, resulting in substrate access to the thrombin's active site. Hydrolysis of a fluorophore labeled peptide then results in a readily detectable optical signal.

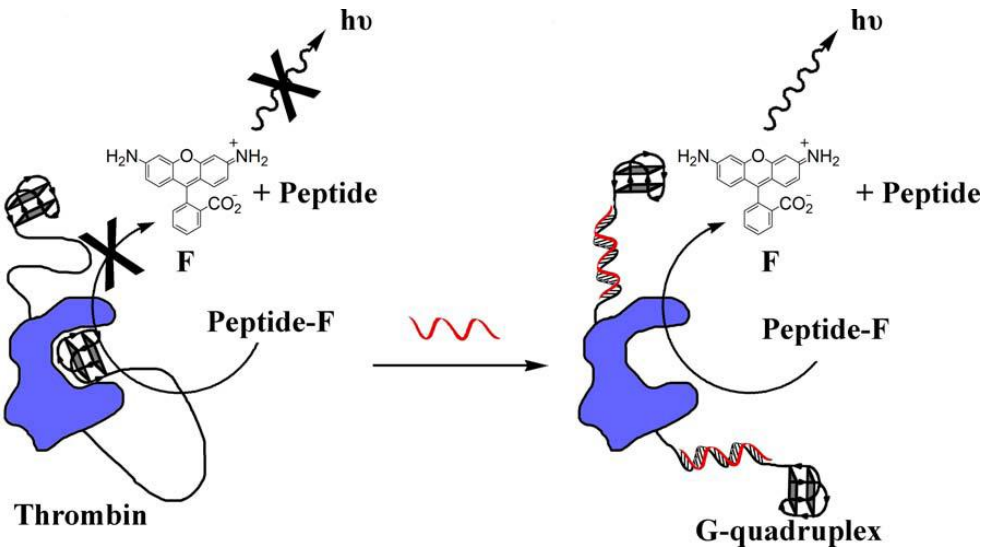

Figure 1.22. Optical detection of DNA by catalytic activation of thrombin upon dissociation of an intramolecular thrombin-TBA complex. (From reference 67)

1.7.5 The use of G-quadruplexes in building nanomachines

The TBA sequence has also been used as the basis for single molecule systems that have been coined "nanomachines" or nanomotors.[69-71] Li and Tan first demonstrated that conformational switching of a DNA oligonucleotide between its duplex and its folded G-quadruplex forms resulted in a flexing motion.[69] They used FRET to follow this

shrinking and expansion motion in real time. In a similar fashion, Alberti and Mergny reported that the conformational equilibrium between DNA duplex and quadruplex defines a nanomolecular machine.[70] Thus, the conformational states of a 21-mer DNA oligonucleotide, modified with 5'-fluorescein donor and 3'-rhodamine acceptor groups, could be readily detected by using FRET techniques. Switching between the folded unimolecular G-quadruplex and a duplex conformation caused a 5-6 nm displacement along the length of the oligonucleotide. This nanomachine could be cycled between its closed G-quadruplex state and open duplex state by sequential addition of other DNA strands, a so-called "C-fuel" and a "G-fuel". The “C-fuel” unfolded the unimolecular G-quadruplex to generate a duplex, while the “G-fuel” strand was used to liberate the labeled 21-mer so that it could refold into a G-quadruplex structure.

Simmel and coworkers recently described a nanomachine that can bind and release thrombin as it undergoes conformational switching (Figure 1.23).[71]

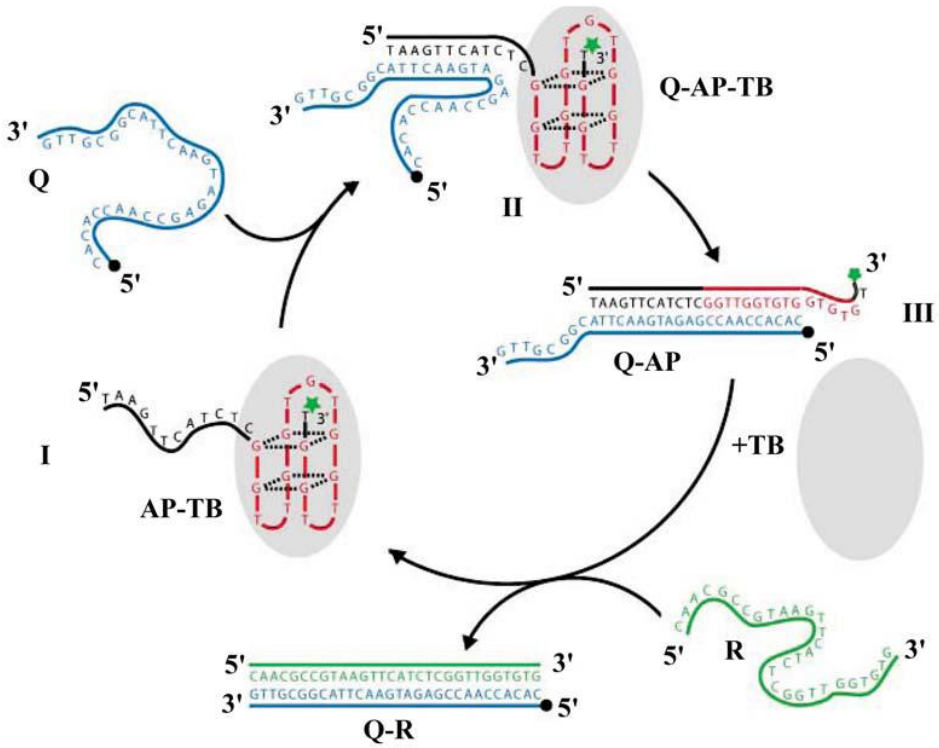

Figure 1.23. A DNA-based nanomachine that binds and releases thrombin. Binding of DNA strand Q to TBA-protein complex release thrombin, and addition of complementary DNA strand R removes Q and shifts equilibrium back to the TBA-thrombin complex. (From reference 71)

In this DNA-based machine, the TBA sequence was fused to another DNA sequence that can partially bind another DNA sequence (Q). Upon addition of the Q DNA

to the TBA-thrombin complex, the G-quadruplex region unfolds and releases the bound thrombin protein. Addition of another DNA strand (R) that is complementary to Q, frees up the TBA sequence and allows it to refold. Thus, this nanomachine represents a new way to control the reversible binding of thrombin in solution.

1.7.6 New G-quadruplex structures from synthetic DNA analogs

Polymers other than canonical DNA and RNA oligonucleotides can also form G-quadruplexes. The ability to alter the polymer backbone may result in G-quadruplexes with a variety of potential applications in supramolecular chemistry, biotechnology and nanotechnology. In addition, studies on nucleic acid analogs may lead to insights into the structural factors that control fundamental issues about the thermodynamics and kinetics of the G-quadruplex motif in the parent DNA and RNA nucleic acids. For example, locked nucleic acids (LNA) have conformationally constrained ribose units that are fixed in a C3´-endo conformation by a methylene bridge between the 2´-O and 4´-C atoms (Figure 1.24).[72,73] This RNA-like C3´-endo sugar pucker reduces backbone flexibility and helps drive the attached nucleobase to adopt an *anti* conformation about the glycosidic bond. Dominick and Jarstfer recently showed that replacement of individual dG residues with LNA nucleotides in the Oxy28 telomeric sequence d ($G_4T_4G_4T_4G_4T_4G_4$) dramatically alter the topology of the resulting G-quadruplex.[74] Oligonucleotides with four G-rich tracts can adopt either parallel or antiparallel intramolecular G-quadruplexes.

For example, the human telomeric sequence d ($AGGG(TTAGGG)_3$) forms a unimolecular propeller structure whose phosphate backbone sections are all parallel to one another. On the other hand, the Oxy28 sequence forms an antiparallel crossover basket, with the G residues alternating in a syn-anti-syn-anti fashion along the individual G4 tracts. Because 3'-endo nucleotides prefer to adopt an anti glycosidic bond, the authors postulated that incorporation of LNA residues into Oxy28 might drive the formation of a parallel G-quadruplex.

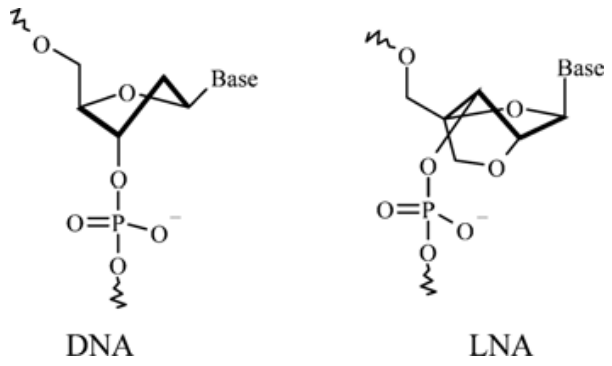

Figure 1.24. Structures of DNA and LNA showing a) DNA in the C2´-*endo* conformation and b) LNA locked into the C3´-*endo* conformation. (From references 72, 73)

Dominick and Jarstfer inserted LNA into specific positions of the Oxy28 sequence and used CD spectroscopy to determine both the folding topology and thermodynamic stability of a family of modified oligonucleotides.[74] In all cases, substitution of an LNA residue led to G-quadruplexes that were destabilized relative to the parent Oxy28 sequence. However, in some cases, even single nucleotide changes shifted the G-quadruplex from an antiparallel to a parallel propeller structure in the presence of K^+ (Figure 1.25). This remarkable finding drives home the point that even single internal modifications within the oligonucleotide backbone can dramatically influence the structure of the resulting G-quadruplex.

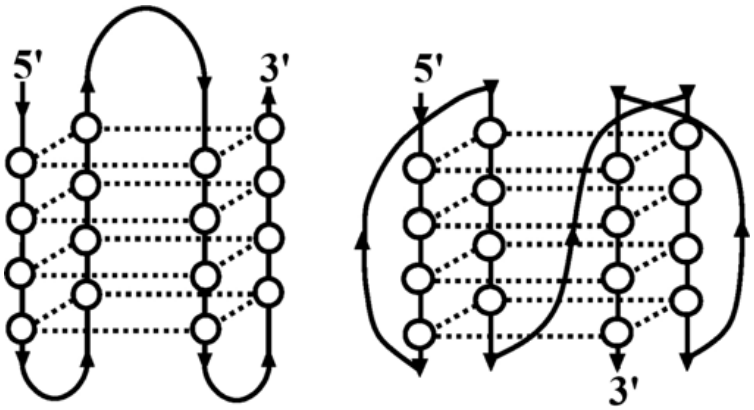

Figure 1.25. Schematic showing a) antiparallel DNA G-quadruplex and b) parallel DNA G-quadruplex. Substitution of a single DNA monomer with a LNA analog results in conformational switching between the two structures. (From reference 74)

In another informative study, Mayol and colleagues demonstrated the significant impact that LNA can have on both the thermodynamics and kinetics of G-quadruplex folding.[75] They used ^{1}H NMR and CD measurements to characterize a well-defined G-quadruplex $[tgggt]_4$ with three stacked G-quartets. Like the analogous $d[TGGGT]_4$, this LNA G-quadruplex formed a symmetric structure with all 4 strands parallel to one another. The LNA G-quadruplex $[tgggt]_4$ was more stable, with a higher melting temperature, than the corresponding DNA and RNA quadruplexes. Importantly, these CD melting and annealing measurements also revealed that the LNA strands had a much faster association rate than do DNA and RNA at micromolar concentrations. Mayol's study indicates that the significant preorganization of the LNA backbone, coupled with the stabilization of *anti*-glycosidic bonds, provides an entropy gain that leads to faster kinetics for G-quadruplex formation.[76] Peptide nucleic acids (PNA), nucleobase oligomers wherein the anionic phosphate backbone is replaced by neutral N-(2-aminoethyl) glycine linkages, also form a variety of G-quadruplex structures. Both DNA and RNA G-quadruplexes can be invaded by a homologous PNA strand to give hybrid PNA_2-DNA_2 G-quadruplexes.[77,78] Armitage and colleagues showed that the PNA H-$G_4T_4G_4$-Lys-NH_2 hybridizes with its homologous DNA d ($G_4T_4G_4$) to give a G-quadruplex consisting of 2 strands of DNA and 2 strands of PNA. FRET measurements using labeled polymers indicated that strands were organized such that the 2 DNA strands are parallel with each other and the 5' ends of the DNA point in the same direction as the N-termini of the PNA strands (Figure 1.26). Of the 2 possible structures envisioned for such a PNA_2-DNA_2 hybrid Armitage favored the "alternating" structure (A) over the "adjacent" structure (B) for two reasons: electrostatic repulsion would be minimized by separating the 2 anionic DNA strands and FRET experiments indicated that the donor and acceptor were closer to one another when both the PNA and DNA strands were labeled. Armitage also made some important observations about G-quadruplex kinetics in comparing the CD melting profiles for this hybrid PNA_2-DNA_2 G-quadruplex with that for the hairpin dimer formed by the homologous DNA. The DNA hairpin dimer showed significant hysteresis upon cooling, indicating that the rate of association of 2 strands to make the hairpin dimer is relatively slow. In contrast, the hybrid PNA_2-DNA_2 showed little hysteresis in the melting and annealing process, indicating that the kinetics for strand association are much faster for the 4-stranded PNA G-quadruplex. Armitage suggested that this faster hybridization kinetics was due to the lack of negative charges along the

PNA backbone and, possibly, due to electrostatic attraction of the PNA's positively charged N-terminus with the anionic DNA. Armitage concluded his paper by noting that, in principle, PNA_4 G-quadruplexes should be possible.

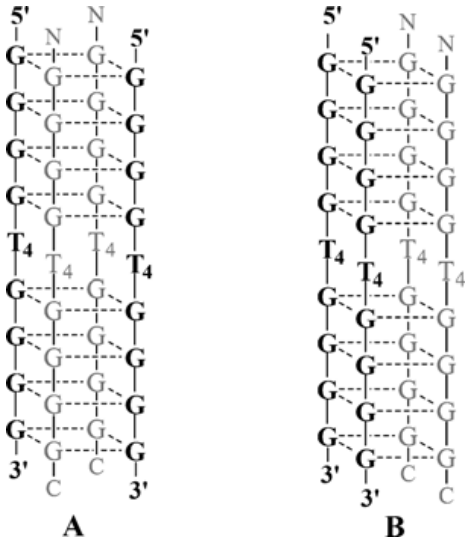

Figure 1.26. Possible structures of hybrid 1:1 PNA_2-DNA_2 quadruplexes (bold = DNA, gray =PNA) where the PNA strands are (A) diagonally opposite or (B) adjacent to each other. (From reference 78)

Shortly after Armitage's paper on hybrid PNA_2-DNA_2 G-quadruplexes, Balasubramanian and colleagues reported formation of intermolecular G-quadruplexes composed solely of 4 PNA strands.[79] Based on the combined ESI-MS, UV and CD data they identified a 4-stranded PNA quadruplex $(Lys\text{-}TG_3\text{-}NH_2)_4$ that aligned in an antiparallel fashion. This PNA sequence, which contains only 1 chiral center at its terminal Lys residue, exhibited an induced CD spectrum characteristic for stacked G-quartet chromophores, with a negative CD band at 270 nm and a positive band at 288 nm. UV melting experiments revealed that this particular PNA G-quadruplex was not nearly as stable, nor as cooperative in its formation, as the corresponding DNA quadruplex $(TG_3)_4$. Subsequent to Balasubramanian's report, Armitage and colleagues showed that another PNA sequence also form intermolecular G-quadruplexes. Thus, depending on the conditions, the PNA $(H\text{-}G_4T_4G_4\text{-}Lys\text{-}NH_2)$ forms either a 4-stranded quadruplex or a two-stranded hairpin dimer (Figure 1.27).[80] Unlike the $(Lys\text{-}TG_3\text{-}NH_2)_4$ G-quadruplex studied by Balasubramanian, this $(H\text{-}G_4T_4G_4\text{-}Lys\text{-}NH_2)$ 4 PNA quadruplex was stabilized by the presence of Na^+ and K^+. Since their backbones are neutral, Armitage noted that a PNA G-

quadruplex might be an excellent candidate for transporting cations across cell membranes.

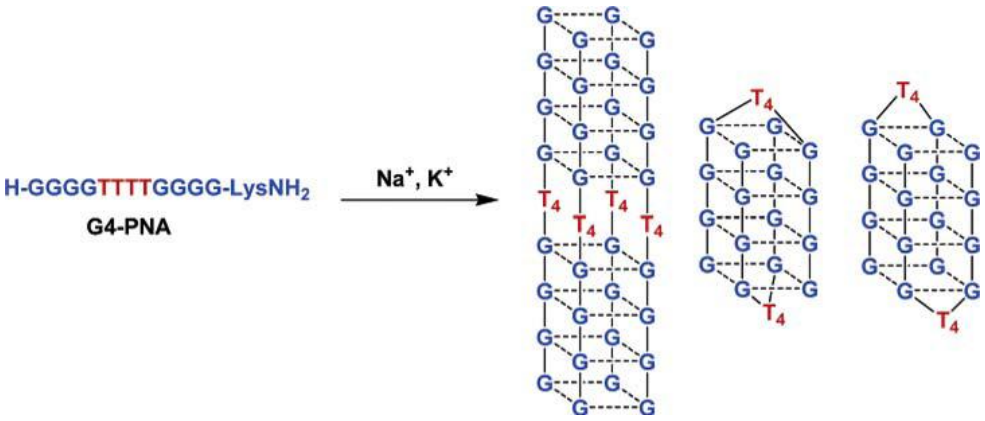

Figure 1.27. Possible G-Quadruplex structures formed by PNA. (From reference 80)

Most recently, Giancola and colleagues reported on the thermodynamic and kinetic properties of G-quadruplexes formed from chimeras 5'-tGGGT-3' and 5'-TGGG-3'-t, sequences that contain a single PNA residue at the ends of a DNA sequence.[81] Using CD spectroscopy and calorimetry, they found that these chimeric PNA-DNA quadruplexes were thermodynamically more stable than the corresponding DNA G-quadruplex. Furthermore, the kinetics of quadruplex formation, as measured by melting and annealing experiments, indicated a reaction order of 4.0 in strand concentration. Both chimeric G-quadruplexes assembled more slowly than the corresponding DNA, as the rate constants at 20 $^{\circ}$C were ($3.0 \pm 0.2 \times 10^7$) for $[5'\text{-TGGGGT-}3']_4$ and ($2.1 \pm 0.2 \times 10^7$) for the chimeras. Giancola et al. also identified a kinetically stable intermediate, suggested to be a dimer during the process of G-quadruplex formation. Their data agreed with a mechanism for G-quadruplex formation, first put forth by Wyatt for DNA,[82] wherein single and double strand species are in an equilibrium favoring single strand, and the step going from dimer to quadruplex is rate limiting. Such a mechanism is consistent with the 4th-order dependence of the association rate on single-strand concentration, but does not require the unlikely event of a four-body collision. Studies on such nucleic acid analogs, showing that incorporation of a single PNA residue into a DNA strand can influence biophysical properties, may well help guide the design of new biopolymer conjugates with improved molecular recognition properties.

Finally, it is important to recognize that folded oligonucleotides can also be functional. For example, Sen's group has described a series of DNA oligonucleotide

aptamers that are catalysts.[83-88] Aptamers, selected with a transition state analog N-methylmesoporphyrin, catalyzed the Cu^{2+} and Zn^{2+} metallation of porphyrins.[83] This catalytic DNA, which requires K^+ for its activity, may either bind the porphyrins by external stacking or by intercalation between G-quartets. Li and Sen concluded that these DNA chelatases used substrate binding energy to distort the porphyrin's planar conformation, making the porphyrin more basic and easier to metallate.[84] They suggested that the G-quartet is sufficiently rigid to enable this substrate distortion. Sen's group also identified G-quadruplex DNA aptamers with peroxidase activity.[86,87] Their DNA-hemin complexes had enhanced peroxidase activity, when compared to the heme cofactor alone. Again, they concluded that the folded DNA activates the bound heme and enhances peroxidase activity.[87] Willner's group used this hemin binding aptamer as the basis for the clever development of a DNA sensor.[66] Most recently Sen and Cinnapen used *in vitro* selection to discover a DNA aptamer that can catalyze the photoreactivation of thymine-thymine cyclobutane dimmers in DNA.[88] Thus, a 42-mer nucleotide repaired a thymine-thymine dimer substrate with 305 nm light, showing an efficiency that rivaled that of the native photolyase enzyme. A G-quadruplex unit, formed by specific guanine bases within this 42-mer deoxyribozyme, was proposed to function as a light-harvesting antenna, with photoreactivation of the thymine-thymine dimer proceeding via electron donation from a excited guanine base within the G-quadruplex. These studies by Sen underscore the potential for using G-quadruplexes to function as catalysts.

1.8 Conclusion

G-quartet systems, in addition to providing models for understanding assembly in DNA and RNA, also have potential impact on sensor development, materials science, and nanoscience. Natural G-quadruplexes can be useful motifs to build new structures and biomaterials. The use of guanine self-assembly to form self-assembled nanomachines, biosensors, therapeutic aptamer and catalysts highlight the many functions that can arise from G-quadruplexes.

References

1. J. W. Steed, D. R. Turner, K. J. Wallace *Core Concepts in Supramolecular Chemistry and Nanochemistry*, Wiley & Sons, Ltd, Chichester, UK, **2007**.
2. Cram, D. J., *Angew. Chem., Int. Ed. Engl*. **1986**, *25*, 1039–1134.
3. a) J.-M. Lehn, *Perspect. Supramol. Chem.* **1994**, *1*, 307; b) F. J. M.Hoeben, P. Jonkheijm, E.W. Meijer, A. P. H. J. Schenning, *Chem.Rev.* **2005**, *105*, 1491; c) D. S. Lawrence, T. Jiang, M. Levett, *Chem.Rev.* **1995**, *95*, 2229; d) A. Ajayaghosh, S. J. George, A. P. H. Schenning, *Top. Curr. Chem.* **2005**, *258*, 83.
4. See for example a few selected papers: a) S. Yagai, T. Seki, T. Karatsu, A. Kitamura, F. Wűrthner, *Angew. Chem.* **2008**, *120*, 3415; *Angew. Chem. Int. Ed.* **2008**, *47*, 3367; b) S. Yagai, T. Kinoshita, M. Higashi, K. Kishikawa, T. Nakanishi, T. Karatsu, A. Kitamura, J. Am. *Chem. Soc.* **2007**, *129*, 13277; c) P. G. A. Janssen, J. Vandenbergh, J. L. J. Van Dongen, E.W. Meijer, A. P. H. J. Schenning, *J. Am. Chem. Soc.* **2007**, *129*, 6078; d) A. Piermattei, M. Giesbers, A. T. M. Marcelis, E. Mendes, S. J. Picken, M. Crego-Calama, D. N. Reinhoudt, *Angew. Chem.* **2006**, *118*, 7705; *Angew. Chem. Int. Ed.* **2006**, *45*, 7543; e) D. B. Amabilino, J. Veciana, *Top. Curr. Chem.* **2006**, *265*, 253; f) L. Brunsveld, B. J. Folmer, E. W. Meijer, R. P. Sijbesma, *Chem. Rev.* **2001**, *101*, 4071.
5. a) B. L. Feringa, R. A. van Delden, N. Koumura, E. M. Geertsema, *Chem. Rev.* **2000**, *100*, 1789; b) K. Kinbara, T. Aida, *Chem. Rev.* **2005**, *105*, 1377; c) S. Yagai, A. Kitamura, *Chem. Soc. Rev.* **2008**, *37*,1520; d) S. Masiero, S. Lena, S. Pieraccini, G. P. Spada, *Angew.Chem.* **2008**, *120*, 3228; *Angew. Chem. Int. Ed.* **2008**, *47*, 3184; e) M.Barboiu, J.-M. Lehn, *Proc. Natl. Acad. Sci. USA* **2002**, *99*, 5201 – 5206.
6. Saenger, W., *Principles of Nucleic Acid Structure*, Springer-Verlag: New York, **1984**.
7. Davis, J. T. *Angew. Chem. Int. Ed.* **2004**, *43*, 668-698.
8. Guschlbauer, W.; Chantot, J. F.; Thiele, D. *J. Biomol. Struct. Dyn.* **1990**, *8*, 491-511.
9. Spada, G. P.; Gottarelli, G. *Synlett* **2004**, 596-602.
10. Simonsson, T. *Biol. Chem.* **2001**, *382*, 621-628.
11. Williamson, J. R. *Annu. Rev. Biophys. Biomolec. Struct.* **1994**, *23*, 703-730.

12. Gellert, M.; Lipsett, M. N.; Davies, D. R. *Proc. Natl. Acad. Sci. U. S. A.* **1962**, *48*, 2013-2018.
13. Fresco, J. R.; Massoulie, J. *J. Am. Chem. Soc.* **1963**, *85*, 1352-1353.
14. Pinnavaia, T. J.; Miles, H. T.; Becker, E. D. *J. Am. Chem. Soc.* **1975**, *97*, 7198-7200.
15. Pinnavaia, T. J.; Marshall, C. L.; Mettler, C. M.; Fisk, C. I.; Miles, H. T.; Becker,E. D. *J. Am. Chem. Soc.* **1978**, *100*, 3625-3627.
16. Wong, A.; Ida, R.; Spindler, L.; Wu, G. *J. Am. Chem. Soc.* **2005**, *127*, 6990-6998.
17. a) F. Aboul-ela, A. I. Murchie, D. M. Lilley, *Nature* **1992**, *360*, 280; b) F. Aboul-ela, A. I. Murchie, D. G. Norman, D. M. Lilley, *J. Mol. Biol.* **1994**, *243*, 458; c) C. Cheong, P. B. Moore, *Biochemistry* **1992**, *31*, 8406; d) C. Kang, X. Zhang, R. Ratliff, R. Moyzis, A. Rich, *Nature* **1992**, *356*, 126; e) G. Laughlan, A. I. Murchie, D. G. Norman, M. H. Moore, P. C. Moody, D. M. Lilley, B. Luisi, *Science* **1994**, *265*, 520; f) P. Schultze, F. W. Smith, J. Feigon, *Structure* **1994**, *2*, 221; g) F. W. Smith, J. Feigon, *Biochemistry* **1993**, *32*, 8682; h) Y. Wang, D. J. Patel, *Biochemistry* **1992**, *31*, 8112; i) Y. Wang, D. J. Patel, *Structure* **1993**, *1*, 263.
18. A few recent collections of research papers or reviews on the biological aspects of supramolecular chemistry of guanosines: a) A. N. Lane, J. B. Chaires, R. D. Gray, J. O. Trent, *Nucleic Acids Res.* **2008**, *36*, 5482 –5515; b) A. N. Lane, J. B. Chaires, R. D. Gray, J. O. Trent, *Nucleic Acids Res.* **2008**, *36*, 5482; c) L. Oganesian, T. M. Bryan, *Bioessays* **2007**, *29*, 155; d) S. Burge, G. N. Parkinson, P. Hazel, A. K. Todd, S. Neidle, *Nucleic Acids Res.* **2006**, *34*, 5402; e) J. L. Huppert, *Chem. Soc. Rev*. **2008**, *37*, 1375; f) D. Monchaud, M.-P. Teulade-Fichou, *Org. Biomol. Chem.* **2008**, *6*, 627.
19. Zhou, S. Y.; Liu, D. *Crit. Rev. Eukaryot. Gene Expr.* **2006**, *16*, 103-118.
20. McEachern, M. J.; Krauskopf, A.; Blackburn, E. H. *Annu. Rev. Genet.* **2000**, *34*, 331-358.
21. Collins, K. *Curr. Opin. Cell Biol.* **2000**, *12*, 378-383.
22. Greider, C. W. *Annu. Rev. Biochem.* **1996**, *65*, 337-365.
23. Bailey, S. M.; Murnane, J. P. *Nucleic Acids Res.* **2006**, *34*, 2408-2417.
24. Blackburn, E. H. *Cell* **2001**, *106*, 661-673.
25. Cech, T. R. *Angew. Chem. Int. Ed.* **2000**, *39*, 34-43.
26. Bryan, T. M.; Cech, T. R. *Curr. Opin. Cell Biol.* **1999**, *11*, 318-324.
27. Rhodes, D.; Giraldo, R. *Curr. Opin. Struct.Biol.* **1995**, *5*, 311-322.

28. Hahn, W. C.; Counter, C. M.; Lundberg, A. S.; Beijersbergen, R. L.; Brooks, M.W.; Weinberg, R. A. *Nature* **1999**, *400*, 464-468.
29. Olaussen, K. A.; Dubrana, K.; Dornont, J.; Spano, J. P.; Sabatier, L.; Soria, J. C. *Crit. Rev. Oncol./Hematol.* **2006**, *57*, 191-214.
30. Jing, N. J.; Sha, W.; Li, Y. D.; Xiong, W. J.; Tweardy, D. J. *Curr. Pharm. Design* **2005**, *11*, 2841-2854.
31. Chen, Z.; Corey, D. R., *Advances In Cancer Research*, *Vol 87*, **2003**, 31-58.
32. Neidle, S.; Parkinson, G. *Nat. Rev. Drug Discov.* **2002**, *1*, 383-393.
33. Perry, P. J.; Arnold, J. R. P.; Jenkins, T. C. *Expert Opin. Investig. Drugs* **2001**, *10*, 2141-2156.
34. Han, H. Y.; Hurley, L. H. *Trends Pharmacol. Sci.* **2000**, *21*, 136-142.
35. Kerwin, S. M. *Curr. Pharm. Design* **2000**, *6*, 441-471.
36. Hurley, L. H.; Wheelhouse, R. T.; Sun, D.; Kerwin, S. M.; Salazar, M.; Fedoroff, O. Y.; Han, F. X.; Han, H. Y.; Izbicka, E.; Von Hoff, D. D. *Pharmacol. Ther.* **2000**, *85*, 141-158.
37. Famulok, M.; Mayer, G.; Blind, M. *Acc. Chem. Res.* **2000**, *33*, 591-599.
38. Bock, L. C.; Griffin, L. C.; Latham, J. A.; Vermaas, E. H.; Toole, J. J. *Nature* **1992**, *355*, 564-566.
39. Macaya, R. F.; Schultze, P.; Smith, F. W.; Roe, J. A.; Feigon, J. *Proc. Natl. Acad. Sci. U. S. A.* **1993**, *90*, 3745-3749.
40. Marathias, V. M.; Bolton, P. H. *Biochemistry* **1999**, *38*, 4355-4364.
41. Vairamani, M.; Gross, M. L. *J. Am. Chem. Soc.* **2003**, *125*, 42-43.
42. Padmanabhan, K.; Padmanabhan, K. P.; Ferrara, J. D.; Sadler, J. E.; Tulinsky, A. *J. Biol. Chem.* **1993**, *268*, 17651-17654.
43. Tasset, D. M.; Kubik, M. F.; Steiner, W. *J. Mol. Biol.* **1997**, *272*, 688-698.
44. Nagatoishi, S.; Nojima, T.; Juskowiak, B.; Takenaka, S. *Angew. Chem. Int. Ed.* **2005**, *44*, 5067-5070.
45. Ueyama, H.; Takagi, M.; Takenaka, S. *J. Am. Chem. Soc.* **2002**, *124*, 14286-14287.
46. Ho, H. A.; Bera-Aberem, M.; Leclerc, M. *Chem.-Eur. J.* **2005**, *11*, 1718-1724.
47. Ho, H. A.; Leclerc, M. *J. Am. Chem. Soc.* **2004**, *126*, 1384-1387.
48. He, F.; Tang, Y. L.; Wang, S.; Li, Y. L.; Zhu, D. B. *J. Am. Chem. Soc.* **2005**, *127*, 12343-12346.

49. Potyrailo, R. A.; Conrad, R. C.; Ellington, A. D.; Hieftje, G. M *Anal. Chem.* **1998**, *70*, 3419-3425.
50. Lee, M.; Walt, D. R. *Anal. Biochem.* **2000**, *282*, 142-146.
51. Hamaguchi, N.; Ellington, A.; Stanton, M. *Anal. Biochem.* **2001**, *294*, 126-131.
52. Li, J. W. J.; Fang, X. H.; Tan, W. H. *Biochem. Biophys. Res. Commun.* **2002**, *292*, 31-40.
53. Yang, C. J.; Jockusch, S.; Vicens, M.; Turro, N. J.; Tan, W. H. *Proc. Natl. Acad. Sci. U. S. A.* **2005**, *102*, 17278-17283.
54. Nutiu, R.; Li, Y. F. *J. Am. Chem. Soc.* **2003**, *125*, 4771-4778.
55. Nutiu, R.; Li, Y. F. *Chem.-Eur. J.* **2004**, *10*, 1868- 1876.
56. Heyduk, E.; Heyduk, T. *Anal. Chem.* **2005**, *77*, 1147-1156.
57. Pavlov, V.; Xiao, Y.; Shlyahovsky, B.; Willner, I. *J. Am. Chem. Soc.* **2004**, *126*, 11768-11769.
58. Seela, F.; Jawalekar, A. M.; Chi, L. F.; Zhong, D. Y. *Chem. Biodivers.* **2005**, *2*, 84-91.
59. Li, Z.; Mirkin, C. A. *J. Am. Chem. Soc.* **2005**, *127*, 11568-11569.
60. Ikebukuro, K.; Kiyohara, C.; Sode, K. *Anal. Lett.* **2004**, *37*, 2901-2909.
61. Hianik, T.; Ostatna, V.; Zajacova, Z.; Stoikova, E.; Evtugyn, G. *Bioorg. Med. Chem. Lett.* **2005**, *15*, 291-295.
62. Xiao, Y.; Lubin, A. A.; Heeger, A. J.; Plaxco, K. W. *Angew. Chem. Int. Ed.* **2005**, *44*, 5456-5459.
63. Xiao, Y.; Piorek, B. D.; Plaxco, K. W.; Heeger, A. J. *J. Am. Chem. Soc.* **2005**, *127*, 17990-17991.
64. So, H. M.; Won, K.; Kim, Y. H.; Kim, B. K.; Ryu, B. H.; Na, P. S.; Kim, H.; Lee, J. O. *J. Am. Chem. Soc.* **2005**, *127*, 11906-11907.
65. Radi, A. E.; Sanchez, J. L. A.; Baldrich, E.; O'Sullivan, C. K. *J. Am. Chem. Soc.* **2006**, *128*, 117-124.
66. Xiao, Y.; Pavlov, V.; Niazov, T.; Dishon, A.; Kotler, M.; Willner, I. *J. Am. Chem. Soc.* **2004**, *126*, 7430-7431.
67. Pavlov, V.; Shlyahovsky, B.; Willner, I. *J. Am. Chem. Soc.* **2005**, *127*, 6522-6523.
68. Fan, C. H.; Plaxco, K. W.; Heeger, A. J. *Proc. Natl. Acad. Sci. U. S. A.* **2003**, *100*, 9134-9137.
69. Li, J. W. J.; Tan, W. H. *Nano Lett.* **2002**, *2*, 315-318.
70. Alberti, P.; Mergny, J. L. *Proc. Natl. Acad. Sci. U. S. A.* **2003**, *100*, 1569-1573.

71. Dittmer, W. U.; Reuter, A.; Simmel, F. C. *Angew. Chem. Int. Ed.* **2004**, *43*, 3550-3553.
72. Koshkin, A. A.; Rajwanshi, V. K.; Wengel, J. *Tetrahedron Lett.* **1998**, *39*, 4381-4384.
73. Obika, S.; Nanbu, D.; Hari, Y.; Andoh, J.; Morio, K.; Doi, T.; Imanishi, T. *Tetrahedron Lett.* **1998**, *39*, 5401-5404.
74. Dominick, P. K.; Jarstfer, M. B. *J. Am. Chem. Soc.* **2004**, *126*, 5050-5051.
75. Randazzo, A.; Esposito, V.; Ohlenschlager, O.; Ramachandran, R.; Mayol, L. *Nucleic Acids Res.* **2004**, *32*, 3083-3092.
76. Mergny, J. L.; De Cian, A.; Ghelab, A.; Sacca, B.; Lacroix, L. *Nucleic Acids Res.* **2005**, *33*, 81-94.
77. Datta, B.; Schmitt, C.; Armitage, B. A. *J. Am. Chem. Soc.* **2003**, *125*, 4111-4118.
78. Marin, V. L.; Armitage, B. A. *J. Am. Chem. Soc.* **2005**, *127*, 8032-8033.
79. Krishnan-Ghosh, Y.; Stephens, E.; Balasubramanian, S. *J. Am. Chem. Soc.* **2004**, *126*, 5944-5945.
80. Datta, B.; Bier, M. E.; Roy, S.; Armitage, B. A. *J. Am. Chem. Soc.* **2005**, *127*, 4199-4207.
81. Petraccone, L.; Pagano, B.; Esposito, V.; Randazzo, A.; Piccialli, G.; Barone, G.; Mattia, C. A.; Giancola, C. *J. Am. Chem. Soc.* **2005**, *127*, 16215-16223.
82. Wyatt, J. R.; Davis, P. W.; Freier, S. M. *Biochemistry* **1996**, *35*, 8002-8008.
83. Li, Y. F.; Sen, D. *Biochemistry* **1997**, *36*, 5589- 5599.
84. Li, Y. F.; Sen, D. *Chem. Biol.* **1998**, *5*, 1-12.
85. Geyer, C. R.; Sen, D. *J. Mol. Biol.* **2000**, *299*, 1387-1398.
86. Travascio, P.; Li, Y. F.; Sen, D. *Chem. Biol.* **1998**, *5*, 505-517.
87. Travascio, P.; Witting, P. K.; Mauk, A. G.; Sen, D. *J. Am. Chem. Soc.* **2001**, *123*, 1337-1348.
88. Chinnapen, D. J. F.; Sen, D. *Proc. Natl. Acad. Sci. U. S. A.* **2004**, *101*, 65-69.

Chapter 2. The G-Quartet in Supramolecular Chemistry: Cation-Templated Self-Assembly

The majority of this Chapter has been published in:

- S. Lena, S. Masiero, S. Pieraccini, G. P. Spada, *Chem. Eur. J.* **2009**, *15*, 7792.
- P. Neviani, E. Mileo, S. Masiero, S. Pieraccini, M. Lucarini, G. P. Spada, *Org. Lett.* **2009**, *11*, 3004.

2.1 Introduction

Since the last two decades, guanosine-related molecules have been of interest in different areas, ranging from structural biology to medicinal chemistry, supramolecular chemistry and nanotechnology. As guanine is a multiple hydrogen bonding unit, capable also to bind cations, it fits very well with contemporary studies in supramolecular chemistry, self-assembly and non-covalent synthesis. This Chapter, after reviewing on the diversification of cation-templated self-organised assemblies from guanosine-based low-molecular-weight molecules, will mainly focus on the use of guanine moiety as a potential scaffold for designing functional materials with tailored physical properties.

2.2 Guanosine Self-Assemble in Nonpolar Solvents

Until the early 1990s it was believed that G-quartet assemblies only formed in water and Guschlbauer, a pioneer of the G-quadruplexes studies, wrote in his 1990 review article:[1] "*water appears to be an indispensable solvent for the autoassociation of guanosine […] organic solvents give rise to poorly organised aggregates*". At that time, appropriate molecular structures and conditions needed for observing guanosine self-assembly in organic solvents were not yet identified. Due to the poor solubility of guanosine, it was not until the ribose hydroxyl groups were modified with protecting groups that it was recognized that lipophilic guanosine nucleosides could self-associate into discrete assemblies in organic solvents.

Concurrently and independently our group in Bologna[2] and Davis' group in Maryland[3] reported in 1995 that (lipophilic) guanosine derivatives can self-assemble and form the G-quartet motif even in organic solvents in the presence of alkali-metal cations. No longer forced to work in water (or other highly polar solvents), it was possible to

extend the structural modification of the guanine moiety exploiting the facility to functionalise guanosine in the sugar hydroxyl groups or in the aromatic base. Since then, it has been found that guanosine derivatives do indeed form a variety of stable, ordered assemblies in organic solvents, some of them templated by cations. In fact, while all supramolecular architectures reported in water are based on the G-quartet motif and are metal-ion template (see Figure 1.5), in organic solvents a high diversification is observed: not only G-quartet-based assemblies were observed, but also ribbon-like, sheet-like (Chapter 3) and continuous helical architectures (see **2.5.1**).

Lipophilic guanosine dG **1** extracted K^+ picrate from water into chlorinated organic solvents to give a discrete and highly stable [dG **1**]$_8$ • K^+ octamer or a columnar polymeric aggregates [dG **1**]$_n$ • nK^+ depending on the experimental conditions (Figure 2.1).

This G-quartet stacked polymer, [dG **1**]$_n$ • nK^+, formed in hydrocarbon solvents, gave hexagonal packed liquid crystals (see **3.2.1**).[7] Similar to the situation in water, the K^+ cation was absolutely essential for templation and stability of the G-quartets.

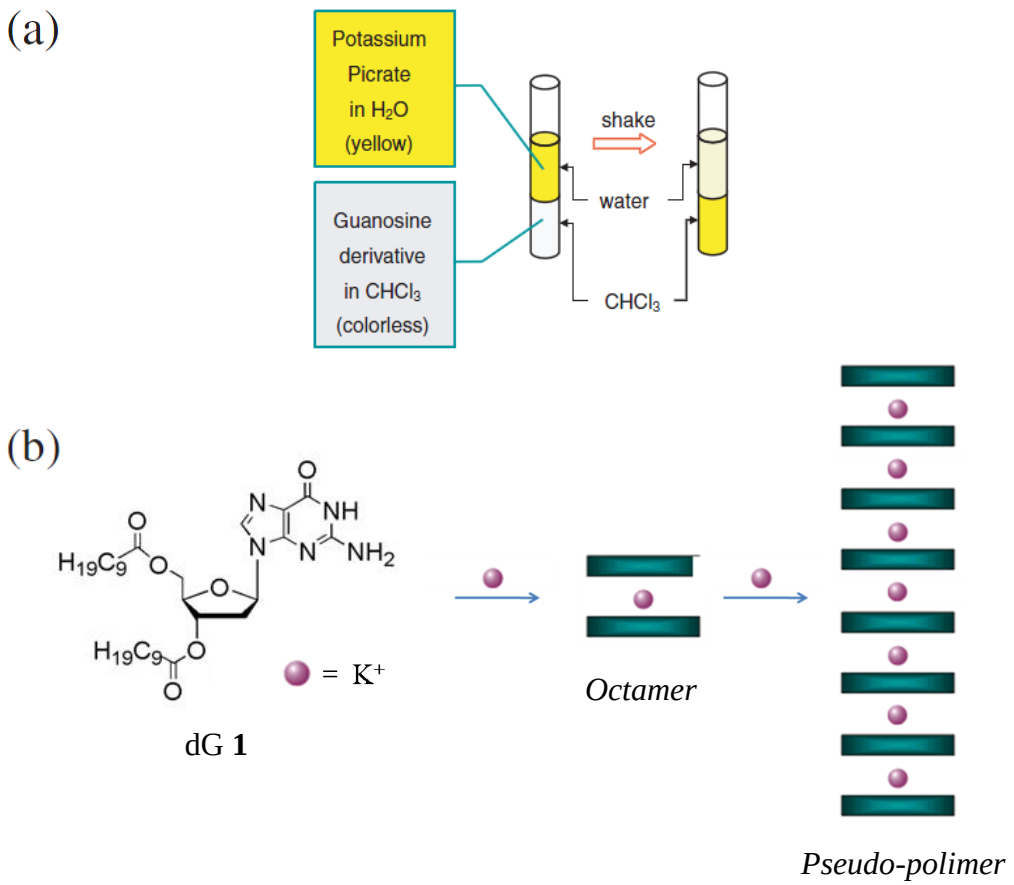

Figure 2.1. The set-up of the extraction experiment (a) and the cation directed self-assembly of lipophilic guanosine dG **1** (b).

It was also observed that hydrogen bonded ribbons were formed by dG **1** in the absence of K^+ (Figure 2.2).[4] Through changing either the sugar substituents or the solvent, our group modulated the specific hydrogen-bonding pattern (obtaining either a ribbon structure with dipole or no dipole as shown in Figure 1.4a and b). These ordered ribbons were shown to have some potential applications in the molecular electronic field (Chapter 3).

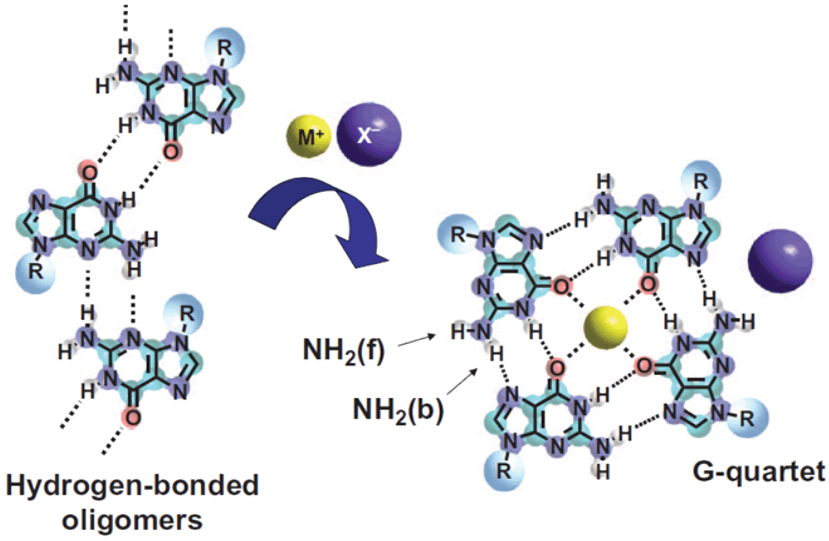

Figure 2.2. Self-assembly of guanosines. In organic solvents, lipophilic guanosine derivatives self-associate into a mixture of hydrogen-bonded oligomers. On addition of salt, the cation can template the formation of G-quartets. (Adapted from reference 49)

2.2.1 C_4-symmetric octamer $G_8 \cdot M^+$

As mentioned above, dG **1** behaves as an ionophore and solutions of it in chloroform are able to extract potassium picrate (KPic) from water (or crystal state) (Figure 2.1a);[2] moreover two different supramolecular assemblies were proposed and later on solved: depending on the relative amount of KPic used in the extraction either a C_4-symmetric octamer $G_8 \cdot M^+$ or a "polymeric" $(G_4 \cdot M^+)_n$ assembly (Figure 2.1b) can be obtained.

Our and Davis' groups collaborated to determine the structure of the octamer dG $\mathbf{1}_8 \cdot K^+$ in chloroform, the first detectable intermediate in the cation-directed self-assembly of dG **1**, by NMR spectroscopy.[5] This octameric assembly is very robust and its stability is impressive for a non-covalent assembly. The ^{1}H NMR spectra, essentially temperature

independent over more than 100 °C, show two sets of signals in a 1:1 ratio corresponding each to nucleosides with different glycosydic conformation (*syn*-like and *anti*-like) (Figure 2.3)

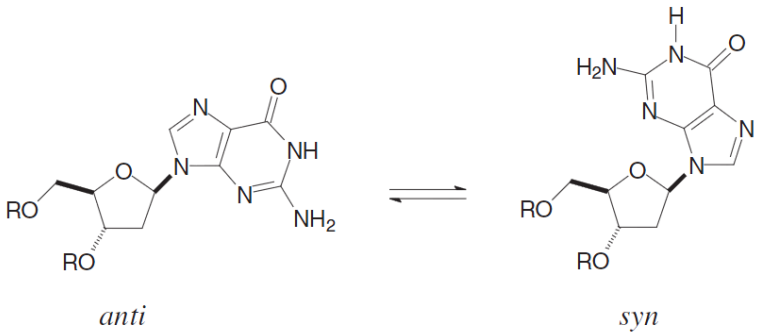

Figure 2.3. Glycosydic conformations.

It should be noted that there is another stereochemical consequence to the cation-templated self-assembly of guanosine derivatives. The two faces of the G-quartets are diasterotopic and can be labelled head and tail (see Figure 2.4a for a definition of these descriptors). In principle, the two quartets in the octamer can be arranged in three different orientations: head-to-tail (C_4 symmetry, see Figure 2.4b), head-to-head and tail-to-tail (D_4 symmetry; in Figure 2.4c the tail-to-tail arrangement is shown). Therefore, considering these two stereochemical aspects (*syn*/*anti* glicosidic conformation and relative G-quartets orientation) several diastereoisomers are possible for the octamer dG $\mathbf{1}_8 \cdot K^+$. Remarkably, the NMR data indicated that this octamer was a single diastereomer of C_4 symmetry. In one G-quartet, all monomers had a *syn* conformation, while the other tetramer had an "all-*anti*" conformation. NOE interactions indicated a relative orientation with the head-side of the "all-*anti*" G-quartet facing the tail-side of the "all-*syn*" G-quartet (Figure 2.4b). This stereoselectivity and stereoregularity for the non-covalent assembly of formula dG $\mathbf{1}_8 \cdot K^+$ is striking.

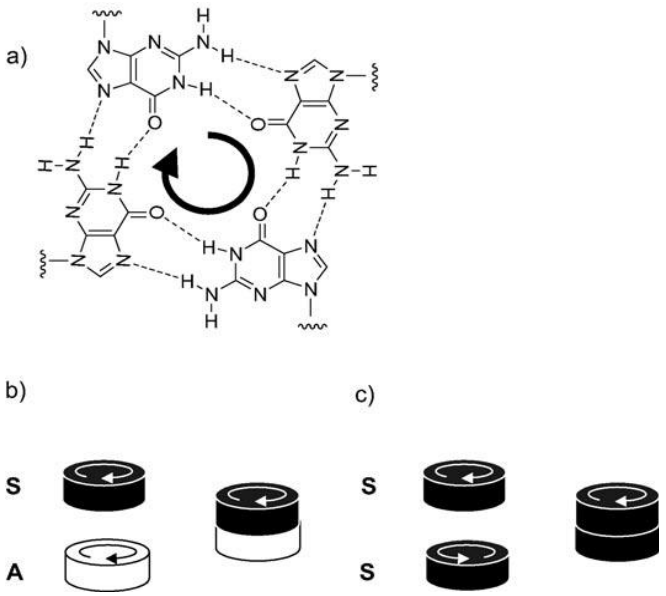

Figure 2.4. a) A G-quartet showing its head diastereotopic face. Schematic drawing of b) a C_4-symmetric and c) a D_4-symmetric octamer. In the C_4-symmetric octamer (obtained, e. g., from dG **1**), an all-*syn* G-quartet (S, black disk) with its tail-side (lower face) stacks on the head-side (upper face) of an all-*anti* (A, white disk) G-quartet. In the D_4-symmetric octamer (obtained, e.g., from **2**), two all-*syn* G-quartet stack facing their tail sides. Clockwise and counter-clockwise arrows refer to the head and tail faces, respectively.

2.2.2 Highly stereoregular D_4-symmetric "polymer" $(G_4 \cdot M^+)_n$

The solution structure of columnar polymeric aggregates [dG **1**]$_n$ • nK$^+$ was solved in our group by NMR (and small-angle neutron scattering (SANS)) spectroscopy.[6] Also this assembly is stable over a temperature range of approximately 100 °C. ^{1}H NMR spectra of the polymeric aggregate are relatively simple, showing three sets of signals (not interconverting on the NMR chemical shift time scale) in a 1:1:1 ratio. Each set corresponds to guanosine monomers with a different conformation (one *anti* rotamer, and two different *syn* conformers, *syn*1 and *syn*2). Like the C_4-symmetric dG $\mathbf{1}_8 \cdot K^+$ octamer, each G-quartet within the dG $(\mathbf{1}_4 \cdot K^+)_n$ polymer is homogeneous in terms of its rotamer composition. NMR data are consistent with a structure composed of three distinct G-quartets displaying an all-*anti* (A), an all-*syn*1 (S1) and an all-*syn*2 (S2) arrangement. The polymer is then a repetition of a dodecamer building block composed from these three different types of stacked G-quartets. Disregarding the stacking orientation, there are three possible sequential arrangements of three quartets into a dodecamer: AS1S2, AS2S1 and S1AS2, but only the first is observed. In addition, considering the diastereotopicity of

the quartet's faces, eight (2^3) different relative orientations of the A, S1 and S2 quartets are possible, in principle, for the AS1S2 arrangement. NOESY experiments confirm that the AS1S2 dodecamer is present as a unique stereoisomer (Figure 2.5): the head-side of the A quartet faces the tail-side of the S1 quartet, while the head-side of the S1 quartet faces the tail-side of the S2 quartet. Finally, the following dodecamer repetition sequence is observed in the polymer: [AS1S2] [S2S1A] [AS1S2] [S2S1A] [AS1S2], wherein two all-*anti* quartets A and two all-*syn*2 quartets S2 are close together, arranged in a tail-to-tail and a head-to-head orientation, respectively. Two structural aspects should be noted. First, the stereochemistry of AS1 arrangement is similar to that reported for C_4-symmetric octamer $G_8 \cdot M^+$, suggesting that the octamer presumably represents the first step of aggregation. Second, the symmetry of this polymeric assembly is different from that observed for the polymeric supramolecular structure of 5'-GMP **6** in water (Figure 1.5): in this latter case, due to the head-to-tail orientation of all the contiguous G-quartets, the polymer has C4 symmetry.

The stereochemical regularity of these columnar polymeric G-aggregates is truly amazing as far as the rotamers around the glycosidic bond within each G-quartet, the repeated sequence of the G-quartets along the columns and their relative stacking orientation are concerned (Figure 2.5). As already mentioned above, in contrast to discrete assemblies, for example, octamers, these columnar aggregates form lyomesophases of the cholesteric and hexagonal types in hydrocarbon solvents above a critical concentration.[7] The elongation ratio of the supramolecular assembly is a crucial factor for the appearance of lyotropic liquid-crystalline phases and only supramolecular polymeric assemblies, like $(G_4 \cdot M^+)_n$ or ribbon structures can self-correlate to produce this type of supramolecular self-organisation (see **3.2.1**)

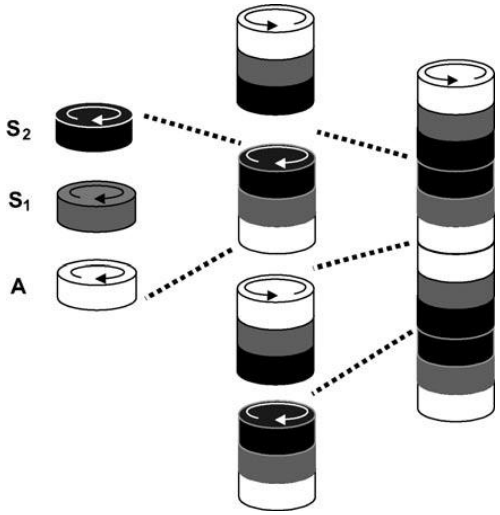

Figure 2.5. "Explosion" cartoon of the assembly of the polymeric aggregate obtained from dG **1**. White, grey and black disks refer to all-*anti* (A), all-*syn*1 (S1) and all-*syn*2 (S2) quartets, respectively; clockwise and counter-clockwise arrows refer to the quartet head and tail faces, respectively.

2.2.3 D_4-symmetric octamer $G_8 \cdot M^+$

While derivative dG **1** forms the K^+-templated C_4-symmetric octamer structure or the polymeric assembly $(G_4 \cdot M^+)_n$ described above in solution, other lipophilic guanosine derivatives (especially those with ribose, as sugar moiety) can give a different stereoregular octamer with a D_4-symmetry.[8-11] For example, in the presence of Na^+ ions N2-modified guanosine derivatives, like 2-*N*-(4-butylphenyl)-2',3',5'-*O*-triacetyl guanosine **2** (Figure 2.6), are found to self-associate into discrete octamers that contain two G-quartets and a central ion.[9b] In each octamer, all eight guanosine molecules are in a syn conformation and the two G-quartets are stacked in a tail-to-tail fashion (Figure 2.4c). Hence, π–π-stacking interactions between the N2-side arms can considerably stabilise the octamer structure although the N-substitution with aryl groups is not a prerequisite for observing D_4-symmetric octamers. Once confirmed that the assembly has an octameric structure (e.g., by DOSY NMR spectroscopy) it is relatively easy to assign its symmetry to the C_4 or D_4 point group: in fact, while in the former case two sets of signals are observed in the ^{1}H NMR spectrum (the two G-quartets are diastereotopic), in the latter case only a single set of signals is observed for the two homotopic G-quartets.

Furthermore circular dichroism is diagnostic of the stacking polarity of two contiguous G-quartets.[12] Similarly to base pairs in DNA, the tetramers do not stack in

register, but are rotated with respect to each other to give, in the 230–300 nm region characteristic of the π–π* transitions of guanine chromophore, a double-signed exciton-like CD signal. This couplet, the sign of which allows the assignment of the stacking helicity (handedness), exhibits opposite signed bands at about 260 and 240 nm for the head-to-tail (C_4-symmetric) stacking in compound dG **1**, while both bands are blue-shifted by 20–30 nm in the D_4-symmetric stacking in compound **3** (Figure 2.7b).

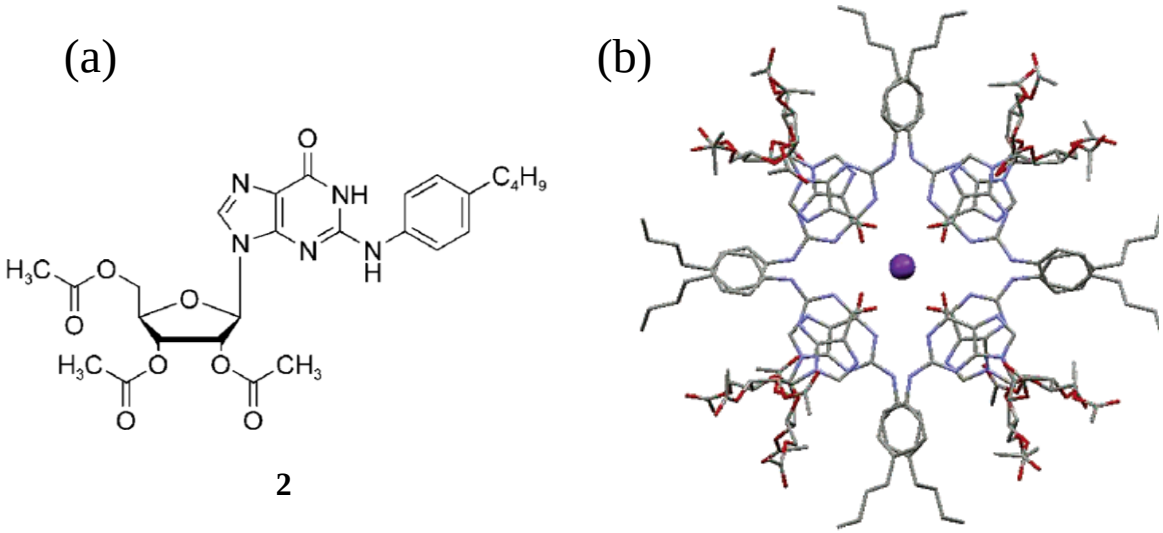

2

Figure 2.6. a) Derivative **2** and b) molecular model (top view) for a D_4-symmetric octamer where the two G-quartets are oriented in a tail-to-tail fashion. (From reference 9a)

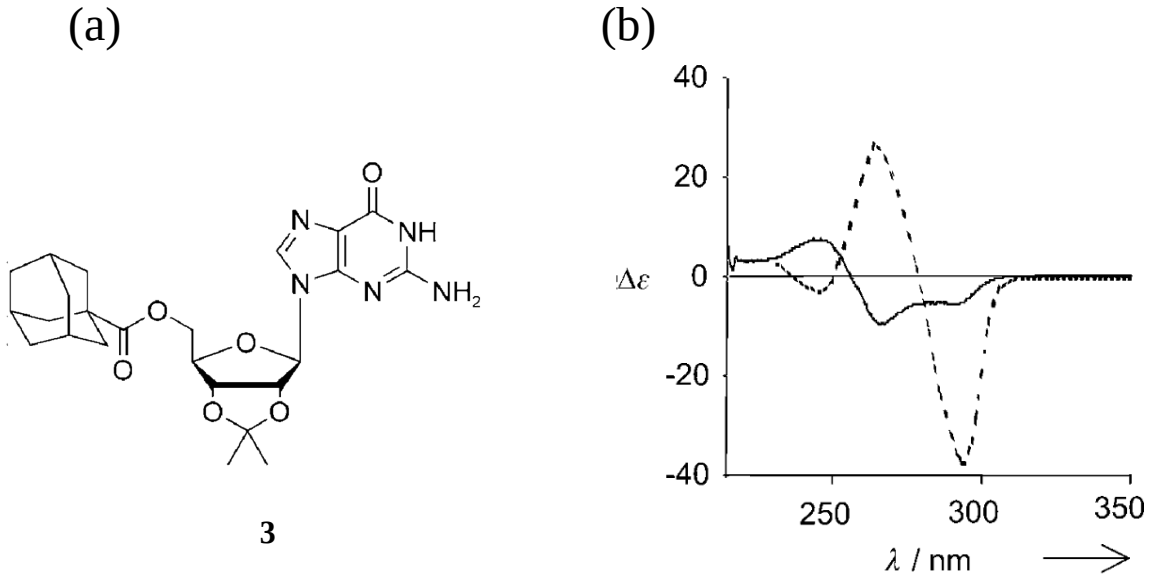

3

Figure 2.7. a) Derivative **3** and b) comparison between CD spectra of C_4-(solid line) and D_4-symmetric (dashed line) octamers $G_8 \cdot M^+$ obtained from **1** and **3**, respectively. (Figure 2.7b from reference 2, 10)

2.2.4 D_4-symmetric hexadecamer $G_{16}\cdot 4M^+$ (or $G_{16}\cdot 2M^{2+}$)

Derivative G **8** was observed to form a different metal-ion template supramolecular structure in the presence of KPic.[8] NMR experiments (including DOSY NMR data)[13] indicated that a D_4-symmetric hexadecamer $G_{16}M^+_4$ composed of four stacked G-quartets is the major species in solution (Figure 2.9). ^{1}H NMR spectra show two sets of signals, present in a 1:1 ratio, assigned to the distinct "outer" and "inner" G-quartets that make up the D_4-symmetric hexadecamer and also experimental diffusion coefficient agree well with the expected value for $G_{16}M^+_4$. X-ray crystallography confirmed that derivative G **8** forms an ordered hexadecamer.[14] This assembly, with empirical formula $G\mathbf{8}_{16}\cdot 3K^+/Cs^+\cdot 4Pic^-$, is stabilised by four co-axial cations and by four picrate anions. It can be described as a pair of head-to-tail C_4-symmetric octamers $G_8\cdot M^+$, with each octamer using its eight carbonyl oxygen atoms to coordinate a K^+ ion, while a third K^+ ion holds the two $G_8\cdot M^+$ octamers together in a head-to-head orientation: this leads to a D_4-symmetric assembly (Figure 2.8a). Finally, a Cs^+ ion loosely bound, in solution caps the structure. In addition to stabilization by cations, four picrate anions form hydrogen bonds to N2 amino groups that extend from the two "inner" G-quartets (Figure 2.8b). The lipophilic G-quadruplex looks like a cation channel with an anionic belt wrapped around its middle. Similar solid-state structures for $G\mathbf{8}_{16}\cdot 2M^{2+}\cdot 4Pic^-_4$ were obtained with the divalent cations Ba^{2+} and Sr^{2+}.[15]

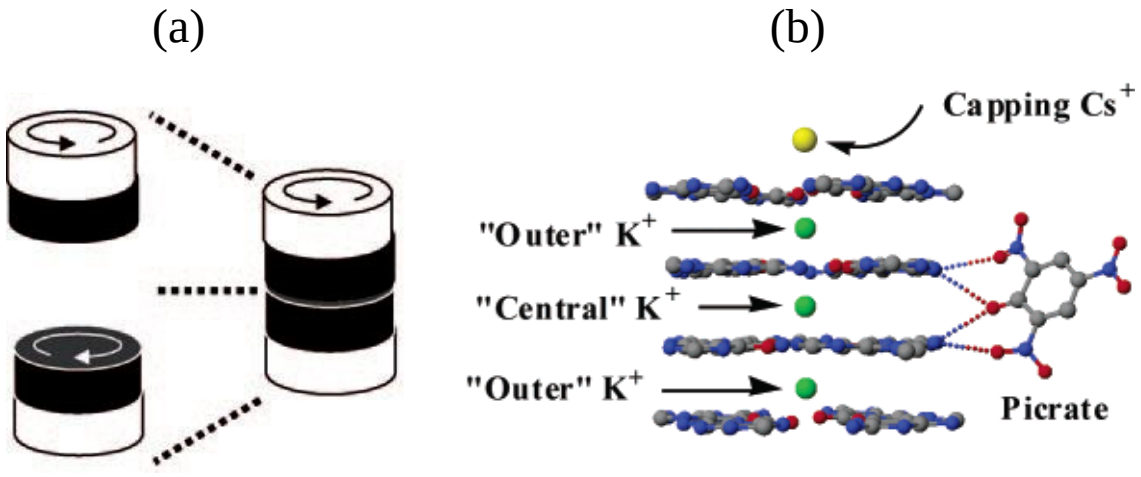

Figure 2.8. a) Schematic cartoon of the quartet assemblies in the D_4-symmetric hexadecamer (black and white refer to inner and outer quartets, respectively; clockwise and counter-clockwise arrows refer to the head and tail faces, respectively); b) a schematic showing the nucleobase–picrate hydrogen bonds in the hexadecamer $G\mathbf{8}_{16}\cdot 3K^+/Cs^+\cdot 4Pic^-$. (Figure 2.8b adapted from reference 13)

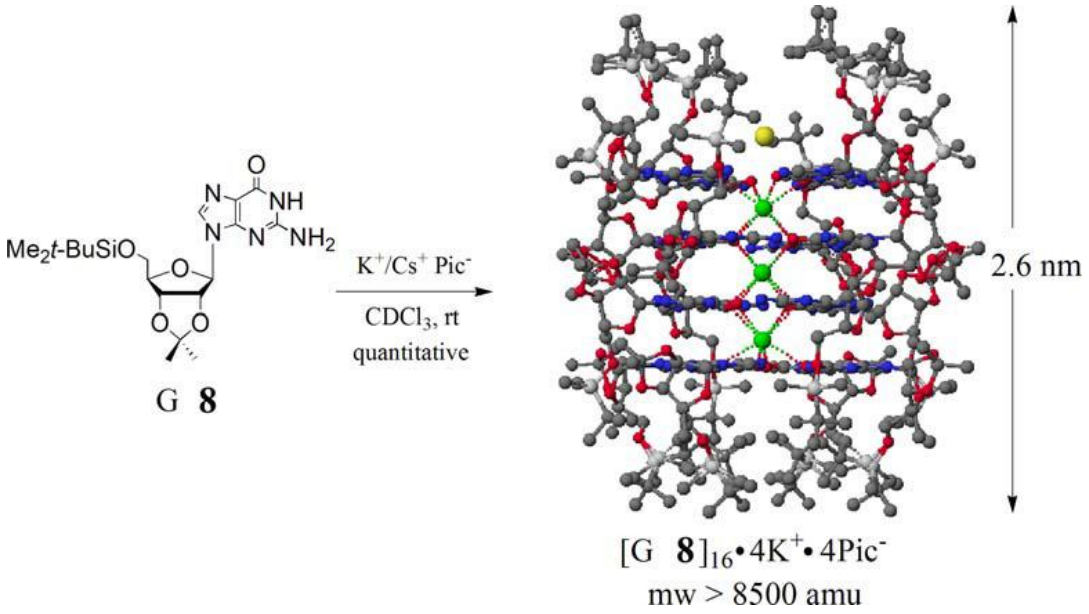

Figure 2.9. Crystal structure shows that the cation-templated self-assembly of 16 equivalents of G **8** gives a lipophilic G-quadruplex [G **8**]$_{16}$ • $3K^+/Cs^+$ • $4pic^-$. (From reference 14)

Moreover, G-quadruplexes containing divalent cations such as Pb^{2+}, Ba^{2+} or Sr^{2+} are both thermodynamically and kinetically more stable than are the corresponding G-quadruplex assemblies that contain monovalent Na^+ or K^+. This enhancement in stability in the presence of the divalent cations over monovalent cations is most likely due to the stronger ion-dipole interactions between the bound cations and the coordinating carbonyl oxygens.

2.2.5 D_5-symmetric decamer isoG$_{10}$·M$^+$

Much like guanosine, the isoguanosine nucleobase also self-associates into discrete hydrogen-bonded assemblies in the presence of cations. For example, the lipophilic analogue 5'-*tert*-butyldimethylsilyl-2',3'-di-*O*-isopropylidene isoguanosine isoG **5** was proposed to form a pentamer isoG$_5$·M$^+$ and/or a decamer isoG$_{10}$·M$^+$ in the presence of monovalent cations.[3,16] Recent diffusion NMR studies concluded that D_5-symmetric decameric species are the only assemblies formed in solution.[17] The crystal structure of isoG **5**$_{10}$·Cs$^+$ revealed that the decamer is composed of two hydrogen-bonded isoG-pentamers (see Figure 2.10) that sandwich a central Cs^+ ion.[16] Computational

studies have supported the experimental findings that isoG forms stable pentameric/decameric assemblies with alkali metal ions.[18]

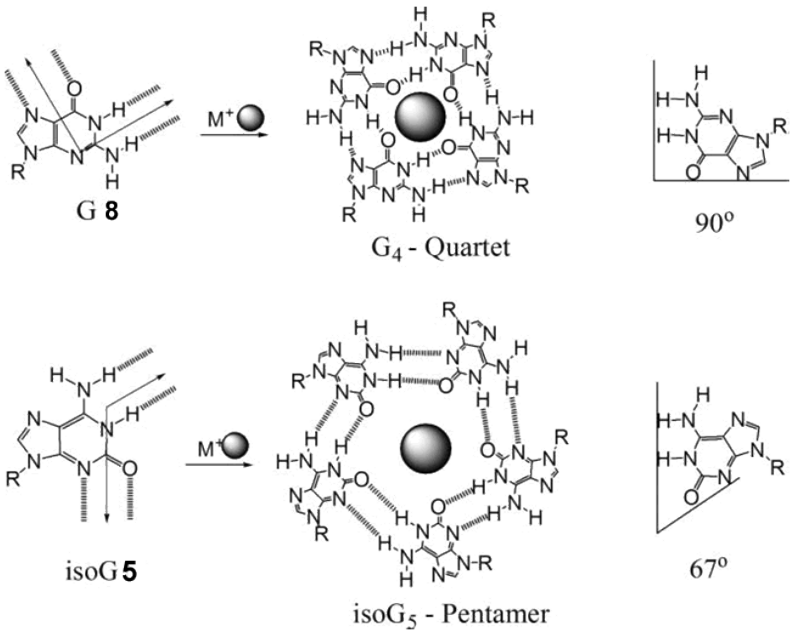

Figure 2.10. Lipophilic nucleosides G **8** and isoG **5** self-associate in the presence of cations to give G_4-quartets or $isoG_5$-pentamers. The orientation of the nucleoside's hydrogen bond donor and acceptor groups determines assembly size. (Adapted from reference 19)

The case of isoG is a nice example on how the self-assembly is determined by the information programmed into the monomers component and even small variations on the building block can alter the supramolecular structure. Isomers guanosine **8** and isoguanosine **5** differ only in the location of an oxygen and a nitrogen atom, yet they self-assemble in very different manners. G-quartets are formed from **8** because the donor and acceptor unites are 90° to each other, thus ensuring a planar tetramer with C_4-symmetry. Unlike guanine, in isoguanine the self-complementary units form a wider angle very close to the theoretical value for a regular pentagon (see Figure 2.10) thus leading to a hydrogen-bonded pentameric structure with C_5 symmetry.

Davis and colleagues conducted a ''*self-sorting*'' study in $CDCl_3$ to illustrate how the cation dictates the self-assembly patterns for G **8** and isoG **5**.[20] An equimolar mixture of the two isomers in $CDCl_3$, in the absence of cations, formed a mix of hydrogen-bonded species. Addition of Ba^{2+} to this mixture gave quantitative formation of two discrete hydrogen-bonded complexes, the G-quadruplex [G **8**]$_{16}$·2Ba^{2+} and the decamer [isoG **5**]$_{10}$ ·Ba^{2+}. This ''*self-sorting*'' illustrated that a cation is needed to template formation of distinct assemblies in solution from this mixture of nucleosides.

2.3 Enantiomeric Self-Association of Lipophilic Nucleosides

The cation's control over self-assembly was also illustrated by the expression of supramolecular stereochemistry by chiral nucleosides. The cation's identity (Ba^{2+} vs. K^+) had a significant influence on the diastereoselectivity in self-association of G **8**.[15a] When K^+ was added to a solution of racemic (D,L)-G **8** the resulting G-quadruplexes were a mixture of heterochiral diastereomers. The divalent cation Ba^{2+}, however, directed enantiomeric self-recognition of (D,L)-G **8**, giving homochiral G-quadruplexes (Figure 2.11). To explain this cation-dependent diastereoselectivity, Davis and colleagues proposed that the increased enthalpy inherent to the divalent cation–oxygen interaction must help overcome the unfavorable entropy associated with enantiomeric ''*self-sorting*''.

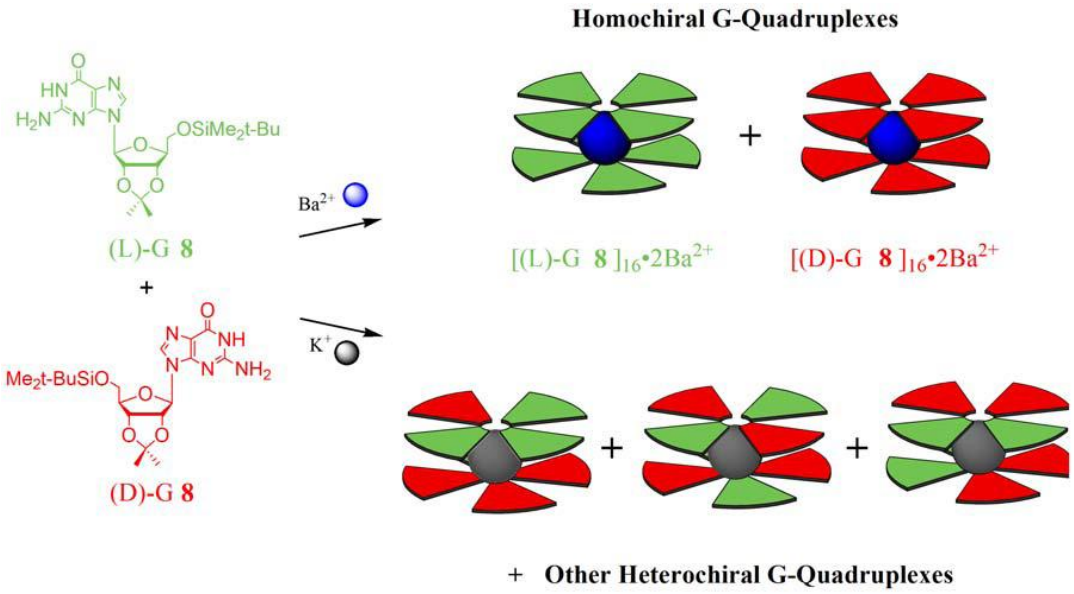

Figure 2.11. G **8** undergoes cation dependant enantiomeric self-association. Racemic (*D*, *L*)-G **8** self-assembles in the presence of Ba^{2+} to give homochiral G-quadruplexes [(*D*)-G **8**]$_{16}$•2Ba^{2+}•4pic^- and [(*L*)-G **8**]$_{16}$•2Ba^{2+}•4pic^-. Addition of K^+ to G **8** gave a diastereomeric mixture of heterochiral assemblies. The green wedges represent (L)-G **8**, while the red wedges represent (D)-G **8**. The blue and gray spheres represent Ba^{2+} and K^+ respectively. (From reference 15a)

Lipophilic G-quartets might potentially be useful as chiral resolving agents. For instance, our group in Bologna showed that G-quartets formed from dG **7** (Figure 2.12) are enantioselective in their ability to extract chiral anions from water into organic solution. Thus, dG **7** extracted a K^+ *N*-dinitrophenyl-(L)-tryptophan salt from water into

$CDCl_3$ with a 3:1 enantioselectivity over the (D)-Trp enantiomer, indicating significant interactions occur between these anions and the chiral G-quadruplex.[21]

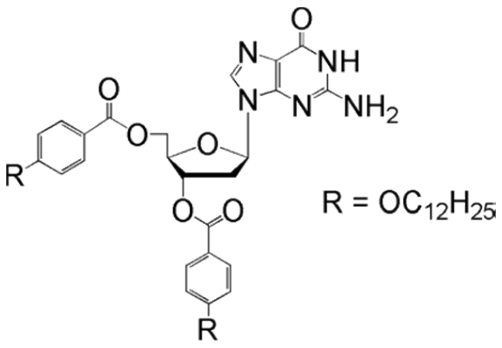

dG **7**

Figure 2.12. Derivative dG **7**.

2.4 "Empty" G-Quartets

Although cations are usually essential for the templation of G-quartets, there have been examples of G-quartets formed in the absence of cations. As already mentioned, generally, guanosine analogs form hydrogen-bonded dimers or ribbons. Sessler and colleagues solved a crystal structure of G **10** that revealed an "empty" G-quartet. G **10** was shown to self-assemble into a G-quartet even without the assistance of a templating cation.[22]

Attachment of sterically bulky groups, a dimethylaniline unit, to the C8 position of the guanine ring gave a conformationally constrained nucleoside that prefers to adopt a *syn* glycosidic bond conformer (Figure 2.3) in both the solid state and solution. This *syn* conformation prevents the nucleoside from any hydrogen-bonded ribbon formation and thus favors formation of the macrocyclic G-quartet (Figure 2.13). This study showed how control over the monomer can have profound impacts in the self-assembly of guanosine analogous.

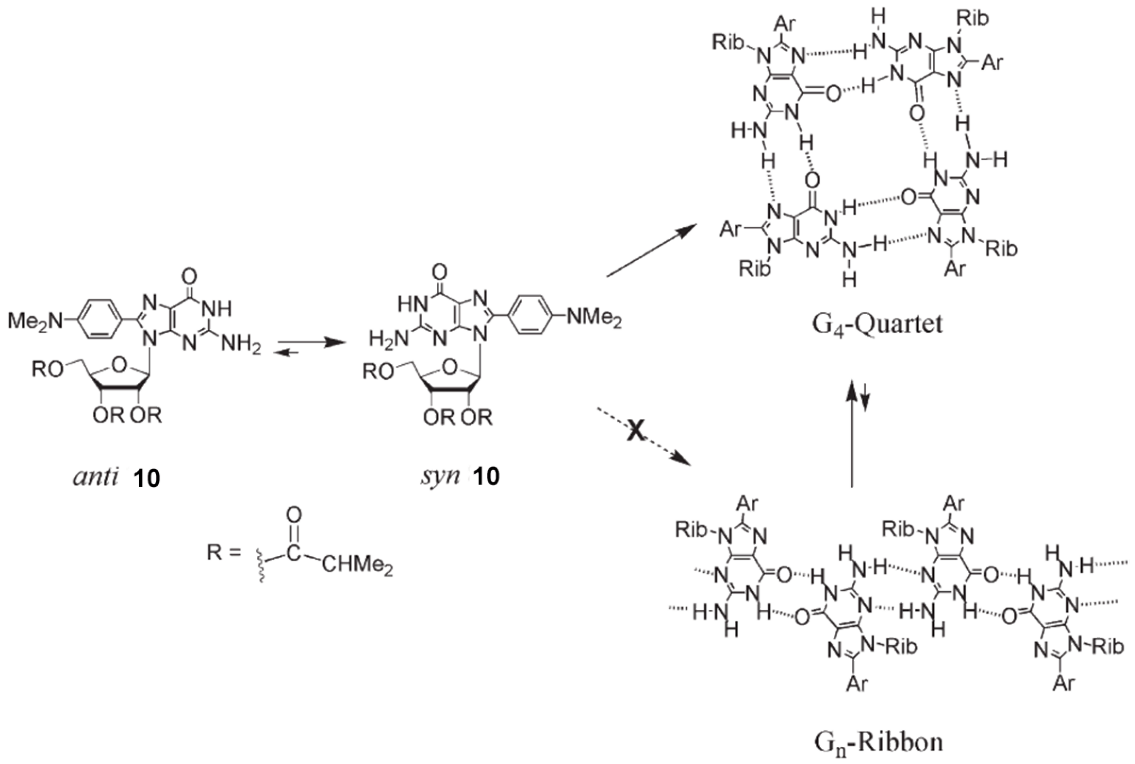

Figure 2.13. Conformationally constrained G **10** forms a G-quartet without presence of a templating cation. (From reference 22)

More recently, Besenbacher and colleagues showed that 'bare' (without any sugar or other substituents in N9) guanine **12** can form a kinetically stable "empty" G-quartet on a gold surface (Figure 2.14).[23] Using AFM they found that the empty G-quartet was not the thermodynamic minimum, as annealing the deposited G-quartet network led to rearrangement into a hydrogen-bonded ribbon. In this case, the available N9-H and the neighboring N3 positions of guanine **12** seem crucial for stabilizing the network of connected G-quartets. The Besenbacher paper is the first demonstration that guanine itself forms cyclic quartets, as other G-quartets have always involved N9-substituted G nucleobases.

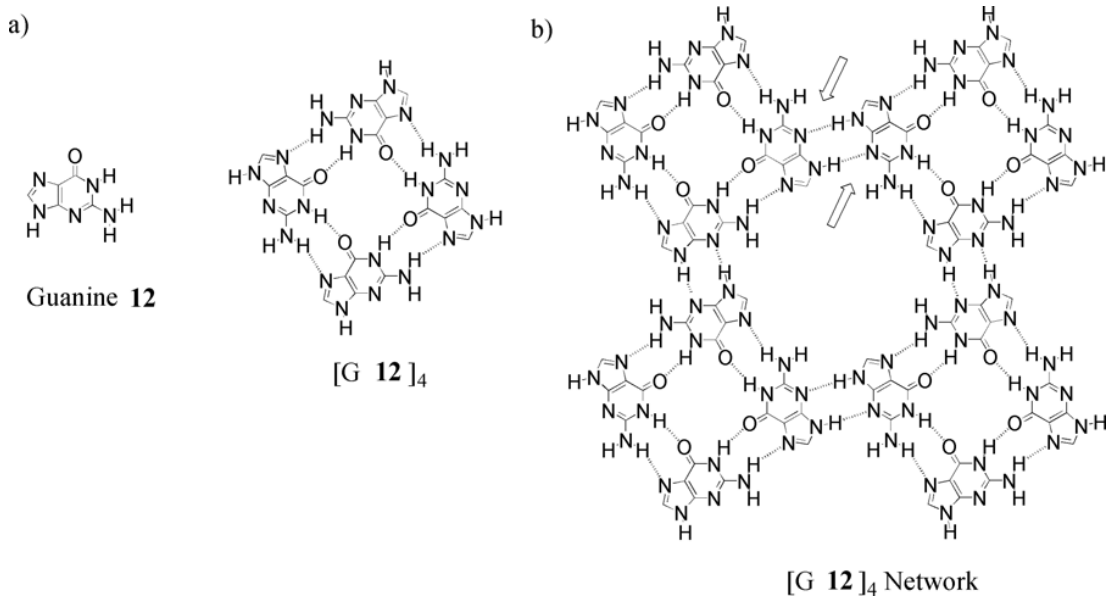

Figure 2.14. a) An empty G-quartet formed by guanine **12**. b) A hydrogen bound network of empty G-quartets. Each G-quartet can form up to eight additional hydrogen bonds with neighboring G-quartets (arrows). (From reference 23)

2.5 New Hydrogen-Bonded Assemblies from Nucleoside Analogs

Recently, Rivera and coworkers reported another way to stabilize G-quartet units by using 8-aryl-dG analogs such as dG **13**.[24] By adding a hydrogen bond acceptor to the C8 position, an additional hydrogen bond was forced between the exocyclic N2 amino hydrogen and the carbonyl of the hydrogen bond acceptor (Figure 2.15).

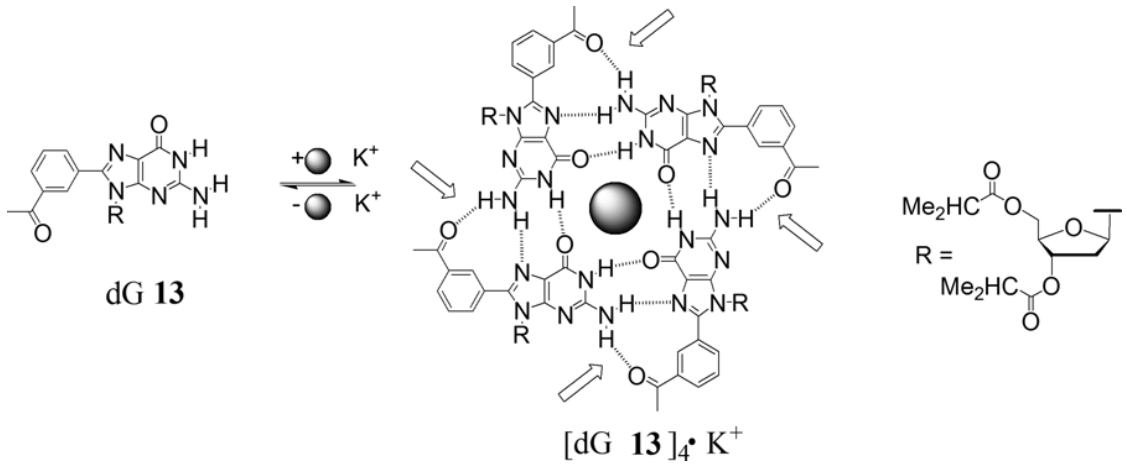

Figure 2.15. A G-quartet formed from dG **13**, a modified nucleobase with an expanded Hoogsteen hydrogen bonding face. Note the additional hydrogen bonds, depicted by arrows, thought to be a reason for increased stability. (From reference 24)

The G-quadruplex [dG **13**]$_{16}$ • 3K$^+$ showed an increased stability when compared with assemblies from the unsubstituted G derivatives as proven by variable temperature and dilution NMR experiments. Rivera proposed that the stability of the 8-aryl-dG analog **13** was due to a combination of factors. Again, the C8 substitution forces the derivative into the *syn* conformation, therefore precluding formation of hydrogen bonded ribbon structures. Additionally, the four additional aromatic rings attached to C8 provide larger surface for π-π interactions between the stacked G-quartets (see also derivative **2** in Figure 2.6). Finally, the C8 substituent in dG **13** enables four additional hydrogen bonds per G-quartet, as depicted by the arrows in Figure 2.15 (see also **2.6.4**)

Sessler and coworkers have synthesized a guanosine-cytidine dinucleoside (**11**) that self-associates into a cyclic trimer in organic solvents (Figure 2.16).[25] They used the potent GC hydrogen-bonding motif to direct assembly formation. An ethylene bridge separates the guanosine and cytidine moieties in derivative **11** and preorganizes these groups for formation of the macrocycle via three GC basepairs. This well-defined supramolecular structure may find use in the construction of self-assembled dendrimers and other nanostructures.

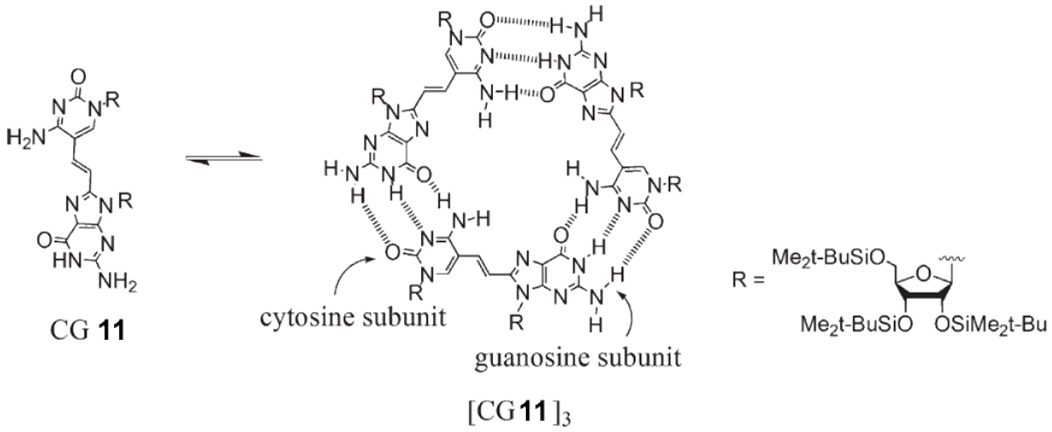

Figure 2.16. Self-assembly of lipophilic dinucleoside CG **11** into cyclotrimer [CG 12]$_3$.

2.5.1 Helical "polymer" (oxoG)$_n$

Recently, our group described another unique structure obtained upon self-assembly of 8-oxo lipophilic nucleosides.[26] Thus, both 8-oxoG **4** and the corresponding 2-deamino analog (8-oxoI) form hydrogen-bonded helices in organic solvents (Figure 2.17). This self-assembly pattern was quite different from the hydrogen-bonded ribbons formed by dG **1** (see Chapter 3).

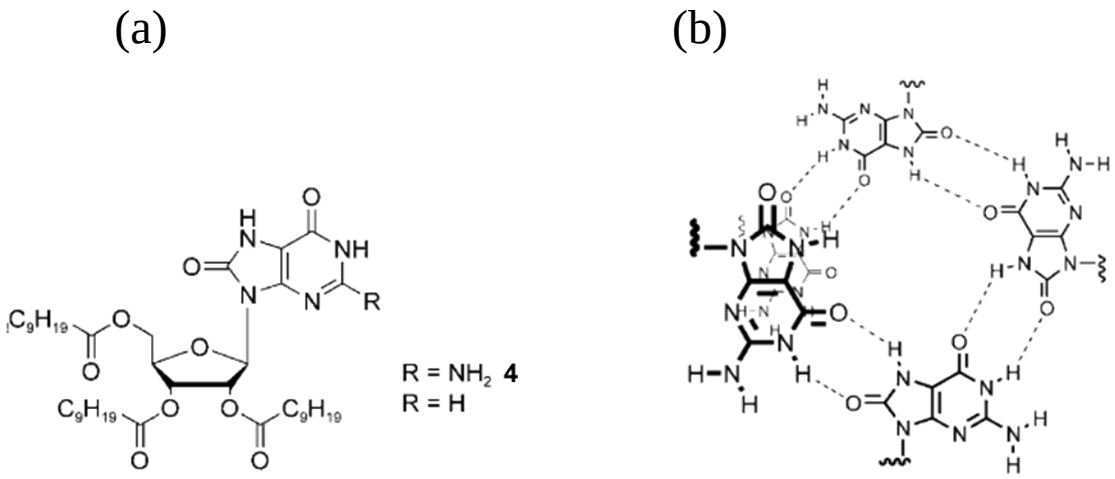

Figure 2.17. a) 8-oxoguanine **4** and its analog and b) the hydrogen-bonded helical structure formed by its self-assembly (the helical configuration has been arbitrary chosen). (From reference 26)

2.6 Guanosine Assemblies as Potential Scaffold for Functional Materials

As shown in the previous sections, guanosine derivatives allow both the control and diversification of self-assembled nanoarchitectures. This opens the possibility of a systematic fabrication of diverse architectures and material morphologies starting from one single molecule (with a minimum of synthetic modifications).

2.6.1 Ion channels

The G-quartet has been proposed as a scaffold for building synthetic ion channels because it is cyclic in nature, and cations can bind to the central cavity (Figure 2.18a). Additionally, G-quartets stack to form channel like structures, where the cations align in the middle of the tubular structure (Figure 2.18b).[14] This structure is reminiscent of the crystal structure of the potassium channel from *Streptomyces lividans* solved by the MacKinnon group.[27]

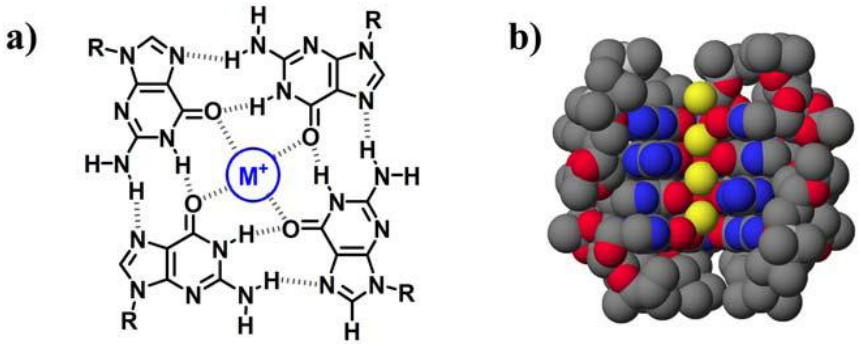

Figure 2.18. a) G-quartet and b) Crystal structure of lipophilic G-quadruplex $[G]_{16} \bullet 4K^+$ with its front partially stripped away for clarity. The yellow spheres correspond to the cations that align the central region of the G-quadruplex. (From reference 14)

Davis and colleagues described a unimolecular G-quadruplex **14** that functions as a transmembrane Na^+ transporter (Figure 2.19).[28] The particular strategy combined non-covalent synthesis and post-assembly modification of a non-covalent G-quadruplex. Reversible olefin metathesis was used to cross-link subunits that had been preorganized within a G-quadruplex. The precursor, G **9** was substituted with two meta-allyl ethers to enable olefin metathesis to be carried out within an individual G-quartet and between G-quartet layers. This unimolecular G-quadruplex **14** apparently folds into a conformation that allows transport of Na^+ cations across phospholipid bilayer membranes. Evidence for the ability of the lipophilic G-quadruplex **14** to transport Na^+ across phospholipid liposomes was obtained using ^{23}Na NMR spectroscopy.

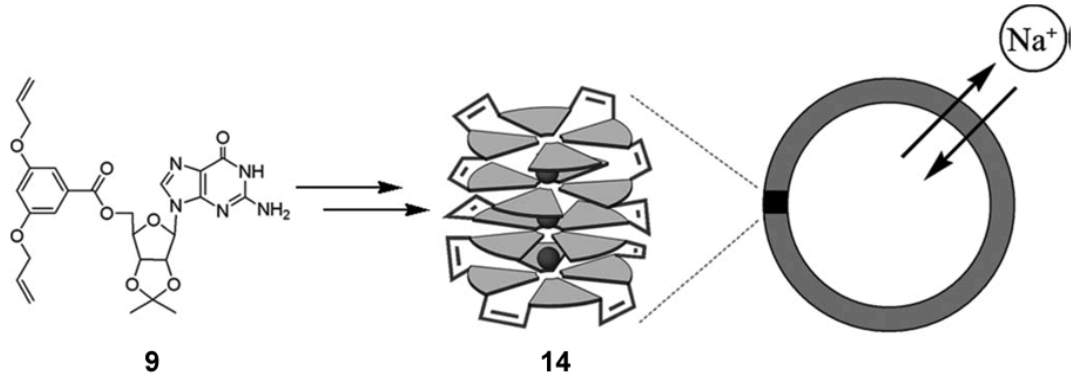

Figure 2.19. Olefin metathesis was used to cross-link sub-units in the lipophilic guanosine **9**. The resulting unimolecular G-quadruplex **14** was shown to transport Na^+ ions across phospholipid bilayer membranes. (Adapted from reference 28)

More recently, Davis and co-workers reported that ditopic guanosinelithocholate **15** (Figure 2.20) forms discrete channels in phospholipid membranes in which guanine moieties form G-quartets.[29] These channels conduct on the 1–20 nS scale. This conductance value indicates that they must necessarily have diameters that are

significantly larger than that provided by a G-quartet with ions moving through the central channel for which smaller conductance values on the order of pS are expected.[30] Regardless of the actual membrane-active structures **15** forms, by self-assembly, large and stable transmembrane channels starting from guanine moiety as scaffold.

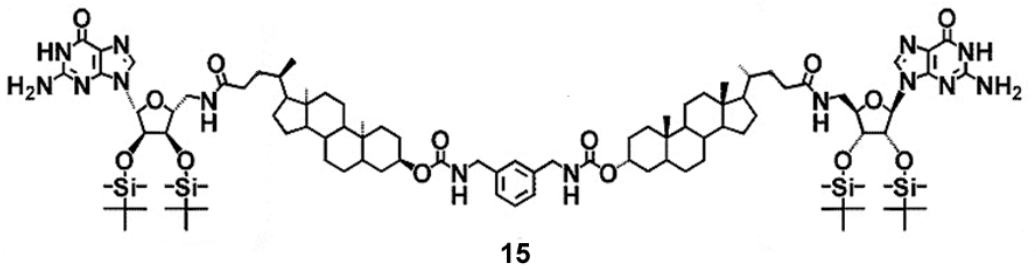

15

Figure 2.20. Ditopic guanosine derivative. (Adapted from reference 29)

2.6.2 Supramolecular scaffolds for molecular engineering

Supramolecular chemistry at the interface is a highly investigated field for the variety of potential technological applications in nanoelectronic, biological coating and catalytic processes.[31] Recently Rowan and co-workers initiated a program aimed at investigating the potential of assembling supramolecular polymers, derived from low-molecular-weight nucleobase-endcapped monomers, on a surface as a way to organize functional groups at the nanoscale and as such act as molecular-scale surface scaffolds (Figure 2.21).[32] The monomer **16** (Figure 2.22) is composed of three components: 1) a hydrocarbon core to enhance adsorption onto a hydrophobic surface in the presence of an aqueous medium, 2) the guanine end groups, to facilitate adsorbate–adsorbate interactions through hydrogen bonding and 3) a triethylene glycol monomethyl ether (TEG) side chain. The goal was using these assemblies to create oligo-(ethylene glycol)-covered surfaces. These grafted assemblies showed the ability to influence biological processes, namely static platelet adhesion.

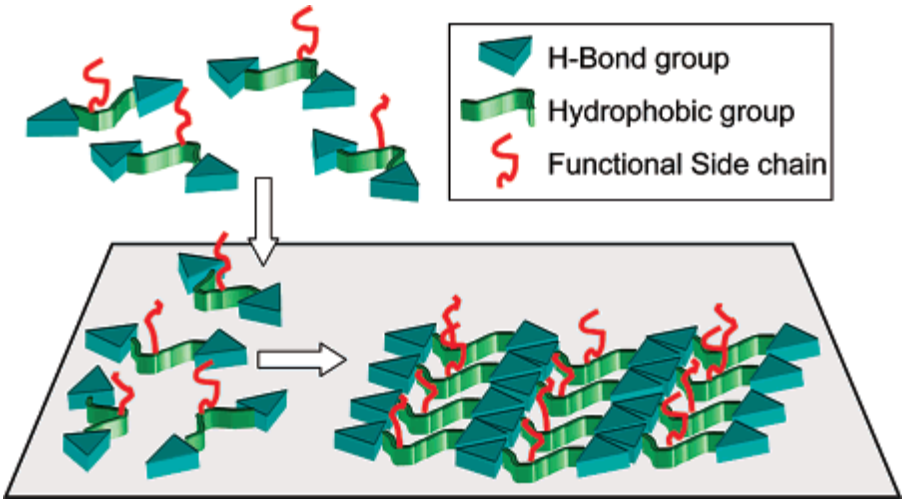

Figure 2.21. Concept of organized functional groups arranged through surface supramolecular polymerization. Monomers are initially in solution followed by adsorption and assembly to form linear band structures that present side groups in an ordered array on a hydrophobic surface. (From reference 32)

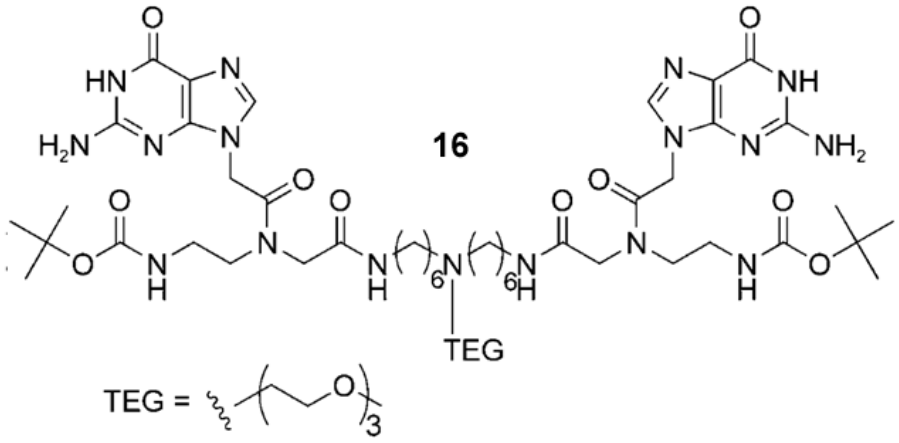

Figure 2.22. Derivative **16**.

2.6.3 Amplification and transcription of functional self-organisation

Many research groups have demonstrated that functional self-organization can be readily transcribed into hybrid nanostructures by using sol–gel processes.[33]

In particular Barboiu and co-workers have reported a synthetic route for preparing self-organized ion-channel systems that have been "frozen" in a polymeric matrix, as a straightforward approach for the design of a novel class of solid hybrid membranes.[34] In this study, the guanine alkoxysilane building block G **17** is used as a molecular precursor to conceive hybrid chiral materials at the nanometric and micrometric scales. The main

strategy consists of generating (amplifying) dynamic supramolecular G-quartets and G-quadruplex by K^+ ion templating, from a dynamic pool of supramolecular dimeric, oligomeric ribbon-type, or cyclic supramolecular architectures (Figure 2.23). The G-quadruplex architectures are then fixed in a hybrid organic-inorganic material by using a sol-gel transcription process, followed by a second inorganic transcription in silica, that is, calcinations.

Moreover, the authors obtain chiral materials by using an achiral guaninesiloxane as a precursor and this shows a new way of embedding supramolecular chirality in materials, a process of interest for the development of a supramolecular approach to nanoscience and nanotechnology in working toward systems of increasing functional complexity.

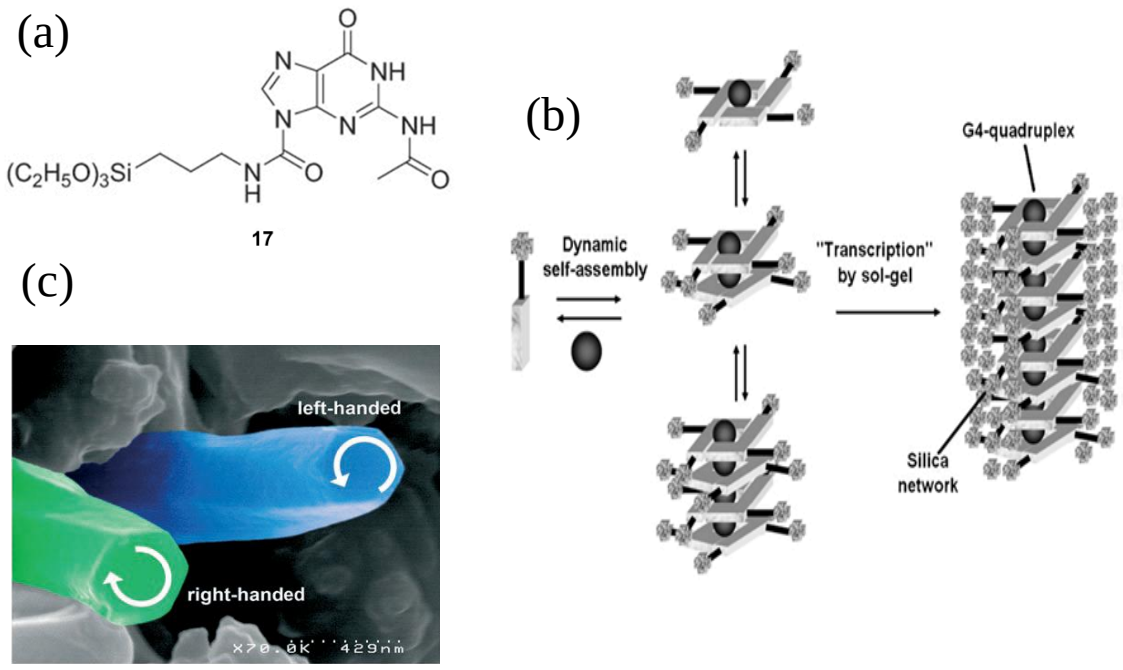

Figure 2.23. a) Derivative **17**, b) representations of the transcription of the G-quadruplex into solid hybrid materials by a sol–gel process in the presence of templating K^+ ions and c) SEM image of the left- and right-handed twisted hexagonal nanorods resulting from sol–gel transcription of the chiral hexagonal G-quadruplex into the organic–inorganic hybrid material. (Adapted from reference 34)

2.6.4 Self-assembled dendrimers

Dendrimers, "tree-shaped" monodispersed macromolecules, are suitable platforms for technological applications, for example, in light harvesting, catalysis, cellular imaging, and drug delivery.[35]

Betancourt and Rivera reported the dendronization of guanosine compound **18a** to lead compound **18b** (Figure 2.24) and the use of this latter derivative in the construction of well-defined and discrete SAD (self-assembled dendrimer) (Figure 2.25).[36] This approach relies on the propensity of guanosine derivative to form hexadecameric D_4-symmetric assemblies in the presence of KI.[9c] The versatility of this approach for the construction of dendrimers is illustrated by the fact that a hexadecameric SAD of **18b** displays 128 protected oxygen atoms at its periphery. In contrast, to achieve the equivalent with a fully covalent dendrimer will require, for example, the synthesis and coupling of four fifth-generation dendrons to a tetrafunctional core (e.g., a porphyrin). Furthermore, these SADs are discrete, well-defined, easy to make, chiral and thermally stable and have a functional core. The fact that these SADs are sustained by multiple noncovalent interactions enables the fine-tuning of their structure and dynamics by using a wide variety of external stimuli.

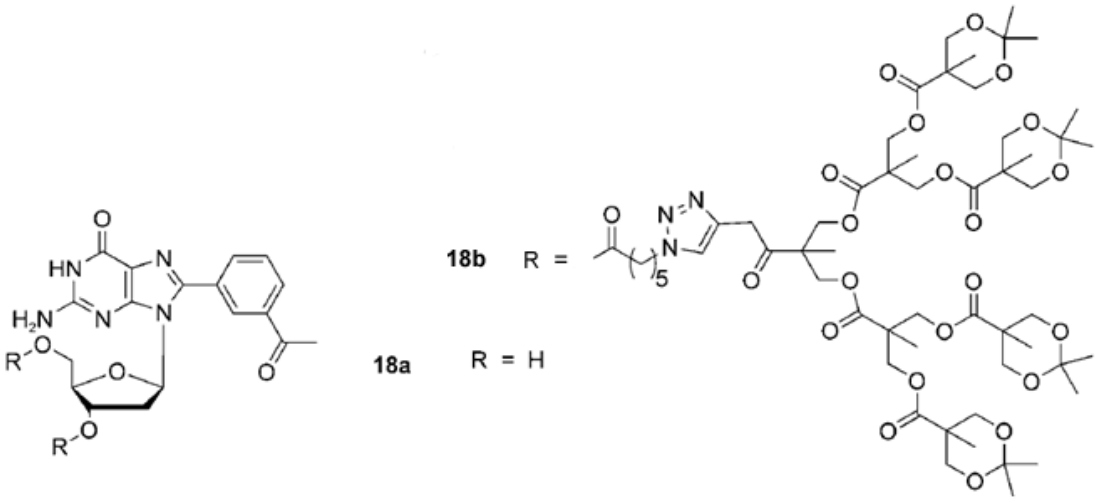

Figure 2.24. Guanosine derivatives.

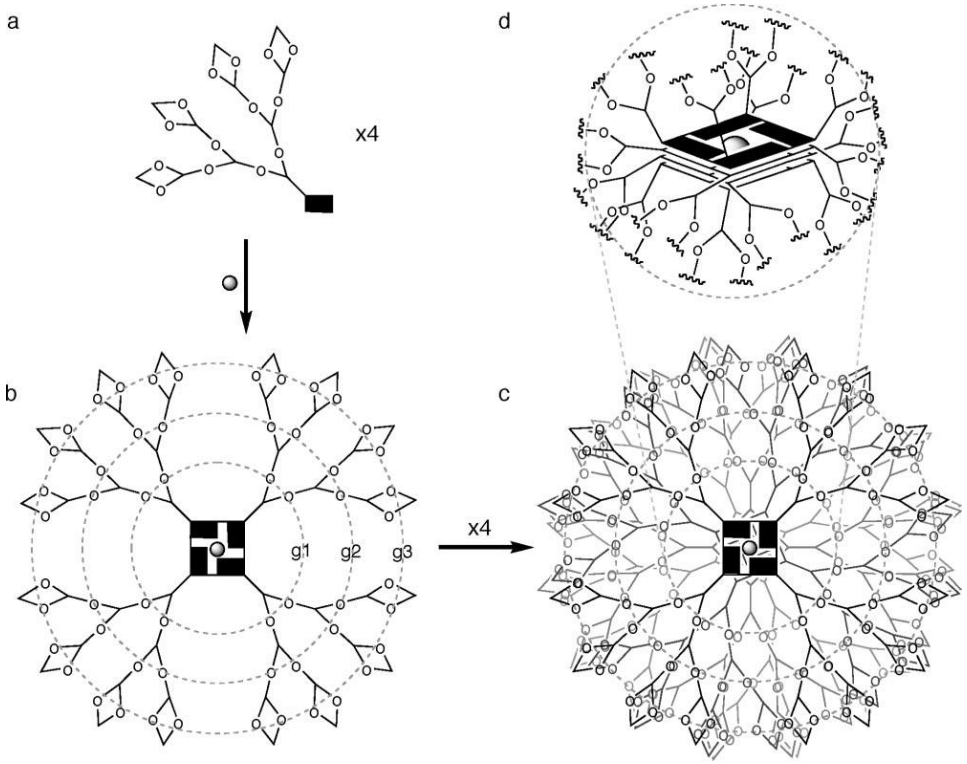

Figure 2.25. Hierarchical formation of a self-assembled dendrimer (SAD). (a) Dendronized **18b** subunits self-assemble into (b) disk-like tetramers, which (c) further stack to form hexadecameric SADs. (d) The resulting SADs have a functional core composed of a modified lipophilic G-quadruplex. (From reference 36)

2.6.5 Guanosine derivatives for functional G-quartet nanosheets

An example of the long-range amplification of G-quadruplex self-organization into macroscopic polymeric functional films has been recently reported by Barboiu and co-workers.[37] The reversible synthesis of bisiminoboronate–guanosine macromonomers **19**, followed by the self-assembly of **19** into G-quartet type structures allowed the preparation of G-quartet polymeric membrane materials on the macroscopic scale (Figure 2.26). The structure and morphology of these solid materials were determined, and the cation transport properties were investigated (mixed cationic Na^+/K^+ or selective K^+ transport). All results, together with the higher conductivity measured on these membranes compared to the non-templated ones, indicate that the G-quadruplexes self-correlate with a directional order that allows the formation of directional transport pathways.

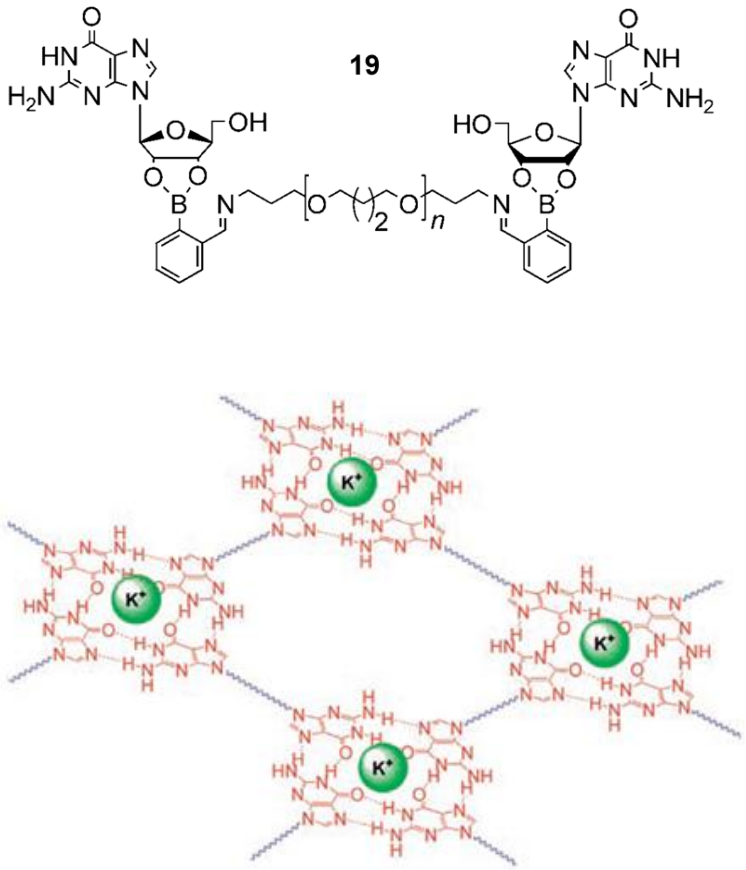

Figure 2.26. The cation-templated hierarchical self-assembly of bisiminoboronate guanosine **19** macromonomer gives G-quartet networks in solid, self-supporting, polymeric membrane films in the presence of templating K^+ ions. (Adapted from reference 37)

Shi and co-workers demonstrated how the anion binding sites in G-quadruplexes can serve as a new synthetic handle to extend the ion-mediated self-assembly of guanosines. They proposed a novel supramolecular architecture by using the covalently-linked dianion 2,2',6,6'-tetranitrobiphenolate ($TNBP^{2-}$) to tether individual G-hexadecamers $[G\mathbf{8}]_{16}\bullet 4Na^+$.[38] A highly ordered nanoscale structure was produced in the solid-state upon cross-linking the lipophilic G-quadruplexes: the non-covalent polymeric nanosheets extend along the horizontal direction without changing the vertical dimension of the complex (3.0 nm) (Figure 2.27).

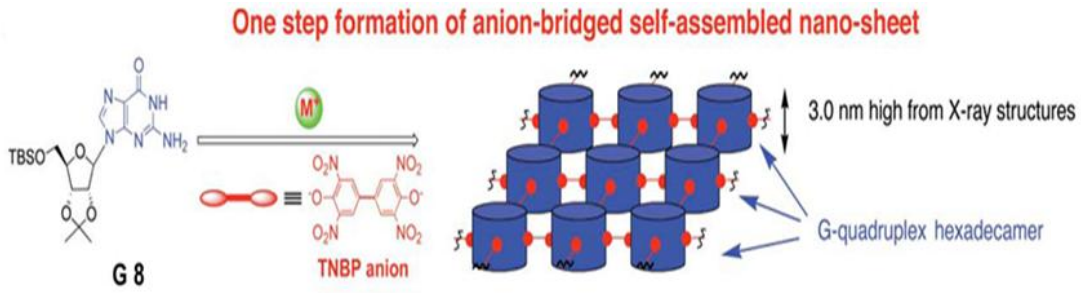

Figure 2.27. Schematic illustration of the nanosheet. (Adapted from reference 38)

2.6.6 G-quartet dynamic covalent chemistry

Dynamic covalent chemistry (DCC) is a major strategy in supramolecular chemistry, enabling amplification of selected compounds from a dynamic combinatorial library (DCL) of equilibrating compounds.[39] In the DCC approach, building blocks that form reversible covalent bonds are used to build a DCL. Stabilization of a particular library member upon addition of a template shifts the equilibrium, amplifying any stabilised product in the mixture.

Lehn and Sreenivasachary described a G-quartet system wherein component selection from a DCL is driven by the physical properties of the product.[39a] They showed that guanosine hydrazide **20** formed thermally reversible gels at moderate pH in the presence of both Na^+ and K^+. These gels presumably are formed by the stacking and crosslinking of G-quartets. The 5'-hydrazide in the G-quartet gels was reacted with a library of aldehydes to form acylhydrazone bonds, allowing the authors to study the effects of sidechain modification on gel properties. While addition of some aldehydes destroyed the hydrogels, other aldehydes (including **21**) formed acylhydrazone gels that were stronger than the parent gel formed from hydrazide G **20**. These findings prompted Lehn and Sreenivasachary to determine whether the thermodynamic stability of the gel phase might actually drive the component selection in their DCL (Figure 2.28). Thus, a mixture composed of 4 acylhydrazones, formed from reaction of aldehydes **21** and **22** with hydrazides G **20** and serine **23**, was generated under conditions where the 5'-acylhydrazones could equilibrate by undergoing reversible bond cleavage and reformation. The product mixture, measured by ^{1}H NMR, was sensitive to temperature. At 80 °C, above the gel transition temperature, the distribution of products was statistical, indicating that the 4 acylhydrazones (A–D) were of similar stability. Between 25–55 °C,

acylhydrazone **B**, in its gel-state, and **C** in solution were favored over acylhydrazones **A** and **D**. In this case, self-assembly of G hydrazide **20** was driven by selection of the components that gave the most stable hydrogels. The stability of the G-quartet hydrogel altered the dynamic equilibrium of acylhydrazones and directed reaction of the G hydrazide **20** with aldehyde **22**. Lehn explained that *''…(t)he process amounts to gelation-driven self-organization with component selection and amplification…based on G-quartet formation and reversible covalent connections.''* This DCC approach may well have broad applications in medicinal chemistry and material science. In fact, hydrogels offer a promising medium for controlled release of bioactive substances, and they are of interest because of their hydrophilic character and potential biocompatibility.

Lehn et al. demonstrated that hydrogelator **20** can incorporate analogue compounds that contain a guanine moiety leading to the formation of mixed G-quartets: ^{1}H NMR spectroscopy was used to study the inclusion of various guanine derivatives into the gel and their releasing rates.[39c]

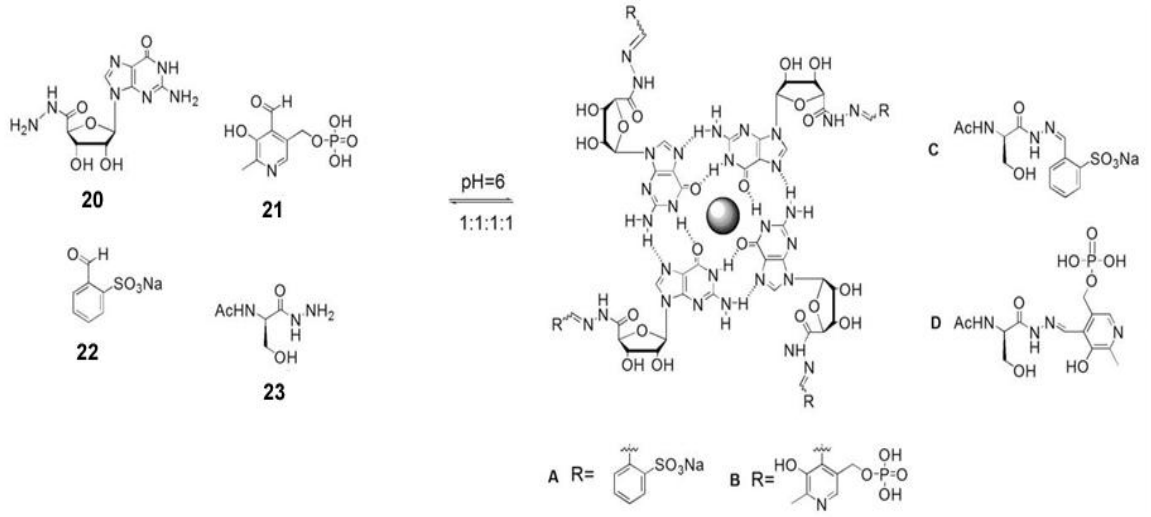

Figure 2.28. Stability of G-quartet hydrogel **B** alters equilibrium of acylhydrazones and directed reaction of G hydrazide **20** with aldehyde **22**. (Adapted from reference 39a)

Ghoussoub and Lehn also recently described another dynamic sol–gel interconversion process, triggered by the reversible binding and release of K^+ by a G-quartet hydrogel.[39d] Hydrogels formed by the ditopic monomer G-G **24** were converted to soluble (G-G)n polymers upon addition of [2.2.2]-cryptand **25**, an ionophore that extracts K^+ from the G-quartet hydrogel. The gel was regenerated upon expelling K^+ from the [K^+ 2.2.2]-cryptate by protonation of the cryptand's bridgehead nitrogen to give [$2H^+$ 2.2.2]

25. In this way, gel–sol interconversion was triggered over multiple cycles by controlling the equilibrium of the bound K^+ between the G-quartet and the [2.2.2] cryptand (Figure 2.29)

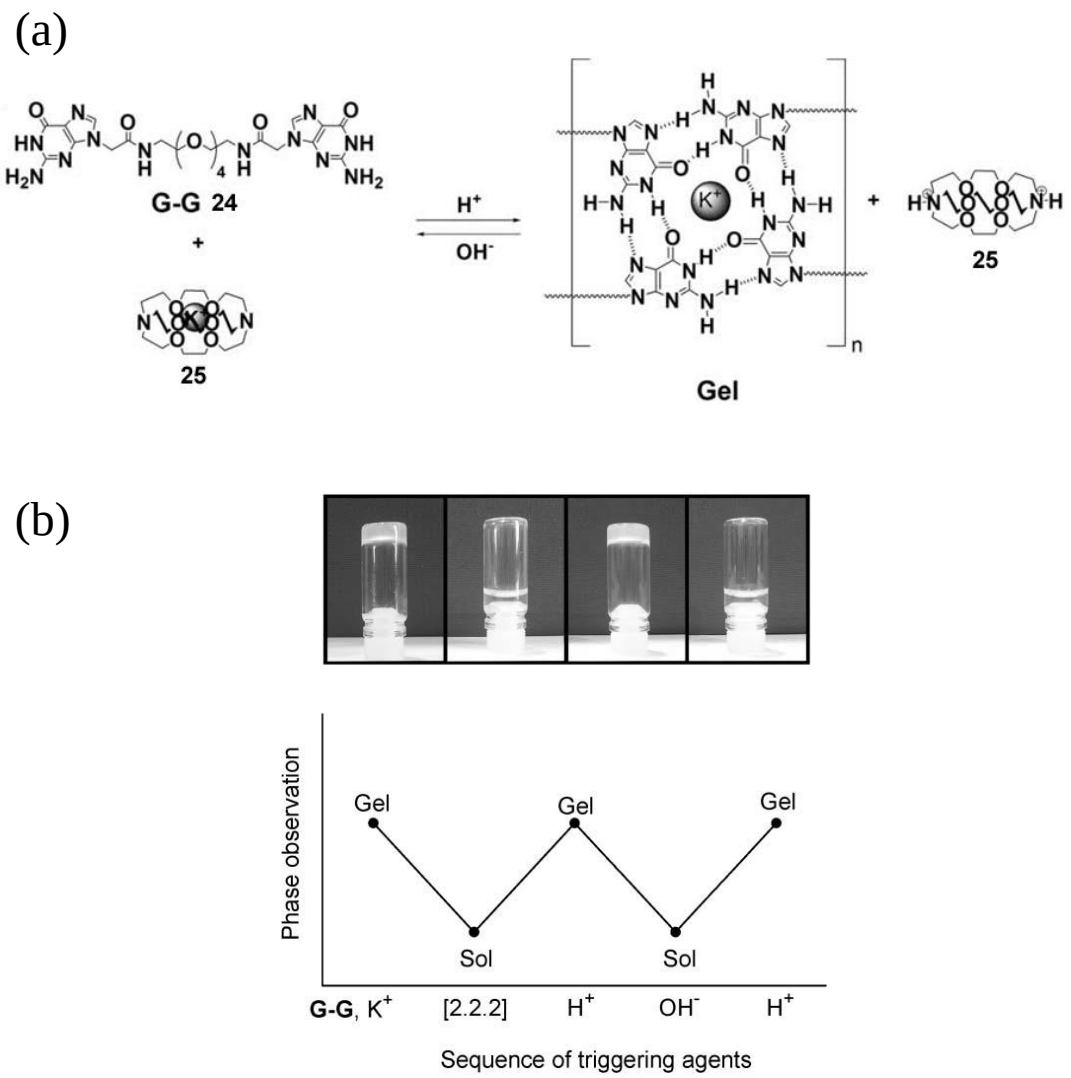

Figure 2.29. (a) Structure of G-G **24** and schematic of the reversible formation of polymeric G-quartet based hydrogels. Changing pH in the presence of [2.2.2 cryptand] **25** modulated the sol–gel equilibrium. (b) Modulation of the gel–sol status induced by the sequence of triggering agents. (Adapted from reference 39d)

In a related system, we demonstrated a strategy for switching between two distinct supramolecular motifs in organic solvents.[40] By modulating the protonation state of the K^+ ionophore [2.2.2] cryptand **25**, we could stabilize either hydrogen-bonded ribbons or a discrete K^+ G-octamer (see Chapter 4).

2.6.7 Ordering of open-shell moieties

Molecular packing or arrangement of open-shell molecules is crucial in originating magnetic properties, such as ferromagnetism, in supramolecular assemblies.[41]

Takui et al. recently reported that the guanine-substituted nitronyl nitroxide permanent radical **26** forms in the crystal state the ribbon-A hydrogen-bonding network (see Figure 1.4a and Chapter 3).[42] Introduction of the radical substituent into the N9 position of the nucleobase results in little disturbance in the propensity of guanine to self-assemble in a ribbon-like motif. This finding confirms the selectivity and directionality of the guanine scaffold and its potential use in governing the molecular packing of open-shell molecular assemblies. In fact, A-type ribbons of guanines upon packing in a direction roughly perpendicular to their planes originate a double chain of nitronyl nitroxide moieties in close proximity (see Figure 2.30). The authors reported that in the crystal state no short contacts around the nitroxide groups leading to exchange interaction were found (neither within nor between the hydrogen-bonded ribbons). However, they found short contacts (close to van deer Waals distance) between nitronyl/nitroxide oxygen atoms of a ribbon and phenyl carbon atoms of the adjacent one. The one-dimensional ferromagnetic chains of the radical moieties explain the magnetic susceptibility found for this solid material.

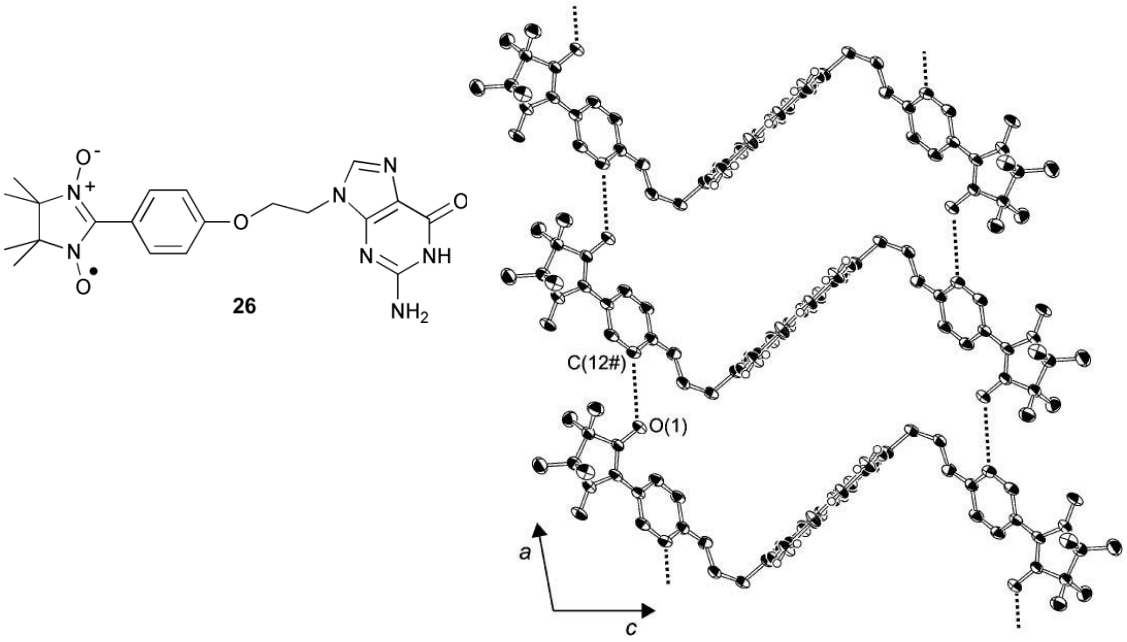

Figure 2.30. The double chain of nitronyl nitroxide moieties in the crystal state of **26**. The guanine A-type ribbons are running along the b axis. (From reference 42)

Another example of open-shell moieties ordered by a supramolecular architecture showing a new (magnetic) property has been reported by our group. Recently we have shown that the scaffolding of the persistent radical unit 4-carbonyl-2,2,6,6-tetramethylpiperidine-1-oxyl (TEMPO), is achieved by taking advantage of the self-assembly templated by potassium ions of the guanosine derivative **27** (Figure 2.31) into a H-bonded network.[43] In the presence of potassium ions, this compound can form in fact a D_4-symmetric octameric assembly $[\mathbf{27}_8K]^+$ (see **2.2.3** and Figure 2.4c) containing eight spin centers showing a weak electron spin-spin exchange interaction. Reversible interconversion, fueled by cation release and complexation (using ionophore **25**), allows the switching between discrete quartet-based assemblies and molecularly dissolved **27** (or its ribbon-like supramolecular oligomers), thus the control of the intermolecular weak spin-spin interactions. This system was the first example of a reversible introduction-suppression of a weak spin-spin exchange in a self-recognizing and self-assembling molecule controlled by the addition/removal of a templating cation.[44]

Our next challenge was to increase the spin exchange difference between the two states to obtain drastic magnetic changes before and after addition of the metal cation.

Here we report on the self-assembly properties of derivative **28a** (Figure 2.31) where two TEMPO units are connected to the guanosine deoxynucleoside at the O5′ and O3′ positions. This target molecule has been chosen for two reasons: (i) in the metal templated assembled species of **28a** the number of paramagnetic units doubles, possibly leading to significant enhancement of magnetic coupling; (ii) passing from ribo-guanosine (such as **27** or derivative **3**) to 2′-deoxyguanosine derivatives (such as dG **1**), the discrete K^+-templated assembly was expected to be C_4-symmetric (see **2.2.1** and Figure 2.4b) and this structural variation could originate a different (higher) spin-spin interaction.

We will show that **28a**, despite the presence of two bulky substituents, forms indeed a K^+-templated octameric assembly giving rise to very strong spin-spin interactions comparable to those observed in very concentrated monoradical solutions. This finding is consistent with the proposed structure consisting of 16 radical units confined within the complex.

Because steric hindrance potentially introduced by the double substitution in O5′ and O3′ could destabilize supramolecular assemblies, CD spectroscopy was initially employed to prove the self-assembly of **28a** to give quartet-based structures in CH_2Cl_2 upon KPic extraction.

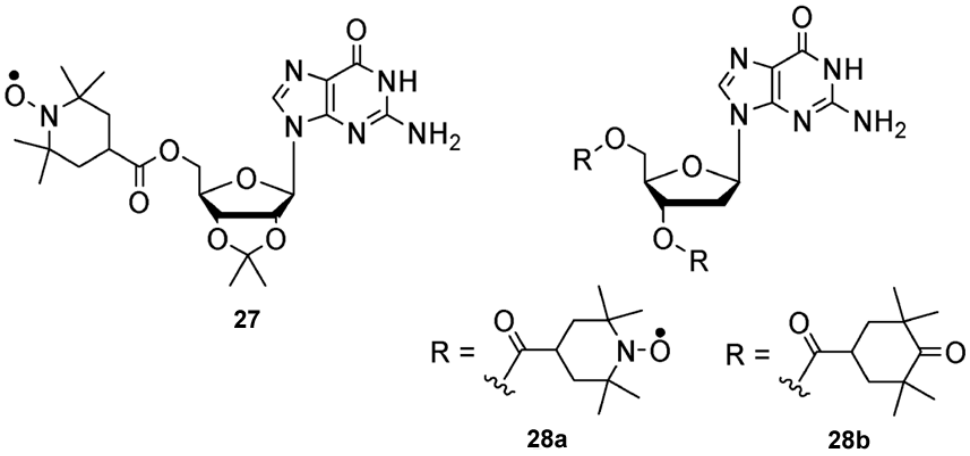

Figure 2.31. Guanosine derivatives.

As we mentioned in section **2.2.3** circular dichroism is diagnostic of either the formation of G-quartet based assemblies[45] or the stacking polarity of two contiguous G-quartets.[12] In fact, the tetramers do not stack in register, but are rotated with respect to each other to give, in the 230-300 nm region, characteristic of the π-π* transitions of guanine chromophore, a double signed exciton-like CD signal. This couplet, whose sign allows the assignment of the stacking helicity (handedness), exhibits opposite signed bands at ca. 260 and 240 nm for the head to tail (C_4-symmetric) stacking while both bands are blue-shifted by 20-30 nm in the D_4-symmetric stacking[12] (Figure 2.7b).

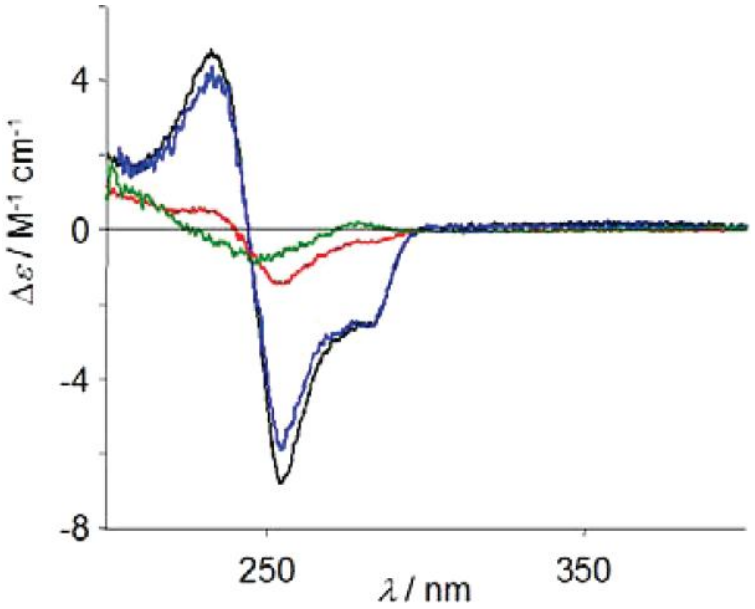

Figure 2.32. CD spectra of **28a** (5 mM) before (red line, the low-intensity negative couplet is due to Na^+ (or K^+) contamination resulting from the synthetic procedure) and after (black line) KPic extraction. CD spectra of **28a**/KPic complex sample after dilution to 0.5 mM (blue line) and after addition of 4 equiv of [2.2.2] cryptand **25** (green line).

Figure 2.32 shows CD spectra of solutions of **28a** recorded before (red trace) and after (black trace) solid-liquid extraction of potassium picrate KPic (i.e., after stirring the guanosine solution with solid KPic; see Experimental Part, Chapter 5).

While the solution of **28a** shows a weak Cotton effect corresponding to the guanine chromophore, in the presence of KPic an intense negative CD coupling with the negative and positive components at around 265 and 245 nm, respectively, is observed: this feature is diagnostic of a C_4-symmetric assembly of (at least) two G-quartets chirally rotated. Intensity and shape of the CD spectrum do not change with concentration, in the range 8-0.5 mM (see Figure 2.32, blue trace), suggesting that in these conditions the self-assembled structure is maintained. The molar ratio between **28a** and KPic has been determined spectrophotometrically to be >8:1 (see Experimental Part, Chapter 5). These findings suggest that the assembly is a C_4-symmetric octamer formed by two head-to-tail stacked G-quartets.

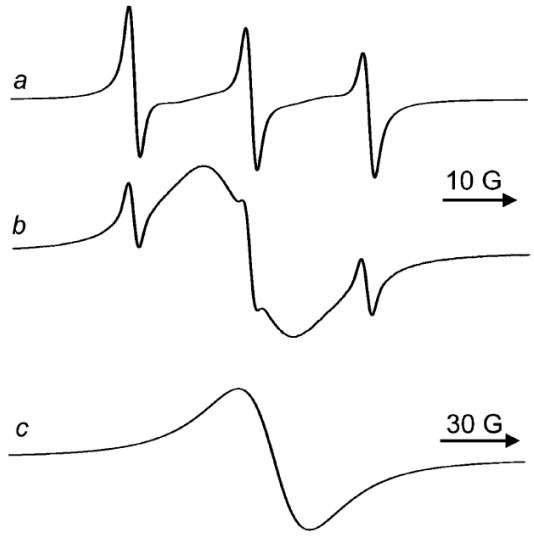

Figure 2.33. ESR spectra of **28a** (0.5 mM) before (a) and after (b) KPic extraction. (c) ESR spectrum recorded at 77 K in CH_2Cl_2 glass in the presence of K^+.

Figure 2.33 shows ESR spectra recorded on **28a** in CH_2Cl_2 (before, trace a, and after, trace b, KPic extraction). In the absence of metal cations, the spectrum is characterized by three equally spaced lines with a broadening between them, this being an indication that intramolecular spin exchange is occurring. In sharp contrast, the ESR spectrum recorded after solid-liquid extraction of potassium picrate shows mainly one broad signal whose integrated intensity corresponds to the initial amount of radicals. The broadening (peak to peak line width = 12 G) of the signal is independent of concentration and temperature, and thus interassembly interactions and motional broadening can be

discounted. This spectrum is reminiscent of those obtained from very concentrated nitroxide solutions (> 0.05 M).[46] Since the spectrum was obtained at 0.5 mM concentration, the signal broadening is ascribed to the proximity of spin centers of **28a** within the framework of the octamer. This signal may contain not only a triplet transition but also other multiplet transitions from higher spin states arising from multiple interactions between the 16 radical units.

At 77 K in CH_2Cl_2 glass, the spectrum of the octamer (see Figure 2.33, trace c) showed only a featureless single peak in the g ≈ 2 region and a weak $|\Delta ms| = 2$ peak at 1660 G. The observation of a $|\Delta ms| = 2$ transition also support the presence of intermolecular spin-spin interaction. However, the signal of $|\Delta ms| = 2$ transition is very weak, indicating that these transition probabilities are extremely small as a result of a small D-value of the high spin-spin states from the octamer. Accordingly to previous investigation[46,47] on symmetric tetraradical, we attributed the lack of resolvable zero field splitting to the time-averaged symmetry of the complex (*vide infra*).

Reversible interconversion between uncomplexed and octameric forms was demonstrated by addition of four equivalents of [2.2.2] cryptand **25** to a solution containing the assembly. Under these conditions the CD and EPR spectra returned to the original signals (see Figure 2.32, green trace, and Figure 2.34b).

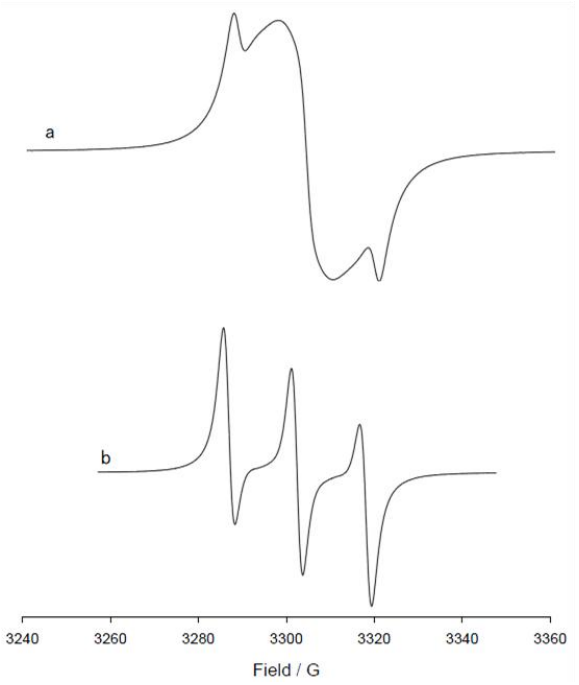

Figure 2.34. (a) EPR spectrum of **28a** (0.5 mM) in CH_2Cl_2 after solid-liquid KPic extraction. (b) EPR spectrum of the same sample after addition of [2.2.2] cryptand **25**.

Because of the presence of two paramagnetic units, the ^{1}H NMR spectra of **28a** are characterized by a very low spectral resolution and their analysis turned out far more complicated than for derivative **27**. Therefore we prepared and characterized by CD and NMR compound **28b** in which the paramagnetic moiety is replaced by the closed-shell structurally related 3,3,5,5-tetramethyl-4-oxocyclohexanecarboxylate fragment. Because of the much higher resolution of NMR spectra, a full characterization of the assembly could be obtained for this derivative.

The proton spectrum of a CD_2Cl_2 solution of **28b** after KPic extraction (Figure 2.36) is characterized by the doubling of almost all of the signals (see **2.2.1**). Integration of the picrate signal at 8.75 ppm and H8 signals (8.03 and 7.48 ppm) supports a 8:1 stoichiometry for the complex. The signal doubling is thus consistent with a C_4-symmetric octamer.

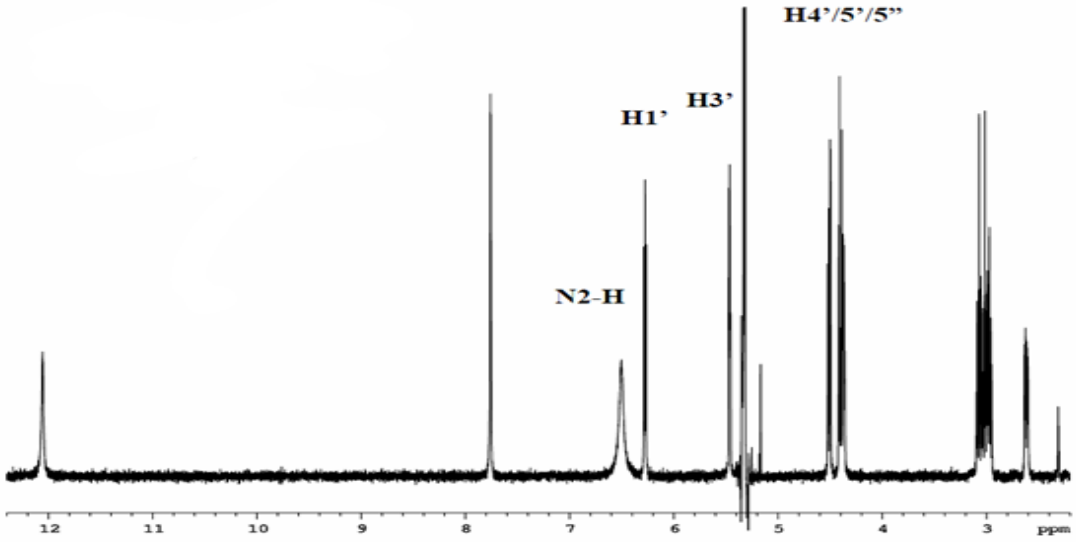

Figure 2.35. Proton spectrum of **28b** before KPic extraction in CD_2Cl_2

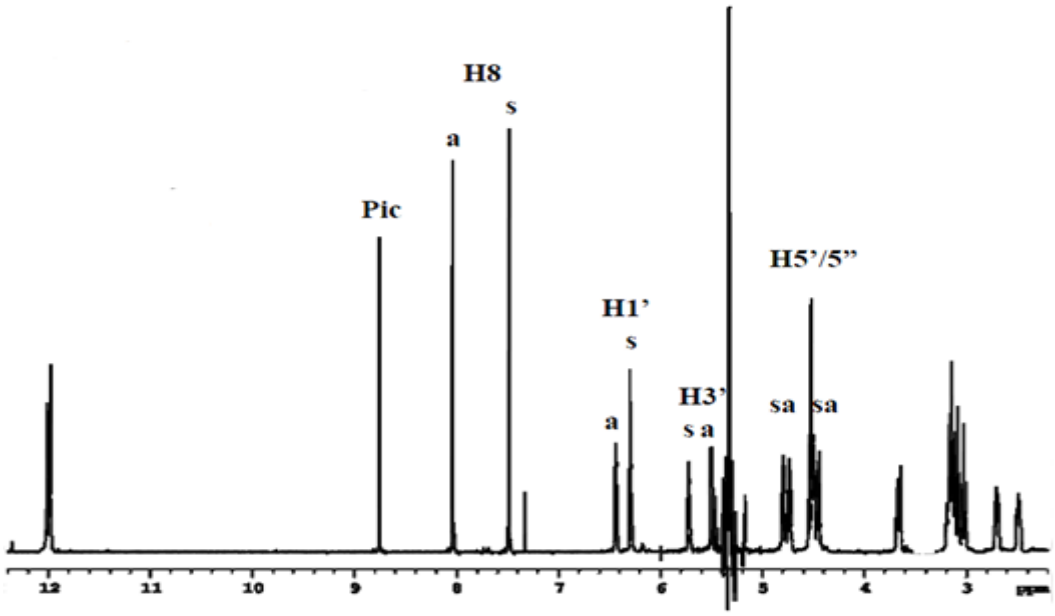

Figure 2.36. Proton spectrum of **28b** after KPic extraction in CD_2Cl_2

This is confirmed by NOESY spectra (Figure 2.37 and Experimental Part, Chapter 5), which show the features of an octamer composed of an all-*anti* quartet stacked on top of an all-*syn* quartet in an head-to-tail relative orientation.[5,9b,8] In particular, the characteristic interquartet correlations between *syn*-H8 (7.48 ppm) and *anti*-H1′ (6.43 ppm) and between *anti*-H8 (8.03 ppm) and *syn*-H5′/H5″ (4.79 and 4.53 ppm) can be observed.

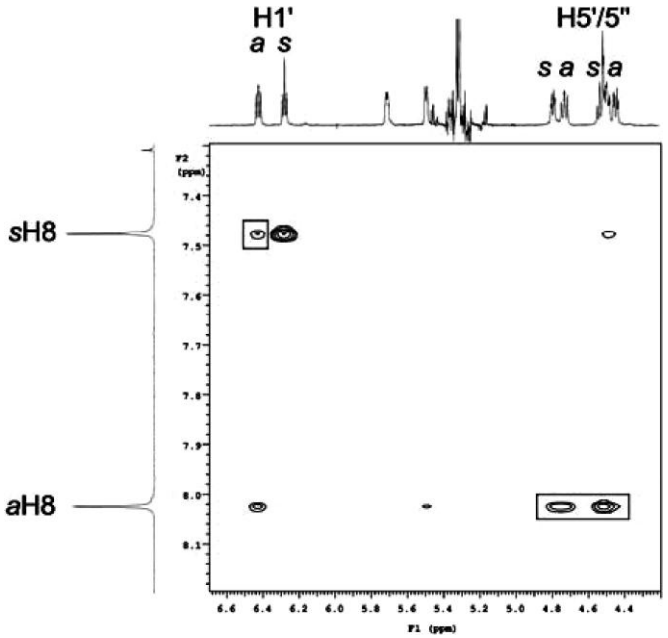

Figure 2.37. Portion of the 600 MHz NOESY spectrum of the octameric complex between **28b** and KPic, recorded at rt in CD_2Cl_2 (mixing time 150 ms) showing the interquartet correlations.

Shape and intensity of CD spectra of **28b** (before and after KPic extraction) are quite similar to those of **28a** (see Figure 2.38) suggesting a similar self-assembly behavior.

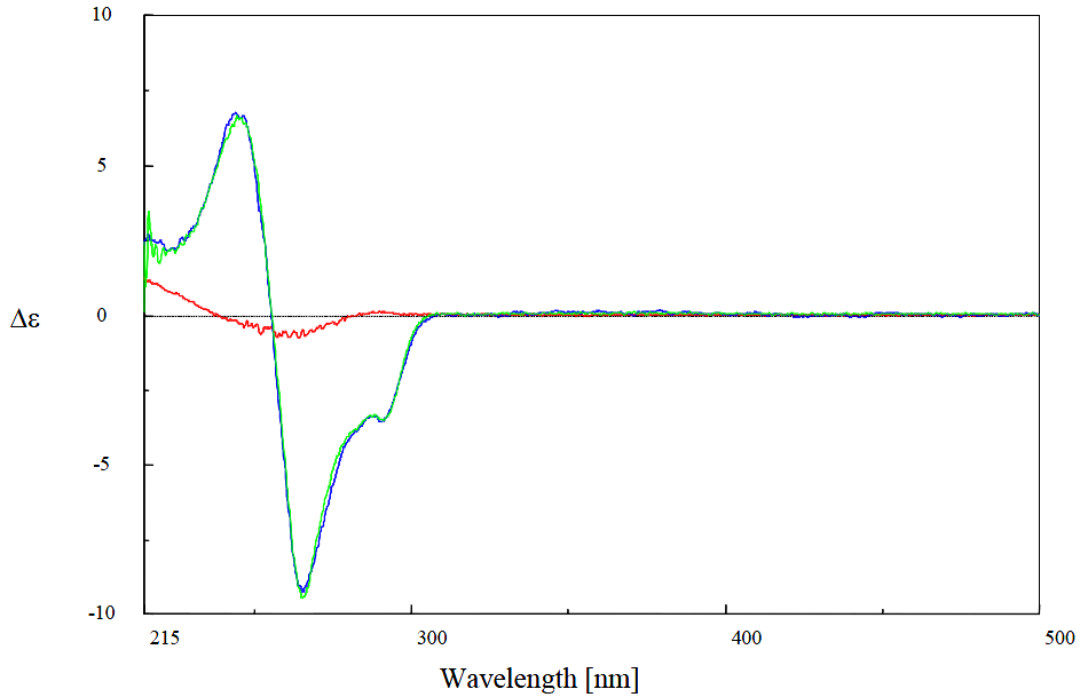

Figure 2.38. CD spectra of **28b** in CD_2Cl_2 (8 mM) before (red) and after (blue) potassium picrate extraction. The green spectrum was obtained upon 1:10 dilution of the 'blue solution' with CD_2Cl_2 .

Based on CD and NMR data we can conclude that in the presence of K^+ both derivatives **28a** and **28b** self-associate into two stacking G-quartets in a head-to-tail arrangement with the metal ion sitting in the central cavity, to form a C_4-symmetric octamer.

To obtain a more detailed picture of the geometry of the octamer, stochastic dynamics (SD) simulations were performed by using the AMBER* force field of Macromodel 7.0 program. Initially, a Monte Carlo conformational search was carried out by rotating all rotable bonds and by preserving all-*anti* quartet stacked on top of an all-*syn* quartet in an head-to-tail relative orientation. The most stable conformation found by this procedure was then used in the dynamic simulation. The simulations were run at 300 K with time steps of 1 fs and an equilibrium time of 500 ps before dynamic run. The total simulation time was set to 5000 ps in order to achieve full convergence. Molecular dynamics calculations (see Figure 2.39 and Experimental Part, Chapter 5) confirm the C_4-symmetric nature of the octamer and indicate the presence of four triradical modules protuding from the two tetramers and pointing outside the assembly (in green) and a

tetraradical module located on top of the all-*anti* quartet (in red). In the triradical module the nitroxide are arranged in isosceles triangles. In each triangle, the distance between the oxygen atoms of the three nitroxides is in the range 9.5-10.5 and 6-7 Å, which is expected to lead to three spin-spin interactions with high *J* values. The tetraradical unit is, instead, arranged in a rombic fashion with an average distance between radical oxygen atoms of 7.5 Å, which is expected given a strong spin-spin interaction between all of them.

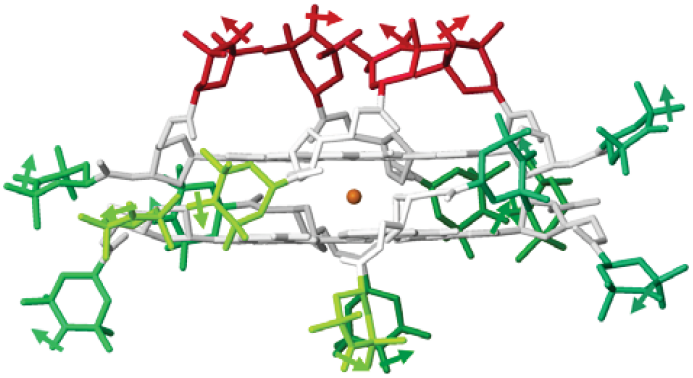

Figure 2.39. Structure of the octamer that refer to the time interval of dynamic simulation between 2000th to the 2250th ps.

In conclusion, here we have shown the advantages of obtaining a supramolecular hexadecanitroxide from **28a**, a derivative with two open-shell moieties; in particular, ESR line-broadening due to dipolar and/or exchange effects is more remarkable because of increasing pathways of the radical-radical contact. This work should be regarded as the first example of a radical-armed self-assembling scaffold showing drastic magnetic changes by addition-removal of diamagnetic alkali metal cations.[48]

Derivative **28a** was prepared in one step from 2′-deoxyguanosine according to Scheme 2.1 (see Experimental Part, Chapter 5).

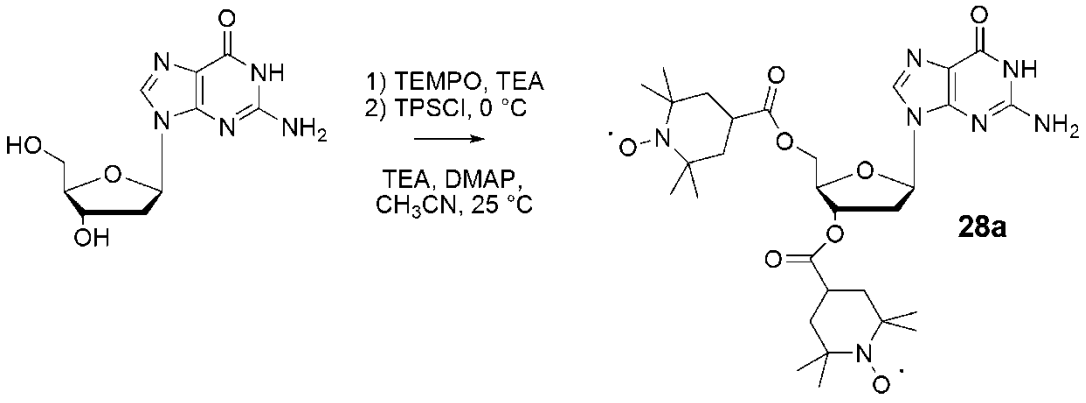

Scheme 2.1. Synthesis of derivative **28a**.

Derivative **28b** was prepared according to Scheme 2.2. Methylation of 4-oxocyclohexanecarboxylic acid (Scheme 2.2a), followed by acylation of 2′-deoxyguanosine (Scheme 2.2b) yielded **28b** (see Experimental Part, Chapter 5).

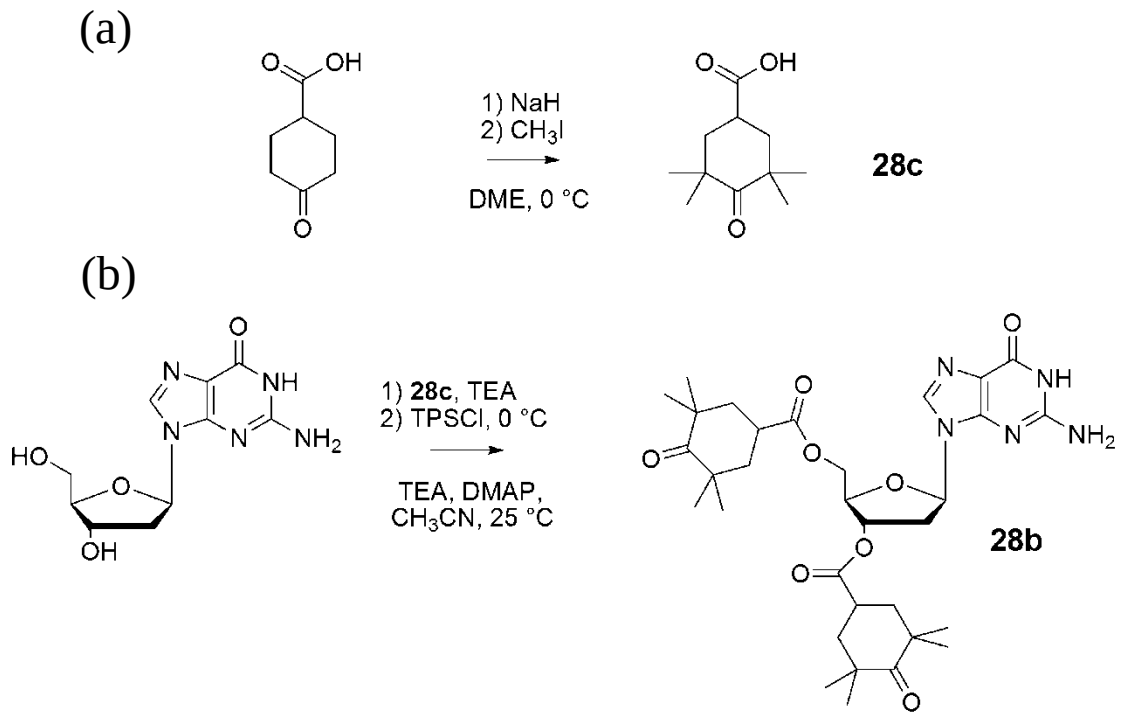

Scheme 2.2. Synthesis of derivative **28b**.

In Scheme 2.3 it's outlined the synthetic strategy to obtain the new open-shell derivative **29**, currently under investigation (see Experimental Part, Chapter 5).

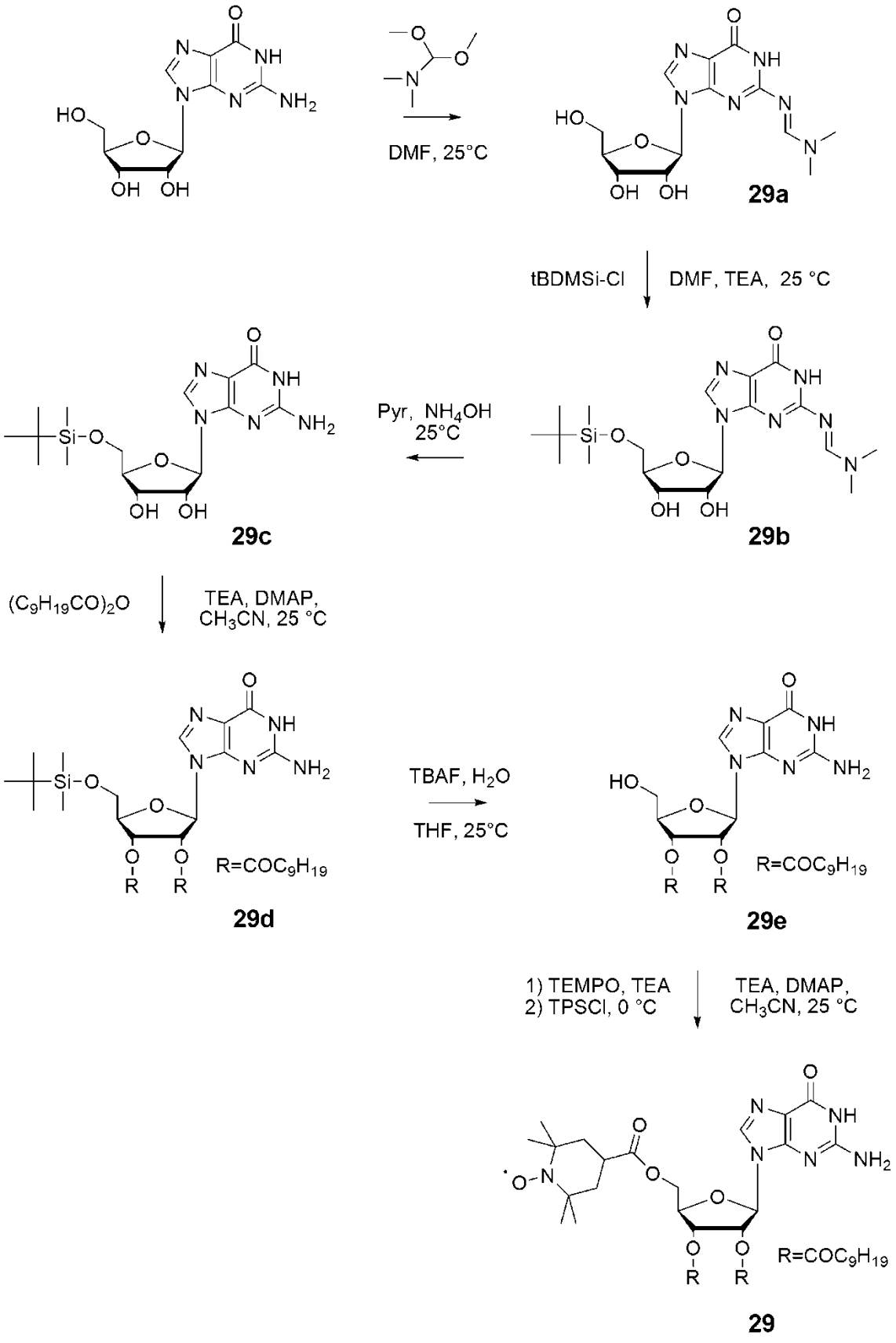

Scheme 2.3. Synthesis of derivative **29**.

Guanosine was first reacted with *N*,*N*-dimethylformamide dimethyl acetal in DMF to give the N2 base-protected **29a**. Derivatization of amidine **29a** with tBDMSi-Cl gave 5'-*O*-silylated **29b**. Deprotection of the amidine group provided 5'-tBDMSi-guanosine **29c**. This compound, with free 2'- and 3'- hydroxyls, was then acylated with decanoic anhydride to afford **29d**. Removal of 5'-silyl group followed by acylation with TEMPO moiety gave the desired product **29**.

In Scheme 2.4 it is shown a different way to obtain compound **29c** from guanosine, leading to a synthetic improvement of the previous pathway (see Experimental Part, Chapter 5).

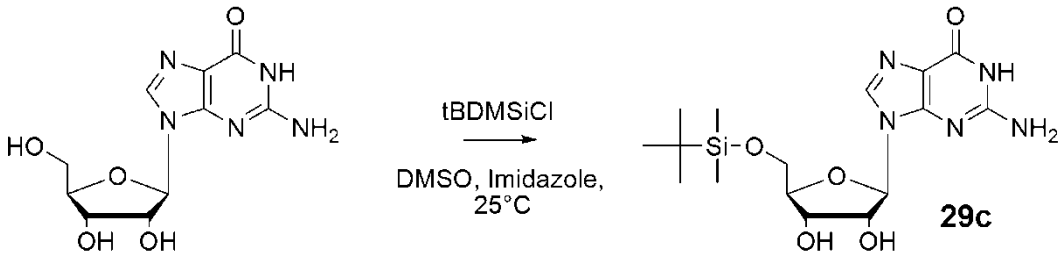

Scheme 2.4. Synthesis of derivative **29c** starting from guanosine.

As already mentioned at the beginning of this Chapter, in the absence of cations lipophilic guanosines can form hydrogen bonded ribbons. Moreover, as in the case of G-quartet columnar aggregates (see **1.5** and **2.2.2**), these guanosine supramolecular architectures may origin lyotropic mesophases in selected organic solvents (see **3.2.1**).

Here we report some ESR results about the gel-like or LC (liquid crystal) phase formed by derivative **28a** in absence of cations. Currently, both the symmetry of the gel-like or LC phase and the magnetic susceptibility properties of derivative **28a** and **29** are under investigation.

When derivative **28a** is dissolved in the minimum amount of dichloromethane and diethyl ether or toluene is added, a biphasic system with a compact birefringent gel-like phase is observed. But a monophasic gel-like phase cannot be obtained neither by changing the concentration nor the relative amount of the solvents.

The gel-like phase turns to an isotropic solution when, by diluting with toluene or Et_2O, the analytical concentration of **28a** becomes $\leq$ 5 mM. The use of the chlorinated solvent is necessary due to the very low solubility of solid **28a** in ethers or aromatic hydrocarbons. When using toluene, it's possible to remove all the chlorinated solvent.

This operation does not, however, affect the gel-like phase. The gel-like phase doesn't form when aliphatic hydrocarbons (for example petroleum ether) instead of toluene are used. In fact, the addition of petroleum ether to a solution of **28a** causes the formation of a precipitate.

The ESR spectrum of **28a** 2.2 mM in toluene solution is interpreted as the superposition of two different species: one containing at 373 K five lines (a(N)=16.60 G, g=2.00599 in CH_2Cl_2), the other consisting of only broad single signal (g=2.0060 in CH_2Cl_2) (Figure 2.40). The first signal is attributed to the **28a** monomer in which the *intramolecular* exchange interaction between the two nitroxidic units is comparable to the hyperfine a(N) interaction. The ESR spectrum shows considerable narrowing of the 2nd and 4th lines when the temperature increases this being an indication that an intramolecular motion is fast modulating the exchange interactions.

The other much more intense broad signal can be attributed to a ribbon-like polyradical showing dipolar coupling and/or relatively strong *intermolecular* exchange interaction.

Figure 2.40. Derivative **28a** 2.2 mM in toluene T=373 K.

The ratio between the two species can be modified by changing the absolute concentration of guanosine. Actually, the spectrum of guanosine 1-10 μm, consists practically only of five lines, suggesting the dominant population of the monomer under very dilute conditions (see Figure 2.41).

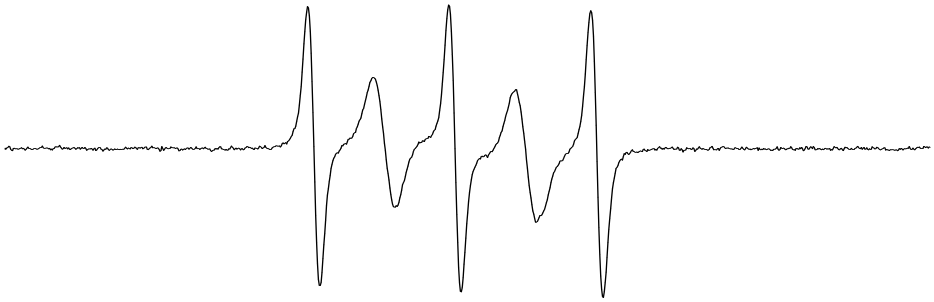

Figure 2.41. Derivative **28a** $1x10^{-6}$ M in toluene T=373 K.

On the contrary above 5 mM the ESR spectrum is dominated by the presence of the broad signal, indicating that the ribbon like structure is the most abundant species under these conditions (see Figure 2.42).

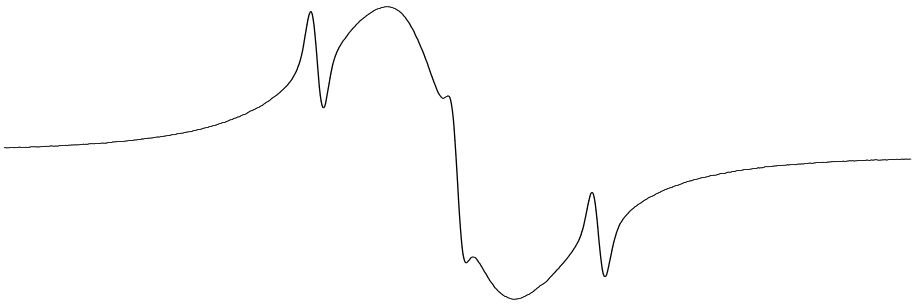

Figure 2.42. Derivative **28a** $5x10^{-3}$ M in toluene T=373 K.

The equilibrium between the two species can be significantly changed also by addition of 1,1,1,3,3,3-hexafluoro-2-propanol. In the presence of this strong hydrogen bond donor the ribbon-like structure is destroyed and the spectrum consists only of one signal due to the monomeric species (Figure 2.43)

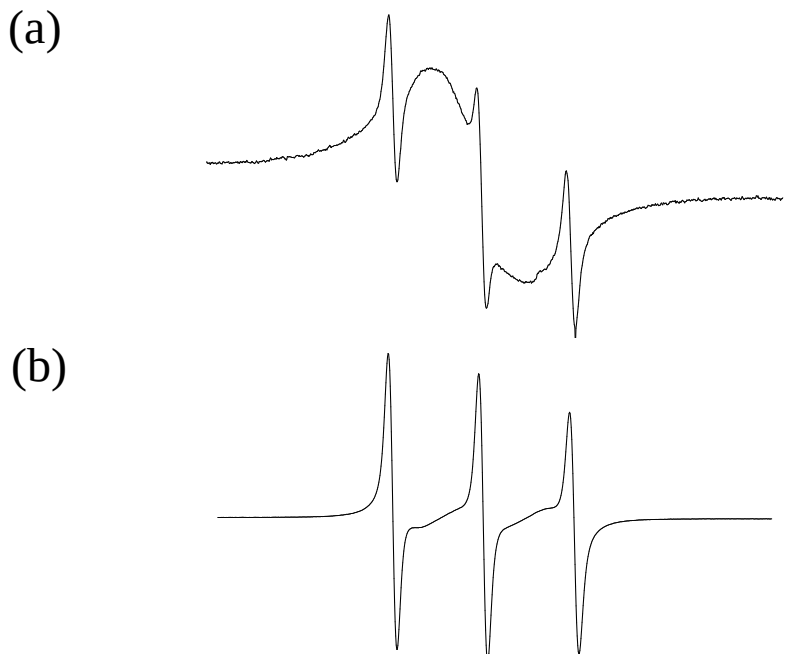

Figure 2.43. ESR spectrum of **28a** 0.1mM in toluene at room temperature in the absence (a) and in the presence (b) of hexafluropropanol (2.0 M).

The ratio between the two species strongly depends also by the nature of the solvent as shown by Figures 2.44-2.47.

In a solvent like DMSO which is known to destroy self-assembled guanosine architecture the monomer is the only detectable species. On the contrary in decane the polyradical species is the predominant one even at high temperature.

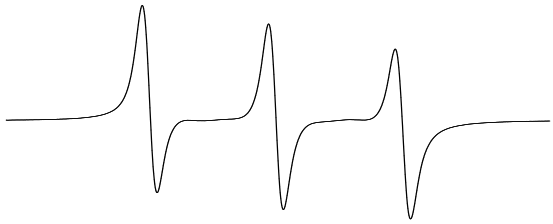

Figure 2.44. Derivative **28a** 1.0 mM in CH_3CN T=298 K.

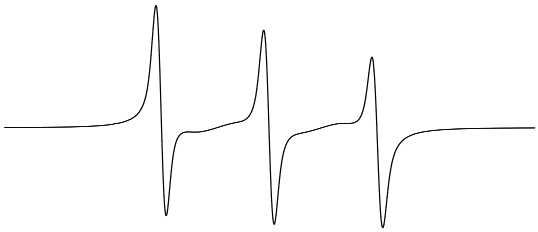

Figure 2.45. Derivative **28a** 1.0 mM in $CHCl_3$ T=298 K.

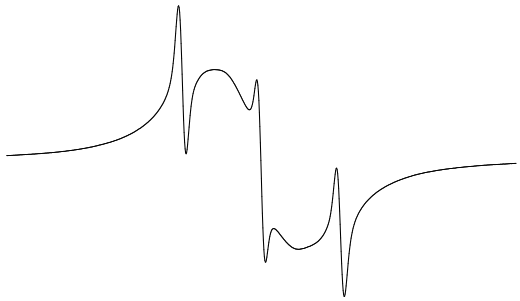

Figure 2.46. Derivative **28a** 1.0 mM in benzene T=298 K.

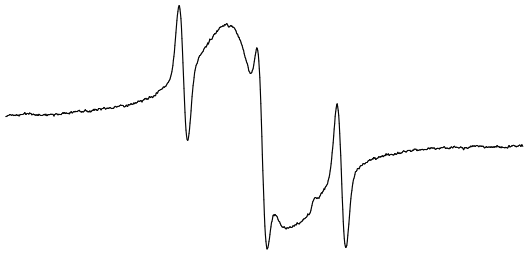

Figure 2.47. Derivative **28a** 1.0 mM in decane T=298 K.

Finally, in Figures 2.48 and 2.49 some optical microscope images of the gel-like or LC phase of derivatives **28a** and **29**.

(a) (b)

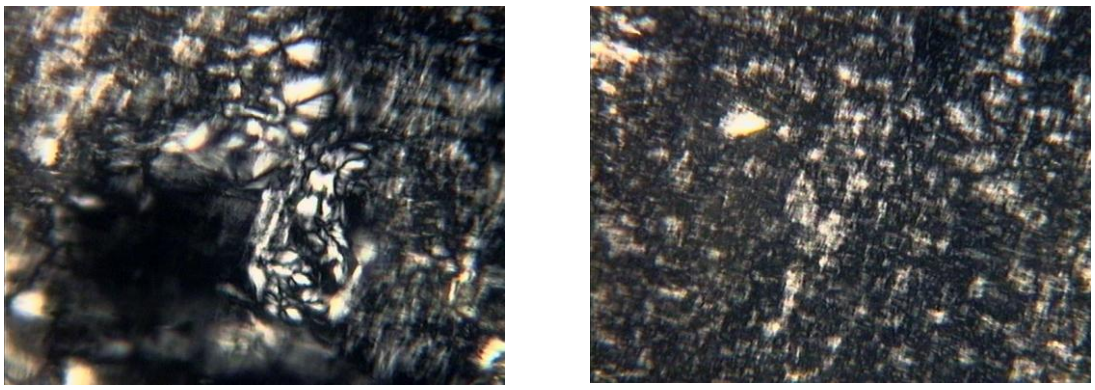

Figure 2.48. Textures of derivative **28a** in toluene. a) and b) details showing the birefringent behaviour of the biphasic gel-like system [c] = 1.8% w/w

(a) (b)

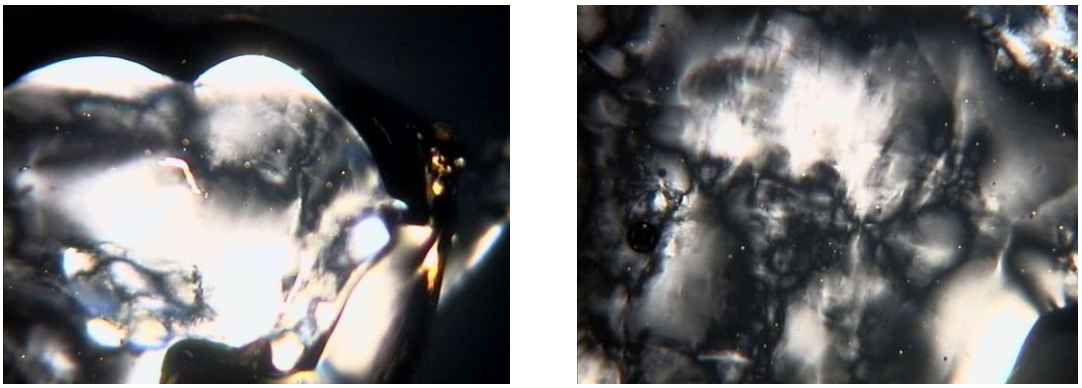

Figure 2.49. a) and b) textures of derivative **29** in toluene [c] = 8% w/w

2.7 Conclusion

Guanine nucleobases have a high ability to form multiple hydrogen bonds and, possibly, base stacking. These directionally controlled, multiple base–base interactions make the guanine moiety a highly useful structural element for design and construction of geometrically well-defined three-dimensional assemblies. Rapid progress of the guanine-related supramolecular and materials chemistry in recent years, which has been briefly reviewed here, is opening the way to a variety of novel functional materials that consist of geometrically well-defined two- or three-dimensional assemblies of nucleobase-containing molecules. Furthermore, guanine self-assembly is employed in molecular manufacturing, intended as the concept of engineering functional structures at the molecular scale to achieve sub-micro, micro or macro scale objects, with the objective to achieve components and/or systems with predictable and controllable properties.

References

1. Guschlbauer, W.; Chantot, J. F.; Thiele, D. *J. Biomol. Struct. Dyn.* **1990**, *8*, 491-511.
2. G. Gottarelli, S. Masiero, G. P. Spada, *J. Chem. Soc. Chem. Commun.* **1995**, 2555.
3. J. T. Davis, S. Tirumala, J. Jenssen, E. Radler, D. Fabris, *J. Org. Chem.* **1995**, *60*, 4167.
4. Giorgi, T.; Grepioni, F.; Manet, I.; Mariani, P.; Masiero, S.; Mezzina, E.; Pieraccini, S.; Saturni, L.; Spada, G. P.; Gottarelli, G. *Chem.-Eur. J.* **2002**, *8*, 2143-2152.
5. A. Marlow, E. Mezzina, S. Masiero, G. P. Spada, J. T. Davis, G. Gottarelli, *J. Org. Chem.* **1999**, *64*, 5116.
6. E. Mezzina, P. Mariani, R. Itri, S. Masiero, S. Pieraccini, G. P. Spada, F. Spinozzi, J. T. Davis, G. Gottarelli, *Chem. Eur. J.* **2001**, *7*, 388.
7. S. Pieraccini, G. Gottarelli, P. Mariani, S. Masiero, L. Saturni, G. P. Spada, *Chirality* **2001**, *13*, 7.
8. M. S. Kaucher, Y.-F. Lam, S. Pieraccini, G. Gottarelli, J. T. Davis, *Chem. Eur. J.* **2005**, *11*, 164.
9. a) X. Liu, I. C. M. Kwan, S. Wang, G. Wu, *Org. Lett.* **2006**, *8*, 3685; b) S. Martic´, X. Liu, S. Wang, G. Wu, *Chem. Eur. J.* **2008**, *14*, 1196; c) V. Gubala, J. E. Betancourt, J. M. Rivera, *Org. Lett.* **2004**, *6*, 4735.
10. C. Graziano, S. Pieraccini, S. Masiero, M. Lucarini, G. P. Spada, *Org. Lett.* **2008**, *10*, 1739.
11. G. P. Spada, S. Lena, S. Masiero, S. Pieraccini, M. Surin, P. Samorì, *Adv. Mater.* **2008**, *20*, 2433.
12. a) D. M. Gray, J.-D. Wen, C. W. Gray, R. Repges, C. Repges, G. Raabe, J. Fleishhauer, *Chirality* **2008**, *20*, 431; b) G. Gottarelli, S. Masiero, G. P. Spada, Enantiomer **1998**, *3*, 429; c) G. Gottarelli, S. Lena, S. Masiero, S. Pieraccini, G. P. Spada, Chirality **2008**, *20*, 471.
13. X. D. Shi, K. M. Mullaugh, J. C. Fettinger, Y. Jiang, S. A. Hofstadler, J. T. Davis, *J. Am. Chem. Soc.* **2003**, *125*, 10830.
14. S. L. Forman, J. C. Fettinger, S. Pieraccini, G. Gottarelli, J. T. Davis, *J. Am. Chem. Soc.* **2000**, *122*, 4060.

15. a) X. D. Shi, J. C. Fettinger, J. T. Davis, *J. Am. Chem. Soc.* **2001**, *123*, 6738; b) X. Shi, J. C. Fettinger, J. T. Davis, *Angew. Chem*. **2001**, *113*, 2909; *Angew. Chem. Int. Ed.* **2001**, *40*, 2827.
16. a) S. Tirumala, A. L. Marlow, J. T. Davis, *J. Am. Chem. Soc.* **1997**, *119*, 2769; b) M. Cai, A. L. Marlow, J. C. Fettinger, D. Fabris, T. J. Haverlock, B. A. Moyer, J. T. Davis, *Angew. Chem.* **2000**, *112*, 1339; *Angew. Chem. Int. Ed.* **2000**, *39*, 1283; c) X. Shi, J. C. Fettinger, M. Cai, J. T. Davis, *Angew. Chem.* **2000**, *112*, 3254; *Angew. Chem. Int. Ed.* **2000**, *39*, 3124.
17. T. Evan-Salem, L. Frish, F. W. B. van Leeuwen, D. N. Reinhoudt, W. Verboom, M. S. Kaucher, J. T. Davis, Y. Cohen, *Chem. Eur. J.* **2007**, *13*, 1969.
18. a) J. C. Chaput, C. Switzer, *Proc. Natl. Acad. Sci. USA* **1999**, *96*, 10614; b) M. Meyer, J. Suhnel, *J. Phys. Chem. A* **2003**, *107*, 1025.
19. J. T. Davis, *Angew. Chem., Int. Ed.*, **2004**, *43*, 668.
20. M. M. Cai, X. D. Shi, V. Sidorov, D. Fabris, Y. F. Lam and J. T. Davis, *Tetrahedron*, **2002**, *58*, 661.
21. V. Andrisano, G. Gottarelli, S. Masiero, E. H. Heijne, S. Pieraccini and G. P. Spada, *Angew. Chem., Int. Ed.*, **1999**, *38*, 2386.
22. Sessler, J. L.; Sathiosatham, M.; Doerr, K.; Lynch, V.; Abboud, K. A. *Angew. Chem. Int. Ed.* **2000**, *39*, 1300-1302.
23. Otero, R.; Schock, M.; Molina, L. M.; Laegsgaard, E.; Stensgaard, I.; Hammer, B.; Besenbacher, F. *Angew. Chem. Int. Ed.* **2005**, *44*, 2270-2275.
24. Gubala, V.; Betancourt, J. E.; Rivera, J. M. *Org. Lett.* **2004**, *6*, 4735-4738.
25. J. L. Sessler, J. Jayawickramarajah, M. Sathiosatham, C. L. Sherman and J. S. Brodbelt, *Org. Lett.*, **2003**, *5*, 2627 and references cited within.
26. Giorgi, T.; Lena, S.; Mariani, P.; Cremonini, M. A.; Masiero, S.; Pieraccini, S.; Rabe, J. P.; Samorì, P.; Spada, G. P.; Gottarelli, G. *J. Am. Chem. Soc.*, **2003**, *125*, 14741; Lena, S.; Cremonini, M. A.; Federiconi, F.; Gottarelli, G.; Graziano, C.; Laghi, L.; Mariani, P.; Masiero, S.; Pieraccini, S.; Spada, G. P. *Chem. Eur. J.*, **2007**, *13*, 3441.
27. Doyle, D. A.; Cabral, J. M.; Pfuetzner, R. A.; Kuo, A. L.; Gulbis, J. M.; Cohen, S. L.; Chait, B. T.; MacKinnon, R. *Science* **1998**, *280*, 69-77.
28. M. S. Kaucher, W. A. Harrell, Jr. and J. T. Davis, *J. Am. Chem. Soc.*, **2006**, *128*, 38.

29. L. Ma, M. Melegari, M. Colombini, J. T. Davis, *J. Am. Chem. Soc.* **2008**, *130*, 2938.
30. N. Sakai, Y. Kamikawa, M. Nishii, T. Matsuoka, T. Kato, S. Matile, *J. Am. Chem. Soc.* **2006**, *128*, 2218.
31. See for example: a) V. Palermo, A. Liscio, D. Gentilini, F. Nolde, K. Müllen, P. Samorì, *Small* **2007**, *3*, 161; b) J. Puigmartí-Luis, A. Minoia, H. Uji-i, C. Rovira, J. Cornil, S. De Feyter, R. Lazzaroni, D. B. Amabilino, *J. Am. Chem. Soc.* **2006**, *128*, 12602.
32. A. M. S. Kumar, S. Sivakova, J. D. Fox, J. E. Green, R. E. Marchant, S. J. Rowan, *J. Am. Chem. Soc.* **2008**, *130*, 1466; A. M. S. Kumar, S. Sivakova, R. E. Marchant, S. J. Rowan, *Small* **2007**, *3*, 783.
33. K. Sada, M. Takeuchi, N. Fujita, M. Numata, S. Shinkai, *Chem. Soc. Rev.* **2007**, *36*, 415.
34. Arnal-Hérault, C.; Banu, A.; Barboiu, M.; Michau, M.; van der Lee, A. *Angew. Chem. Int. Ed.*, **2007**, *46*, 4268.
35. a) G. R. Newkome, C. N. Moorefield, F. Vogtle, *Dendritic Molecules: Concepts, Synthesis Perspectives*, VCH, Weinheim, **1996**; b) F.W. Zeng, S. C. Zimmerman, *Chem. Rev.* **1997**, *97*, 1681.
36. J. E. Betancourt, J. M. Rivera, *Org. Lett.* **2008**, *10*, 2287.
37. C. Arnal-H_rault, A. Pasc, M. Michau, D. Cot, E. Petit, M. Barboiu, *Angew. Chem.* **2007**, *119*, 8561; *Angew. Chem. Int. Ed.* **2007**, *46*, 8409.
38. C. Zhong, J. Wang, N. Wu, G. Wu, P. Y. Zavalij, X. Shi, *Chem. Commun*. **2007**, 3148.
39. a) N. Sreenivasachary, J-M. Lehn, *Proc. Natl. Acad. Sci. USA* **2005**, *102*, 5938; b) V. Setnicka, M. Urbanova, K. Volka, N. Sreenivasachary, J-M. Lehn, *Chem. Eur. J.* **2006**, *12*, 8735; c) N. Sreenivasachary, J.-M. Lehn, *Chem. Asian J.* **2008**, *3*, 134; d) A. Ghoussoub, J.-M. Lehn, *Chem. Commun.* **2005**, 5763.
40. Pieraccini, S.; Masiero, S.; Pandoli, O.; Samorì, P.; Spada, G. P. *Org. Lett*., **2006**, *8*, 3125.
41. *Magnetism: Molecules to Materials, Vol. I–IV* (Eds.: J. S. Miller, M. Drillon), Wiley-VCH, Weinheim, **2001–2003**.
42. K. Maekawa, D. Shiomi, T. Ise, K. Sato, T. Takui, *Org. Biomol. Chem.* **2007**, *5*, 1641.

43. Graziano, C.; Pieraccini, S.; Masiero, S.; Lucarini, M.; Spada, G. P. *Org. Lett.* **2008**, *10*, 1739–1742.
44. Self-assembled spin cage containing four radical centers have also been reported: Nakabayashi, K.; Ozaki, Y.; Kawano, M.; Fujita, M. *Angew. Chem., Int. Ed.* **2008**, *47*, 2046–2048.
45. Paramasivan, S.; Rujan, I.; Bolton, P. H. *Methods* **2007**, *43*, 324–331; Gottarelli, G.; Spada, G. P.; Garbesi, A. In *Comprehensive Supramolecular Chemistry*; Sauvage, J.-P.; Hosseini M. W., Eds.; Pergamon: Oxford, 1996; Vol. 9, pp 483-506.
46. Wertz, J. E.; Bolton, J. R. *Electron Spin Resonance*; Chapman and Hall: New York, 1986.
47. (a) Rajca, A.; Mukherjee, S.; Pink, M.; Rajca, S. *J. Am. Chem. Soc.* **2006**, *128*, 13497–13507. (b) Kirste, B.; Grimm, M.; Kurreck, H. *J. Am. Chem. Soc.* **1989**, *111*, 108–114.
48. Metal-induced magnetic exchange coupling in paramagnetic azacrowns have also been reported: Igarashi, K.; Nogami, T.; Ishida, T. *Chem. Commun.* **2007**, 501–503.
49. David González-Rodríguez, Joost L. J. van Dongen, Martin Lutz, Anthony L. Spek, Albertus P. H. J. Schenning, E. W. Meijer *Nature Chemistry* **2009**, *1*, 151.

Chapter 3. Supramolecular Organisation of Guanosine Derivatives Not-Mediated By Ions

The majority of this Chapter has been published in:

- G. Gottarelli, S. Masiero, E. Mezzina, S. Pieraccini, J. P. Rabe, P.Samorì, G. P. Spada, *Chem. Eur. J.* **2000**, *6*, 3242.

In section **3.4** *it is briefly summarized part of the work done during my PhD training at the CNRS (Strasbourg) under the supervision of Prof. Nicolas Giuseppone:*

- P. Neviani, D. Sarazin, M. Schmutz, C. Blanck, N. Giuseppone, G. P. Spada, *Manuscript submitted*.

3.1 Introduction

Almost all the supramolecular architectures described so far (Chapter 2) require the presence of a cation (usually alkali-metal, but also earth-alkali or lanthanide, ions)[1] which stabilizes, via dipole-ion interactions, the macrocyclic G-quartet that can, in turn, stack in columnar G-quadruplex arrangements. In addition, guanosine can polymerize via hydrogen bonding to give a variety of supramolecular networks including linear ribbons such as A and B-types (chart below). This complex supramolecular behavior confers to the guanine-guanine interactions their upper interest among all the homonucleobases studied and, as in the case for cation-templated structures, linear ribbons from guanosine derivatives are considered as potential scaffolds for functional materials.

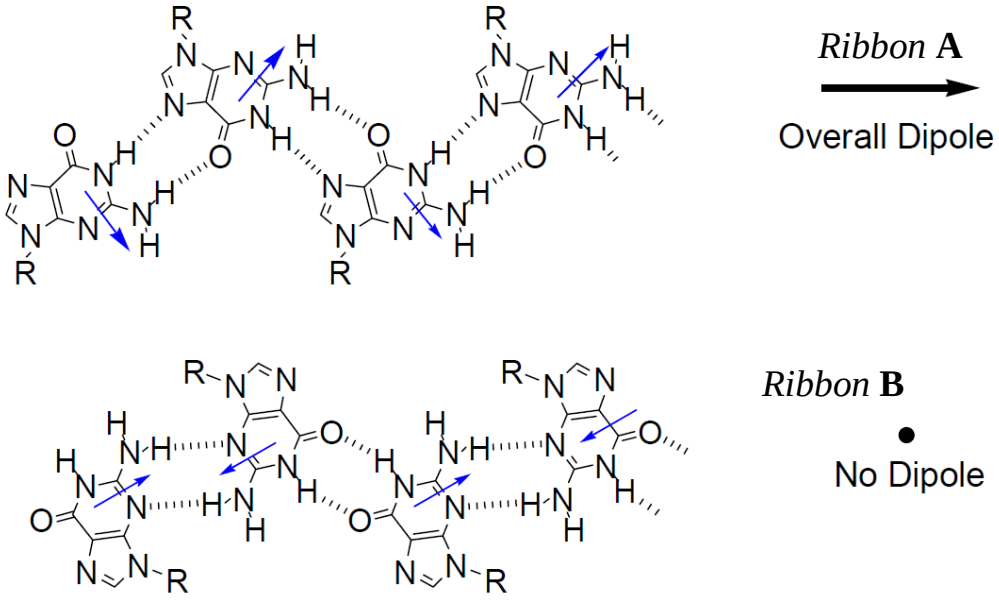

3.2 Ribbon Structures

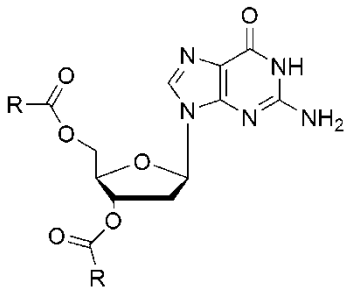

R= C_9H_{19} dG **1**

R= *p*-($C_{12}H_{25}O$)C_6H_4 dG **7**

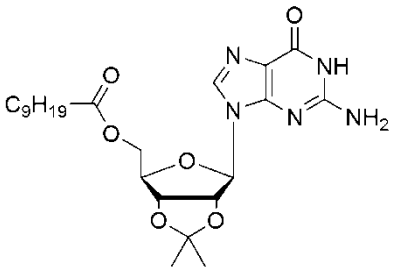

G **30**

Figure 3.1. Guanosine derivatives.

NMR data show the existence of two types of self-assembled, ribbon-like structures (A and B-type, see chart above) which are connected at the guanine moieties through two different H-bonded networks. The first species (A), which is stable in the solid state and characterized by cyclic NH(2)-O(6) and NH(1)-N(7) hydrogen bonds, is detected soon after dissolving the polycrystalline powder in rigorously anhydrous $CDCl_3$. This metastable species slowly undergoes a structural transition towards a thermodynamically stable ribbon characterized instead by NH(1)-O(6) and NH(2)-N(3) cyclic hydrogen bonds (B). Moreover STM imaging at submolecular resolution (see Figure 3.6) indicate a molecular packing of type A, like the one detected in the solid state. This indicates that, upon adsorption at solid-liquid interface, the guanosine moieties undergo a structural rearrangement from B-type to an A-type ribbon.

In this section it is described in detail the NMR studies, performed by our group between 1998-2000, that clearly demonstrate the presence of these supramolecular aggregates in solution for derivatives shown in Figure 3.1.

In previous research,[2] some of us have studied the self-assembly of derivative dG **1**. It was concluded that dG **1** self-assembles into the ribbon-like structure B. A similar study on derivative dG **7** revealed that, while the H(8) signal is at δ=7.7 in the NMR spectrum of dG **1** (Figure 3.2c), the H(8) signal in the NMR spectrum of derivative dG **7**, dissolved in rigorously anhydrous $CDCl_3$, is found above δ=8, independent of concentration. Moreover, the freshly prepared solution, even if diluted, displays a considerable broadening of all bands. Over a few hours, the H(8) signal moves slowly upfield and eventually reaches the 'standard' value of δ=7.7. Furthermore, with

dideuterotetrachloroethane as a solvent, the H(8) signal of dG **7** is above δ=8, but after a heating-cooling cycle the spectrum returns immediately to standard, that is H(8) signal at δ=7.7. The newly assembled form (A) is prevalent when the H(8) signal is above δ=7.7, the deshielding presumably being cause by involvement of N(7) as a proton acceptor in the self-assembling process. The presence of water in solution increase the rate of formation of the B polymeric form, whose H(8) signal falls to around δ=7.7. These observation indicate that freshly prepared solutions maintain a memory of the solid-state.[3] As time passes, or after heating, a structure is achieved that is more stable in solution. Our group therefore re-examined the self-assembly of derivative dG **1** to demonstrate that previous NMR data were obtained at the equilibrium, where only the more stable ribbon (B-type) is detectable.

A 0.03 M solution of derivative dG **1** in rigorously anhydrous $CDCl_3$ shows a broad H(8) signal centred at δ=8.1 (Figure 3.2a). Within a few hours, the signal moves upfield and sharpens. After twelve hours it is recorded at δ=7.95 and after four days it reaches δ=7.89 (Figure 3.2b). Addition of water (1 μL) finally moves the signal to δ=7.7 (Figure 3.2c).

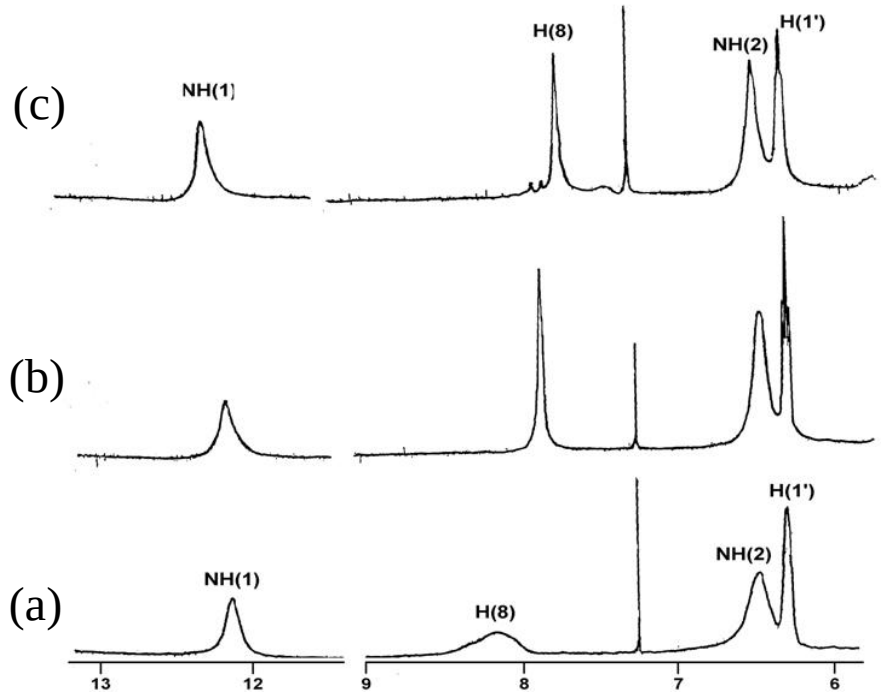

Figure 3.2. ^{1}H NMR spectra of derivative dG **1** (0.03 M in $CDCl_3$): a) immediately after dissolution, b) after four days, c) after equilibration upon addiction of 1 μL of water.

The absence of two separate signals for H(8) seems to exclude a slow equilibrium (on the NM timescale) between two species (ribbon A and B). This seems to contradict

the observation that the transformation from A-type to B-type ribbon is slow. The two observations can be reconciled by considering a mechanism in which the first aggregate A rearranges through a continuous transformation, in which the proton shifts gradually change, into the more stable assembled species B. As the ribbon-like structure A was previously found in the guanosine crystal by X-ray diffraction[3] we conclude that the A form is present in freshly prepared $CDCl_3$ solutions.

In order to further characterize the two forms in solution, some ^1H-^1H nuclear Overhouse effect (NOE) spectra were recorded at different times. Ribbon A is characterized by the proximity of H(8) and NH(1) and of H(8) and NH(2) (see Figure 3.3a). On the other hand , the B form is characterized by NOE enhancements due to the proximity between H(1'), H(2'), H(2''), and the α-protons of the 3'-*O*-decanoyl group of one molecule, and NH(1) and NH(2) of the closest molecule (Figure 3.3b).[2]

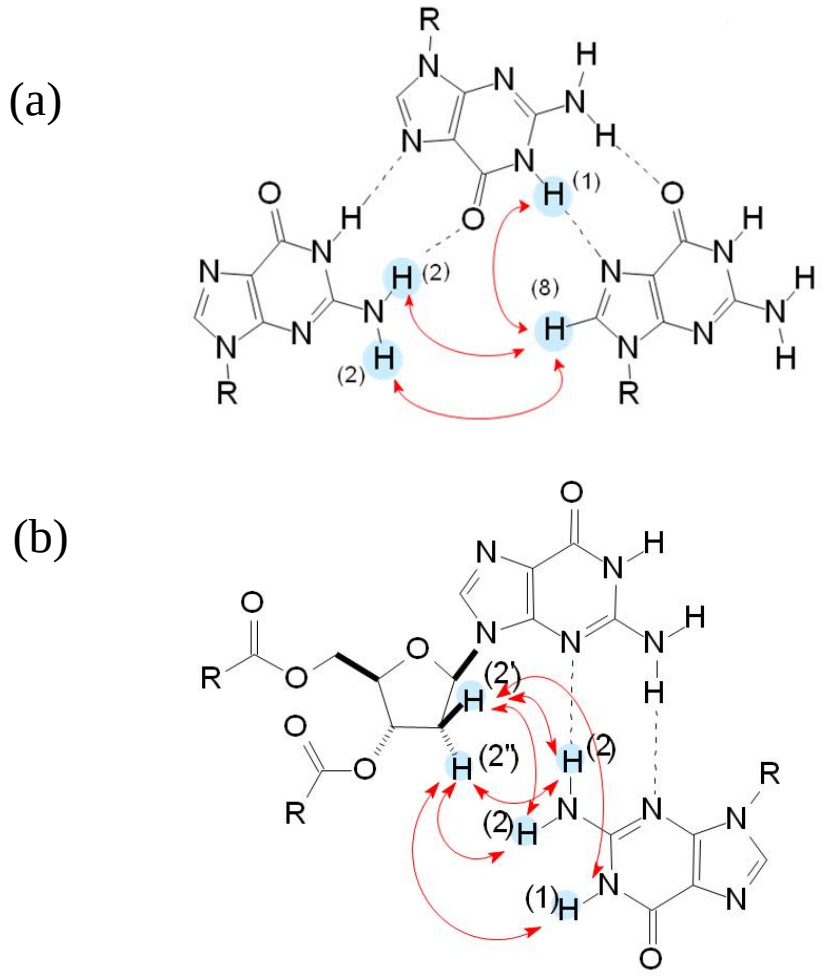

Figure 3.3. The NOE interaction characteristic of (a) A-type and (b) B-type ribbon as indicate by double-head arrows.

For sake of simplicity, we are only going to consider the data obtained by irradiating H(8) (A form) and H(2') and H(2'') (B form).

All NOE experiments recorded immediately after the dissolution of compound dG **1** in anhydrous $CDCl_3$ (H(8) at δ=8.1) show significant enhancement of NH(1) (4.5%) and NH(2) (7.4%) caused by the saturation of H(8). On the other hand, the characteristic NOEs of the B aggregate obtained by irradiating H(2') [NH(1)/NH(2') and NH(2)/NH(2')] are almost negligible (< 1%). The situation changes if the same NOEs are recorded after 24 hours. Saturation of H(8) gives smaller increments of NH(1) (3%) and NH(2) (5.5%). Saturation of NH(2') and NH(2'') induces increased enhancement of NH(1) (4.3 and 3.8%, respectively) and of NH(2) (5.3 and 3.9%, respectively).

Measurements of NOE increments carried out after three days confirm the increase in amount of structure B at the expense of structure A (even if the solution still shows small amounts of structure A after several days). These results indicate a transformation to the more stable structure B: the chemical shift value of H(8) gives a qualitative measure of the shift.

As the position of the H(8) signal is a probe for analysing the prevalent species in solution, it has been used to check the H-bond network structure of the fibre[2] obtained from slow evaporation of a solution of derivative dG **1** in $CHCl_3$. In the previous work,[2] structure B was assigned to the ribbon present in the fibre on the basis of NMR data obtained at the equilibrium. In fact, the ^{1}H NMR spectrum obtained by dissolution of the fibre in anhydrous $CDCl_3$ has a broad H(8) signal at δ=8.3, thus confirming that the fibre as the same structure as the solid[3] (form A). Also in this case, the signal moves slowly upfield towards the standard δ=7.7 value. As the NMR spectra of derivative dG **7** behave in a similar way (at the equilibrium, the δ value of NH(2) shifts downfield with concentration indicating progressive engagement in H-bonding, just as in the case of derivative dG **1**), an analogous self-assembly into ribbon-like structures A and B can also be inferred for this compound.

A similar NMR study was also performed on guanosine derivative G **30**, in order to demonstrate a similar behaviour in solution as for deoxyguanosine derivatives.

The ^{1}H NMR spectrum of G **30** was recorded in $CDCl_3$ and the signals (Table 3.1) were assigned by means of two-dimensional COSY and NOESY experiments.

	δ [ppm]	J_{HH} [Hz]
H(8)	7.59 (s)	
H(1′)	5.95 (d)	1.8
H(2′)	5.25 (dd)	6.3, 1.8
H(3′)	4.97 (m)	
H(4′)	4.42 (m)	
H(5′)[a]	4.69 (dd)	11.2, 5.9
H(5″)[a]	4.12 (dd)	11.2, 6.3
N-H(1)	12.12 (brs)	
N-H(2)	6.06 (brs)	

Table 3.1. ^{1}H NMR data of a 2.60×10^{3} mol L^{-1} solution of G **30** in $CDCl_3$. Other resonances: 2.32 (t, J=7.5 Hz, CH_2CO), 1.60 (m, 5H, acetonide CH_3, C*H*$_2$CH$_2$CO); 1.38 (s, acetonide CH_3), 1.25 (m, 12H, CH_2); 0.86 (t, J=6.5 Hz, CH_2CH_3). [a] H(5') and H(5'') protons were not individually assigned.

The spectrum shows a broad singlet centred at δ=12.1, corresponding to an hydrogen-bonded imino proton NH(1), (in [D_6]DMSO, where solute-solute hydrogen-bonds are weakened by competition with the solvent, the same signal falls at lower frequencies (δ=10.7)) which does not shift when the solute concentration is increased. The H(8) signal is around δ=7.6 and the H(2) resonance falls from δ=6.1 to 6.3 in a concentration range of 2.6×10^{-3}-5×10^{-2} mol L^{-1}. The sugar proton signals are well separated and appear between δ=4 and 6. The analysis of the cross-peak intensities made on the basis of a COSY experiment allows one to distinguish the single resonances of the ribose moiety. In particular, H(1')/H(2') and H(3')/H(4') are correlated by small coupling constants, while H(2') and H(3') show larger cross-peak intensities due to a larger coupling constant.

Structural information on the assembled species in solution was obtained by ^{1}H-^{1}H NOESY experiments on compound G **30**, and the results compared with those of derivative dG **1**. For both compounds, dG **1** and G **30**, the NH_2 signal shifts downfield when the concentration is increased, an observation that indicates progressive involvement of this group in hydrogen bonding. Ribo derivative G **30** shows more extensive aggregation than dG **1** at room temperature in nonanhydrous $CDCl_3$: the spectra recorded at the same concentration values used for compound dG **1** display broader signals for all the protons.

NOESY data (mixing times 0.05-0.2 ms) for a 0.01 mol L^{-1} solution of G **30** confirm the presence of ribbon-like self-assembled species. Ribbon B ('solution' aggregate) is prevalent in nonanhydrous $CDCl_3$, and is identified by a strong

intermolecular interaction between NH_2 and H(1') and a less intense cross-peak between NH_2 and H(2') protons (Figure 3.4).

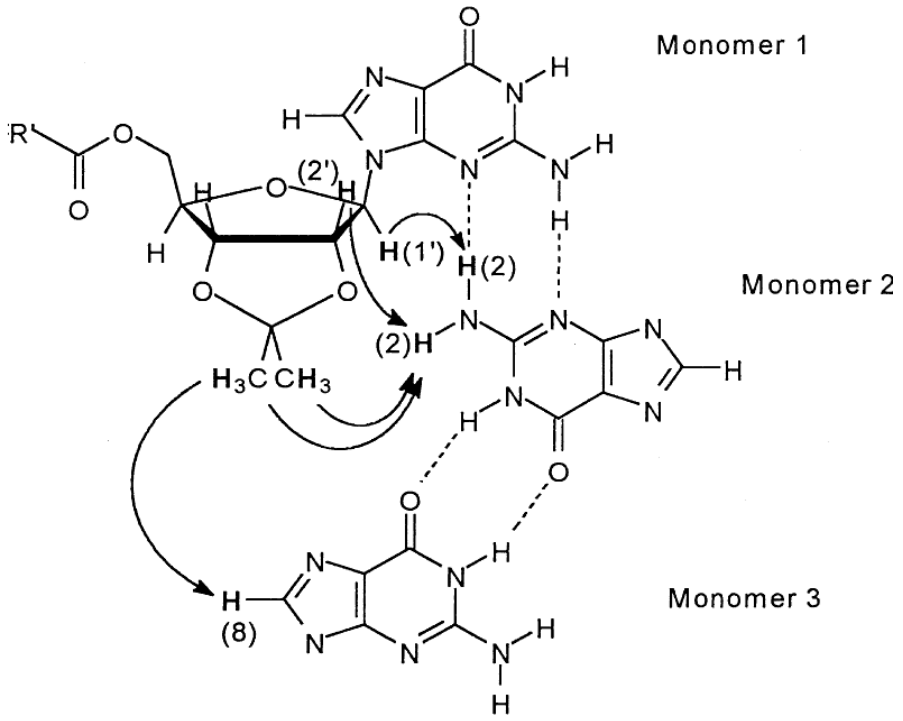

Figure 3.4. Important intermolecular interactions determined from NOESY experiments showing B-type ribbon aggregate formed by derivative G **30**.

These results parallel those obtained for deoxyribo derivative dG **1**. Additional cross-peaks confirming the hydrogen-bonding pattern are generated by the intrinsic structure of the compound under investigation. Important intermolecular interactions between methyl protons of the acetonide ring of one molecule and the NH_2 of the one closest to it, and between the methyl protons and the H(8) of the next closest one, allow the sequential connection between three molecules and thus confirm the hydrogen-bonding framework characterizing the 'solution' aggregate (ribbon B): the former spatial interaction, CH_3-NH_2 , is what is expected for the relative arrangement of monomer 1 and monomer 2 in which hydrogen-bonding to N(3) is involved; the latter, CH_3-H(8), is what is expected for the relative arrangement of monomer 2 and monomer 3 in which H(1)/O(6) hydrogen-bonds are present.

NOESY spectra of freshly prepared solutions also show small amounts of the hydrogen-bonded ribbon structure A (solid state) , which is characterized by cross-peaks connecting H(8) with H(1) and H(8) with H(2) intermolecularly.

It is interesting to note that in order to detect NOESY cross-peaks relating the intra-intermolecular protons for solutions of lower concentration (4×10^{-3} mol L^{-1}) longer mixing times are required; this suggests the presence of shorter ribbons.

The data obtained are a confirmation of the general behavior of some lipophilic derivatives of guanosine and deoxyguanosine. These compounds self-associate, in the absence of added alkali metal ions, to give ribbon-like structures characterized by two different hydrogen-bonding networks in the solid state and in chloroform. In both ribbon-like polymers the glycosidic bond adopts an *anti* conformation (see Figure 2.3). The formation of ribbon-like polymers seems to be a quite general behaviour, at least for derivatives that can adopt an *anti* conformation (see **2.4**). It should be pointed out that the two ribbons possess a different symmetry and, for example, while ribbon A has a permanent dipole moment, ribbon B has no net dipole (see **3.1**, chart). This feature has been exploited in organic electronic prototype devices (see **3.3**).

Moreover CD spectra of these aggregates are very weak and almost identical to those of the monomers: the chirality of the nucleosides is not expressed at the supramolecular level.[4,5]

The self-assembled G-ribbons have been ‘‘seen’’ with the scanning probe microscopies.[6]

The picture in Figure 3.5 is a Scanning Force Microscopy (SFM) image of derivative dG **7** and shows a dried nanoribbon formed on the basal plane of the substrate (mica). Its width, around 6.2 nm, is consistent with its proposed structure.

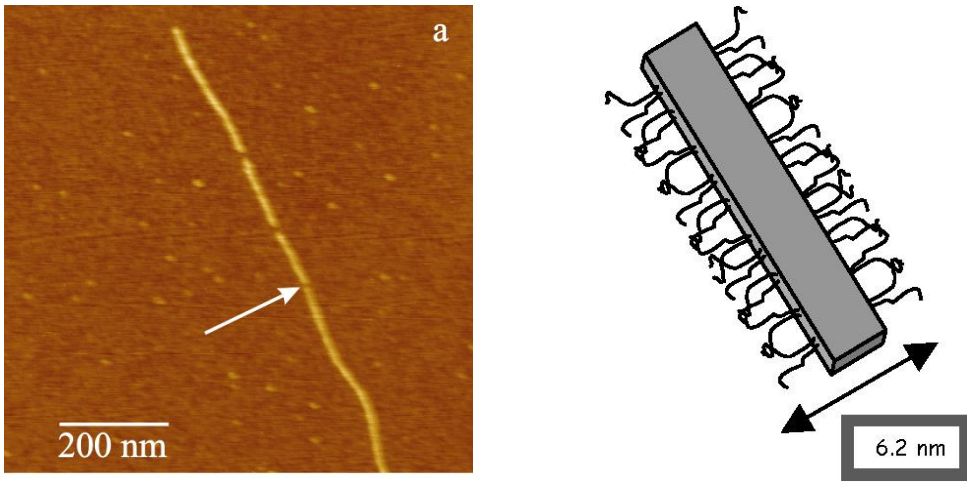

Figure 3.5. SFM picture of dG **7** nanoribbon.

The picture on Figure 3.6 is a Scanning Tunnelling Microscopy (STM) image (at the interface graphite/solution) of closely packed arrays of H-bonded ribbons that interdigitate. The unit cell dimension b perfectly matches that of the ribbon A found in Single Crystal by X-ray.[3]

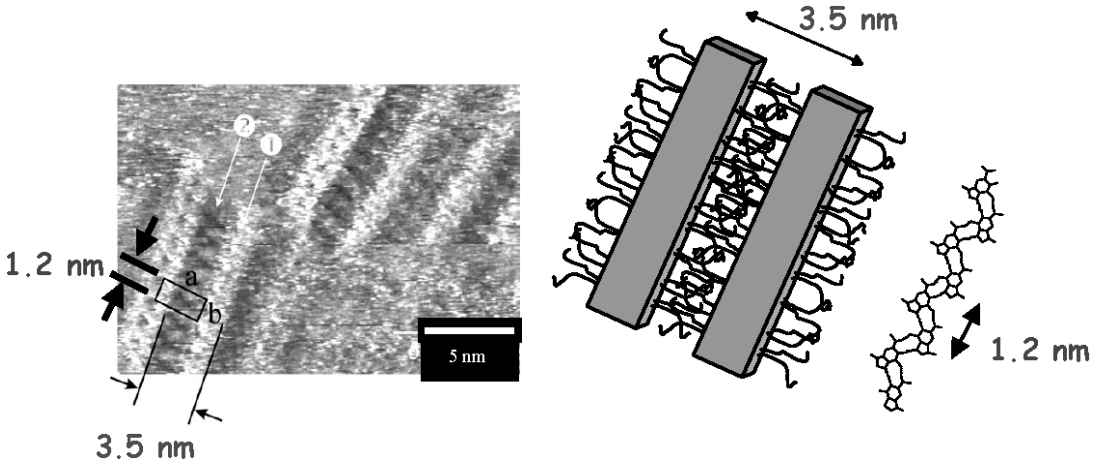

Figure 3.6. A quasi-molecular resolution Scanning Tunneling Microscopy (STM) image (at the graphite/solution interface) of closely packed arrays of H-bonded ribbons (A-type) formed by self-assembly of dG **7**.

3.2.1 Guanosines as organogelators and/or lyotropic mesogens

In recent years there has been immense interest in studying gels derived from low molecular mass gelators (supramolecular, or simply molecular gels). The motivation for this is not only to understand the fundamental aggregate structures in the gels at different length scales, but also to explore their potential for futuristic technological applications.

Gels have been made sensitive to external stimuli like light and chemical entities by incorporating a spectroscopically active or a receptor unit as part of the gelator molecule. This makes them suitable for applications such as sensing and actuating. The diversity of gel structural architectures has allowed them to be utilized as templates to prepare novel inorganic superstructures for possible applications in catalysis and separation. Gels derived from liquid crystals (anisotropy gels) that can act as dynamically functional materials have been prepared, for example, for (re-writable) information recording. Supramolecular gels can be important, for example, in controlled release applications, in oil recovery and for gelling cryogenic fuels. They can also serve as media for a range of applications.

The ability of guanylic nucleotides and oligonucleotides to form hydrogels or liquid-crystalline phases in aqueous solutions has been known for a long time.[7-9]

This behavior is a consequence of the formation of a self-assembled structure, in which the basic unit is a chiral columnar aggregate based on G-quartets (see **1.5**) held together by non-covalent interactions. Depending on concentration, temperature and amount of added salts, these aggregates can originate viscous gel-like phases or self-correlate to generate mesophases of either the cholesteric or hexagonal type (Figure 3.7).

Also lipophilic columnar G-quadruplex structures, as mentioned in Chapter 2, give liquid-crystalline phases in organic solvents just as the ordinary G-rich oligonucleotides do in water.[10] This result may seem obvious, but is instead surprising considering the subtle contributions of different intermolecular forces in the formation of lyotropic phases.[11] Subsequently, Kato and coworkers found that lipophilic folic acid derivatives, which also form hydrogen-bonded tetrads, could also give liquid crystalline phases under the appropriate conditions.[12]

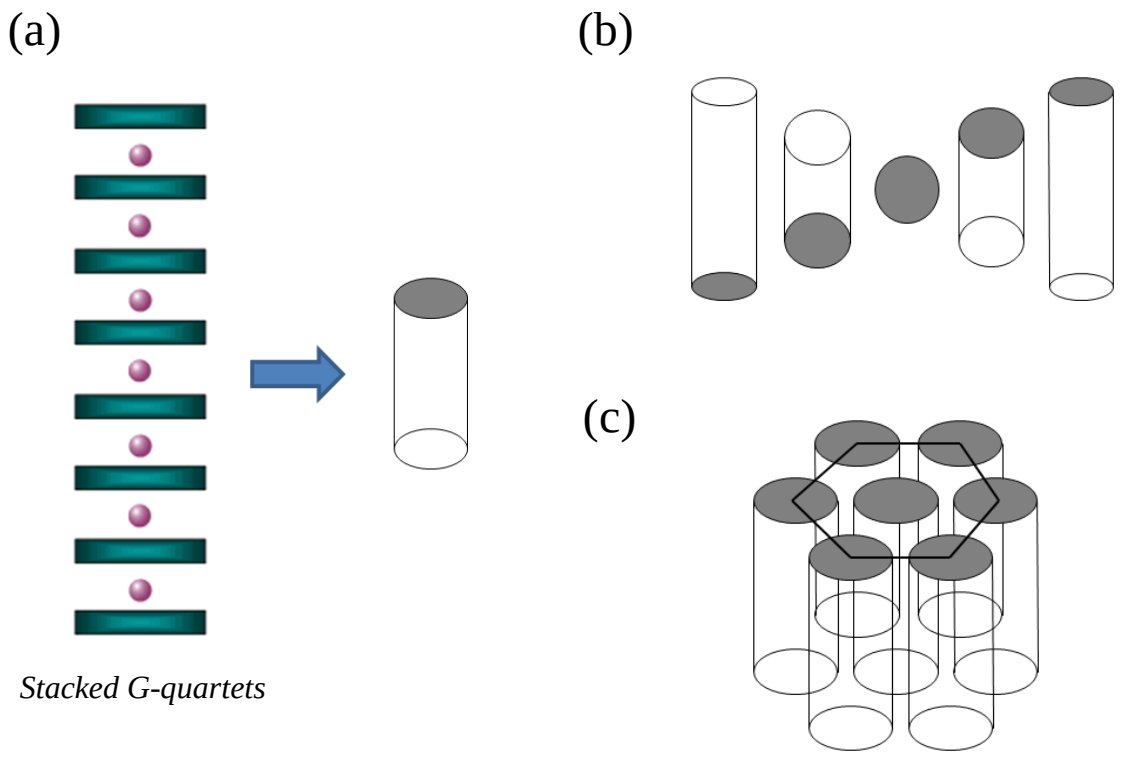

Figure 3.7. Lyotropic liquid crystals from (a) self-assembled guanosines. The symmetry of the (b) cholesteric and (c) hexagonal phase.

Even in the absence of templating cations, guanosine supramolecular architectures may origin lyotropic mesophases:[13] for example, dG **1** in hexadecane gives,

above a critical concentration, a viscous birefringent (LC) phase. A texture of this phase is reported in Figure 3.8.

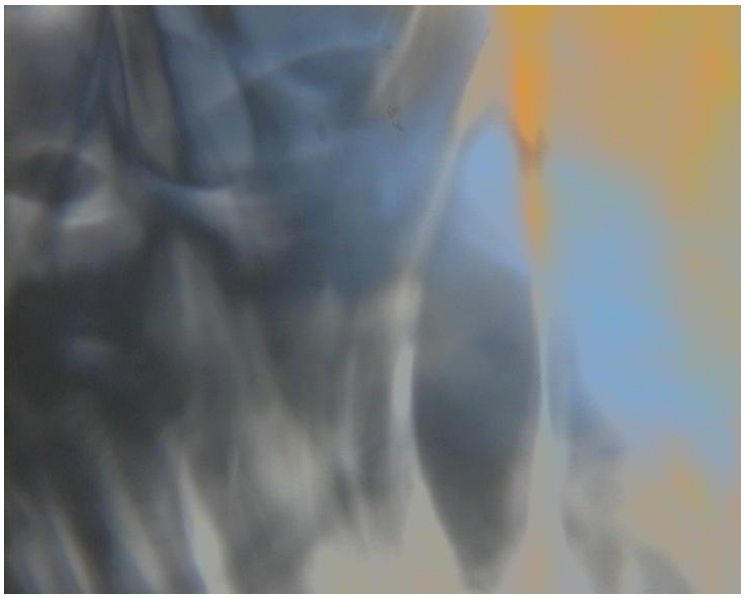

Figure 3.8. Optical texture of dG **1** in hexadecane (c=9% w/w).

X-ray diffraction measurements gave narrow Bragg reflections whose reciprocal spacing is indicative of a two-dimensional square packing of extended hydrogen bonded elements with the alkyl chains and solvent molecules filling the lateral gap between the tapes (Figure 3.9).

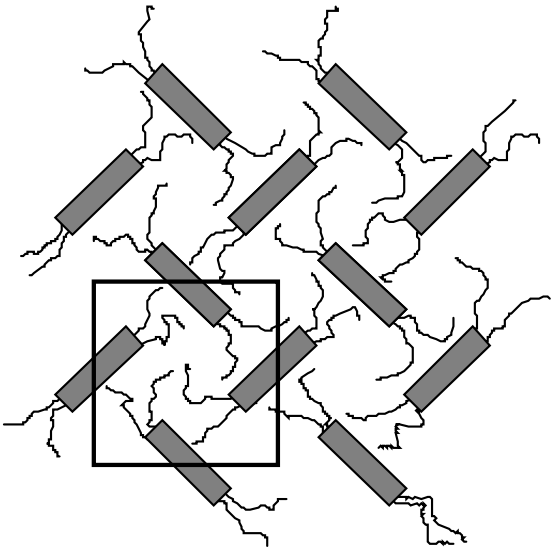

Figure 3.9. A model for the square LC phase of dG **1** in hydrocarbon solvents.

3.2.2 Two-dimensional guanosine layers

Araki and co-workers reported a sheet-like assembly obtained from a guanosine derivative with non-polar and flexible alkylsilyl groups, for example, dG **31** (Figure 3.10a) which is an efficient organogelator for alkanes.[14] From an in-depth structural analysis, Araki concluded that the basic structure of these gels is a sheet-like assembly. This supramolecular structure, as sketched in Figure 3.10b, is composed of anti-parallel G-ribbons of type A, with additional double inter-tape hydrogen bonds between NH(2) and N(3) of two guanine units located in adjacent ribbons. The gel-liquid-crystal phase transition for organogels from dG **31**, triggered by heating, has been observed and this transition was shown to be due to the selective cleavage of the inter-tape hydrogen bonds.

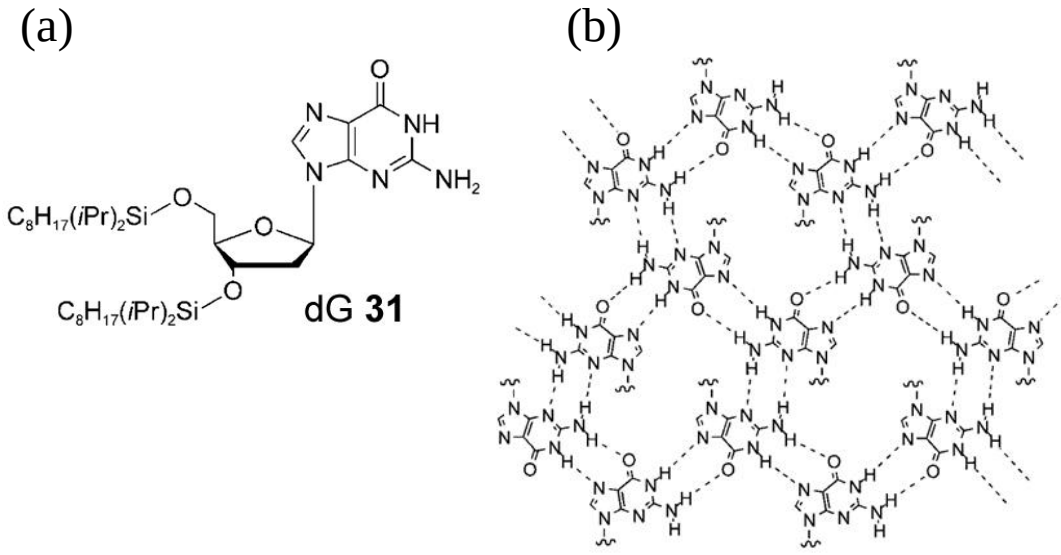

Figure 3.10. a) Deoxyguanosine derivative, b) two-dimensional H-bonded sheet of guanine moieties. (Figure 3.10b from reference 14b)

More recently the same author proposed a different supramolecular structure for 2',3'-*O*-isopropylideneguanosine organogelators having bulky alkylsilyl moieties in *O*-5'.[15] The gelation is mediated by the formation of self-complementary G-G base pairs through double N(2)-H---N(3) hydrogen bonds which further develop into a 2D supramolecular assembly (Figure 3.11).

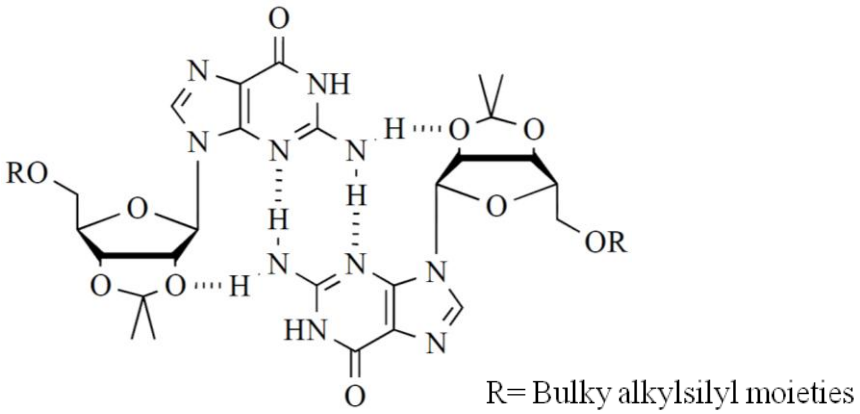

Figure 3.11. G-G base pair as propobed by Araki et al. (From reference 15).

3.3 Systems of Interest in Molecular Optoelectronics

(Bio)molecular electronics is gaining an increasing attention worldwide due to the appealing possibility of realizing cheap and easy-to-fabricate devices that exploit the self-assembly, self-recognition and self-repairing capability of engineered organic or bio-inspired molecules. Self-assembling guanosines are, therefore, promising candidates for fabrication of electronic nanodevices. Rinaldi et al. have proposed the use of nanoribbons formed from guanine units dG **1** in the design of molecular electronic nanodevices.[16a–c]

Self-assembled nanoribbons obtained by drop casting were used to interconnect gold nanoelectrodes fabricated by electron beam lithography (Figure 3.12).

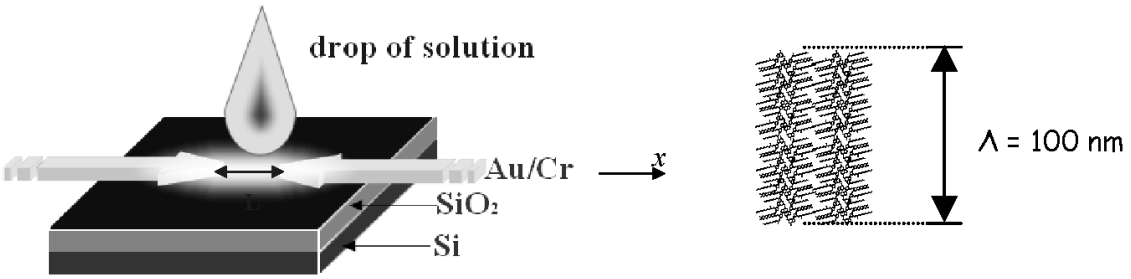

Figure 3.12. Schematic preparation of a G-based electronic nanodevice.

The formation of nanoribbons between the nanoelectrodes with different gaps were followed in loco with SFM. The typical length of the oriented arrays of ribbons (a nanocrystal) is 100 nm. The dependence Current Intensity vs Voltage is recorded. For contact gap of 60 nm or less only one nanocrystal is probed. Under these conditions a

clear diode-like behaviour is exhibited (Figure 3.13a), with currents of the order of the μA for positive bias and nA for negative bias. This rectifying feature points out to the existence of the strong dipole in each nanocrystal: this originates from the dipole of the guanine units ordered in the ribbon-like structure (A-type ribbon) of the nanocrystals. If a three-terminal device is prepared, the system behaves as a "Field Effect Transistor" when the guanosine nanoribbons are used to interconnect the drain and source terminals.[16b] The situation changes dramatically in the 120 nm device (Figure 3.13b). In this case few nanocrystals are probed by the electrodes and the total dipole of the sample between the electrodes averages to zero because the nanocrystals are randomly oriented. The I-V plot is non-linear, symmetric with a zero-current region (between -2V and +2V). At higher bias, the current increase at sub-μA levels, and the behaviour is typical of a metal-semiconductor- metal device. An interesting property of this 120 nm device is its high photoresponsivity:[16c] the current increases from sub-μA level in the dark to sub-mA levels under few mW power illumination.

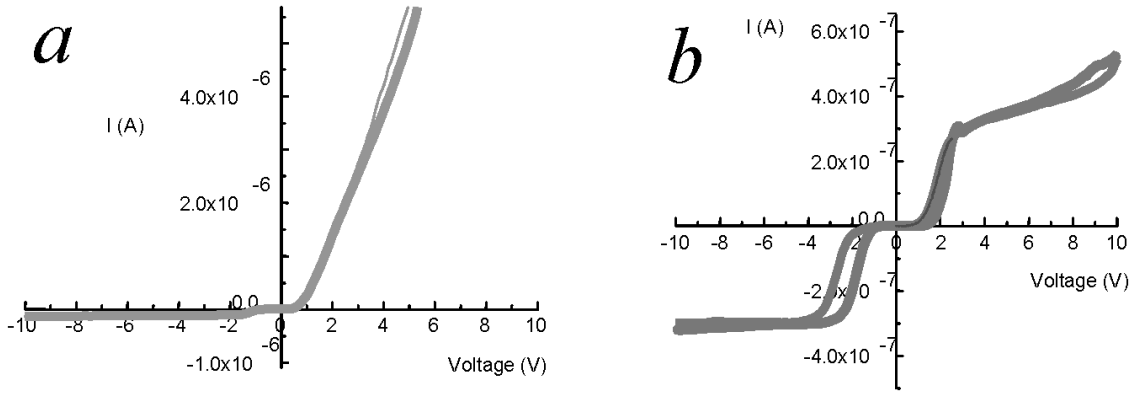

Figure 3.13. I-V plot for 60 (a) and 120nm (b) contact gap devices.

Recently, Neogi et al. fabricated a two-terminal diode assembly of derivative dG **1** on a GaN semiconductor substrate. Due to polarity induced along the direction of the guanosine nanocrystal wires during the self-assembly process, the output current of the GaN-based photodiodes is significantly higher than hybrid Si/self-assembled guanosine-based photodiodes at similar input voltage.[16d] Semiconductor quantum dots have the potential to become fluorescent bioprobes for many biological applications. Self-assembled guanosines conjugated to luminescent quantum dots have been recently proposed for biophotonic applications.[16e] A significant enhancement of photoluminescent emission is observed when the G-ribbons are conjugated to GaN quantum dots. This

novel material system could allow the development of biocompatible nanophotonic sensors sensitive to UV wavelength (as most of biological agents absorb or emit in this region).

3.4 Hierarchical Formation of Fibrillar and Lamellar Self-Assemblies from Guanosine Motifs

Although the formation of the linear ribbons and their H-bonding patterns have been demonstrated in solution (as well as in the crystal state[3] and on graphite surface), only very few investigations have been performed so far toward the determination of the length of these supramolecular polymers, as well as on their possible hierarchical self-assemblies in higher scale structures. As mentioned in section **3.2**, NMR spectroscopic indications of the supramolecular polymerisation come from the shifting and broadening of the resonance signals upon concentration of the solution. In addition, the observation of negative enhancements (or positive cross-peaks) in NOE (or NOESY) experiments indicates that guanosine derivatives behave as large molecules with $M_W > 1000$ ($\omega\tau_c > 1$).[2]

In sections **3.4.3**-**3.4.4** we report on the investigation of the supramolecular polymerisation of dG **1** and G **30** in chloroform by using light scattering technique, as well as transmission electronic microscopy (TEM). This line of studies reveals the formation of supramolecular polymers with high molecular weights that produce hierarchical structuring of very soft self-assemblies displaying either fibrillar (dG **1**) or lamellar (G **30**) organizations. The elucidation of these structures furnishes an explanation to the physical behaviour of guanosine units which display organogelator properties.

It's important to underline that our first goal was to use DOSY technique in order to obtain data concerning the length of these supramolecular polymers. As shown in some examples in Chapter 2, diffusion NMR is demonstrated as a valuable technique in characterizing the size of lipophilic G-quadruplexes. Some details of this powerful technique are described below.

However, during our investigation, it seems that its use in 1-D polymers is limited by the fact that the form factor of very long ribbons could not fit with the model used. Work is currently in progress to overcome this limitation.

3.4.1 Pulsed field gradient NMR

Characterization of supramolecular structures is often difficult and a continuous challenge in the field. Even with the advancement of nanoscale synthesis of functional material that has had a large degree of success in supramolecular chemistry,[17-19] solid-state structures through crystallization of these structures is often difficult or not possible. Furthermore, packing forces may give solid-state structures that are not well-populated or present in solution. Mass spectrometry,[20] analytical ultracentrifugation,[21-23] dynamic light scattering,[24] gel permeation chromatography, and vapor pressure osmometry have been used to determine sizes of supramolecular complexes. Unfortunately, these techniques don't provide the atomic resolution offered by NMR spectroscopy. On the other hand, standard NMR techniques are excellent at determining molecular composition, but defining the sizes of high-symmetry complexes can be difficult or not possible. Pulsed field gradient (PFG) NMR, a method for measuring diffusion rates, provides information about the sizes of molecules in solution.[25-29] PFG-NMR, used to study self-association of natural products,[30-32] peptides,[33,34] and proteins,[35-39] is also an emerging technique in supramolecular chemistry. Diffusion NMR has been used to define the aggregation state of ion pairs and other organometallic assemblies,[40-44] as well as determine the sizes of dendrimers, supramolecular polymers and nanoparticles.[45-48] The Cohen group have been pioneers in utilizing diffusion NMR in combinatorial and supramolecular chemistry.[49] Cohen and colleagues used diffusion NMR in host-guest chemistry, with detailed studies of macrocyclic complexes.[49-53] Recently, this technique has been used to investigate issues of structure and mechanism in molecular self-assembly. Hydrogen-bonded rosettes, calixarene-nucleoside conjugates and stacked bisphenylenes have been sized using diffusion NMR.[54-56] Solvation's key role in stabilizing resorcinarene capsules has been revealed through this technique.[57-59] In addition to structural characterization, diffusion NMR can also provide insight into dynamic processes that occur during self-assembly.[60-63]

3.4.2 PFG-NMR theory

PFG-NMR spectroscopy is a powerful technique for measuring diffusion coefficients in solution. Translational diffusion is the thermally random movement of molecules. The net distance traveled from where the molecule starts to where it ends is measured, the path the molecule travels is irrelevant. Figure 3.14 shows a molecule diffusing in two dimensions. Many variables can affect molecular diffusion such as the molecule's hydrodynamic properties, temperature, concentration, chemical exchange, reactions, restricted motion, and solvent viscosity.[25]

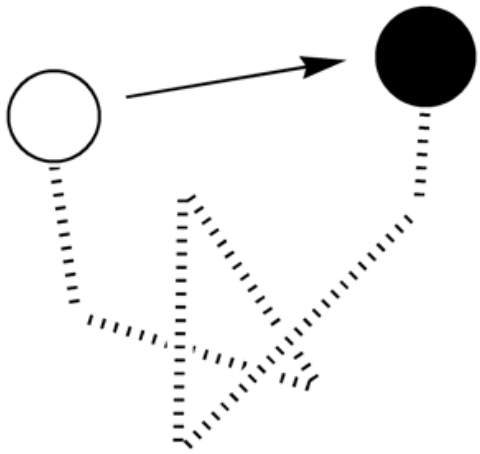

Figure 3.14. Translational motion of a molecule in two dimensions.

From the Stokes-Einstein equation and equations for the hydrodynamic frictional coefficients, the diffusion coefficient can be estimated from the size of the molecule. The Stokes-Einstein equation relates the diffusion coefficient to the hydrodynamic frictional coefficient, which is a function of the shape and size of the molecule (Equation 3.1), where k is the Boltzmann constant and T is the temperature in Kelvin. Using the hydrodynamic frictional coefficient for a sphere (Equation 3.2), the diffusion coefficient of a sphere is a function of the radius (Equation 3.3), where η is the solvent viscosity and R is the radius of the sphere. In this simplified approach, if two different diffusion coefficients of different spheres were measured in the same environment, the ratio of these diffusion coefficients would be inversely related to the radii of the spheres (Equation 3.4).[64]

$$D = \frac{k \cdot T}{f}$$

Equation 3.1. Diffusion coefficient related to the hydrodynamic frictional coefficient.

$$f = 6 \cdot \pi \cdot \eta \cdot R$$

Equation 3.2. Hydrodynamic frictional coefficient for a sphere.

$$D = \frac{k \cdot T}{6 \cdot \pi \cdot \eta \cdot R}$$

Equation 3.3. Diffusion coefficient related to the radius of a sphere.

$$\frac{D_a}{D_b} = \frac{\left(\frac{k \cdot T}{6 \cdot \pi \cdot \eta \cdot R_a} \right)}{\left(\frac{k \cdot T}{6 \cdot \pi \cdot \eta \cdot R_b} \right)} = \frac{R_b}{R_a}$$

Equation 3.4. Ratio of two diffusion coefficients related to a sphere.

Since the radius of a sphere is a function of its volume, the hydrodynamic radius can be estimated from a given volume (Equation 3.5). For shapes and geometries other than spheres (for example, in the case of the ribbon-like structures usually a rod-like model is applied) there are other equations for the hydrodynamic frictional coefficient. These equations and subsequent theories are well developed and mathematically derived.[65,66]

Using Equation 3.5, the relationship of a monomer to a dimer can be calculated by assuming that the dimer is a sphere of twice the volume. Relating the volume (v) to the radius of a monomer is calculated in Figure 3.15. Similarly, calculating the radius of a dimer that is twice the volume of a monomer is shown in Figure 3.16. Using these two radii, the ratio of diffusion coefficient of a dimer to the diffusion coefficient of a monomer should be equal to 0.794 (Figure 3.17).

$$v = \frac{4}{3} \cdot \pi \cdot R^3$$

Equation 3.5. Volume of a sphere, where R equals the radius.

$$v = \frac{4}{3} \cdot \pi \cdot \left(R_{monomer}\right)^3 \qquad R_{monomer} = \sqrt[3]{\frac{v}{\frac{4}{3} \cdot \pi}}$$

Figure 3.15. Calculation of the radius of a monomer of a sphere of a specific volume.

$$2 \cdot v = \frac{4}{3} \cdot \pi \cdot \left(R_{dimer}\right)^3 \qquad R_{dimer} = \sqrt[3]{\frac{2 \cdot v}{\frac{4}{3} \cdot \pi}} = \sqrt[3]{2} \cdot \sqrt[3]{\frac{v}{\frac{4}{3} \cdot \pi}}$$

Figure 3.16. Calculation of the radius of a dimer that is twice the volume of its monomer.

$$\frac{D_{dim}}{D_{mon}} = \frac{R_{mon}}{R_{dim}} = \frac{\sqrt[3]{\frac{x}{\frac{4}{3} \cdot \pi}}}{\sqrt[3]{2} \cdot \sqrt[3]{\frac{x}{\frac{4}{3} \cdot \pi}}} = \frac{1}{\sqrt[3]{2}} = 0.794$$

Figure 3.17. The ratio of the diffusion coefficients of a dimer to monomer.

The hydrodynamic radius is a function of both the size of the molecule and its solvation sphere(s). The solvation spheres observed are time averaged spheres.[67] In aqueous medium, the hydration spheres are complex and often difficult to predict accurately.[68-70] This is typically true for hydrogen bonding solvents, where solvent-solute interactions are strong. Fortunately, the solvation spheres in organic solvents are less of a problem due to the apolar nature of the solvents.

As mentioned before, there are several techniques for measuring diffusion coefficients but PFG-NMR has advantages of requiring low concentrations and being

noninvasive.[25] PFG-NMR utilizes a gradient field to measure the diffusion coefficients of molecules in an NMR tube. When a magnetic gradient field is applied to a sample, a magnetic field is generated in the z-axis of the NMR tube (Figure 3.18b). This magnetic gradient field is linear, so molecules on the bottom of the NMR tube feel the effects stronger than do the molecules at the top of the NMR tube.[49] The magnetic gradient field phase shifts the peaks in the NMR spectrum to a different frequency due to them being in different environments of the gradient field. This first magnetic gradient field pulse dephases the NMR spectrum by making it nonhomogenous. After a period of time (Δ), a second magnetic gradient field is applied in the opposite direction, which should rephase the system if the molecules are not diffusing (Figure 3.18b).[64] Under the correct conditions, the molecules should diffuse to another position in the NMR tube over time Δ.

When the molecules diffuse to a different position in the NMR tube, they will be in a different environment, and consequently the rephasing will not yield a coherent signal (Figure 3.18c). This scrambling of signals leads to the diminishing of peak intensities in the NMR spectrum, which can be plotted as a function of the diffusion coefficient.[71]

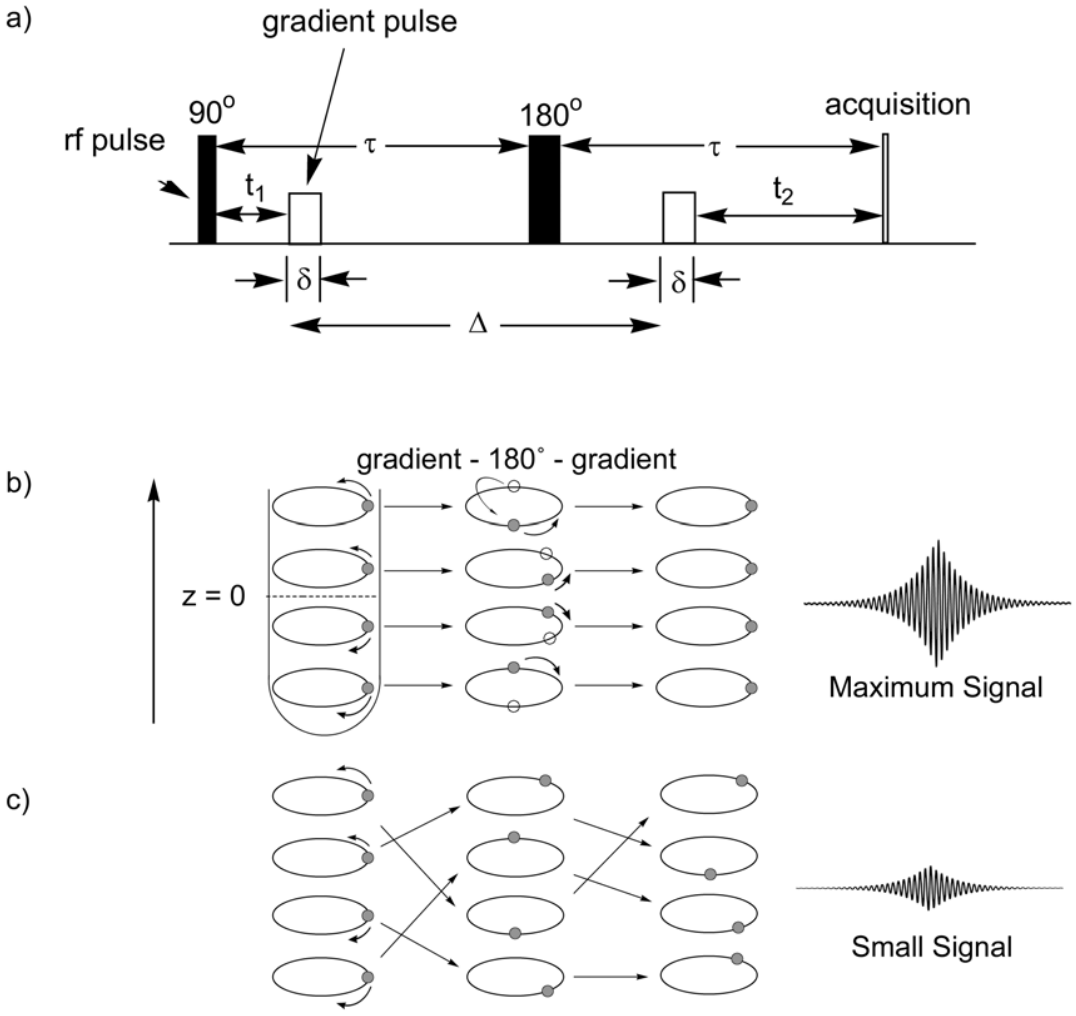

Figure 3.18. a) STE-PFG pulse sequence.[64] See text for more information. The effect of signal intensity from the PFG-NMR experiment b) without and c) with diffusion. The 90° rf pulse magnetically rotates the spins from the z-axis to the x-y axis. After application of a linear magnetic field gradient, the spins are phase shifted depending on the strength of the gradient. Following a 180° refocusing pulse, another magnetic field gradient is applied to shift the spins back into phase.[27]

The stimulated echo (STE) PFG sequence is shown in Figure 3.18a.[64] This sequence has the standard 90°- τ –180°- τ – acquire pulse sequence with the two gradient pulses inserted. The first 90° pulse causes the nuclei to align on the y-axis, after which a gradient is applied for specific duration (δ) and gradient strength (g). This gradient has the effect of dephasing the spectrum as previously mentioned. After time τ, a 180° pulse is delivered to refocus the net nuclear magnetic moment. After this refocusing pulse, another gradient is delivered in the opposite direction to rephase the spectrum. Finally, after another time period of τ, the spectrum is acquired. Following this sequence, the dephasing of the spectrum can be affected by the gradient strength (g), gradient duration (δ), and the mixing time (Δ) between the two opposite gradients.[64] The NMR signal

intensity is also a function of the diffusion coefficient as seen in Equation 3.6, where γ is the gyromagnetic ratio of the nucleus being studied. In theory, only two NMR spectra are needed to yield the diffusion coefficient, which would be an NMR spectrum without a gradient pulse and an NMR spectrum at a certain g, δ, and Δ. Stejskal-Tanner plots of the normalized signal intensity ($\ln(I/I_0)$) as a function of the gradient (Equation 3.7) are often used to calculate the diffusion coefficient from the slope of the line. Furthermore, this plot is used to evaluate if there is any exchange or other species overlapping with the signal. If there is one species, there is a single ordered exponential decay observed, while two different sized species would yield a second ordered exponential decay and so forth.

In the standard pulse sequence, once the δ and Δ are optimized, these values are kept constant, while the gradient strength is varied. In theory and in practice, changing one of these variables, while keeping the other two constant, produces the same results.[72-73]

$$I = I_0 \cdot e^{\left[(-D)\cdot(2\cdot\pi\cdot\gamma\cdot g\cdot\delta)^2\cdot\left(\Delta-\frac{\delta}{3}\right)\right]}$$

Equation 3.6. Intensity related to the diffusion coefficient and the gradient pulse.

$$\ln\left(\frac{I}{I_0}\right) = -D\cdot(2\cdot\pi\cdot\gamma\cdot g\cdot\delta)^2\cdot\left(\Delta-\frac{\delta}{3}\right)$$

Equation 3.7. Normalized intensity as a function of the diffusion coefficient and gradient pulse.

PFG-NMR is diverse in that a number of nuclei may be use to measure the diffusion coefficient. Nuclei such as ^{1}H, ^{13}C, ^{15}N, ^{31}P, and ^{10}F have been used to measure diffusion coefficients.[35,74] These nuclei are chosen depending on their resolution, abundance, and relaxation times, which affect the time and accuracy of the PFG-NMR experiment.

In PFG-NMR experiments, the diffusion coefficient is calculated from well resolved peaks to ensure accurate measurement of diffusion coefficients. Furthermore, the area, as opposed to the peak intensity, is used to give more accurate measurement of diffusion coefficients. In terms of hardware setup, certain steps are needed to ensure

accurate measurements of diffusion coefficients. First, the stability of the NMR spectrometer is critical. Vibrations may create fluctuations in the NMR, which can cause the diffusion coefficients to be unstable. Also, spinning causes similar disturbances, creating inaccurate measurements of the diffusion coefficient. Temperature control over the system is critical, since temperature plays a key role in the measurement of diffusion coefficients. The flow rate of nitrogen to cool the sample must be done at an optimal flow rate to cool the sample sufficiently, while not causing the sample to fluctuate. Along the same lines, convection currents caused by large volumes of solvent cause fluctuations in the sample. To limit these currents, Shigemi tubes are used to keep the solvent height of the NMR tube to 1 cm (Figure 3.19).[75-77] Furthermore, the sample height is kept at 1 cm so that it is in the radio frequency of the coils and so that the z-axis is linear to the volume occupied by the sample.[78] At this height, the sample will respond linearly to the power applied.[78] In addition, when comparing two samples, it is critical to keep the temperature and concentrations the same. The use of an internal standard in these experiments helps ensure that these conditions are identical. It is imperative that the gradient hardware and probe are calibrated for these experiments. Typically, nuclei that have a reasonable relaxation time are used for practical reasons concerning the length of the experiment.

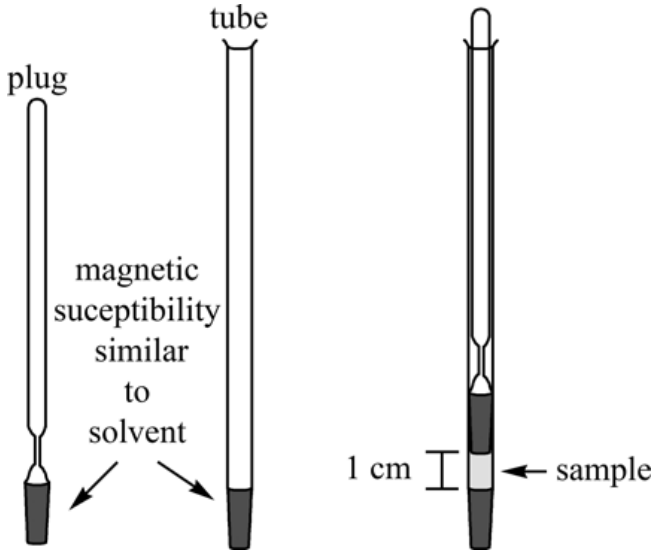

Figure 3.19. Shigemi tubes: plug, tube, and plug and tube assembled.

3.4.3 Static light scattering

The multi angle laser light scattering is the common technique[79] for determining the shape of the polymers through the mean square radius of gyration $< R_G >_Z$ and their structure through the particle scattering factor $P_Z(q)$, the molecular weight M_W, and the second virial coefficient A_2. Theory took great interests long time ago giving statistical sense to these parameters.[79-83] When A_2 is near zero and solutions considered as athermal according to general polymer theories[83] one may deal with the apparent molecular weight $M_{W,app}$ and use the so-called statistical dimensions determined at discrete concentrations[82] instead the one extrapolated at $c \to 0$. Looking at the variation of $M_{W,app}$ versus concentration or temperature allows equilibrium constant K to be evaluated which opens fields to dynamics of the scaffolds and to their assembly ability. The form factor $P_Z(qR)$ may be also useful to determine structural changes of the objects during the diffusion process of elementary unimers.[82] If the scattering window qR>>1, it is often necessary to fit the measurements with the whole form function P(qR). The form factor may derive from calculations especially when the structure of the coil is well known. Theoretical aspects are shortly reviewed in Chapter 5 (Experimental Part). It is shown typical processes for data calculations leading to zimm plot which yield to the molecular dimensions and solution thermodynamics.[79-81]All the data obtained for guanosines dG **1** and G **30** are summarized in Table 3.2.

reference	$<M>_w$ g/mole	$<R_G^2>_z^{1/2}$ nm	A_2 mol ml/g^2	dn/dc
dG **1**	3620	57	3.5 10^{-4}	0.0769
G **30**	5.93 10^5	43	-6.4 10^{-4}	0.083

Table 3.2. Molecular weights, radii of gyration, Virial cofficients and Differential refraction indexes determined in chloroform solutions for guanosines dG **1** and G **30**.

The zimm plot obtained from guanosine dG **1** at 25°C in $CHCl_3$ for different concentrations is shown in Figure 3.20. In this range of concentration, the apparent molecular weight was determined to be relatively stable below the gelation threshold. The linear regression reveals a modest molecular weight of 3620 (corresponding to an aggregation number of 6 to 7 units) but with a radius of gyration of 57 nm which

indicates the presence of large objects. The discrepancy between these two parameters is explained by the high polydispersity of the supramolecular polymer with an average of small ribbons together with a smaller population of large objects. Indeed, the gyration radius being determined from M_W, the importance of the large structures becomes predominant. The molecular weight of the polymers depends largely on the concentration range and a study between 5 and 50 mM reveals a power law of 0.75 which is higher than the value (0.6) for regular swollen coils and which is the signature for rigid objects of about 200 nm in length. Finally, the association constant was determined by plotting the molecular weight as a function of the concentration and shows a relatively small value K_0 = 400 L mol^{-1}.

When the polymer is homogeneous Flory Krigbaum[84] derived the more realistic model for A_2 introducing the κ enthalpy and ψ entropy parameter respectively. By comparison with the Flory-Huggins theory[85] these parameters are seen to be related by $\psi - \kappa = 1/2 - \chi$ where χ is the Flory Huggins interaction parameters. For ideal behaviour $\psi = \kappa$ and $A_2 = 0$ so the theta point is reached, with theta temperature being given by $\theta = T\frac{\kappa}{\psi}$ where T is the absolute temperature. The theory leads to some basics which are the equivalent size of the solvent and monomers respectively and a number of association for statistical calculations.

These statistical basics hold for derivative G **30** but comments on guanosine dG **1** may lie in the expression of idealized lattice model for second virial coefficient. It is obvious that one of the optimal conditions for association is an athermal solution which is what we found for derivative G **30** (Table 3.2).

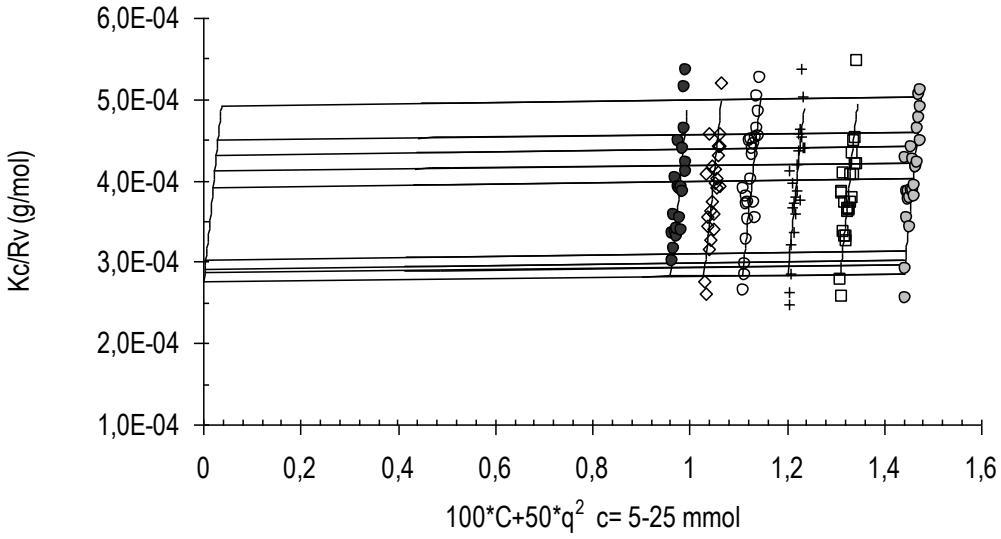

Figure 3.20. Zimm analysis by a two power law linear regression (full line) which yield to a good molecular size for molecule dG **1** from both extrapolations to $q, c \to 0$. M_W = 3620 Dalton and $<R_G^2>_z^{1/2}$ = 57 nm A_2= 3.5 10^{-4} mol ml/g^2 (●) = 1.44 10^{-2} g/ml ; (□) =1.31 10^{-2} g/ml ; (+) = 1.2 10^{-2} g/ml ; (○) = 1.11 10^{-2} g/ml.

In the case of guanosine G **30**, the light scattering shows a quite different behavior of the self-assembly process. The zimm plot in Figure 3.21 shows a smaller polidispersity than what is measured for derivative dG **1** together with higher molecular weights (M_W = 5.93 10^5; Dp = 1250), but with a close radius of gyration (43 nm) which might correlate with the formation of more compact objects. This expectation is confirmed by plotting the M_W in the range of concentration 7 to 14 mM. The experimentally determined power law of 0.3 is the signature for very compact objects such as spheres. Finally, the determination of the equilibrium constant for guanosine G **30** shows a strong association process (K_0 = 6.75 10^5 L mol^{-1}) and a complex behavior of a sigmoid type (Figure 3.22). This non-linear effect indicates a cooperative process and the hierarchical association between the linear supramolecular ribbons with their organization in higher ordered self-assembled structures that in turn stabilize the primary association.

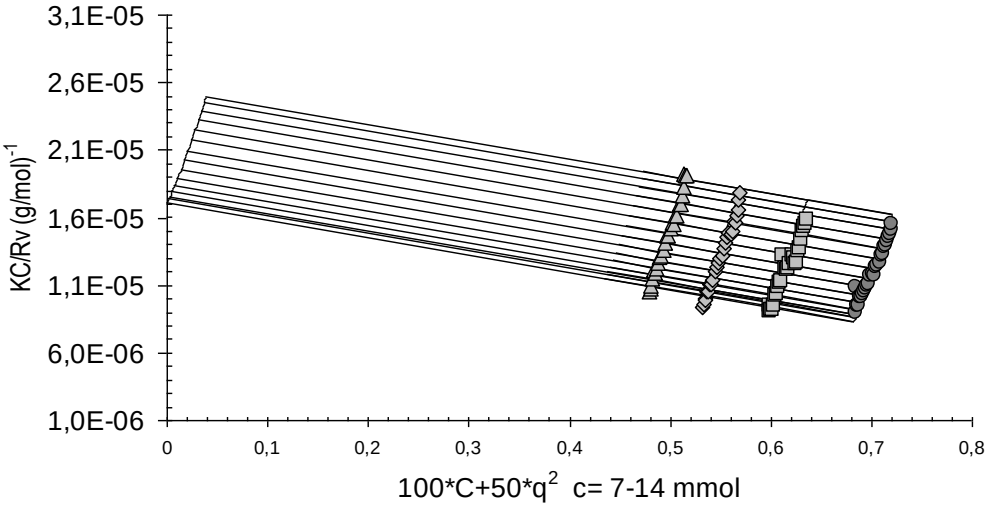

Figure 3.21. Zimm analysis by a two power law linear regression (full line) which yield to the molecular size for molecule G **30** from both extrapolations to $q, c \rightarrow 0$. M_W = 5.93 10^5 Dalton and $<R_G^2>_Z^{1/2}$ = 43 nm A_2 = -6.4 10^{-4} mol ml/g^2 (●) = 6.82 10^{-3} g/ml ; (■) =5.97 10^{-3} g/ml; (♦) = 5.31 10^{-3} g/ml ; (▲) = 4.78 10^{-3} g/ml.

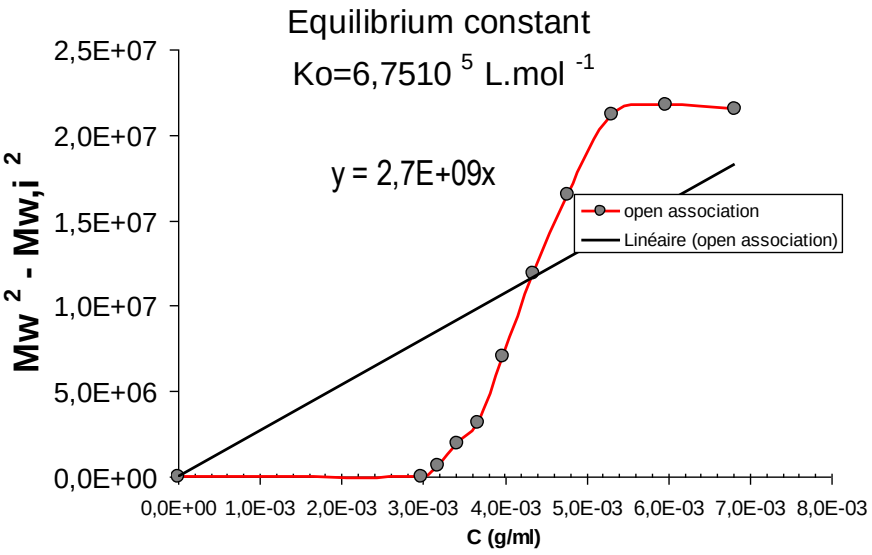

Figure 3.22. M_W, i is the molecular weight of the initial monomer starting the association. From the straight line it is possible to calculated the equilibrium constant of the association K_0 = 6.7 10^5 L mol^{-1} for derivative G **30**.

3.4.4 Transmission electron microscopy

Structural observation of self-assembled system can easily be achieved by TEM approaches, these has been widely used and described in the literature.[86] The samples are prepared in standard conditions as described in literature.[87]

Guanosine derivative dG **1** in bromoform (50 mM) forms small short fibers (Figure 3.23). These fibers present a diameter of 6 nm and a length of approximatively 200 nm. The precise length cannot be determined as the fibers present a high entanglement ratio but is in agreement with the light scattering data. The small individual fibers self-assemble in larger ones to form bundles of 30 nm. These latter can be formed during the preparation step as the diameter of the bundles varies from one experiment to another. The distribution of the fibers within a clear network illustrates the organogelator properties of guanosine dG **1**.

Guanosine derivative G **30** in bromoform (8.14 mM) forms small aggregates and small lamellar structures. It shows a high variability of sizes but never highly ordered structures (Figure 3.24). The aggregation of the ribbons within highly compact lamellar structures is also in good agreement with the light scattering experiments that indicates mainly the presence of pseudo-spherical objects with a strong cooperative effect occurring between the ribbons and their higher scale self-assemblies.

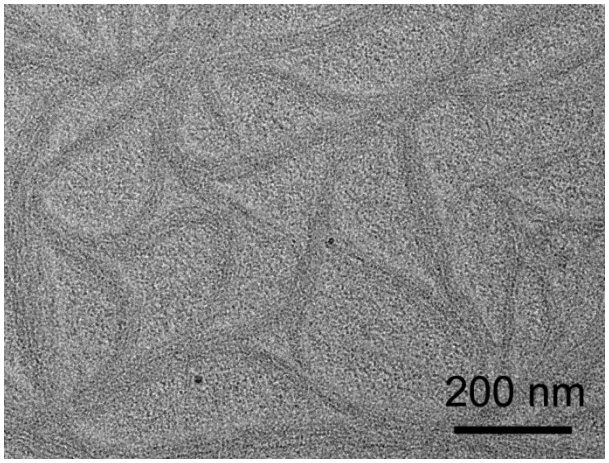

Figure 3.23. TEM image of guanosine derivative dG **1**

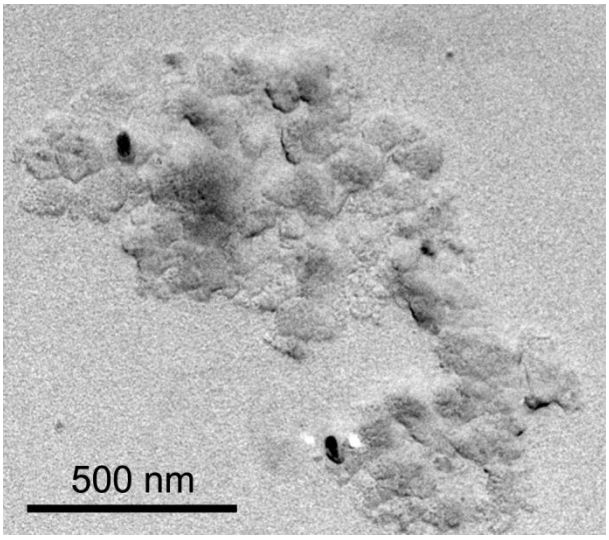

Figure 3.24. TEM image of guanosine derivative G **30**.

In conclusion, in these last sections we have shown the hierarchical polymeric natures of the self-assemblies obtained from the ribbon forming guanosine derivatives dG **1** and G **30**. The light scattering measurements appeared as an appropriate technique for the molecular weight determination versus the structure of this objects that are both concentration sensitive. The main conclusions were confirmed by TEM. Lipophilic guanosine dG **1** forms very soft fibrillar objects of 6 nm of diameter and 200 nm in length and that in turn produces bundles of networked fibers with 30 nm of diameter. Despite its closely related structure, guanosine G **30** forms much longer ribbons with molecular weights up to 6 10^5 that in turn fold in very compact aggregates with lamellar structures. This process has been shown to be highly cooperative by the determination of the molecular weight as a function of the concentration.

These investigations furnish an explanation to the gelation properties of these two derivatives and can be used to rationalize the synthesis of functional guanosine-based soft materials.

3.5 Conclusion

One particular intriguing objective in supramolecular self-assembly is to reach a high level of control over the shape and size of the supramolecular architectures, in order to produce well-defined functional nanostructures by rational design. In this direction, many investigation have been pursued toward the construction of self-assembled objects

from numerous low-molecular weight scaffolds, for instance by exploiting multiple directional hydrogen-bonding interactions. In particular, the possibility of producing well-define and highly ordered guanine supramolecular structures like the ribbons presented here may be of interest for the fabrication of molecular nanowires within the framework of future molecular electronic applications.

References

1. a) I. C. M. Kwan, A. Wong, Y-M. She, M. E. Smith, G. Wu, *Chem. Commun.* **2008**, *682*; b) I. C. M. Kwan, Y-M. She, G. Wu, *Chem. Commun.* **2007**, *4286*.
2. G. Gottarelli, P. Mariani, S. Masiero, E. Mezzina, M. Recanatini, G. P. Spada *Helv. Chim. Acta* **1998**, *81*, 2078.
3. U. Thewalt, C.E. Bugg, R.E. Marsh, *Acta Crystallogr. Sect. B* **1970**, *26*, 1089-1101.
4. R. J. H. Hafkamp, M. C. Feiters, R. J. M. Nolte, *J. Org. Chem.* **1999**, *64*, 412- 426.
5. For an exhaustive review on the chirality transfer in self-assembly processes see: M. C. Feiters, R. J. M. Nolte, in *Advances in Supramolecular Chemistry, Vol. 6* (Ed.: G. W. Gokel), JAI, Stamford, **2000**, p. 41; L. Brunsveld, Ph.D. Thesis, University of Eindhoven, **2001**.
6. Samorì, P., Pieraccini, S., Masiero, S., Spada, G. P., Gottarelli, G., & Rabe, J. P. *Colloids and Surfaces B* **2002**, *23*, 283.
7. a) G. Gottarelli, G. P. Spada, A. Garbesi in *Comprehensive Supramolecular Chemistry: Templating, Self-assembly and Self-organisation, Vol. 9* (Eds.: J. M. Lehn, J.-P. Sauvage, M. W. Hosseini), Pergamon, Oxford, **1996**, Chapter 13.
8. The serendipitous discovery of the self-assembly of simple guanilates leading to liquid-crystal phases was narrated in: G. Gottarelli, G. P. Spada, *Chem. Rec.* **2004**, *4*, 39.
9. W. Guschlbauer, J. F. Chantot, D. Thiele, *J. Biomol. Struct. Dyn.* **1990**, *8*, 491.
10. S. Pieraccini, G. Gottarelli, P. Mariani, S. Masiero, L. Saturni, G. P. Spada, *Chirality* **2001**, *13*, 7.
11. S. Pieraccini, T. Giorgi, G. Gottarelli, S. Masiero, G. P. Spada, *Mol. Cryst. Liq. Cryst.* **2003**, *398*, 57.
12. K. Kanie, T. Yasuda, S. Ujiie and T. Kato, *Chem. Commun.*, **2000**, 1899 and references cited within.
13. G. Gottarelli, S. Masiero, E. Mezzina, S. Pieraccini, G. P. Spada, P. Mariani *Liq. Cryst.* **1999**, *26*, 965.
14. a) K. Araki, I. Yoshikawa, *Top. Curr. Chem.* **2005**, *256*, 133; b) T. Sato, M. Seko, R. Takasawa, I. Yoshikawa, K. Araki, J. *Mater. Chem.* **2001**, *11*, 3018.
15. Yoshikawa, I.; Yanagi, S.; Yamaij, Y.; Araki, K. *Tetrahedron*, **2007**, *63*, 7474.

16. a) R. Rinaldi, G. Maruccio, A. Biasco, V. Arima, R. Cingolani, T. Giorgi, S. Masiero, G. P. Spada, G. Gottarelli, *Nanotechnology* **2002**, *13*, 398; b) G. Maruccio, P. Visconti, V. Arima, S. D'Amico, A. Biasco, E. D'Amone, R. Cingolani, R. Rinaldi, S Masiero, T Giorgi, G. Gottarelli, *Nano Lett.* **2003**, *3*, 479; c) R. Rinaldi, E. Branca, R. Cingolani, S. Masiero, G. P. Spada, G. Gottarelli, *Appl. Phys. Lett.* **2001**, *78*, 3541; d) H. Liddar, J. Li, A. Neogi, P. B. Neogi, A. Sarkar, S. Cho, M. Morkoç, *App. Phys. Lett.* **2008**, *92*, 013309; e) A. Neogi, J. Li, P. B. Neogi, A. Sarkar, H. Morkoc, *Electron. Lett.* **2004**, *40*, 1605.
17. Reinhoudt, D. N.; Crego-Calama, M. *Science* **2002**, 295, 2403-2407.
18. Whitesides, G. M.; Simanek, E. E.; Mathias, J. P.; Seto, C. T.; Chin, D. N.; Mammen, M.; Gordon, D. M. *Acc. Chem. Res.* **1995**, *28*, 37-44.
19. Prins, L. J.; Reinhoudt, D. N.; Timmerman, P. *Angew. Chem. Int. Ed.* **2001**, *40*, 2383-2426.
20. Schalley, C. A. *Mass Spectrom. Rev.* **2001**, *20*, 253-309.
21. Isaacs, L.; Witt, D.; Lagona, J. *Org. Lett.* **2001**, *3*, 3221-3224.
22. Michels, J. J.; O'Connell, M. J.; Taylor, P. N.; Wilson, J. S.; Cacialli, F.; Anderson, H. L. *Chem.-Eur. J.* **2003**, *9*, 6167-6176.
23. Schubert, D.; Tziatzios, C.; Schuck, P.; Schubert, U. S. *Chem.-Eur. J.* **1999**, *5*, 1377-1383.
24. Fenniri, H.; Deng, B. L.; Ribbe, A. E. *J. Am. Chem. Soc.* **2002**, *124*, 11064-11072.
25. Price, W. S., In *New Advances in Anal. Chem.*, Ed.: Atta-ur-Rahman, E., Gordon and Breach Science Pub: Amsterdam, **2000**, 31-72.
26. Stilbs, P. *Prog. NMR Spectrosc.* **1987**, *19*, 1-45.
27. Price, W. S. *Concepts Magn. Resonan.* **1997**, *9*, 299-336.
28. Price, W. S. *Concepts Magn. Reson.* **1998**, *10*, 197-237.
29. Johnson, C. S. *Prog. Nucl. Magn. Reson. Spectrosc.* **1999**, *34*, 203-256.
30. Lo, M. C.; Helm, J. S.; Sarngadharan, G.; Pelczer, I.; Walker, S. *J. Am. Chem. Soc.* **2001**, *123*, 8640-8641.
31. Daranas, A. H.; Fernandez, J. J.; Morales, E. Q.; Norte, M.; Gavin, J. A. *J. Med. Chem.* **2004**, *47*, 10-13.
32. Shikii, K.; Sakamoto, S.; Seki, H.; Utsumi, H.; Yamaguchi, K. *Tetrahedron* **2004**, *60*, 3487-3492.
33. Mayo, K. H.; Ilyina, E.; Park, H. *Protein Sci.* **1996**, *5*, 1301-1315.

34. Yao, S. G.; Howlett, G. J.; Norton, R. S. *J. Biomol. NMR* **2000**, *16*, 109-119.
35. Altieri, A. S.; Hinton, D. P.; Byrd, R. A. *J. Am. Chem. Soc.* **1995**, *117*, 7566-7567.
36. Ilyina, E.; Roongta, V.; Pan, H.; Woodward, C.; Mayo, K. H. *Biochemistry* **1997**, *36*, 3383-3388.
37. Krishnan, V. V. *J. Magn. Reson.* **1997**, *124*, 468-473.
38. Price, W. S.; Tsuchiya, F.; Arata, Y. *J. Am. Chem. Soc.* **1999**, *121*, 11503-11512.
39. Wills, P. R.; Georgalis, Y. *J. Phys. Chem.* **1981**, *85*, 3978-3984.
40. Otto, W. H.; Keefe, M. H.; Splan, K. E.; Hupp, J. T.; Larive, C. K. *Inorg. Chem.* **2002**, *41*, 6172-6174.
41. Beck, S.; Geyer, A.; Brintzinger, H. H. *Chem. Commun.* **1999**, 2477-2478.
42. Keresztes, I.; Williard, P. G. *J. Am. Chem. Soc.* **2000**, *122*, 10228- 10229.
43. Martinez-Viviente, E.; Pregosin, P. S.; Vial, L.; Herse, C.; Lacour, J. *Chem.-Eur. J.* **2004**, *10*, 2912-2918.
44. Valentini, M.; Ruegger, H.; Pregosin, P. S. *Helv. Chim. Acta* **2001**, *84*, 2833-2853.
45. Gorman, C. B.; Smith, J. C.; Hager, M. W.; Parkhurst, B. L.; Sierzputowska-Gracz, H.; Haney, C. A. *J. Am. Chem. Soc.* **1999**, *121*, 9958-9966.
46. Kohlmann, O.; Steinmetz, W. E.; Mao, X. A.; Wuelfing, W. P.; Templeton, A. C.; Murray, R. W.; Johnson, C. S. *J. Phys. Chem. B* **2001**, *105*, 8801-8809.
47. ten Cate, A. T.; Dankers, P. Y. W.; Kooijman, H.; Spek, A. L.; Sijbesma, R. P.; Meijer, E. W. *J. Am. Chem. Soc.* **2003**, *125*, 6860-6861.
48. Valentini, M.; Vaccaro, A.; Rehor, A.; Napoli, A.; Hubbell, J. A.; Tirelli, N. *J. Am. Chem. Soc.* **2004**, *126*, 2142-2147.
49. Cohen, Y.; Avram, L.; Frish, L. *Angew. Chem. Int. Ed.* **2005**, *44*, 520-554.
50. Avram, L.; Cohen, Y. *J. Org. Chem.* **2002**, *67*, 2639-2644.
51. Frish, L.; Sansone, F.; Casnati, A.; Ungaro, R.; Cohen, Y. *J. Org. Chem.* **2000**, *65*, 5026-5030.
52. Frish, L.; Vysotsky, M. O.; Matthews, S. E.; Bohmer, V.; Cohen, Y. *J. Chem. Soc.-Perkin Trans. 2* **2002**, 88-93.
53. Gafni, A.; Cohen, Y. *J. Org. Chem.* **1997**, *62*, 120-125.
54. Kotch, F. W.; Sidorov, V.; Lam, Y. F.; Kayser, K. J.; Li, H.; Kaucher, M. S.; Davis, J. T. *J. Am. Chem. Soc.* **2003**, *125*, 15140-15150.
55. Shenhar, R.; Wang, H.; Hoffman, R. E.; Frish, L.; Avram, L.; Willner, I.; Rajca, A.; Rabinovitz, M. *J. Am. Chem. Soc.* **2002**, *124*, 4685-4692.

56. Timmerman, P.; Weidmann, J. L.; Jolliffe, K. A.; Prins, L. J.; Reinhoudt, D. N.; Shinkai, S.; Frish, L.; Cohen, Y. *J. Chem. Soc.-Perkin Trans. 2* **2000**, 2077-2089.
57. Avram, L.; Cohen, Y. *J. Am. Chem. Soc.* **2002**, *124*, 15148-15149.
58. Avram, L.; Cohen, Y. *Org. Lett.* **2002**, *4*, 4365-4368.
59. Avram, L.; Cohen, Y. *Org. Lett.* **2003**, *5*, 1099-1102.
60. Cabrita, E. J.; Berger, S. *Magn. Reson. Chem.* **2002**, *40*, S122-S127.
61. Johnson, C. S. *J. Magn. Reson. Ser. A* **1993**, *102*, 214-218.
62. Lin, M. F.; Larive, C. K. *Anal. Biochem.* **1995**, *229*, 214-220.
63. Regan, D. G.; Chapman, B. E.; Kuchel, P. W. *Magn. Reson. Chem.* **2002**, *40*, S115-S121.
64. Stejskal, E. O.; Tanner, J. E. *J. Chem. Phys.* **1965**, *42*, 288-192.
65. Crank, J., *The Mathematics of Diffusion*. 2nd Ed., Claxendon Press: Oxford, **1975**.
66. Cussler, E. L., *Diffusion: Mass Transfer in Fluid Systems*. Cambridge University Press: Cambridge, **1984**.
67. Mayzel, O.; Gafni, A.; Cohen, Y. *Chem. Commun.* **1996**, 911-912.
68. Halle, B.; Denisov, V. P., *Methods Enzymol*. **2001**, *338*, 178-201.
69. Otting, G. *Prog. Nucl. Magn. Reson. Spectrosc.* **1997**, *31*, 259-285.
70. Gerothanassis, I. P. *Prog. Nucl. Magn. Reson. Spectrosc.* **1994**, *26*, 171 -237.
71. Hahn, E. L. *Phys. Rev.* **1950**, *80*, 580.
72. Price, W. S.; Walchli, M. *Magn. Reson. Chem.* **2002**, *40*, S128-S132.
73. Price, W. S.; Stilbs, P.; Jonsson, B.; Soderman, O. *J. Magn. Reson.* **2001**, *150*, 49-56.
74. Pregosin, P. S.; Kumar, P. G. A.; Fernandez, I. *Chem. Rev.* **2005**, *105*, 2977-2998.
75. Martin, G. E.; Crouch, R. C.; Zens, A. P. *Magn. Reson. Chem.* **1998**, *36*, 551-557.
76. Reynolds, W. F.; Yu, M.; Enriquez, R. G.; Leon, I. *Magn. Reson. Chem.* **1997**, *35*, 505-519.
77. Crouch, R. C.; Martin, G. E.; Musser, S. M.; Grenade, H. R.; Dickey, R. W. *Tetrahedron Lett.* **1995**, *36*, 6827-6830.
78. Lapham, J.; Rife, J. P.; Moore, P. B.; Crothers, D. M. *J. Biomol. NMR* **1997**, *10*, 255-262.
79. P. Debye, *Phys. Coll. Chem*. **1947** , *51*, 18; B. H. Zimm, *J. Chem. Phys.* **1948**, *16*, 1093.

80. H. C. Benoit, J. S. Higgins, *Polymers and Neutron scattering*, Clarendon Press, Oxford, 1994.
81. B. Chu, *Laser light scattering*, 2nd Edition, Academic Press Limited, London, 1991.
82. M. B. Huglin, *Light scattering from polymer solutions*, Academic Press N.Y., 9, p 397 (1972); Elias H.G. in "*Light scattering from polymer solutions*" Ed. M. B. Huglin academic press, London, **1972**, p. 428.
83. A. Libeyre, D. Sarazin, J. François, *J. Polym. Bull*. **1981**, *4*, 53.
84. P.J. Flory and W. R. Krigbaum, *J. Chem. Phys.* **1950**, *18*, 1086.
85. PJ Flory, *Principles of polymer chemistry*, Cornell University Press, N.Y. 1957.
86. Schmidt et al., *Langmuir* **2002**, *18*, 5668; A. Petitjean, L. A. Cuccia, M. Schmutz, J.-M. Lehn, *J. Org. Chem*. **2008**, *73*, 2481.
87. V. Berl, M. J. Krische, I. Huc, J.-M. Lehn, M. Schmutz, *Chem. Eur. J.* **2000**, *6*, 1838.

Chapter 4. Photoresponsive Supramolecular Self-Assemblies

The majority of this Chapter has been published in:

- S. Yagai, A. Kitamura, *Chem. Soc. Rev.* **2008**, *37*, 1520.
- S. Lena, P. Neviani, S. Masiero, S. Pieraccini, G. P. Spada, *Ang. Chem. Int. Ed*, **2010**, DOI: 10.1002/anie.201000805

'the use of photochromic molecules in supramolecular self-assemblies is the most reasonable method to noninvasively manipulate their degree of aggregation and supramolecular architectures.'

4.1 Introduction

Dynamic supramolecular self-assembly can be controlled either by changing the external environment or by in situ morphological transformation of building blocks.

Specifically, the former strategy might be achieved by varying the temperature and the concentration of solutions, or the polarity of medium. On the other hand, the latter strategy requires external input leading to a large mechanical motion of building blocks.

The modification of photochromic molecules with noncovalent interaction sites or the incorporation of photochromic molecules into self-assembling modules makes light an ideal external input to establish this strategy. Photoinduced mechanical motion (photoisomerization) of photochromic molecules generally leaves no chemical waste, and furthermore it can be repeated reversibly without addition of any chemical substance. If two photoisomers absorb different wavelengths of light, fully controlled two-state photoswitchable molecular systems and materials can be created.[1–13] Especially for multicomponent self-assemblies, a large number of photoresponsive systems exhibiting a photocontrollable degree of aggregation and/or self-assembled architectures have been successfully created so far.[14]

4.2 On Switches: What is a Photochromic Molecular Switch?

Organic molecular photochromic switches are molecules that can be interconverted reversibly between two (meta)-stable states, **A** and **B**, by stimulus with light (Figure 4.1) This change is the result of *cis→trans* photoisomerization, photocyclisation or a combination of the two. For the switch to be useful, it should meet three criteria: (1) it should be thermally stable; (2) the states **A** and **B** should have

different properties, such as a large change in molecular geometry, polarity, UV–Vis absorption, etc., and (3) both states of the switch should be separately addressable. In principle, an ideal photochromic switch would exhibit perfect photocontrol. This means that irradiation at different wavelengths (λ_1 and λ_2) allows quantitative photoconversion to states **A** and **B**, respectively. The ability to address each isomer selectively necessitates that **A** and **B** possess significant differences in their UV–Vis absorption spectra. In many cases this change in absorption is a desirable property in itself.[15,1] Systems with excellent photoequilibria have the obvious advantage that the change in property conveyed by the isomerization is maximized. In practice, however, this is rarely the case. Below it is present a brief description of several of the different types of switches such as spiropyrans, azobenzenes, dithienylethenes and other alkenes, i.e., switches based on C=C double bond *cis→trans* isomerization.

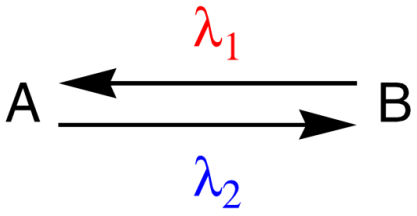

Figure 4.1. Schematic representation of a molecular photochromic switch.

4.2.1 Spiropyrans

Spiropyrans are molecular switches that can undergo reversible photoisomerization between a stable state and a metastable state using UV and/or visible light. They are well suited to control the surface free energy by light, since the relatively hydrophobic ‘closed’ spirocyclic isomer can be reversibly converted to a highly polar hydrophilic zwitterionic merocyanine isomer that has a much larger dipole moment as sketched in Figure 4.2. The thermal conversion from the merocyanine isomer back to the closed spirocyclic form occurs typically with a half-life at room temperature of tens of minutes in non-polar media, while the photochemical isomerization with visible light occurs on a much faster timescale.[16-18]

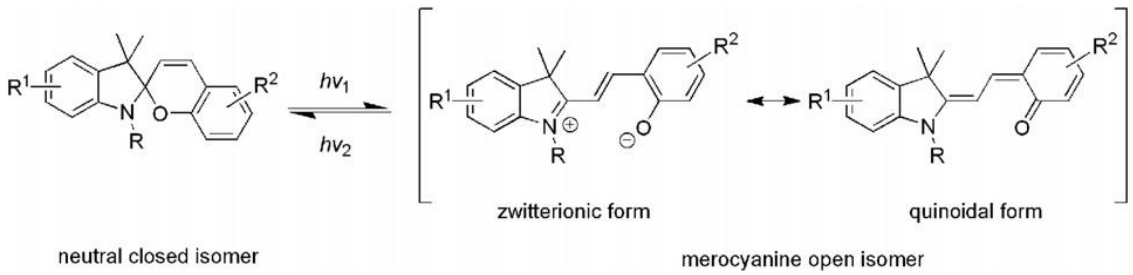

Figure 4.2. Schematic representation of the reversible photoisomerization of spiropyran moieties.

4.2.2 Azobenzenes

Functionalized azobenzenes have received considerable experimental and theoretical attention because they undergo light-driven *trans*→*cis* isomerization. Their *cis*- and *trans*-isomers have a different spatial arrangement of the aromatic moieties, and consequently show significantly different physical and chemical properties, as shown in Figure 4.3.[19] A major advantage of azobenzene switches is that they are easy to synthesize.

However, an important drawback is that, depending on the nature of the substituents on the aromatic groups, these switches often undergo thermal *cis*→*trans* isomerization at room temperature.

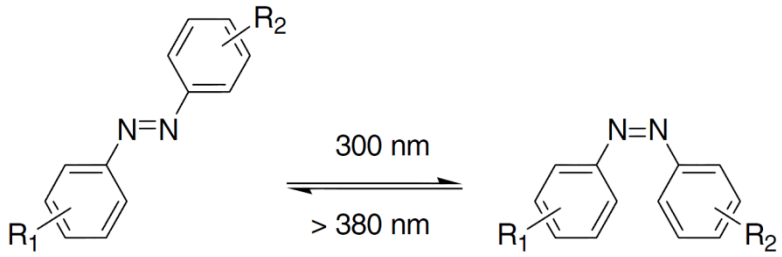

Figure 4.3. Reversible photoisomerization of azobenzene moieties upon UV–Vis irradiation. The *trans*-isomer is planar and the *cis*-isomer is bent and more compact.

4.2.3 Dithienylethenes

1,2-Dithienylethenes are reversible molecular switches consisting of conjugated parts connected by a switching element.[20,21] There are two isomers, i.e., a closed form and an open form of the molecule as sketched in Figure 4.4. The π-conjugation extends over the entire molecule in the closed form whereas it is restricted to each half of the molecule

in its open form. As a consequence, the closed form is expected to exhibit intrinsically better electrical conductance properties than the open form. The transition from closed to open form takes place for wavelengths $500 < \lambda < 700$ nm; for the reverse, one requires $300 < \lambda < 400$ nm. Furthermore, dithienylethenes usually exhibit excellent thermal stability.

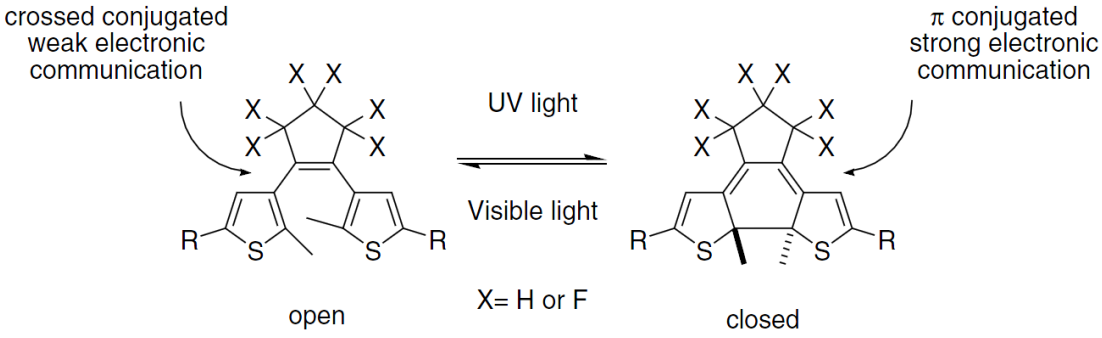

Figure 4.4. Reversible photocyclisation of 1,2-dithienylethene moieties upon UV–Vis light irradiation.

4.2.4 Alkenes

The last class of switches dealt with here are olefins which undergo a *cis*→*trans* photoisomerization schematically shown in Figure 4.5, a process which forms the basis for vision.[10] The best-studied group among these systems is the stilbenes, the photochemical isomerization process of which have been reviewed extensively.[10,22] While simple stilbenes also undergo undesired photochemical side reactions making them unattractive as switches, other robust switches have been prepared from olefins including overcrowded alkenes[23] and maleimides.[24] A key advantage of these systems is that they are generally thermally stable and photochemically robust. As with the switches discussed previously, the properties of stilbenes can be highly sensitive to the precise structure, including examples with perfect photocontrol.[25] Additionally, these molecular switches have formed the basis for light-driven molecular rotary motors.[26]

The photoisomerization of alkenes can also be used to indirectly modulate the strength of association between hydrogen-bonded systems, which form the basis of molecular shuttles constructed from interlocked molecules such as rotaxanes or catenanes.[27] Stimuli-responsive rotaxanes are molecular shuttles in which the macrocycle is interlocked onto the thread with one, two or more different binding sites (‘stations’)

and terminated with two bulky stoppers.[27,28] The architecture of various types of rotaxanes permit large amplitude motion of the mechanically interlocked subunits in response to an external trigger like light, electrons, temperature, pH, nature of the environment, reversible covalent bond formation, etc.[27–29] Switchable rotaxanes have been successfully used to vary physical properties such as conductivity,[30] induced circular dichroism,[31] or fluorescence[32] and are therefore viewed as potential elements for artificial molecular machinery.

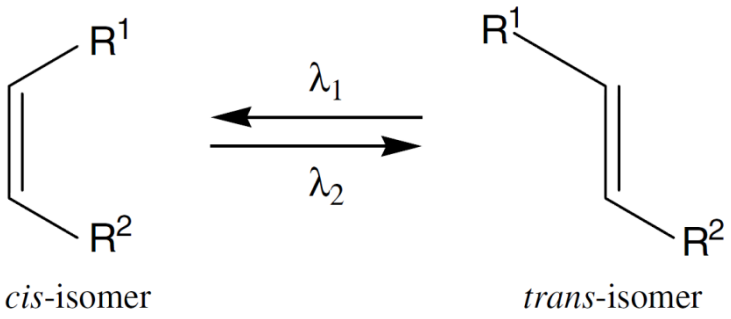

Figure 4.5. General scheme for the photochemical interconversion between the *cis* and *trans* configurations of an alkene.

4.3 Photoresponsive Self-Assembling Systems: General Strategy

The basic idea for manipulating supramolecular self-assemblies by external light input has already been put forward by Shinkai et al. in 1987.[33] They prepared self-complementary azobenzene derivatives **32** functionalized on one end by an ω-ammoniumalkyl and on the other by a crown ether (Figure 4.6a). The self-aggregation properties of these molecules in organic media can be controlled by light because their *trans*-isomers favor cyclic oligomerization whereas their *cis*-isomers undergo intramolecular complexation between the two interactive sites, generating a closed monomer. On the other hand, photocontrollable polymeric assemblies were achieved by mixing symmetrically crown-functionalized azobenzene **33** and oligomethylene-α,ω-diammonium cations **34** (Figure 4.6b).[34]

In both the systems, the bent conformation of *cis*-azobenzene isomer plays an important role as non-aggregative building blocks by forming ‘‘closed’’ supramolecular species. The same approach was employed for the construction of photoresponsive self-assemblies of cyclic oligopeptides.[35]

More easily, if the molecular structure or the chemical property of either photoisomer is less aggregative compared to the other, or if we can adjust conditions (e.g., solvent polarity, concentration and temperature) to be unfavorable for the aggregation of either photoisomer, we can make photoresponsive self-assemblies where the degree of aggregation can be controlled by light input. For instance, the *cis*-isomer of azobenzene is morphologically less aggregative because of its bent conformation disadvantageous for dense molecular packing. Moreover, *cis*-azobenzene is more polar compared to the *trans*-isomer,[36] and thereby less aggregative in polar media (see **4.3.2**).[37,38] A variety of photoresponsive self-assemblies have been established based on these principles, which include photoresponsive micelles, supramolecular polymers and organogels.[14,39,40]

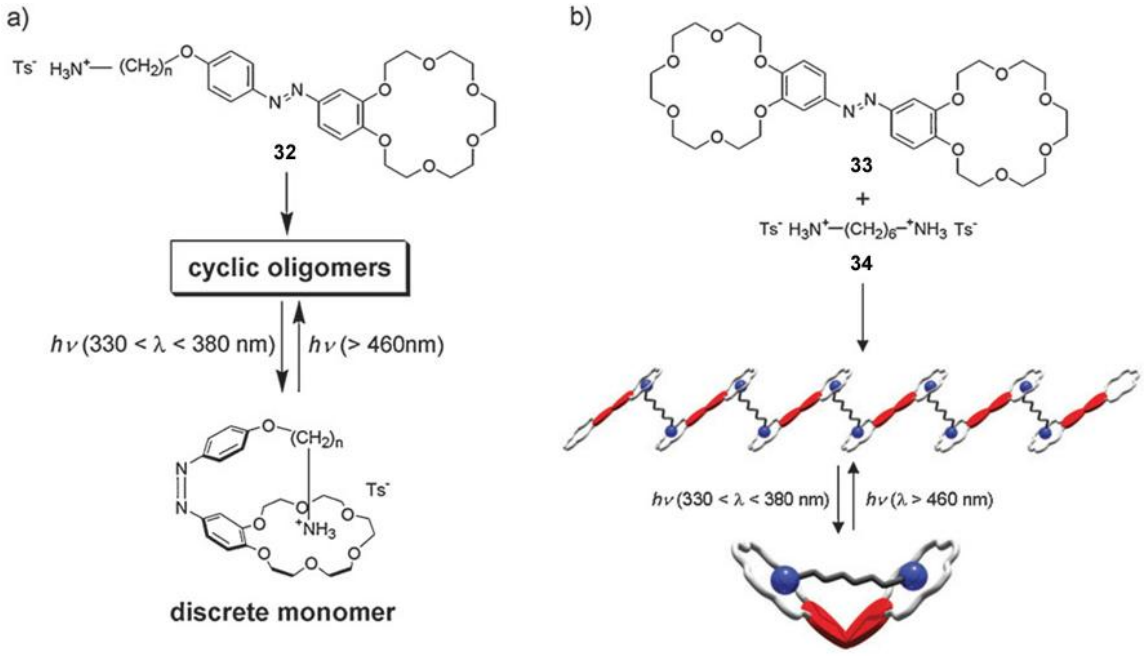

Figure 4.6. Photoresponsive self-assemblies established by Shinkai et al. (a) One-component system achieved by self-complementary azobenzene **32** functionalized on one end by an ω-ammoniumalkyl and on the other by a crown ether. (b) Two-component system achieved by the mixture of symmetrical azocrown **33** and α,ω-diammoniumalkane **34**.

Self-aggregation of **35a**[41] and **35b**[42] based on diarylethene photochromic molecules[21] shows contrasting photoresponses (Figure 4.7). In the case of **35a**, the flexible 'open' isomer is more aggregative than the rigid 'closed' isomer. In sharp contrast, the 'open' isomer of **35b** is not capable of aggregating and vice versa. This

might be related to the fact that the hydrogen-bonding interaction of **35b** is more directional and specific, thereby vulnerable to the conformational freedom of the building blocks. Analogues of **35a** have recently been applied as building blocks for substantially important photoresponsive self-assemblies where supramolecular chirality of ensembles can be transcribed into molecular chirality by external light input.[43-47] Self-aggregation of diarylethene **35c** occurs in aqueous media through a π-π stacking interaction, which can be controlled photochemically due to the change in molecular planarity upon open (aggregative)–close (dissociative) isomerization.[48]

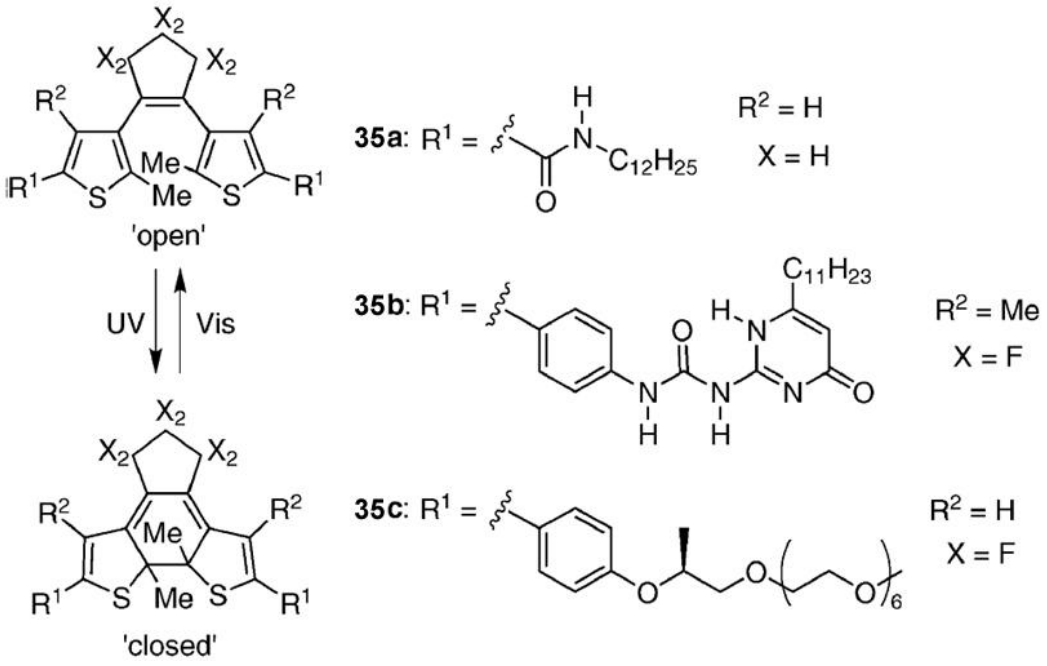

Figure 4.7. Self-assembling diarylethene photochromic molecules **35a**–**c**.

Thus, the systems introduced in this section exemplify generally employed strategies to obtain photoresponsive smart self-assemblies.

4.3.1 Controlling two distinct extended supramolecular structures

The use of two distinct conformations of photochromic molecules given by photoisomerization as building blocks for the extended supramolecular polymerization provides self-assemblies where two extended supramolecular architectures can be guided by light input. However, the construction of such systems appears to be extremely difficult because one of the two photoisomers of most photochromic molecules are

generally flexible, and thereby unsuitable as building blocks for extended supramolecular architectures. One example of this type of photoresponsive self-assembly has been reported by Sleiman and co-workers. They found that the *trans*- and the *cis*-isomers of azodibenzoic acid derivative **36** self-assemble into distinct higher-order structures (Figure 4.8).[49] Vapor pressure osmometry (VPO), NMR, single crystal and powder X-ray measurements and semiempirical calculations demonstrated that the *trans*-isomer forms linear tapelike aggregates whereas the *cis*-isomer generates a discrete tetramer.

Remarkably, hierarchically organized rod-like superstructures have been visualized for the *cis*-isomer by using transmission electron microscopy, which was proposed to be constructed through extended π-π stacking of the tetrameric *cis*-isomers.

This is a quite rare example where the bent conformation of *cis*-azobenzene is elaborately used as a building block of a well-defined supramolecular edifice. As a result of the tetramerization (and further stacking of the resulting tetramers as suggested by a ^{1}H NMR spectral change), the thermal *cis*-to-*trans* isomerization was significantly suppressed in CH_2Cl_2 compared to the molecularly dissolved state in a hydrogen bond-competing solvent (DMSO).

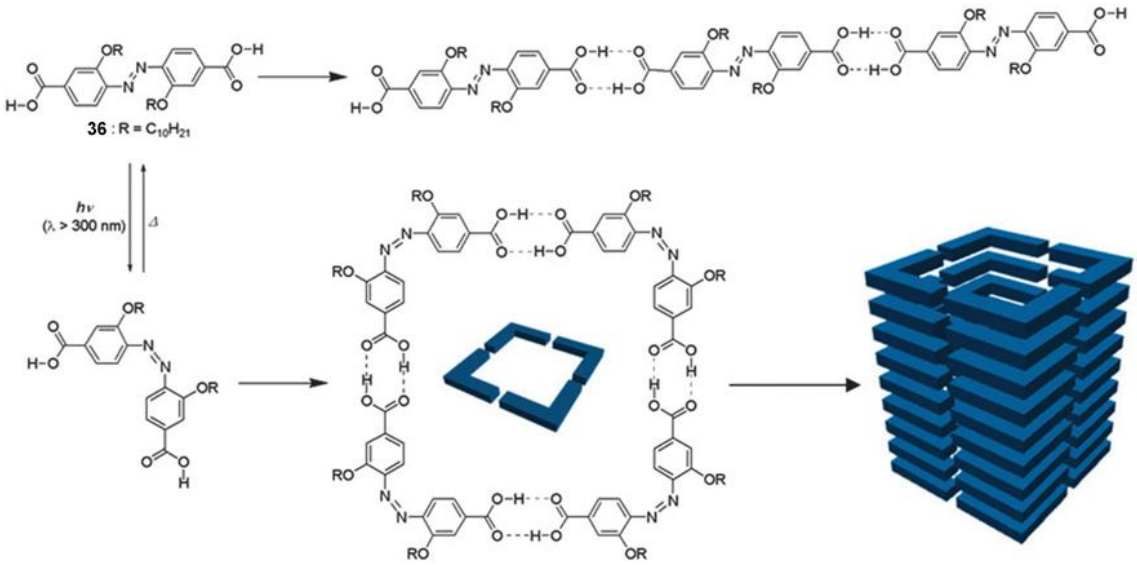

Figure 4.8. Photoresponsive self-assemblies of azodibenzoic acid derivative **36**.

4.3.2 Reversible monomer–aggregate interconversion

Recently Sortino et al.[50] have shown a reversible formation and destruction of H-type aggregates of an anionic porphyrin that can be controlled exclusively through light inputs exploiting the different interactions with the two isomeric forms of a cationic photoresponsive azobenzene-based surfactant. In particular, they have explored the possibility of controlling the aggregation↔disaggregation process of TPPS in water medium through a cationic surfactant whose molecular structure, and consequently its interactions with TPPS, can be reversibly changed by light stimuli of different energy. To this end, they have designed and synthesized the amphiphilic molecule **37** which integrates the photochromic azobenzene moiety in its molecular skeleton. They demonstrate that the *trans*↔*cis* photoisomerization of **37** deeply affects the extent of its interaction with TPPS allowing repeated H-aggregate↔monomer interconversion by means of alternate UV and visible light excitation (Figure 4.9).

Trans-isomer of derivative **37** encourages the formation of premicellar H-type aggregates of TPPS, these aggregates are mainly stabilized by Coulombic interactions between the two oppositely charged species and the hydrophobic clustering of the surfactant.

On the other hand the *cis*-isomer of **37** show a remarkably different behavior. The more polar structure of the *cis*-isomer prevents the stabilization of the supramolecular structures showing that the relevance of the hydrophobic contribution to the stabilization of the aggregate is much smaller than that of the parent *trans* in water medium.

Interestingly, this example represents the first supramolecular approach for reversibly controlling the monomer–aggregate interconversion of porphyrins in an aqueous medium by exploiting exclusively light inputs absorbed by a secondary photoswitching unit non-covalently linked to the porphyrin center.

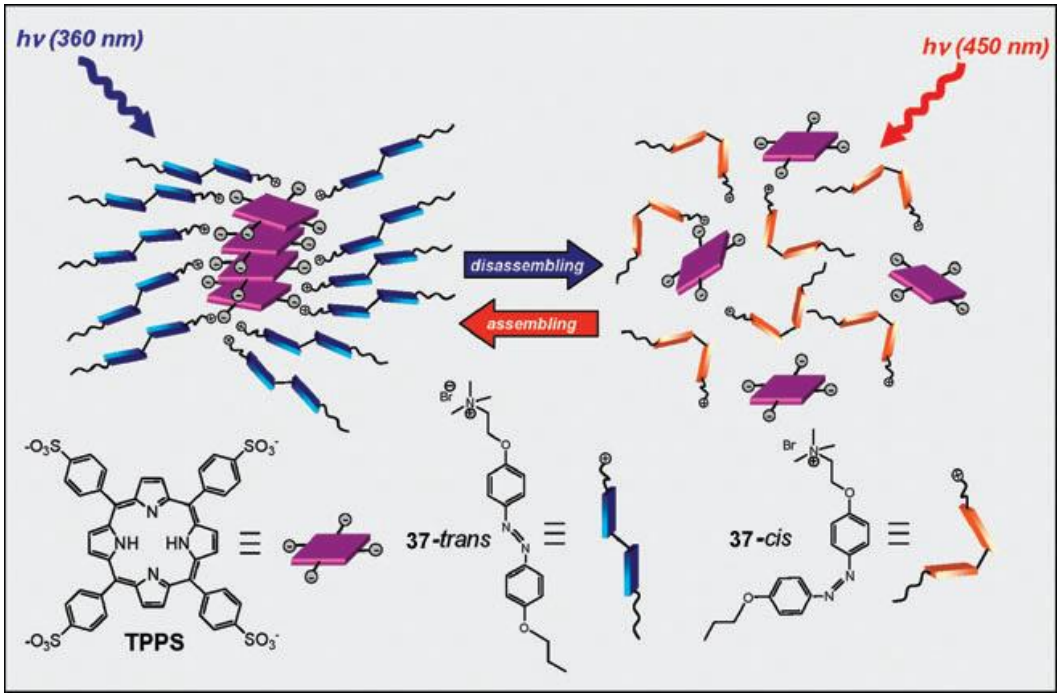

Figure 4.9. A schematic view of the light-powered assembling–disassembling of TPPS mediated by **37**. (From reference 50)

4.3.3 Rosette assemblies showing diverse photoresponses

Kitamura's group has studied a series of photoresponsive hydrogen-bonded macrocycles so-called rosettes,[51] formed from azobenzene-appended melamines and barbiturates/cyanurates through complementary triple-hydrogen-bonding interactions (Figure 4.10). The uniqueness of these photoresponsive rosettes might be the expression of diverse photoresponses even though the same supramolecular motif (hydrogen-bonded rosette) is employed. The type of photoresponse depends on the substituent of the building blocks.

The simplest result was observed for rosette I, which is given by mixing AzoMel **38** and **BAR**, both lacking sterically hindered substituents.[52] Rosette I prepared in chloroform is only kinetically stable, giving rise to an irreversible precipitation as a result of transformation into insoluble extended tapelike supramolecular polymers in the timescale of days (Figure 4.11a and b). Upon 100 h aging, more than half of the components precipitate. The azobenzene moieties of rosette I efficiently photoisomerize upon UV-irradiation with maintaining the rosette architectures as evidenced by ^{1}H NMR (Figure 4.11a and c). In a photostationary state achieved for the [c]=5 mM solution upon 1 h irradiation, the *trans* : *cis* ratio was 12 : 88.

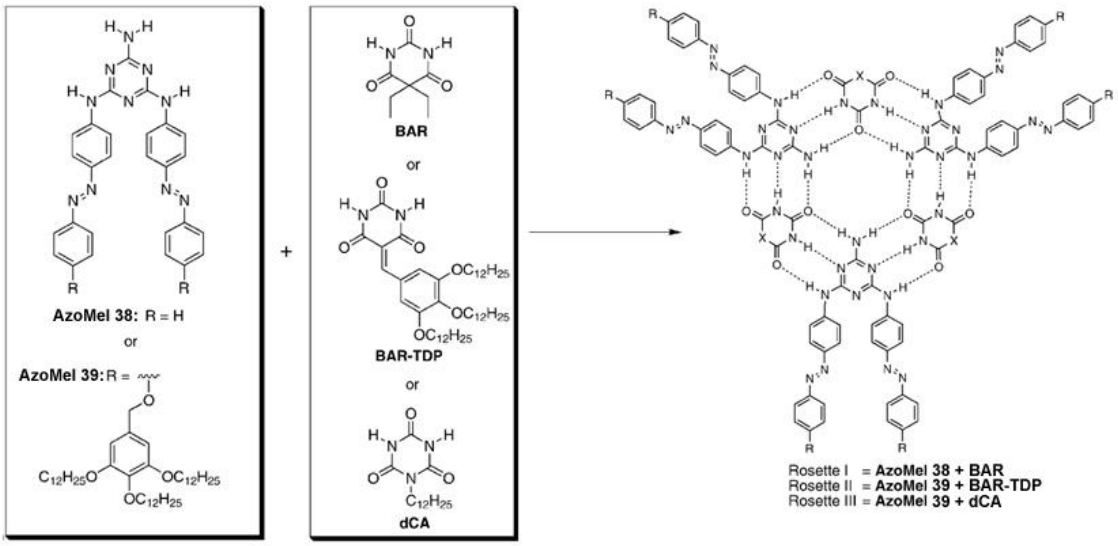

Figure 4.10. Supramolecular rosettes I–III formed by mixing azobenzene-appended melamines AzoMel **38** or AzoMel **39** and barbiturates **BAR** or **BAR-TDP** or dodecyl cyanurate **dCA**.

This result showed that the isomerization of azobenzene moieties has seemingly no impact on the self-assembly of rosette I. However, the group notice that the UV-irradiated solution does not produce any precipitates upon aging over 300 h (Figure 4.11c and d), the situation of which is considerably different from the solution without UV-irradiation.

This observation clearly demonstrates that the *cis*-azobenzene moieties suppress irreversible denaturation of rosette into tapelike assemblies. Probably, the *cis*-azobenzene moieties of AzoMel **38** increase the solubilities of competing tapelike oligomers, which must always be equilibrated with rosettes to a small extent, preventing their phase-separation (precipitation) by open-ended polymerization.[51-53]

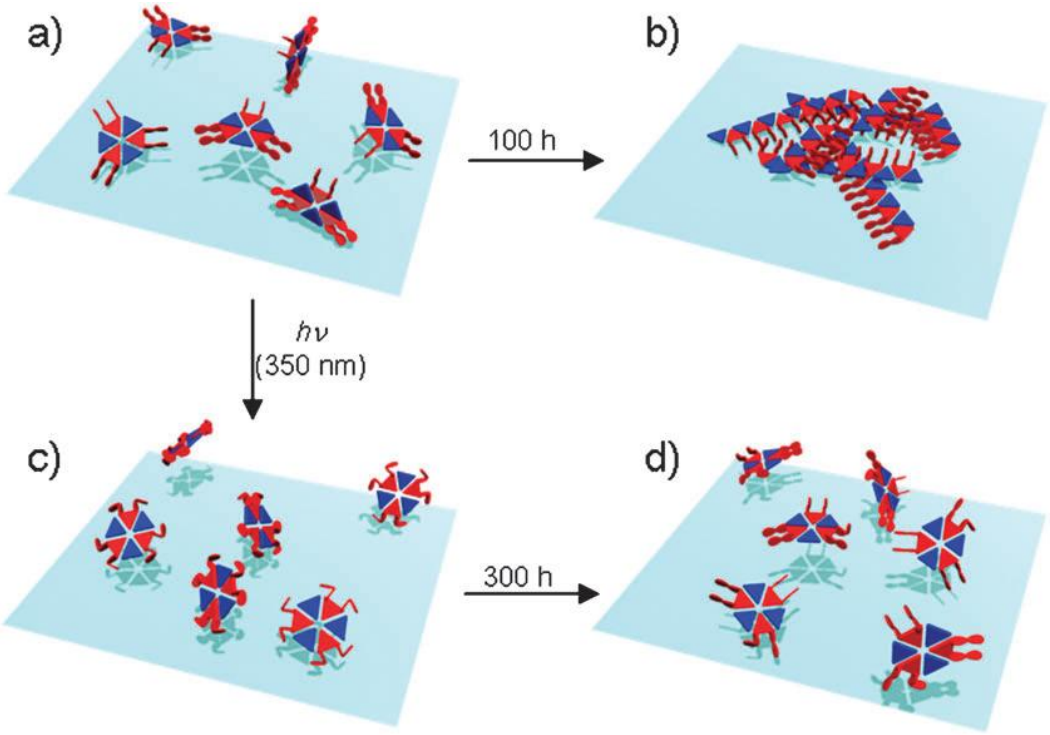

Figure 4.11. Schematic representation of the photoinduced stabilization of rosette I.

The next attempt was to induce different types of photoresponse for azobenzene-functionalized rosettes. The group considered that the modification of both azobenzene-appended melamines and barbiturates with sterically-demanding substituents such as the tridodecyloxyphenyl (**TDP**) ‘‘wedge’’ might endow a more direct photoresponse with the self-assembly of a rosette. Thus AzoMel **39** and **BAR-TDP** were prepared and their mixture was shown to form thermodynamically stable rosette II in apolar solvents, which can be detected even by size exclusion chromatography (SEC) without decomposition.[54]

As a compensation for the increased thermodynamic stability, however, the azobenzene moieties of rosette II displayed a low photoisomerization efficiency due to the steric crowding within the rosette: the *trans* : *cis* ratio in a photostationary state achieved by the best conditions is only 75 : 25. Statistically, this ratio means that only one or two of the six *trans*-azobenzene moieties in a rosette isomerized to the *cis*-isomer. This seemingly undesired outcome implies that AzoMel **39** possessing two *cis*-azobenzene moieties (*cis*,*cis*-AzoMel **39**) no longer complexes with **BAR-TDP** to construct the rosette architecture. Indeed, the 1:1 mixture of preliminary-photogenerated *cis*,*cis*-AzoMel **39** and **BAR-TDP** showed no trace of rosette formation on SEC analysis. Thus, in situ generation of aggregative *trans*,*trans*-AzoMel **39** in the pool of monomers upon irradiation with visible light triggered the generation of rosettes (Figure 4.12), and the

amount of rosette II could be quantitatively regulated by visible (increasing the concentration of the rosette) and UV light (keeping the concentration of the rosette).

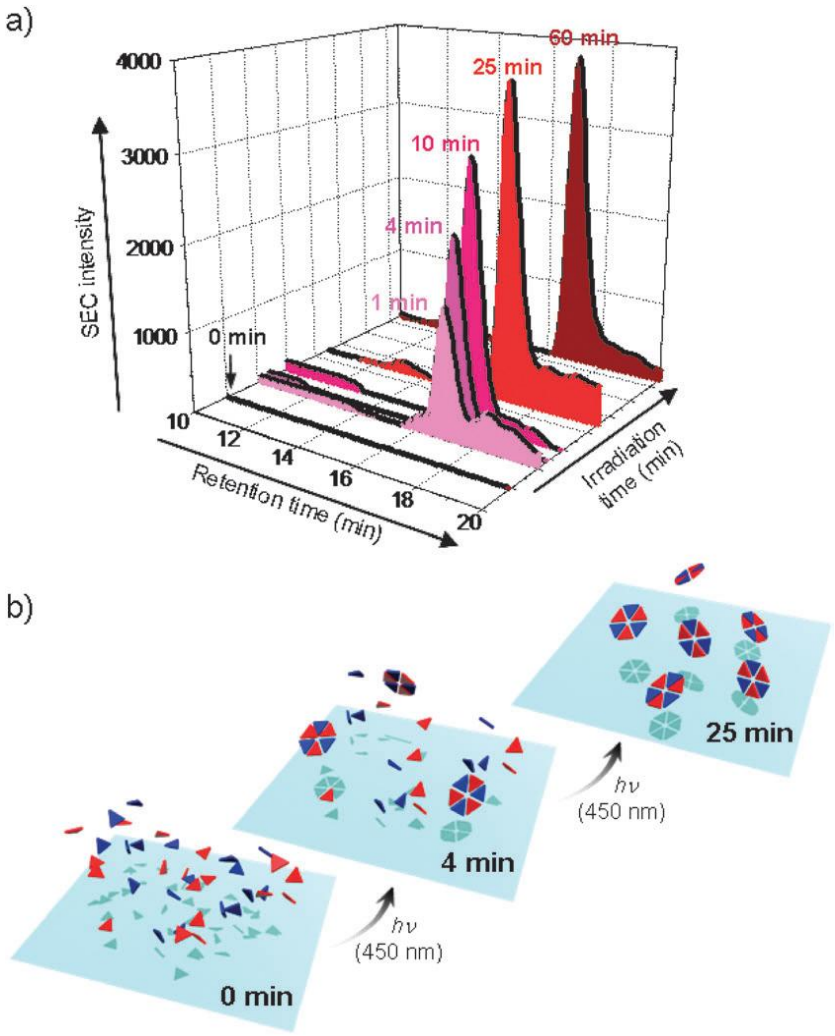

Figure 4.12. Phototriggered formation of supramolecular rosette II. (a) Change of size exclusion chromatogram of the mixture of AzoMel **39** and **BAR-TDP** in toluene upon irradiation with 450 nm light, and (b) the corresponding schematic representation of the phototriggered formation of rosettes.

Despite the low photoisomerization efficiency of the rosette II, the expression of a further different type of photoresponse may come true if disk-shaped rosettes hierarchically organize into higher-order columnar structures.[55] This assumption is derived from the idea that the π-π stacking interaction is vulnerable to the perturbation of the aromatic surface, allowing the control over the organization of disc-shaped supramolecules even by a small geometrical change. However, rosette II was found to intrinsically lack the capability to organize into extended columnar superstructures even

in the least aliphatic solvent such as cyclohexane, probably due to the bulky **TDP** wedge in the barbiturate component (**BAR-TDP**), noncoplanar to the hydrogen-bonded core.

Thus, rosette III consisting of AzoMel **39** and dodecyl cyanurate (**dCA**) has been prepared, affording columnar assemblies stable in apolar solvents.[56] In a high concentration regime (410 mM), solvent molecules were confined in the developed fibrous networks composed of bundled rosette columns, giving organogels (Figure 4.13a).

The *trans-cis* photoisomerization of the azobenzene moieties occurred even in the hierarchically organized state, showing a *cis*-content of ca. 45% under the best conditions.

The morphological change of rosette III accompanying the isomerization of azobenzene moieties impairs its stacking ability, which was demonstrated by the photoinduced gel-to-sol transition (Figure 4.13a and b).[39] The resulting solution could be reconverted to the gel state upon irradiation with visible light and subsequent aging.

Thus, by varying the number of the bulky **TDP** wedges, different types of photoresponse, i.e., photoinduced stabilization, phototriggered formation, and eventually photoregulatable stacking have been achieved for the hydrogen-bonded macrocycles.

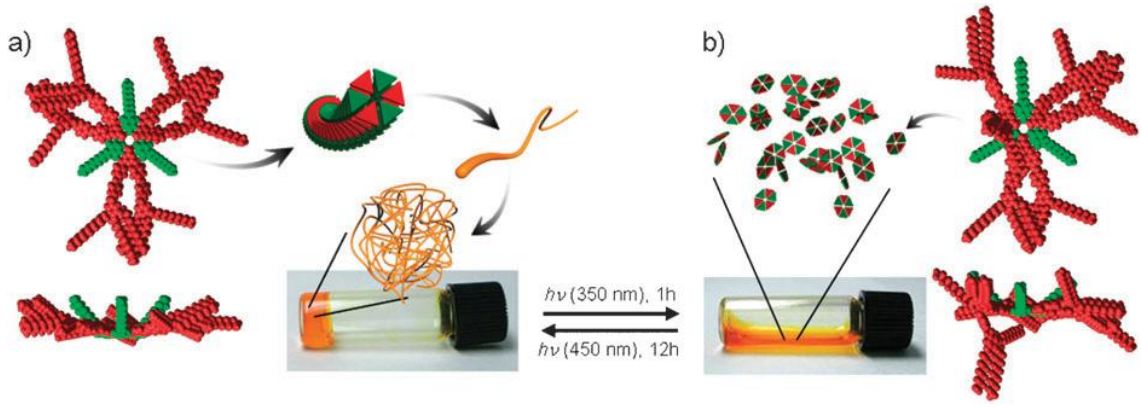

Figure 4.13. Photoresponsive hierarchical organization of supramolecular rosette III in cyclohexane. (a) Organization of rosette III possessing all *trans*-azobenzene moieties. (b) Supramolecularly-dissolved rosette III possessing one *cis*-azobenzene moiety.

4.3.4 Photo-manipulation of helical nanostructures

As a new paradigm of photoresponsive self-assembly, it is finally shown self-assembled nanofibers whose helical morphologies can be transformed by means of external light input. There is a growing interest in self-assembled helical nanoarchitectures because of their potential applications as liquid crystals, nonlinear optics, chiral sensing and separation and templates for inorganic materials.[57]

Manipulation of self-assembled helical nanostructures by external light input thus allows us to fabricate smart nanomaterials, chiroptical properties and functions of which could be controlled at will. One of such systems has been recently reported by Iwaura and Shimizu, who succeeded in the photoinduction/deletion of the helical feature in self-assembled nanofibers, using photoinduced dimerization of thymine nucleobase.[58]

Amphiphile **40** terminated by thymidylic acid self-assembles in aqueous media through π-π stacking interactions between bases and solvophobic interactions between oligomethylene chains, forming nanofibers (Figure 4.14a–d). Scanning electron microscopic observation revealed that the resulting nanofibers have 10 nm thickness and 80 nm width as typical dimensions and the overall morphology is nonhelical (Figure 4.14b–d). Interestingly, when the aqueous solution of **40** was irradiated by 280 nm light for several hours, right-handed helical twisting was induced (Figure 4.14e–g). Irradiation for 3 days rendered all the nanofibers helical.

UV/Vis spectroscopy demonstrated that 63% of the thymine moieties dimerized upon the irradiation, indicating that the helical twisting is indeed induced by the photodimerization of thymine moieties. MALDI-TOF MS measurements of helicity-induced nanofibers showed exclusive generation of dimerized **40** (Figure 4.14a), and no oligomeric species even trimer were detected. Thus the torque of the helical twisting is considered to be intermolecular dimerization of two neighboring thymine moieties within nanofibers. Deletion of helicity was subsequently achieved by irradiation with 240 nm light, which reconverts the thymine photodimer to the monomer (Figure 4.14h–j).

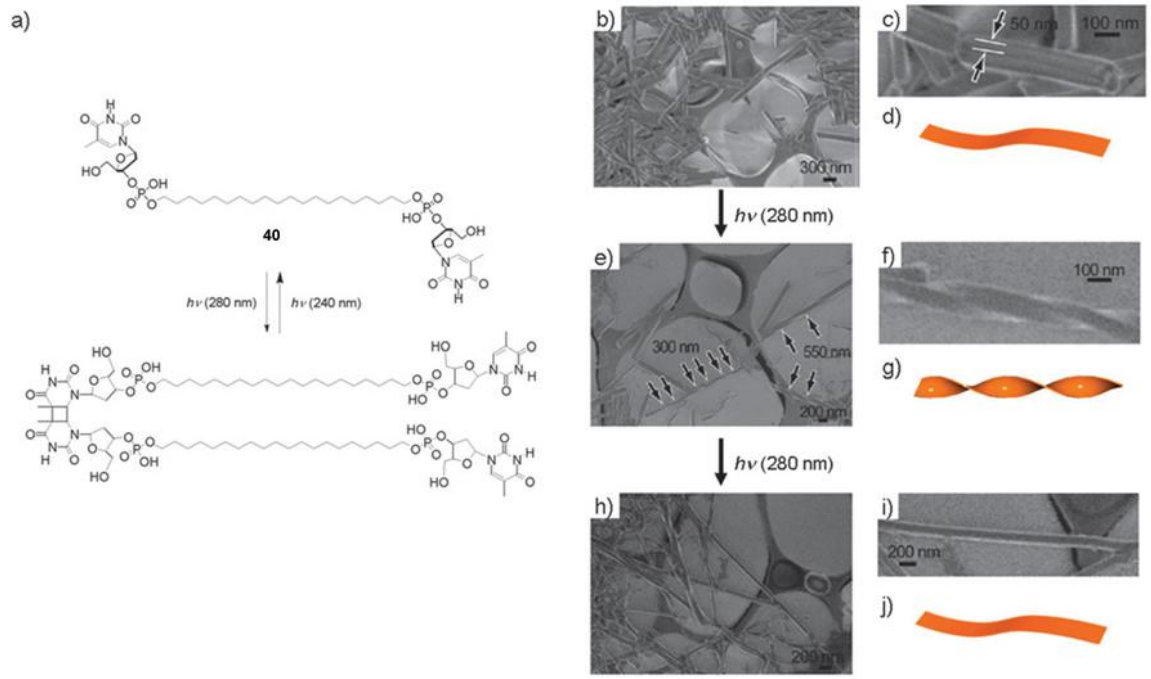

Figure 4.14. (a) Photodimerization of thymine-terminated bolaamphiphile **40**. (b,c,e,f,h,i) SEM images of photoinduced helical twisting of self-assembled nanofibers of **40** and (d,g,j) the corresponding schematic representation of the helical twisting of elemental aggregate. (b–d) As-prepared fibers with no helical structure. (e–g) Helically-twisted fibers by 3 h irradiation of 280 nm UV-light and (h–j) subsequent depletion of helical structure by 3 h irradiation with 240 nm UV-light. (From reference 58)

Another system where helical nanostructures can be manipulated by light stimulus has been reported by Stupp et al.[59] Amphiphile **41** (Figure 4.15a) possessing terminal *trans*-azobenzene substituents self-organizes in cyclohexyl chloride to form superhelical nanofibers (Figure 4.15b). The helical pitch visualized by atomic force microscopy is ca. 78 nm and uniform for all the nanofibers (Figure 4.15c and d). Interestingly, irradiation of nanofibers dispersed in cyclohexyl chloride at 360 nm diminished the helical pitches to 40–70 nm (Figure 4.15e–g). This morphological change can be explained in terms of an increase in the torsional strain upon isomerization of *trans*-azobenzene into the less planar (sterically bulky) *cis*-isomer. The decrease in the helical pitch varied from nanofiber to nanofiber due to the inhomogeneous isomerization efficiency among nanofibers.

In contrast, the helical pitch is uniform in each nanostructure, indicating that the photoinduced decrease in the helical pitch is a relaxation process throughout the entire nanostructure.

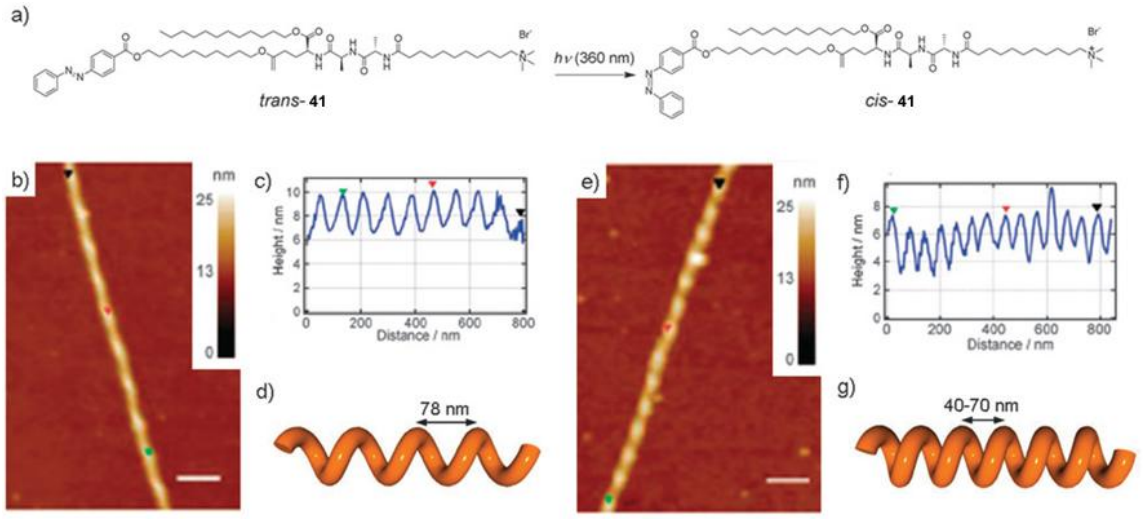

Figure 4.15. (a) Photoisomerization of azobenzene-functionalized amphiphile **41**. (b, e) AFM height images and (c, f) the corresponding height profiles and schematic representation of the helical morphologies for the photoinduced actuation of a helical nanofiber of **41** (b–d) before and (e–g) after irradiation of UV-light. (From reference 59)

4.4 Triggering of Guanosine Self-Assembly by Light

As previously mentioned in section **2.6.6**, Ghoussoub and Lehn were able to control the mesoscale dynamic sol-gel interconversion, i.e., from a disordered guanine solution to gel-forming ordered G-quartet architectures, through reversible cation binding and release (Figure 2.29). However, a great challenge was to control the switching between two or more highly ordered guanine-based supramolecular motifs making use of an external agent.

In 2006, our group demonstrated the tunable interconversion between two highly ordered supramolecular motifs (G-quartet K^+-templated column and G-ribbon) of a lipophilic guanosine derivative (dG **1**, Figures 2.1 and 3.1) fueled by cation complexation and release in a [2.2.2] cryptand **25** containing guanosine solution. The process was controlled by the sequential addition of acid and base as shown in Figure 4.16.

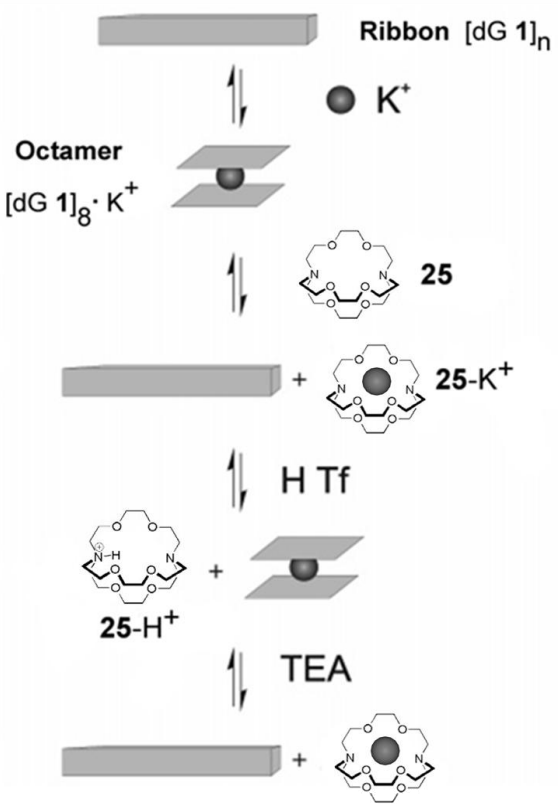

Figure 4.16. The stepwise reversible interconversion between the ribbon [dG **1**]$_n$ and the octamer [dG **1**]$_8$•K^+. The cation complexation/release is controlled by sequential addition of acid (HTf) and base (TEA).

Moreover, this chemically driven switching between different supramolecular motifs allows the fine control of the physical-chemical properties of guanosines scaffolding function groups such as open-shell (see **2.6.7**) or oligothiophene moieties.[60a]

Our next challenge was to control guanosine molecular assembling by photons; this will offer the great advantage of leaving the system in its constitutional state without affecting temperature or other important parameters such as pH and ionic strength by addition of any chemical substance.

Below we report on the photocontrolled self-assembly of a modified guanosine nucleobase. Compound ***E*-42** in the presence of a measured amount of KI self-assembles into a D_4-symmetric complex (see **2.2.3**) consisting of two stacked G-quartets. Photoisomerization to the *Z* isomer determines the decomposition of the octameric complex, which is re-formed when the molecule is reverted to the *E* form either by thermal or photochemical back isomerization.

Following our experience on photoswitchable systems,[60b-d] in order to introduce a photochemical control over guanosine self-assembly, our first approach was to introduce an azobenzene moiety in the 8 position of the guanine base. We expected that, if the

photoactive moiety were placed close to the sites of base recognition, the geometrical changes associated with photoisomerization of the azo chromophore would have resulted in strong effects over guanine self assembly. Unfortunately, the compounds obtained did not show the desired supramolecular behavior. While this work was in progress, interesting results were reported in the literature by Ogasawara and coworkers[61] for oligonucleotides containing a modified guanosine in which an arylvinyl moiety had been introduced at the 8 position. We therefore turned our attention to the 8-styrylguanine moiety as the photoswitching unit.

Derivative ***E*-42** was obtained in three steps from natural guanosine, according to Scheme 4.1: bromination at the 8-position with NBS followed by Suzuki coupling with 2-phenylvinylboronic acid and esterification of the hydroxy functions with acetic anhydride afforded ***E*-42** in a 48% overall yield as pure isomer (see Experimental Part, Chapter 5).

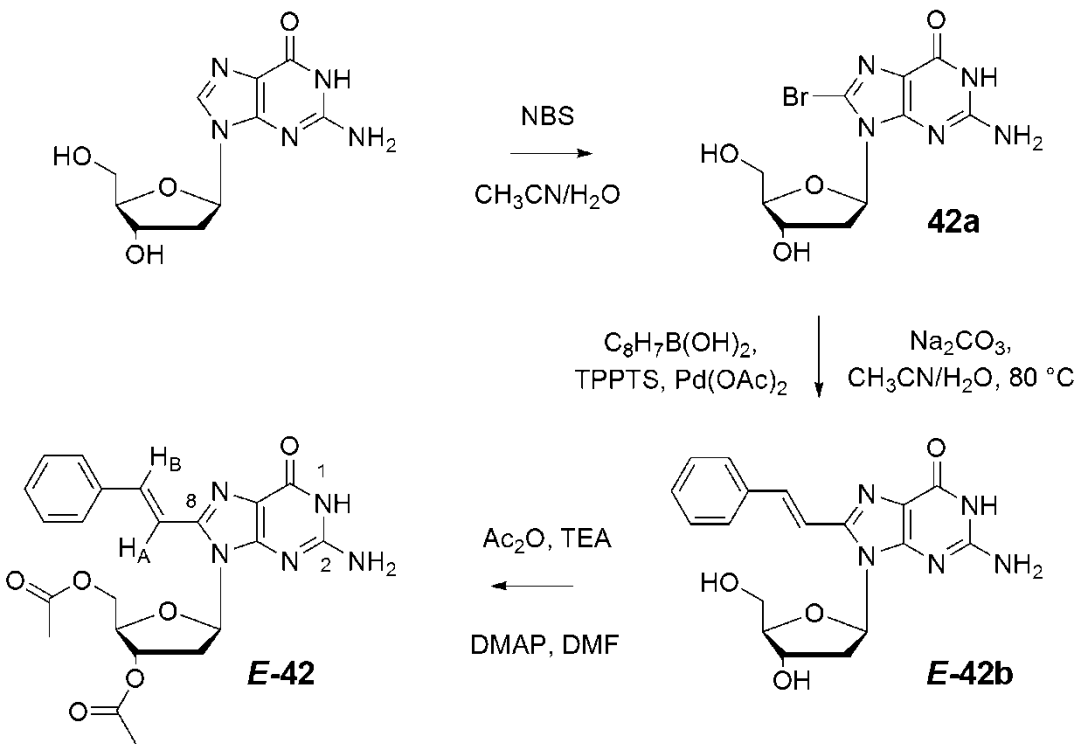

Scheme 4.1. Synthesis of ***E*-42**.

Compound ***E*-42** dissolves readily in MeCN. The ^{1}H-NMR spectrum of ***E*-42** (Figure 4.17a) in CD_3CN (5 mM) shows sharp signals, suggesting that no extensive self assembly to form ribbon like aggregates (see Chapter 3) is occurring under these conditions.

This is supported by NOESY spectra, which show no cross peak attributable to intermolecular correlations (Figure 4.18). Extensive self-assembly takes place upon increasing concentration above 20 mM: the imino N1-H and amino N2-H protons, which resonate at 9.30 and 5.50 ppm, respectively in 5mM solution, shift downfield to 10.47 and 6.33 ppm in a 30 mM solution (Figure 4.17b). This indicates progressive involvement of these groups in H-bonding. Accordingly, the NOESY spectrum now clearly shows an intermolecular correlation between N2-H and H1' of adjacent guanosines (Figure 4.19).

Interestingly, spectra in Figures 4.18-4.19 indicate a conformational change around the glycosidic bond as a function of concentration. In diluted samples (below 5 mM), a cross peak correlating H1' and H_A suggests a *syn* conformation around the glycosidic bond, but at higher concentrations (20 mM and above) this cross peak is no longer apparent while the presence of an intermolecular peak relating N2-H and H1' of adjacent guanosines indicates that a ribbon-like architecture is present and the *anti* conformation is now predominant.

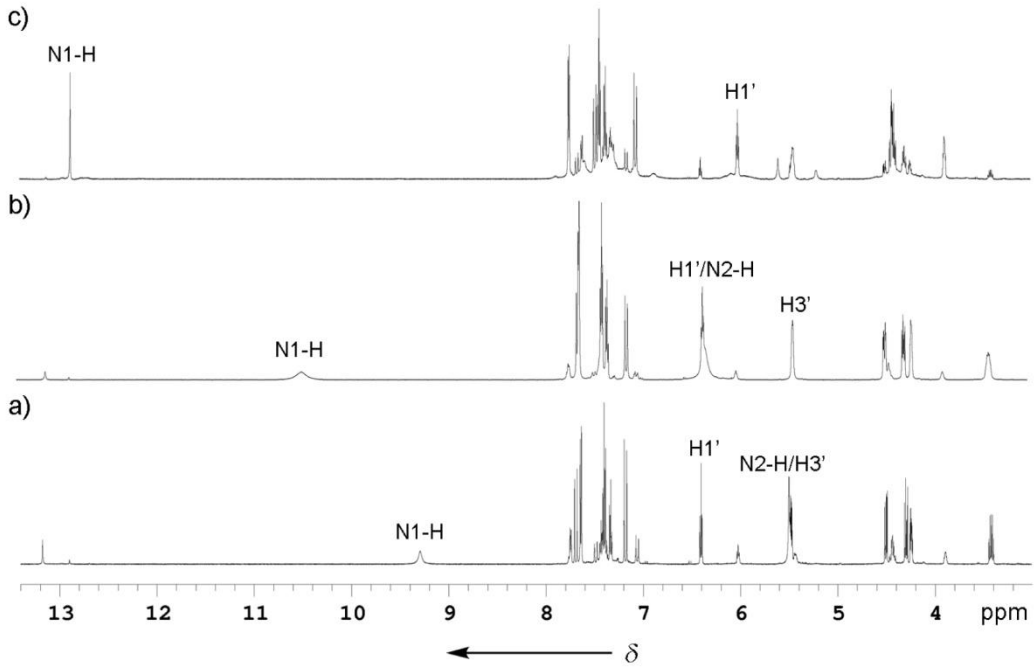

Figure 4.17. a) ^{1}H NMR spectra for a 5 mM solution of ***E*-42** in CD_3CN, b) for a 30 mM solution of ***E*-42** in CD_3CN, and c) for a 5 mM solution of ***E*-42**/KI in CD_3CN.

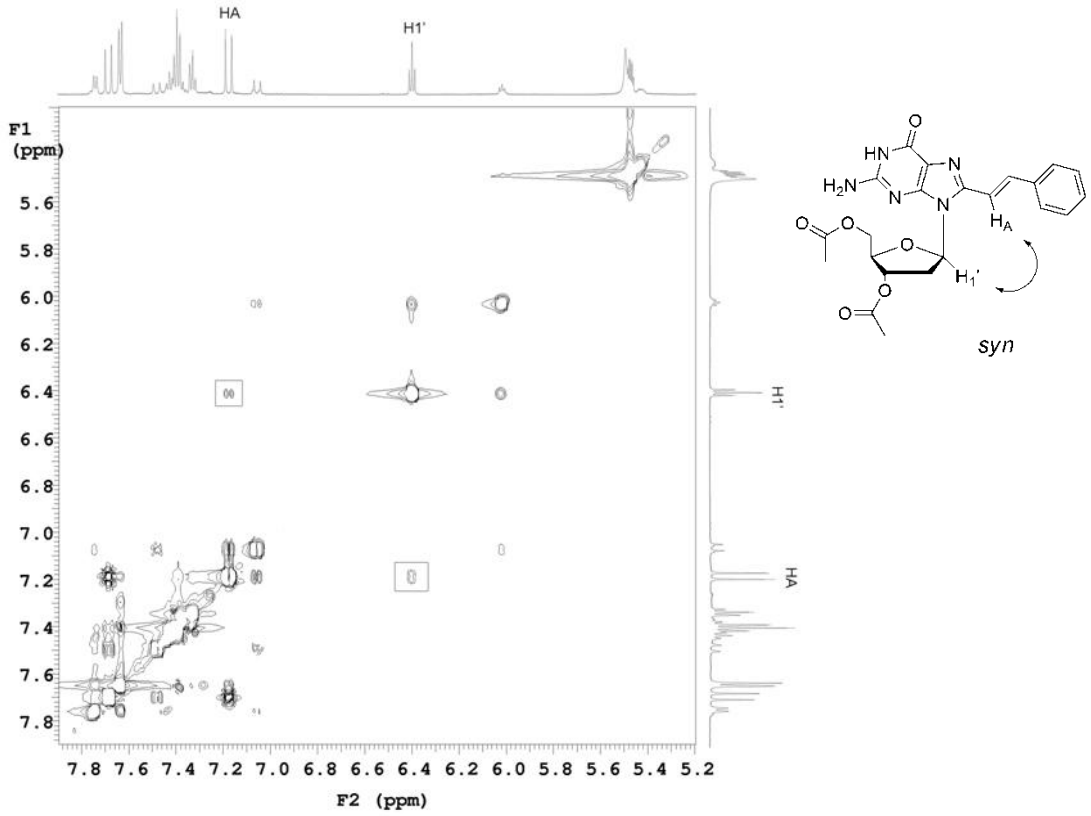

Figure 4.18. Portion of NOESY spectrum of ***E*-42** (5 mM) in CD_3CN. Mixing time 200 ms.

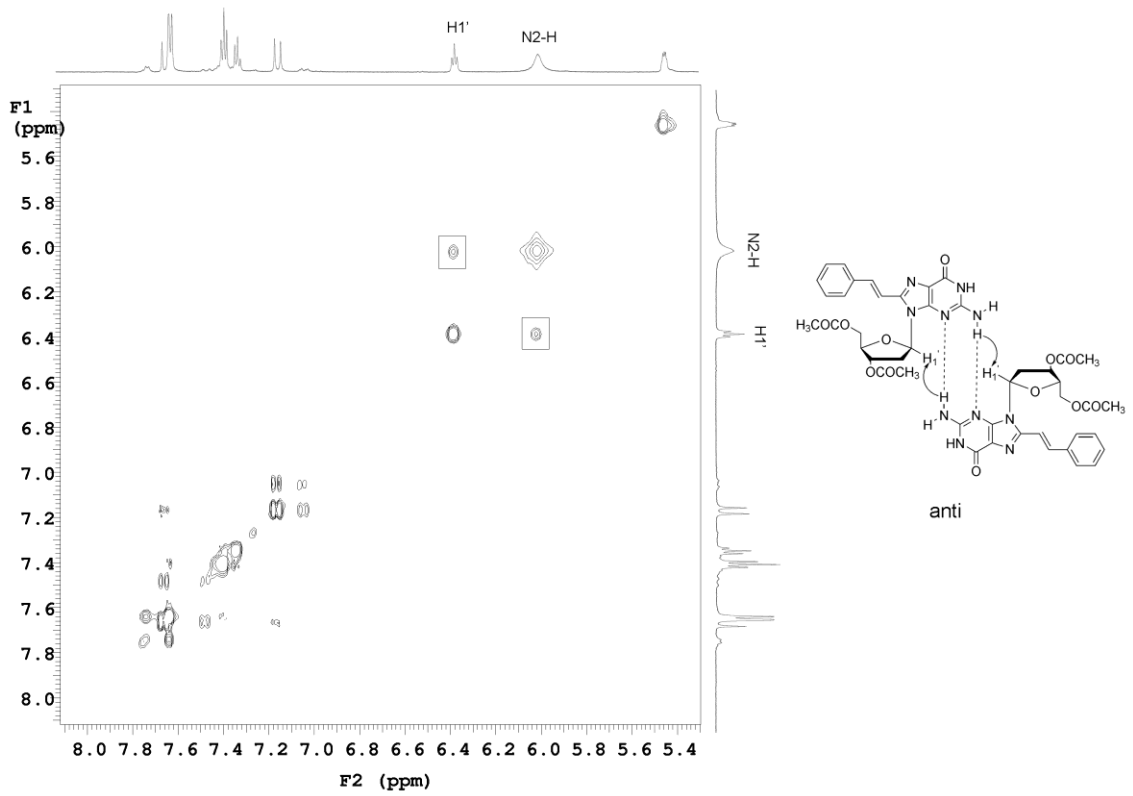

Figure 4.19. Portion of NOESY spectrum of ***E*-42** (20 mM) in CD_3CN. Mixing time 200 ms.

The CD spectrum of ***E*-42** in MeCN shows only a weak (negative) signal. The profile is almost superimposable to the CD spectrum of ***E*-42** in MeOH, a competing solvent for hydrogen bonding, suggesting the presence of a disaggregate form of ***E*-42** (Figure 4.20).

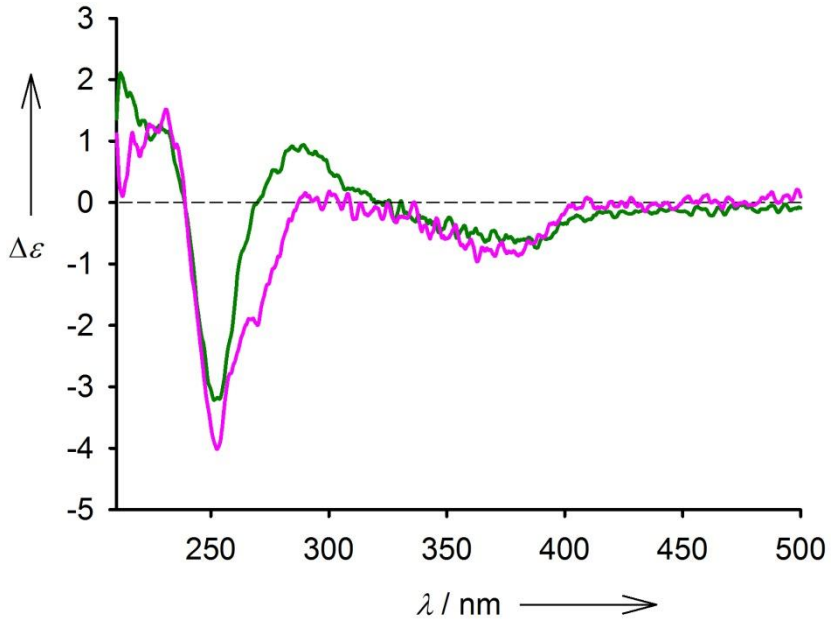

Figure 4.20. CD spectra of a 5 mM solution of ***E*-42** in acetonitrile (pink line) and in methanol (green line).

Upon irradiation of this MeCN solution at 365 nm, ***E*-42** isomerizes to the *Z* form and a *Z* photostationary state (*Z*-PSS, Z=85%) is reached in 28 min (Figure 4.21a), as estimated from UV-Vis spectroscopy by spectral subtraction.[62] The process is perfectly reversible: the *Z* isomer reverts back to the *E* form either by irradiation at 254 nm (30 min, Figure 4.21b) or thermally in the dark (150 min).

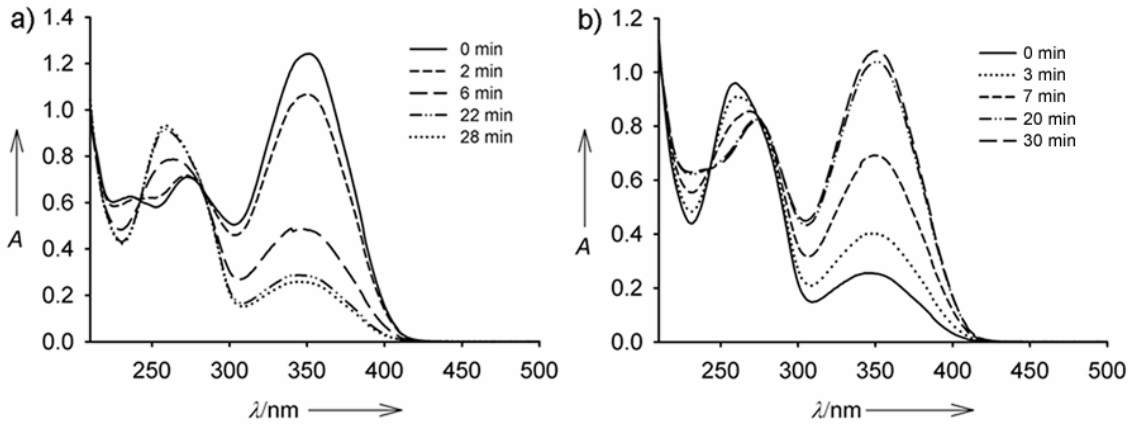

Figure 4.21. a) Absorption spectra for photoisomerization of ***E*-42** upon irradiation at 365 nm, and b) photoisomerization of ***Z*-42** upon irradiation at 254 nm.

When a weighted amount of KI (0.125 mol per mol of guanine, i.e. 1/8) is added to a MeCN solution of ***E*-42**, ^{1}H-NMR and CD spectra change dramatically, as expected when formation of stacked G-quartets templated by the cation occurs. In particular, in the ^{1}H- NMR spectrum (Figure 4.17c) the imino proton shifts downfield more than 3 ppm while the H1' moves upfield by 0.4 ppm and the amino signal becomes unobservably broad at room temperature. No doubling of signals appears in the ^{1}H-NMR spectrum: this suggests the formation of an octameric species composed of two stacked G-quartets arranged in a D_4 simmetry. NOESY spectra show a correlation between H1' and H_A both for diluted and concentrated samples, implying that in the octameric supramolecular complex all of the guanosines adopt a *syn* conformation around the glycosidic bond, regardless of concentration (Figure 4.22)

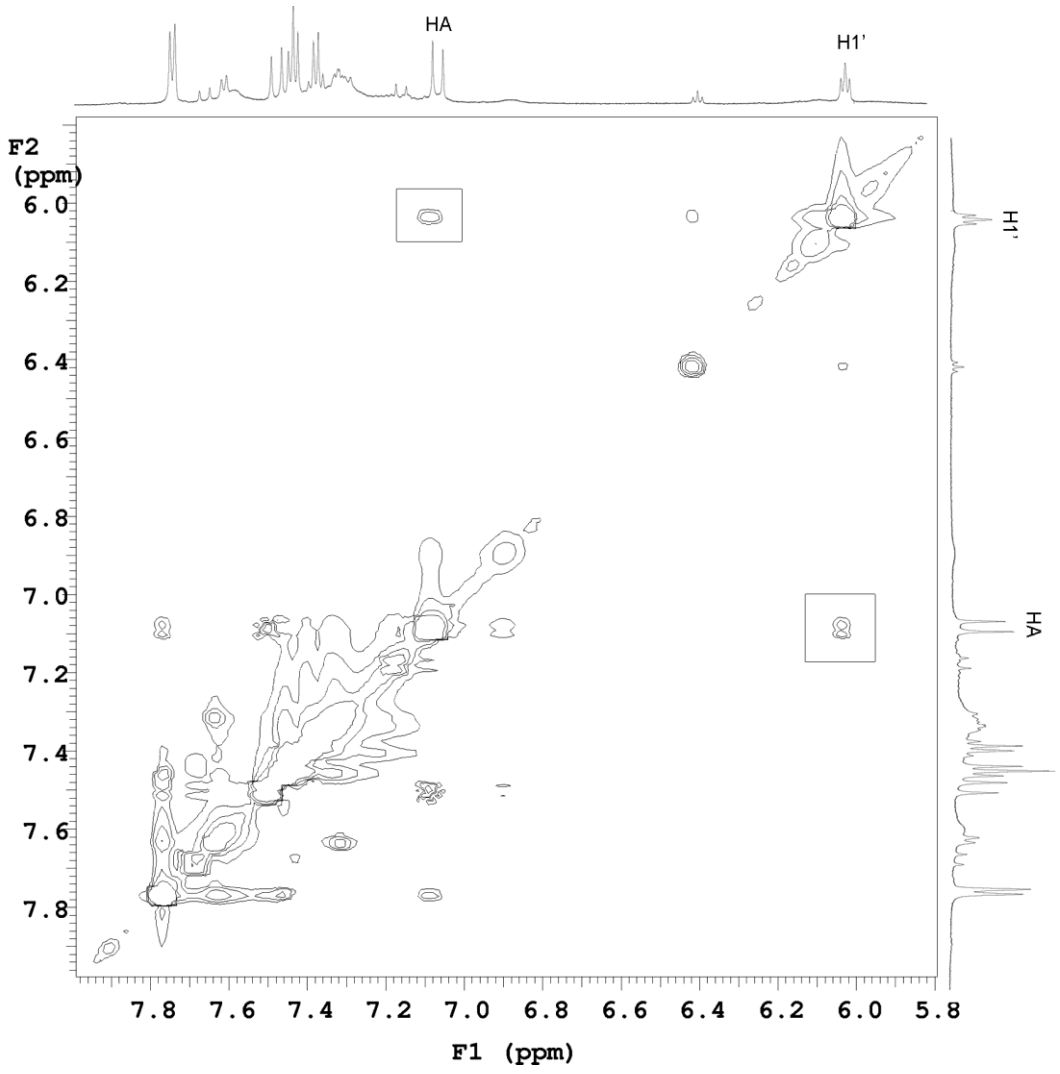

Figure 4.22. Portion of NOESY spectrum of ***E*-1**/KI (20 mM) in CD_3CN. Mixing time 200 ms.

In the CD spectrum (Figure 4.23a) of the ***E*-42**/KI octameric complex, a positive band at 255 nm and a very strong, positive band at 350 nm can be observed. Although no detailed information on the electronic transitions are available so far for 8-styrylguanine chromophore, the spectral changes observed upon addition of potassium ion closely resemble those reported for other unmodified lipophilic guanosines. The strong increase of the CD signal associated with the formation of the ***E*-42**/K^+ aggregate can analogously be attributed to interchromophore couplings taking place in the stacked complex. When samples of the ***E*-42**/K^+ octameric complex are irradiated at 365 nm, photoconversion to the *Z* isomer takes place and the *Z*-PSS is reached in 30 min. for a 5 mM sample. The photoisomerization has a dramatic effect on the assembled species.

The CD spectrum of the solution of **42**/KI recorded at the *Z*-PSS shows very weak signals: this spectrum is practically superimposable to the CD spectrum of ***Z*-42** prior to KI addition and it is similar to that of uncomplexed ***E*-42**. The comparison between CD and UV spectra for ***E*-42** before and after K^+ extraction points to the conclusion that the intensity of the CD signal is mainly attributable to interchromophoric interactions: in particular, the *E* form before K^+ complexation shows a weak CD spectrum, in spite of the strong absorbance in the corresponding UV. Accordingly, the weak CD signal shown by the system at the *Z*-PPS results from the disgregation of the stacked supramolecular complex and is not directly related to the lower molar absorptivity of the *Z* isomer. The disappearance of the strong CD bands at 255 and 350 nm is an evidence of the complex decomposition: stacked G-quartets no longer exist in solution.

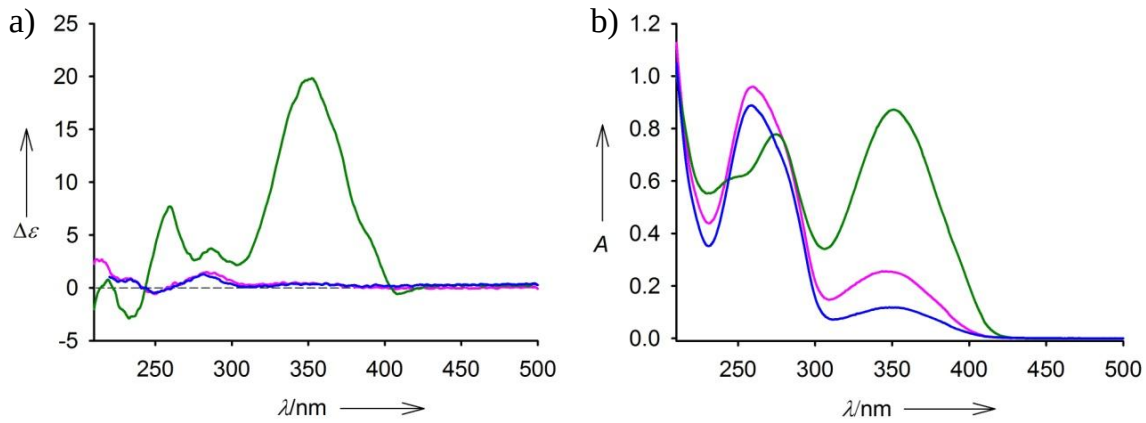

Figure 4.23. a) CD spectra (panel a) and UV-Vis (panel b) of a 5 mM solution of ***E*-42**/KI (green line), of ***Z*-42**/KI (blue line) and ***Z*-42** (pink line) in acetonitrile.

Unfortunately, no NMR studies could be carried out on the *Z*-PSS solution: the photoisomerization with standard Hg lamps of samples large enough to be suitable for NMR analysis produced substantial amounts of photocycloaddition products, in the time required to attain the *Z*-PPS under these conditions (Figure 4.24a).

Hence, direct detailed information on the type and extent of self-assembly undergone by **42** when in the *Z* form in the presence of K^+ could not be obtained. While the disappearance of the stacked octameric structure is evident from the CD spectrum, the organization of ***Z*-42** into other self-assembled species cannot be ruled out.

a)

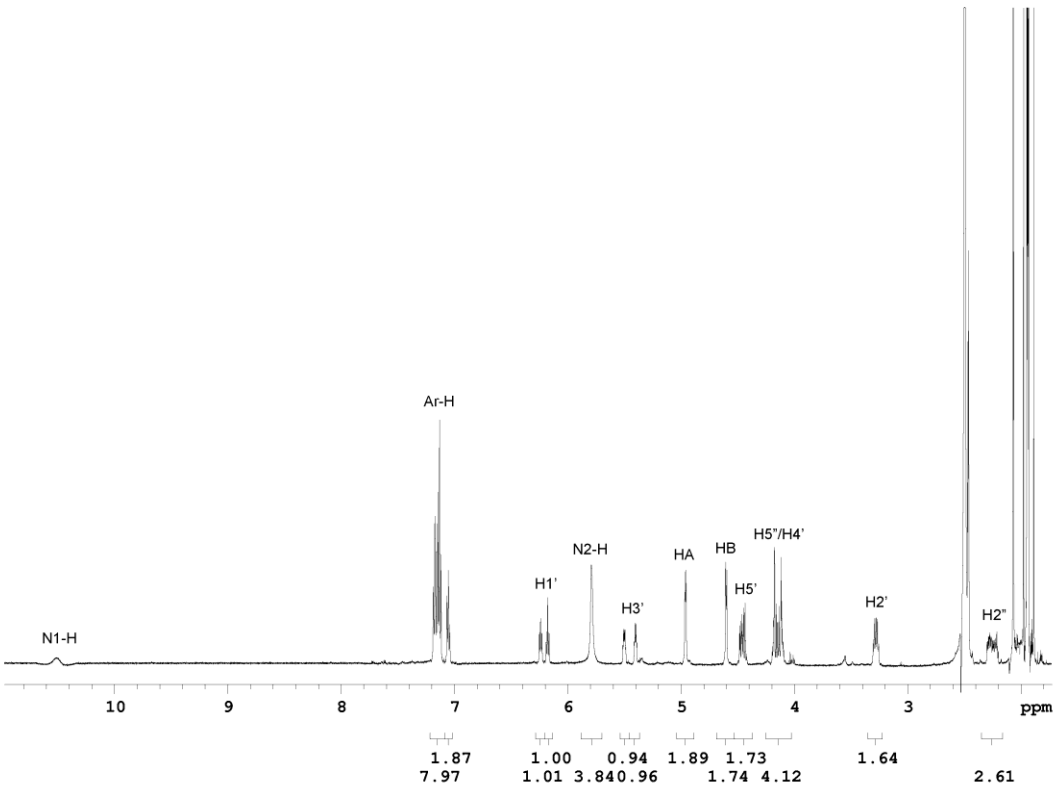

b)

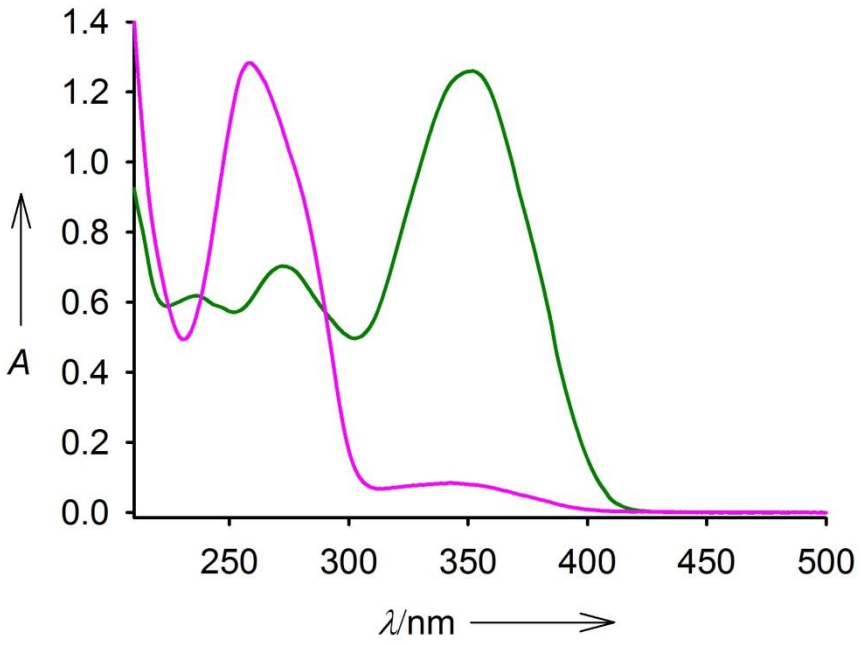

Figure 4.24. a) ^{1}H-NMR spectrum of photocycloaddition product after irradiation of ***E*-42** (8 hours) at 365 nm in CD_3CN; b) absorption spectrum of photocycloaddition product after irradiation at 365 nm for 3 days (pink line) of a 5 mM solution in CH_3CN of ***E*-42** (green line).

As stated above, the *Z* form can be converted back to the *E* form either photochemically, by irradiating at 254 nm, or thermally. Retroisomerization to the *E* isomer determines, at the supramolecular level, the recreation of the octameric complex: the CD spectrum of the solution at this point perfectly overlaps to the starting $(\boldsymbol{E}\textbf{-42})_8 \bullet K^+$ trace.

Thus, the G-quartet based complex can be cyclically assembled and disassembled by light. As shown in Figure 4.25, the process is perfectly reversible: no change in molar absorptivity was observed for both *E* and *Z* states after five cycles.

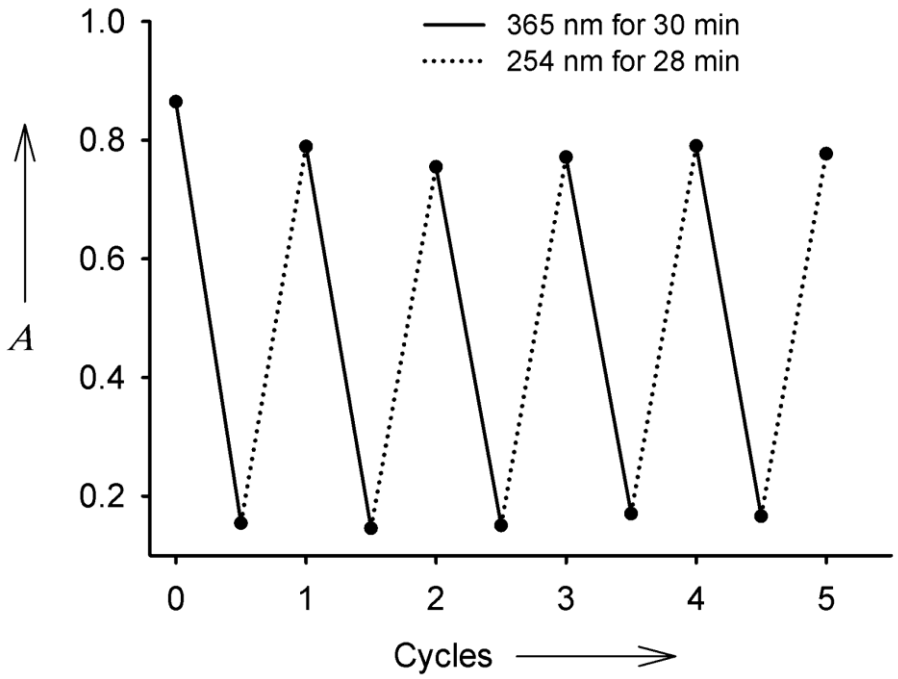

Figure 4.25. Switching cycles between ***E*-42**/KI and ***Z*-42**/KI by alternate irradiation with 365 nm and 254 nm light.

In conclusion, by the introduction of a photoactive moiety at C8 in a lipophilic guanosine derivative it is possible to operate a photocontrol over the self-assembly of the molecule, where the existence of G-quartets can be alternately switched on and off as depicted in Figure 4.26.

Octamer *No stacked G-quartet*

Figure 4.26. Cartoon showing the photocontrolled guanosine self-assembly.

Nevertheless no NMR studies could be carried out on the *Z*-PSS solution in CD_3CN, ^{1}H-NMR spectrum of the *Z*-PSS could be obtained by photoisomerization of a CD_3OD solution. In fact, in this competing solvent for hydrogen bonding, it's possible to detect the new set of signals which belong to *cis*-isomer as shown in Figure 4.27.

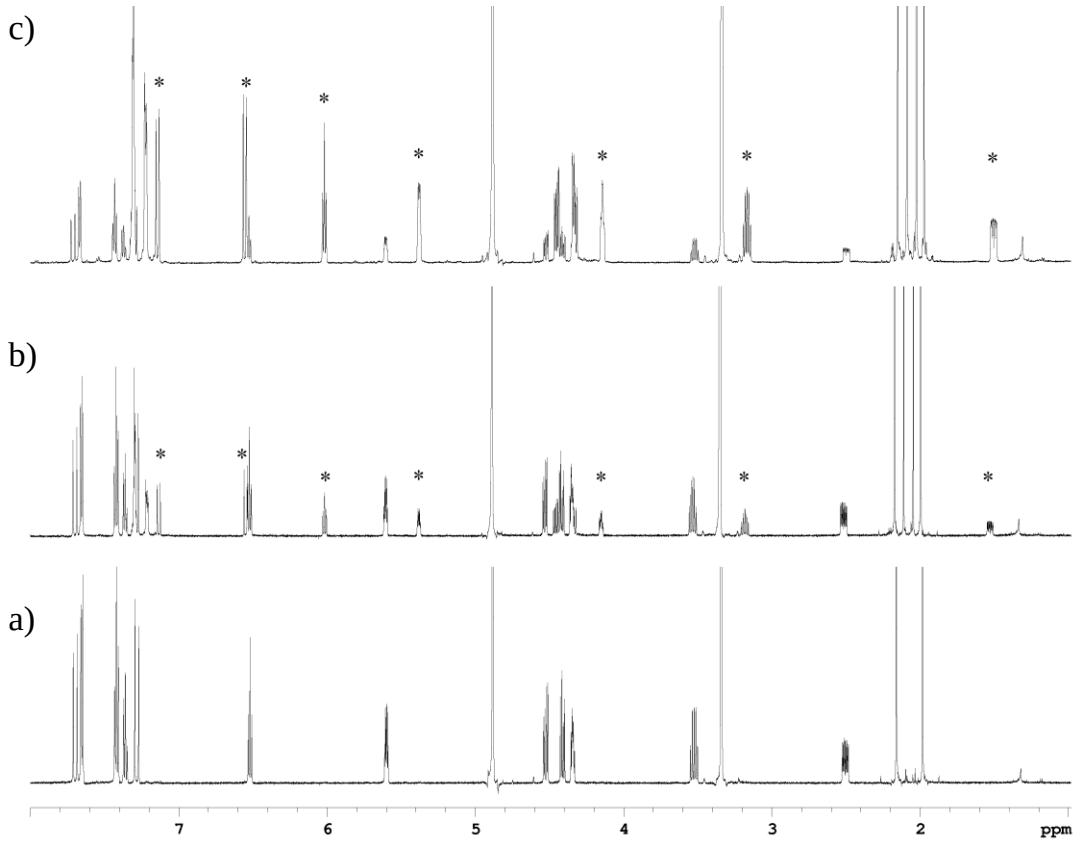

Figure 4.27. ^{1}H-NMR spectra (5 mM) in CD_3OD of a) ***E*-42**, b) ***E*-42** after 4 hours of irradiation at 365 nm and c) ***E*-42** after 1 day of irradiation at 365 nm. Stars indicate some clear signals corresponding to *cis*-isomer. The *trans-cis* ratio in the photostationary state (spectrum c) is 25:75.

Finally, below it is shown UV-Vis absorption spectra for a MeOH solution of ***E*-42**.

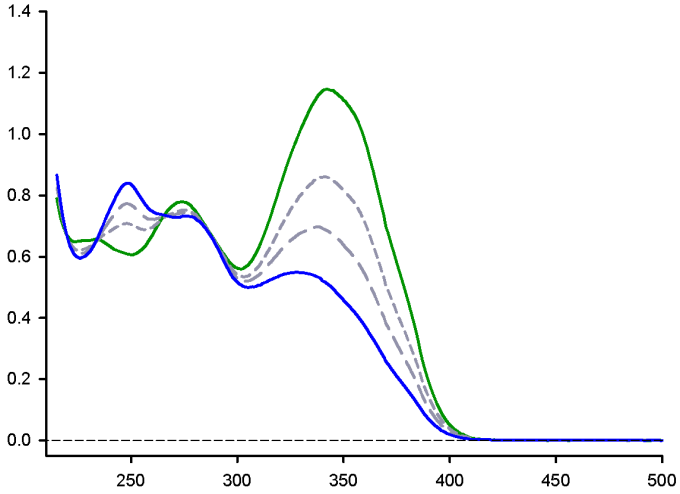

Figure 4.28. Absorption spectra (5 mM) in MeOH of ***E*-42**: before (green line) and after irradiation at 365 nm for 30 minutes (pink line).

4.4.1 Solid-liquid interface approach

While the self-assembly of guanines into G_4 based architectures (not templated by a metal center) on solid surfaces has been studied by Scanning Tunneling Microscopy (STM) under ultrahigh vacuum (UHV) as pointed out in section **2.4**, STM explorations at the solid-liquid interface have been primarily carried out on guanosine derivatives (see **3.2**, Figure 3.6). Although the structure of guanine quadruplex templated by a metal center was introduced over 40 years ago as mentioned in Chapter 1 (see **1.5**), to date, its visualization by STM once assembled at the solid-liquid interface has been reported for the first time by Samorì and our group.[63]

In particular, we provided the first direct evidence on the sub-nm scale of a dynamer operating at surfaces by means of STM. The versatile guanine **43** (Figure 4.29) molecule was reversibly interconverted at the solid-liquid interface between two highly ordered supramolecular motifs (Figure 4.30) as well as we reported for lipophilic guanosines in solution (Figure 4.16). Hence, it was possible to switch between H-bonded ribbon and G_4 based architectures upon subsequent addition of cryptand [2.2.2] **25** molecules, potassium picrate and trifluoromethanesulfonic acid.

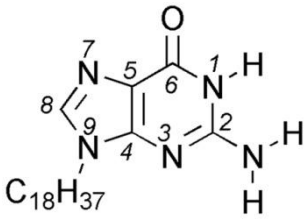

43

Figure 4.29. Guanine derivative

Clearly, inspired by previous results in solution, our next challenge is to control this reversible assembly/re-assembly process at the solid-liquid interface by photons. To this aim in Scheme 4.2 it is shown the synthetic pathway for photochromic derivative **44**, currently under investigation.

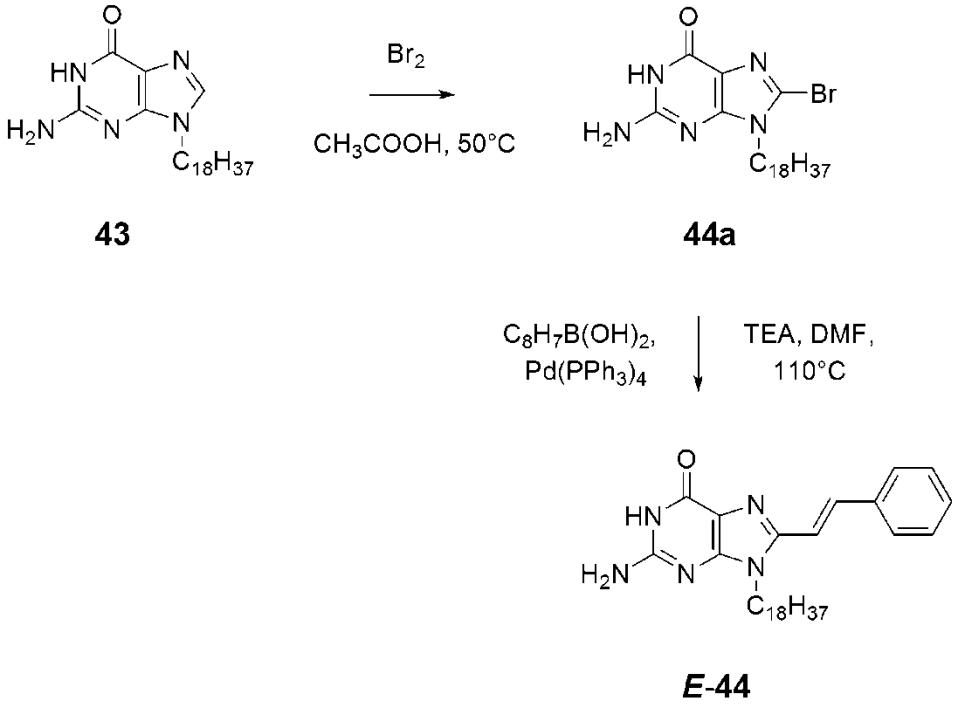

43 **44a** ***E*-44**

Scheme 4.2. Synthesis of derivative **44**.

Bromination at the 8-position of derivative **43** followed by Suzuki coupling with 2-phenylvinylboronic acid afforded the desired product ***E*-44** (see Experimental Part, Chapter 5).

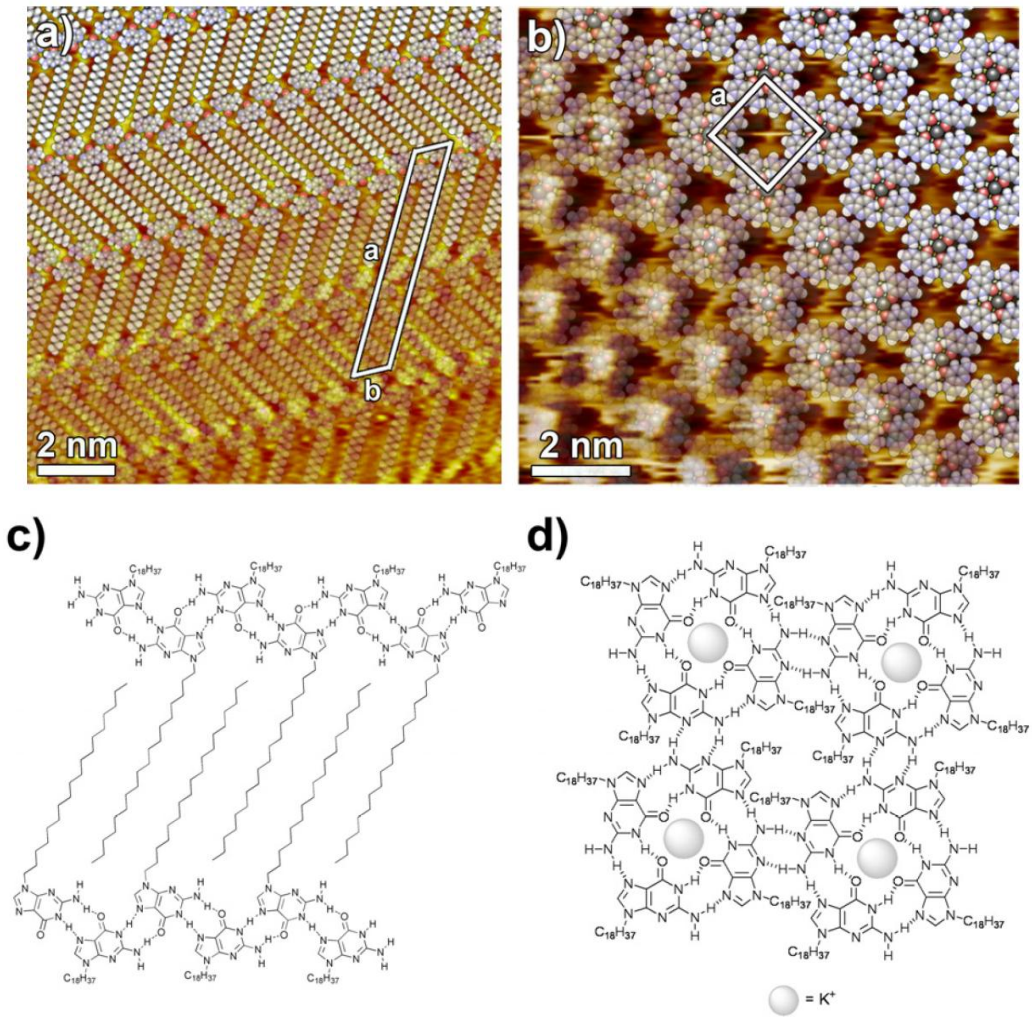

Figure 4.30. STM images of monolayers of supramolecular architectures of **43** at the solid-liquid interface self-assembled from TCB solution; a) ribbon-like structure and b) G_4 based architecture. The model of their packing motif are shown in c) and d), respectively. Tunneling parameters: a) average tunneling current (*It*)= 15 pA, bias voltage (*Vt*) = 350 mV; b) *It* = 5 pA, *Vt* = 200 mV.

The visualization of such supramolecular interconversion at the solid-liquid interface opens new avenues towards understanding the mechanism of formation and functioning of complex nucleobase architectures like DNA or RNA.

Furthermore, the *in-situ* reversible assembly and re-assembly between two highly ordered supramolecular structures at the surfaces represents the first step towards the generation of nanopatterned responsive architectures.

4.4.2 Ditopic guanosine derivative

Finally, concerning photoswitchable systems based on guanosine nucleobase, in Scheme 4.3 it is shown the synthetic strategy to obtain derivative **45**.

Currently we focus on characterization of the multiple cross-linking interconnections that this ditopic guanosine can generate in presence of cations. The networks formed may be considered to encompass the various superstructures resulting from a combination of a chain of G_4 units interconnected in a double-linear fashion and of a fully cross-linked array; in addition, assemblies of internally-bridged G-quartets may be considered (Figure 4.31).

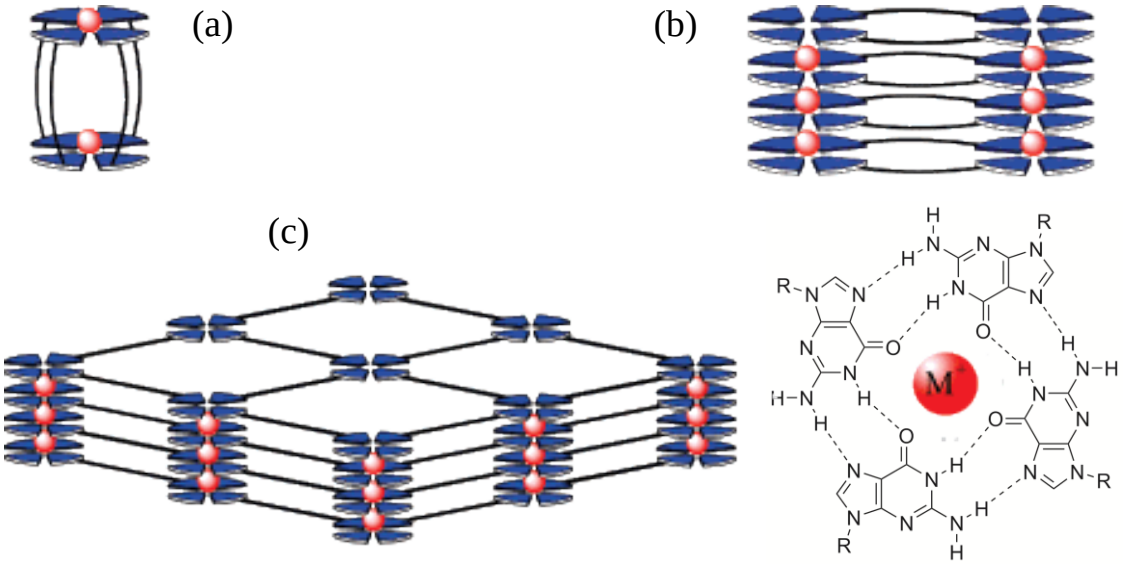

Figure 4.31. Possible supramolecular entities formed by ditopic guanosine derivative **45** through association into G-quartets stabilized by K^+ binding: (a) internally-bridged assembly; (b) linear chain of doubly-bridged G_4 units; (c) fully cross-linked regular array of G_4 units.

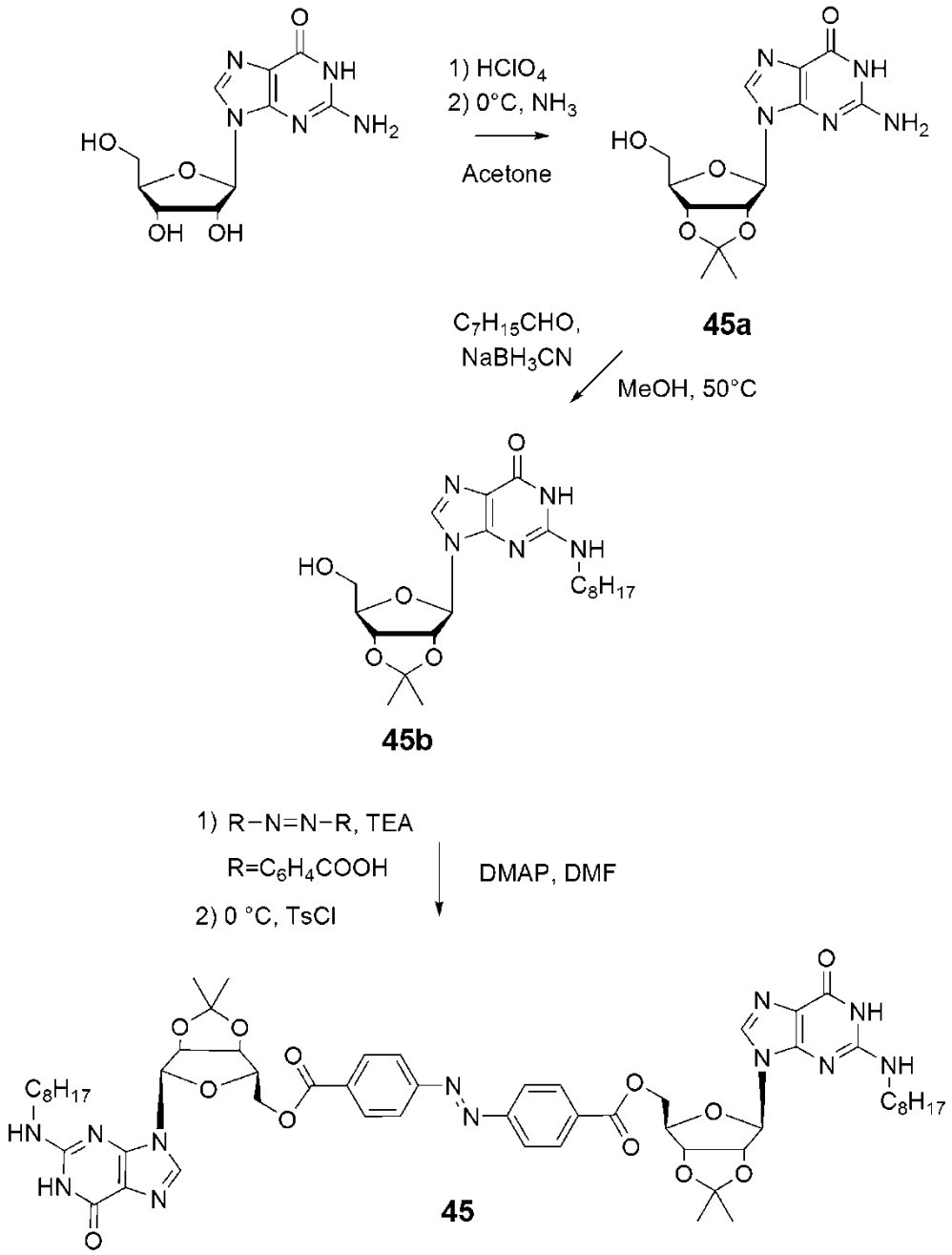

Scheme 4.3. Synthesis of ditopic guanosine derivative **45**.

Derivative **45** was synthesized in three steps starting from guanosine. After protection of free 2'- and 3'-hydroxyls, reductive amination of octanal with the N2 amine of the nucleobase followed by acylation with azobenzene-4,4'-dicarboxylic acid afforded the desired compound (see Experimental Part, Chapter 5).

4.5 Cyclodextrins: Photoresponsive Host-Guest Assemblies

'Mankind is divisible into two great classes: hosts and guests'.
Max Beerbohm (b. 1872), *Hosts and Guests*

4.5.1 Concerning cyclodextrins

Cyclodextrins are a class of chiral, cyclic oligosaccharides that have moleculesized cavities. They are preorganised and have a defined bowl shape that is held together by an intramolecular hydrogen bonding network. Cyclodextrins are the most widely used receptors in *host–guest inclusion chemistry*, with a broad range of applications and industrial production of over a thousand tons per annum. They are used in the food and cosmetics industries and the pharmaceutical sector as stabilising agents, and for the slow release of drugs.

Cyclodextrins commonly comprise between six and eight d-glucopyranoside units that are linked together by a 1,4-glycosidic link. There are three important crystalline, homogeneous and non-hygroscopic cyclodextrins, i.e. α-, β- and γ- cyclodextrin, consisting of six, seven and eight glucopyranose units, respectively (Figure 4.32).

The shapes of cyclodextrins are generally represented as a cylindrical funnel (Figure 4.33) by analogy to the calixarene family. Cyclodextrins have an upper (wide) and lower (narrow) rim. The upper rim consists of the secondary hydroxyl groups and the lower of primary hydroxyl groups. The large number of hydrophilic hydroxyl groups around the rims, plus the hydrophobic nature of the cavity, gives these molecules their unique ability to form inclusion complexes in water.

Cyclodextrins can easily be derivatised by modification of the hydroxyl groups. There are a large number of cyclodextrin derivatives in the literature, containing groups such as alkyl, hydroxyalkyl, carboxyalkyl, amino, thiol and tosyl, which often contain ether or ester linkages. Derivatisation improves the hosts' solubility, increases their affinity for a particular guest target, allows the attachment of specific catalytic groups or allows grafting onto a polymer support for use in chromatographic separation technologies.

Cyclodextrins usually form 1:1 host–guest complexes, although 1:2 and 2:2 complexes are also possible. In aqueous solution, the hydrophobic (or at best 'semi-polar') cavity is filled with water. This water is relatively unstable, due to unfavourable polar–apolar interactions, and the water molecules can be easily replaced by another guest

molecule less polar than water. For example *p*-xylene forms a 1:1 complex with β-cyclodextrin (Figure 4.34).[64]

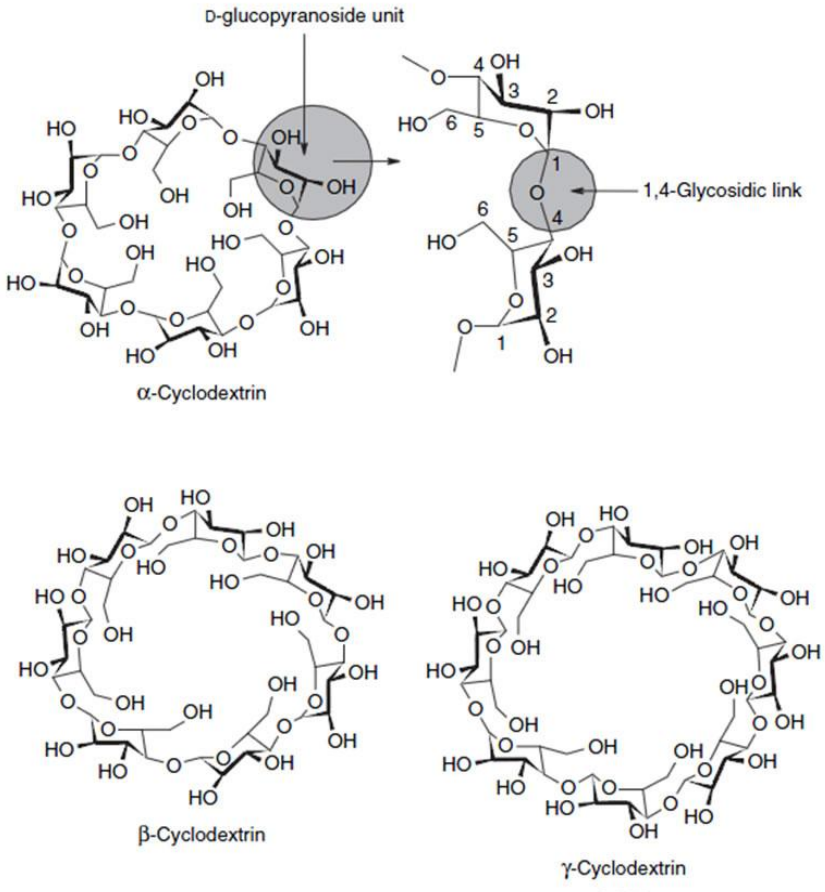

Figure 4.32. The structures of the three most common cyclodextrins (From reference 64).

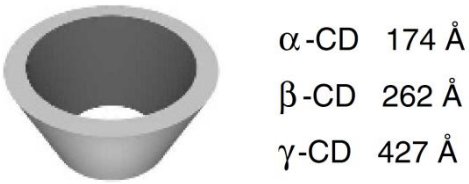

Figure 4.33. Schematic of the common cyclodextrins (CDs), highlighting the cavity volume (From reference 64).

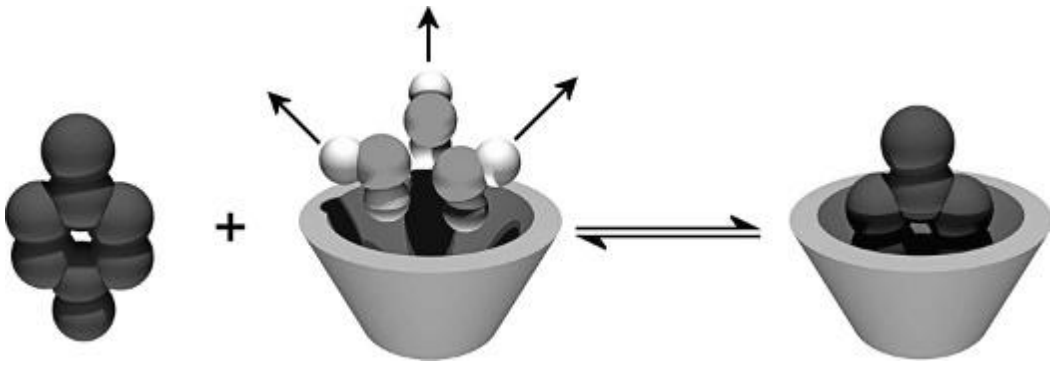

Figure 4.34. Schematic of the cyclodextrin inclusion complex with *p*-xylene in water (From reference 64).

4.5.2 Controlling self-assembly of polymers

Most photoresponsive self-assemblies, as those described above in this Chapter, possess photoswitchable moieties in building blocks in order to induce morphological transformation. From this viewpoint, the photoresponsive self-assemblies of water-soluble polymer p(AA/C12) reported by Harada et al. is unique because the photochromic molecule is used as a 'photoresponsive key'[65] which does not take part in the ensembles (Figure 4.35a).[66] They utilized photo-tunable binding affinities of azobenzene dicarboxylic acid (ADA) guests with α-cyclodextrin (αCD) host. Similar to the unsubstituted azobenzene,[67] *trans*-ADA shows higher binding affinity to αCD compared to the *cis*-isomer.

Poly(acrylic acid)s p(AA/C12) modified by dodecyl groups self-assemble in water through solvophobic interaction between the aliphatic side chains (Figure 4.35b), affording hydrogels. When αCD is added to the gels, gel-to-sol conversion is observed because αCDs capture dodecyl groups, disrupting their solvophobic interactions (Figure 4.35b and c). Remarkably, the addition of *trans*-ADA to this binary mixture converts the solution to the original gel state since *trans*-ADA can predominantly complexes with αCD, thus rendering the dodecyl chains free (Figure 4.35c and d). This ternary mixture including p(AA/C12), ADA and αCD is therefore capable of photoswitching between gel and solution states owing to the photo-tunable binding affinity between ADA and αCD.

Indeed, irradiation of the gel of the ternary mixture with UV-light resulted in a gel-to-sol conversion as a result of lower binding affinity of photogenerated *cis*-ADA to αCD than that of dodecyl group (Figure 4.35d and e). Subsequent irradiation of the

photogenerated solution with visible light again induced gelation due to preferential complexation of αCD with *trans*-ADA (Figure 4.35e and d). This system might be categorized as a unique photoresponsive self-assembly driven by a ‘‘photoresponsive key’’. A similar but irreversible photoinduced disaggregation has been reported for supramolecular polymers of quadruple hydrogen-bonding modules.[68]

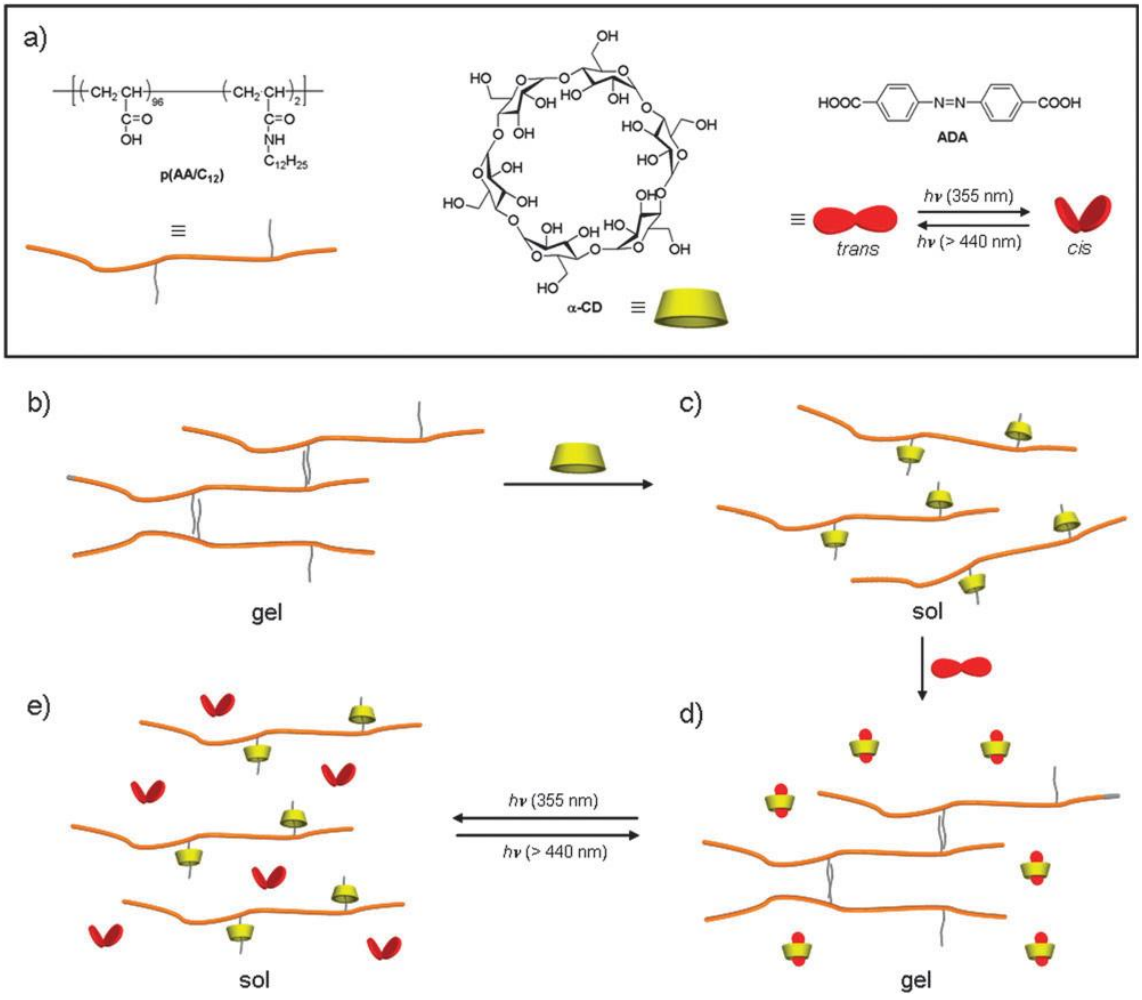

Figure 4.35. (a) Structures and cartoon representations of aqueous polymer p(AA/C12), azobenzene dicarboxylic acid (ADA) and αCD. (b–e) Schematic representation of the self-assembly of aqueous polymer p(AA/C12) controlled by the photoresponsive complexation between ADA and αCD.

Other fascinating photoresponsive self-assemblies of polymers have been reported by the same group.[69] They prepared water soluble polymers p3αCD and p6αCD possessing cyclodextrin pendant groups (Figure 4.36a). For p3αCD, αCD is connected at the 3-position of a glucose ring whereas for p6αCD it is connected at the 6-position.

pC12Azo is the complementary photoresponsive polymer bearing an azobenzene group on the toe of the dodecamethylene (C12) side chains. The mixtures of these host

and guest polymers, i.e., p3αCD/pC12Azo and p6αCD/pC12Azo, were anticipated to generate cross-linked assemblies through the complexation between azobenzene-C12 and αCD moieties. The steady-state viscosity (Z) measurements of semidilute solutions showed that these mixtures have dramatically different Z values despite the fact that both the assemblies are based on the same host–guest interactions. The Z value of p6αCD/pC12Azo was two orders of magnitude larger than that of p3αCD/pC12Azo. This already suggests that local binding affinities between αCD and azobenzene moieties are different for the two binary mixtures. The mixtures were further investigated by 2-D NMR (NOESY) technique, uncovering different local interaction modes. For p3αCD/pC12Azo, interactions were mainly observed between azobenzene and αCD moieties (Figure 4.36b, left) whereas for p6αCD/pC12Azo, interactions were predominantly observed between C12 and αCD moieties (Figure 4.36c, left).

Surprisingly, such a small different in local interaction modes causes contrasted Z changes for the two binary mixtures upon alternative irradiation with UV and visible light.

The mixture p3αCD/pC12Azo showed a further decrease in viscosity upon irradiation with UV-light (Figure 4.36b, from left to right) whereas p6αCD/pC12Azo showed a further increase in viscosity (Figure 4.36c, from left to right). When these UV-irradiated mixtures were subsequently irradiated with visible light, reversal changes were observed for each mixture, i.e., increase and decrease in viscosity for p3αCD/pC12Azo and p6αCD/pC12Azo, respectively (Figure 4.36b and c, from right to left). These interesting observations suggest the occurrence of quite different changes in the local interaction modes for the two binary mixtures upon *trans*-to-*cis* isomerization of azobenzene moieties. NOESY measurements of the UV-irradiated mixtures revealed that azobenzene-C12 and αCD moieties of p3αCD/pC12Azo no longer interact (Figure 4.36b, right) whereas C12 and αCD moieties of p6αCD/pC12Azo interact even after UV irradiation, suggesting that p6αCD and pC12Azo are interlocked upon *trans*-to-*cis* isomerization of azobenzene moieties (Figure 4.36c, right). The positive effect of *trans*-to-*cis* isomerization of azobenzene on supramolecular assemblies (i.e., enhancement of noncovalent interaction or increase in degree of aggregation) is a unique photoresponse.

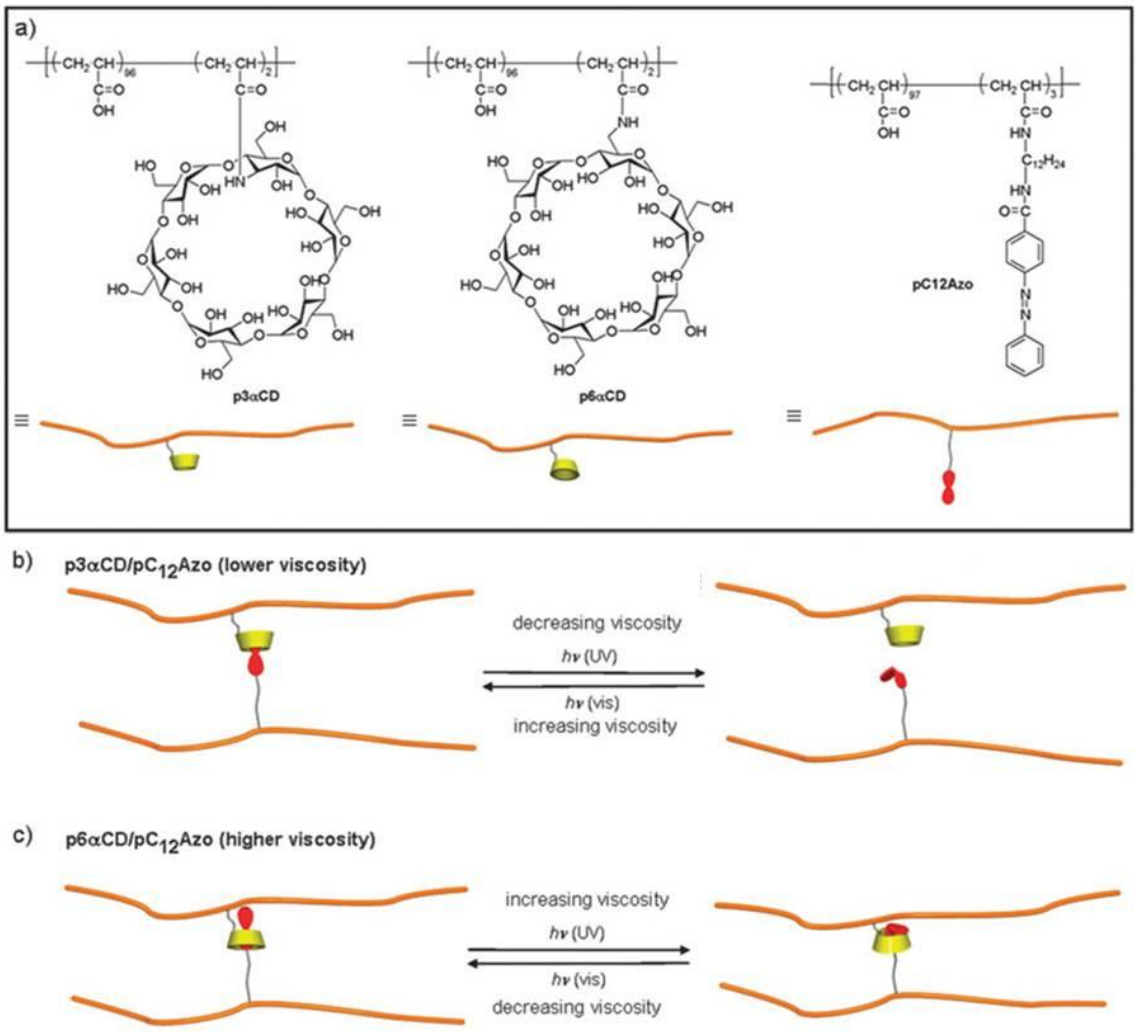

Figure 4.36. (a) Structures of crown-appended polymers p6αCD and p3αCD, and azobenzene-C12-modified polymer pC12Azo. (b and c) Schematic representations of photoresponsive self-assemblies of polymer mixtures p3αCD/pC12Azo and p6αCD/pC12Azo, respectively.

4.5.3 Self-assembling/disassembling of αCD–guest conjugates

Recently our group showed a prototype of a light-powered engine, i.e. the direct conversion of light into continuous mechanical energy by photoreversible self-assembly.[60b]

The main idea was based on one intriguing aspect of photoreversible isomerization of azobenzene: the *Z* isomer has an energy content higher (about 50 kJ mol^{-1}) than the *E* form, meaning that, during photoisomerization, some energy is "harvested" from light and "stored" in the *Z* isomer in the form of a potential. Usually

this energy is dissipated thermally during the back-isomerization to the *E* form, and the thermal effects of this process are so weak that they are useless for practical purposes.

With the aim of finding a way to collect this energy and transform it into a useful form, one can reason that the energy content of a chemical system depends on several factors besides temperature, and in particular, it depends on the number of particles which constitute it. Thus, if the photoisomerization can be coupled to a change in system concentration, this could pave the way to the conversion of the stored energy into an exploitable form (e.g. mechanical work). If a continuous conversion of energy is sought, this concentration change must be reversible, like photoisomerization itself. In addition, the variation of the number of particles does not necessarily imply that matter enters or leaves the system: the system just has to be fooled to believe it. A supramolecular approach was best suited to implement these qualities into an azobenzene-based molecular structure.

The first step was therefore to design an azobenzene derivative with a built-in capability of undergoing an aggregation change as a consequence of photoisomerization.

To this purpose, azodicarboxylic acid **46** (Figure 4.37) was synthesized. As shown in Figure 4.38 conformational constrictions make the *Z* isomer exist as an intramolecularly H-bonded, soluble monomer (in contrast, for example, to the system described in section **4.3.1**). On the other hand, owing both to the solvent polarity and its ability to compete for H-bonding, the *E* isomer exists in solution as a dynamic distribution of intermolecularly H-bonded, low order supramolecular oligomers. These oligomers, on growing, become insoluble and precipitate to form an extensively H-bonded solid. Hence, there is a twofold control operated by light on the number of particles in solution, as the *E* isomer seems aggregated in solution while the *Z* isomer is not.

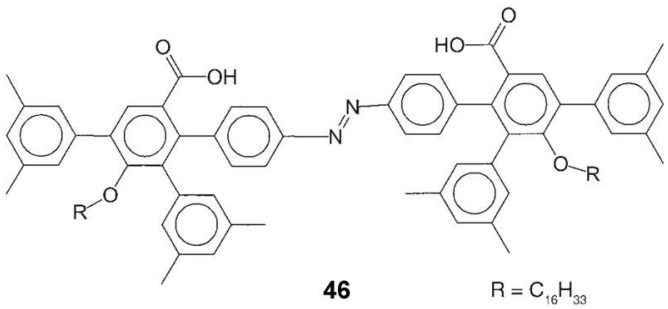

46 $R = C_{16}H_{33}$

Figure 4.37. Azodicarboxylic acid derivative.

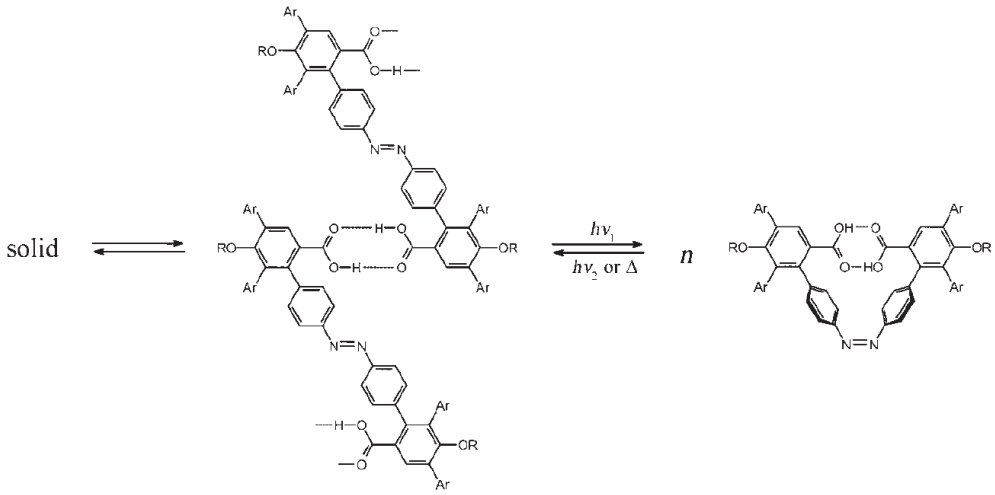

Figure 4.38. Photoresponsive self-assemblies of derivative **46**.

The second step was to build up an osmotic cell (Figure 4.39) in which photoisomerization could be carried out in both compartments: during alternating irradiation (UV/Vis light) a flow of solvent takes place from one compartment to the other as a result of a change in system concentration due to assembling/deassembling process.

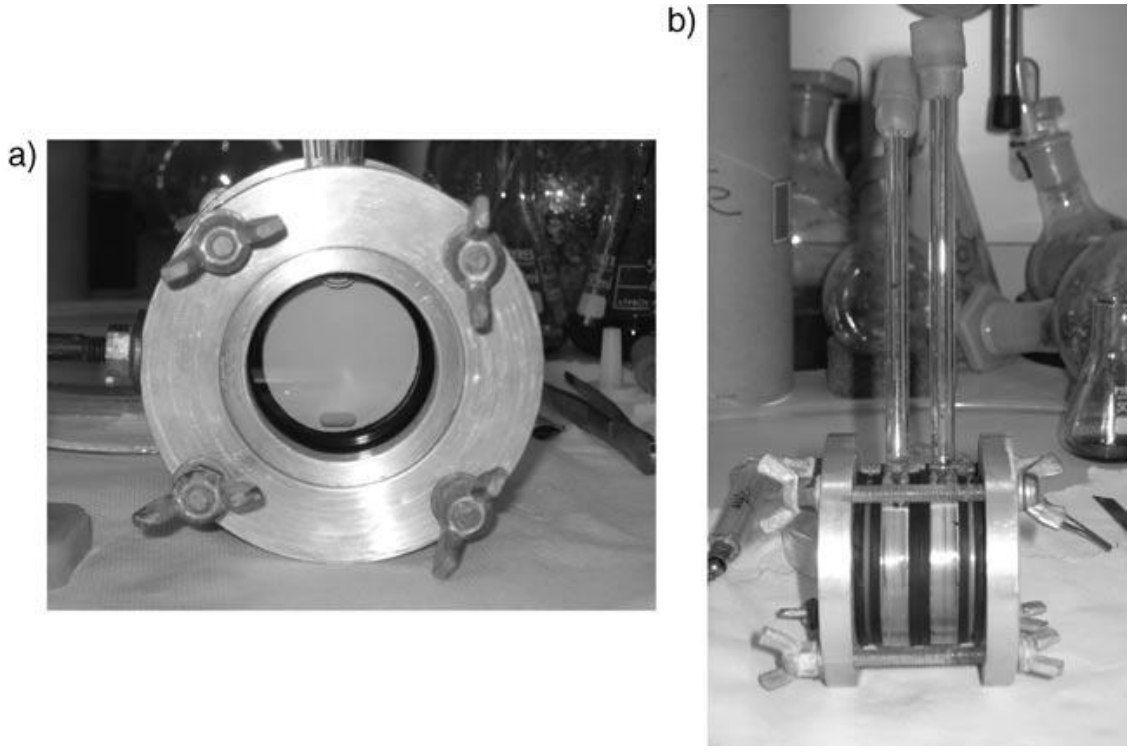

Figure 4.39. Side (a) and front (b) views of the osmotic cell.

Hence, Masiero et al. built up a system in which the energy harvested from light and stored in the molecules upon photoisomerization can be converted into a

macroscopic form by taking advantage of colligative properties and, in particular, of osmosis. This system has been developed to demonstrate the feasibility of the idea of converting light into mechanical energy by means of a photoreversible self-assembly/disassembly process.

Nevertheless enhancement concerning cell design and materials could be devised, currently our challenge is to improve the solvent-solute system of this light-powered engine. To this aim, thanks to the photo-tunable binding affinities of azobenzene guests with α-cyclodextrin (αCD) host (see **4.5.2**), we focus on developing αCD–azobenzene conjugates such as those, recently synthesized, depicted in Figure 4.40.

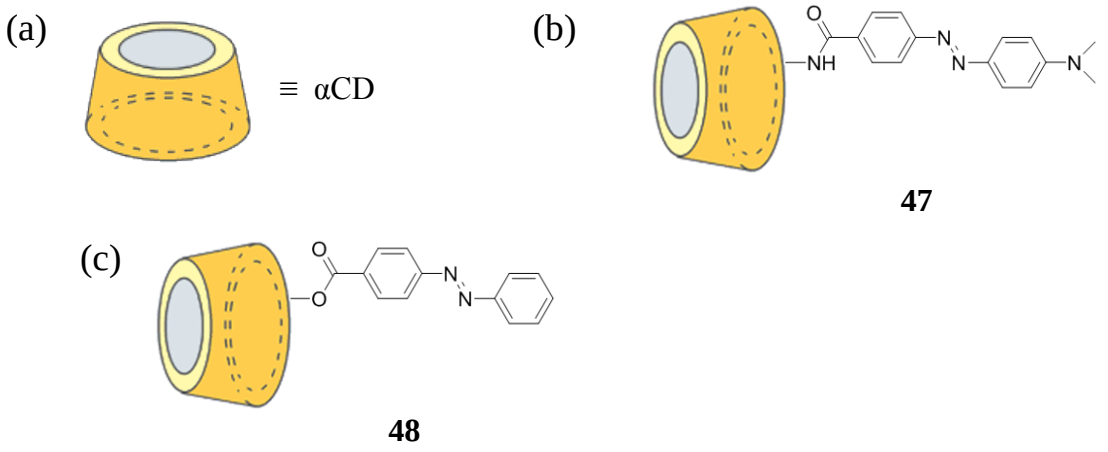

Figure 4.40. αCD-azobenzene dyads.

As well described in literature by Harada et al.,[70] when an appropriate guest moiety is covalently attached to a CD molecule in a suitable way, they may form intramolecular complexes or intermolecular complexes to give supramolecular oligomers and polymers (Figure 4.41).

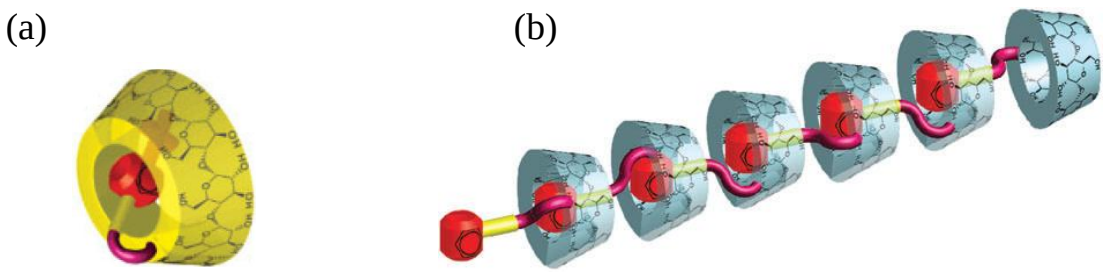

Figure 4.41. Cartoons showing (a) 6-*p*-*tert*-Boc-cinnamoylamino-β-cyclodextrin intramolecular complex (adapted from reference 70a) and (b) 3-cinnamoylamino-α-cyclodextrin supramolecular polymers. (Adapted from reference 70b)

Hence, as shown in Figure 4.40, we attached photoresponsive azobenzene moiety to the secondary side (wider side) of αCD both *via* amide (3-*NH*-αCD-derivative **47**) and ester linkage (2-*O*-αCD-derivative **48**). Taking advantage of the binding affinity between *trans*-azobenzene and αCD, it could be possible to give rise to intermolecular complexes leading to supramolecular oligomers and polymers if the photoresponsive guest is included from the narrower side of αCD (Figure 4.42, see also Figure 4.36b, left). On the other hand, irradiation with UV light will lead to disassemble the supramolecular structure as a result of lower binding affinity of photogenerated *cis*-azobenzene to αCD (Figure 4.42, see also Figure 4.36b, right).

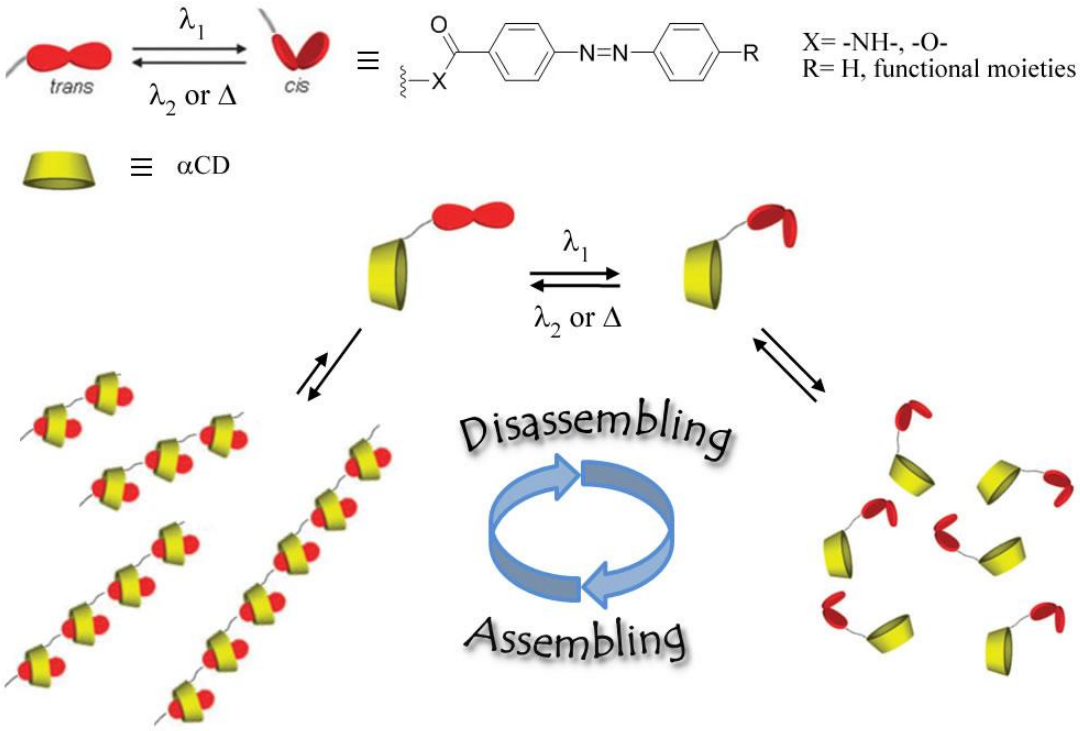

Figure 4.42. A schematic view of the light-powered assembling–disassembling of αCD-azobenzene conjugates.

αCD-azobenzene dyads will improve the light-powered engine previously described for three main reasons: i) using αCD, the system will work in aqueous medium instead of organic medium; ii) the system will be homogeneous (oligomers formed by *trans*-isomer **46**, on growing, become insoluble and precipitate leading to a phase separation) inducing a faster change in system concentration during photoisomerization process (in the previous system dissolution process of *trans*-isomer **46** aggregates needs

to take into account); iii) an easier synthetic approach to control aggregate/monomer interconversion, i.e assembling/deassembling process.

In conclusion, controlled disassembly can be in some instances a valuable process itself, and the use of colligative properties can be a way to link dynamic phenomena that occur at a molecular or nanoscopic level with the macroscopic world. On considering that, according to the van't Hoff equation, a 1 mol L^{-1} solution of a non-electrolyte develops a pressure of about 24 atm (i.e. 18 m Hg) at room temperature, we believe there is room for future development of such systems.

Finally, it is shown the synthetic strategy to obtain derivatives **47** and **48**. An important problem in the synthesis of secondary face monofunctionalized cyclodextrins remains the separation of the reaction mixtures. Because of the presence of many, more or less equally reactive hydroxyl groups, chemo- and regioselective monofunctionalization occurs only rarely. Consequently, comprehensive and scale-limited purification methods using selective precipitation, recrystallization, reverse phase chromatography, and size exclusion chromatography are often needed, and moderate yields are unavoidable. The use of partially silylated cyclodextrins, in which the primary hydroxyls are converted to silyl ethers, turned out to be an important step for better defined synthetic routes to selectively modified cyclodextrins.[71] Silylated cyclodextrins are soluble in various organic solvents, can be purified on a large scale by common silica gel chromatography, and open possible routes to differentiate between the remaining C(2)- and C(3) – hydroxyls (see Figure 4.32).[71-73]

Here we report the monofunctionalization of α-cyclodextrins at the secondary face by two methods. In the first method (Scheme 4.4) an amino-functionalized group is introduced at the C(3)-position of the cyclodextrin by prior tosylation of a secondary hydroxyl group of silylated cyclodextrin and subsequent nucleophilic ring-opening of the intermediate cyclodextrin manno-epoxide. Subsequent acylation followed by deprotection of the silylated primary hydroxyls of the cyclodextrin afforded derivative **47** (see Experimental Part, Chapter 5).

The second method (Scheme 4.5) proceeds by direct and selective introduction of the functional group to the secondary hydroxyl face of silylated cyclodextrin *via* acylation of the C(2)-hydroxyl, leaving the configuration of all glucose units in the cyclodextrin intact. Deprotection of the silylated primary hydroxyls yielded compound **48** (see Experimental Part, Chapter 5).

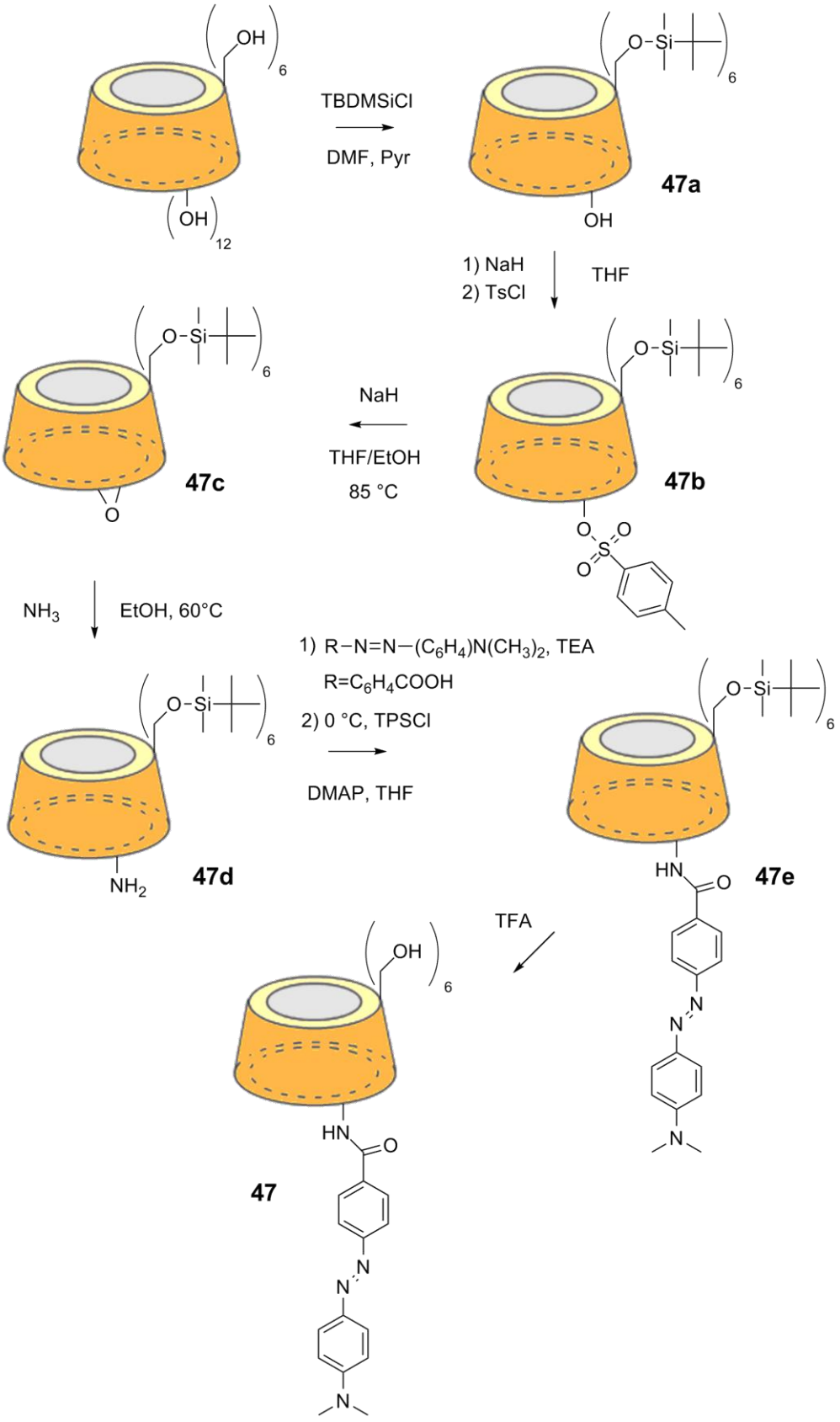

Scheme 4.4. Synthesis of derivative **47**.

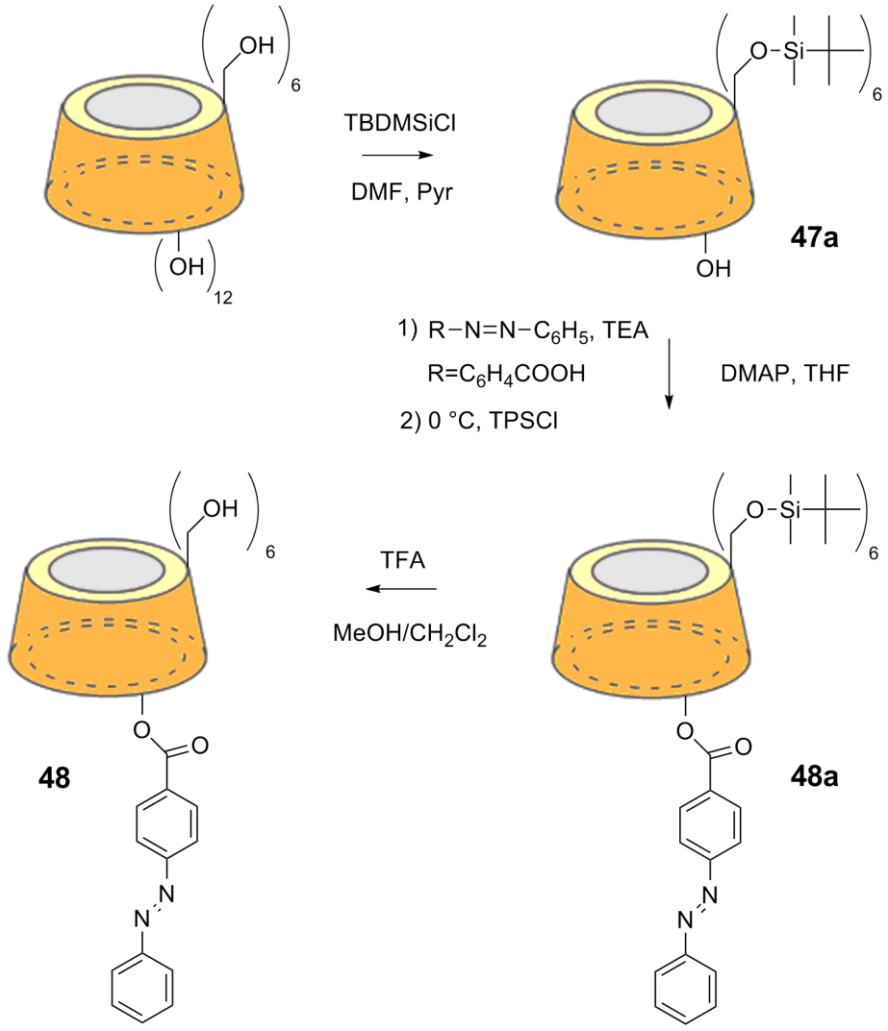

Scheme 4.5. Synthesis of derivative **48**.

4.6 Conclusion

Here, we have shown recently reported supramolecular self-assemblies, some of which could be considered as new paradigms of photoresponsive self-assembling systems. These examples illustrate that there remains a possibility to discover unprecedented photoresponsive molecular ensembles, if one can elaborately combine photochromic molecules with specifically-designed supramolecular building blocks. The incorporation of photoresponsive molecules showing more elaborate mechanical motions[46,74,75] would enhance the quality of photoresponse (e.g., more precise control of aggregation number and supramolecular architecture), enabling the creation of photoresponsive self-assemblies with high sensitivity. On the other hand, the translation of signals emanating from multicomponent self-assemblies by light-stimulus (i.e.,

changes in aggregation number and supramolecular architecture) to other chemical signals, as seen in light-sensed biological processes such as vision, is a topic that need to be addressed for the creation of further complex systems. The accumulation of insight into the construction principle, mechanism and concept of such light-driven supramolecular self-assemblies is crucial for the realization of such complex light-driven systems and practical smart functional materials in various fields of science and technology.

References

1. B. L. Feringa, R. A. van Delden, N. Koumura and E. M. Geertsema, *Chem. Rev*., **2000**, *100*, 1789–1816.
2. R. Ballardini, V. Balzani, A. Credi, T. M. Gandolfi and M. Venturi, *Acc. Chem. Res.*, **2001**, *34*, 445–455.
3. C.-H. Huang and D. M. Bassani, *Eur. J. Org. Chem*., **2005**, 4041–4050.
4. G. A. Woolley, *Acc. Chem. Res*., **2005**, *38*, 486–493.
5. O. Pieroni, A. Fissi, N. Angelini and F. Lenci, *Acc. Chem. Res*., **2001**, *34*, 9–17.
6. T. Seki, *Bull. Chem. Soc. Jpn*., **2007**, *80*, 2084–2109.
7. J.-i. Anzai and T. Osa, *Tetrahedron*, **1994**, *50*, 4039–4070.
8. A. Natansohn and P. Rochon, *Chem. Rev.*, **2002**, *102*, 4139–4176.
9. T. Kinoshita, *J. Photochem. Photobiol., B*, **1998**, *42*, 12–19.
10. C. Dugave and L. Demange, *Chem. Rev*., **2003**, *103*, 2475–2532.
11. S. Yagai, *J. Photochem. Photobiol., C*, **2006**, *7*, 164–182.
12. C. J. Barrett, J.-i. Mamiya, K. G. Yager and T. Ikeda, *Soft Matter*, **2007**, *3*, 1249–1261.
13. K. Kinbara and T. Aida, *Chem. Rev.*, **2005**, *105*, 1377–1400.
14. S. Yagai, T. Karatsu and A. Kitamura, *Chem. Eur. J.*, **2005**, *11*, 4054–4063.
15. N.Y.C. Chu, in: H. Durr, H. Bouas-Laurent (Eds.), *Photochromism. Molecules and Systems*, Elsevier, Amsterdam, **1990**.
16. R. Rosario, D. Gust, M. Hayes, J. Springer, A. Garcia, *Langmuir* **2003**, *19*, 8801–8806.
17. R. Rosario, D. Gust, M. Hayes, F. Janke, J. Springer, A.A. Garcia, *Langmuir* **2002**, *18*, 8062–8069.
18. R. Rosario, D. Gust, A.A. Garcia, M. Hayes, J.L. Taraci, T. Clement, J.W. Dailey, S.T. Picraux, *J. Phys. Chem. B* **2004**, *108*, 12640–12642.
19. H. Rau, *Photoisomerization of azobenzenes*, in: J.F. Rebek (Ed.), *Photochemistry and Photophysics*, CRC Press, Boca Raton, **1990**.
20. B.L. Feringa (Ed.), *Molecular Switches*, Wiley-VCH, Weinheim, **2001**. B.L. Feringa (Ed.), Wiley-VCH, Weinheim, **2001**, p. 001.
21. M. Irie, *Chem. Rev.* **2000**, *100*, 1683–1684.
22. D.H. Waldeck, *Chem. Rev*. **1991**, *91*, 415–436.
23. B.L. Feringa, *Acc. Chem. Res*. **2001**, *34*, 504–513.

24. E.R. Kay, D.A. Leigh, *Hydrogen bond-assembled synthetic molecular motors and machines*, in: T.R. Kelly (Ed.), *Molecular Machines, Topics Curr. Chem*. **2005**, *262*.
25. R.A. van Delden, M.K.J. ter Wiel, B.L. Feringa, *Chem. Commun*. **2004**, 200–201.
26. N. Koumura, R.W.J. Zijlstra, R.A. van Delden, N. Harada, B.L. Feringa, *Nature* **1999**, *401*, 152–155.
27. E.R. Kay, D.A. Leigh, *Synthetic molecular machines*, in: T. Schrader, A.D. Hamilton (Eds.), *Functional Artificial Receptors*, Wiley-VCH, Weinheim, **2005**.
28. V. Balzani, A. Credi, F.M. Raymo, J.F. Stoddart, *Angew. Chem. Int. Ed.* **2000**, *39*, 3349–3391.
29. J.F. Stoddart, *Acc. Chem. Res*. **2001**, *34*, 410–411.
30. A.H. Flood, R.J.A. Ramirez, W.-Q. Deng, R.P. Muller, W.A. Goddard III, J.F. Stoddart, *Aust. J. Chem.* **2004**, *57*, 301–322; T.J. Huang, B. Brough, Ch.-M. Ho, Y. Liu, A.H. Flood, P.A. Bonvallet, H.-R. Tseng, J.F. Stoddart, M. Baller, S. Magonov, *Appl. Phys. Lett*. **2004**, *85*, 5391–5393.
31. G. Bottari, D.A. Leigh, E.M. Pérez, *J. Am. Chem. Soc*. **2003**, *125*, 13360–13361.
32. Q.-C. Wang, D.-H. Qu, J. Ren, K. Chen, H. Tian, *Angew. Chem. Int. Ed.* **2004**, *43*, 2661–2665; A.M. Brower, C. Frochot, F.G. Gatti, D.A. Leigh, L. Mottier, F. Paolucci, S. Roffia, G.W.H. Wurpel, *Science* **2001**, *291*, 2124–2128; D.-H. Qu, Q. C. Wang, J. Ren, H. Tian, *Org. Lett*. **2004**, *6*, 2085–2088; E.M. Pérez, D.T.F. Dryden, D.A. Leigh, G. Teobaldi, F. Zerbetto, *J. Am. Chem. Soc.* **2004**, *126*, 12210–12211.
33. S. Shinkai, T. Yoshida, K. Miyazaki and O. Manabe, *Bull. Chem. Soc. Jpn.*, **1987**, *60*, 1819–1824.
34. S. Shinkai, T. Yoshida, O. Manabe and Y. Fuchita, *J. Chem. Soc., Perkin Trans. 1*, **1988**, 1431–1437.
35. M. S. Vollmer, T. D. Clark, C. Steinem and M. R. Ghadiri, *Angew. Chem., Int. Ed.*, **1999**, *38*, 1598–1601.
36. D. J. Bullock, C. W. N. Cumper and A. I. Vogel, *J. Chem. Soc*., **1965**, 5316–5323.
37. O. Pieroni, A. Fissi, J. L. Houben and F. Ciardelli, *J. Am. Chem. Soc*., **1985**, *107*, 2990–2991.
38. 24. S. Shinkai, K. Matsuo, M. Sato, T. Sone and O. Manabe, *Tetrahedron Lett*., **1979**, *22*, 1409–1412.

39. T. Ishi-i and S. Shinkai, *Top. Curr. Chem*., **2005**, *258*, 119–160.
40. N. M. Sangeetha and U. Maitra, *Chem. Soc. Rev*., **2005**, *34*, 821–836.
41. L. N. Lucas, J. van Esch, B. L. Feringa and R. M. Kellogg, *Chem. Commun*., **2001**, 759–760.
42. M. Takeshita, M. Hayashi, S. Kadota, K. H. Mohammed and T. Yamato, *Chem. Commun.*, **2005**, 761–763.
43. J. J. D. de Jong, L. N. Lucas, R. M. Kellogg, J. H. van Esch and B. L. Feringa, *Science*, **2004**, *304*, 278–281.
44. J. J. D. De Jong, T. D. Tiemersma-Wegman, J. H. Van Esch and B. L. Feringa, *J. Am. Chem. Soc*., **2005**, *127*, 13804–13805.
45. S. Hecht, *Small*, **2005**, *1*, 26–29.
46. B. L. Feringa, *J. Org. Chem*., **2007**, *72*, 6635–6652.
47. J. J. D. de Jong, B. L. Feringa and J. H. van Esch, in *Molecular Gels: Materials with Self-assembled Fibrillar Networks*, ed. R. G. Weiss and P. Terech, Springer, Dordrecht, **2006**, pp. 895–927.
48. T. Hirose, K. Matsuda and M. Irie, *J. Org. Chem*., **2006**, *71*, 7499–7508.
49. F. Rakotondradany, M. A. Whitehead, A.-M. Lebuis and H. F. Sleiman, *Chem. Eur. J*., **2003**, *9*, 4771–4780.
50. F. L. Callari, S. Sortino, *Chem. Commun.*, **2008**, 6179–6181.
51. G. M. Whitesides, E. E. Simanek, J. P. Mathias, C. T. Seto, D. Chin, M. Mammen and D. M. Gordon, *Acc. Chem. Res.*, **1995**, *28*, 37–44.
52. S. Yagai, T. Karatsu and A. Kitamura, *Chem. Commun*., **2003**, 1844–1845.
53. A. G. Bielejewska, C. E. Marjo, L. J. Prins, P. Timmerman, F. de Jong and D. N. Reinhoudt, *J. Am. Chem. Soc*., **2001**, *123*, 7518–7533.
54. S. Yagai, T. Nakajima, T. Karatsu, K. Saitow and A. Kitamura, *J. Am. Chem. Soc.*, **2004**, *126*, 11500–11508.
55. H. M. Keizer and R. P. Sijbesma, *Chem. Soc. Rev*., **2005**, *34*, 226–234.
56. S. Yagai, T. Nakajima, K. Kishikawa, S. Kohmoto, T. Karatsu and A. Kitamura, *J. Am. Chem. Soc.*, **2005**, *127*, 11134–11139.
57. *Materials-Chirality*, *Topics in Stereochemistry*, ed. M. M. Green, R. J. M. Nolte, and E. W. Meijer, Wiley Interscience, New Jersey, **2003**, *24*.
58. R. Iwaura and T. Shimizu, *Angew. Chem., Int. Ed*., **2006**, *45*, 4601–4604.
59. L.-s. Li, H. Jiang, B. W. Messmore, S. R. Bull and S. I. Stupp, *Angew. Chem., Int. Ed*., **2007**, *46*, 5873–5876.

60. a) G. P. Spada, S. Lena, S. Masiero, S. Pieraccini, M. Surin, P. Samorì, *Adv. Mater*. **2008**, *20*, 2433–2438; b) S. Masiero, S. Lena, S. Pieraccini, G. P. Spada, *Angew. Chem. Int. Ed.* **2008**, *47*, 3184-3187; c) S. Pieraccini, G. Gottarelli, R. Labruto, S. Masiero, O. Pandoli, G. P. Spada, *Chem. Eur. J.* **2004**, *10*, 5632-5639; d) F. Cisnetti, R. Ballardini, A. Credi, M. T. Gandolfi, S. Masiero, F. Negri, S. Pieraccini, G. P. Spada, *Chem. Eur. J.* **2004**, 10, 2011-2021.
61. a) S. Ogasawara, M. Maeda, *Angew. Chem. Int. Ed*. **2008**, *47*, 8839-8842; b) S. Ogasawara, M. Maeda, *Angew*. *Chem. Int. Ed*. **2009**, *48*, 6671-6674.
62. a) N. R. King, E. A. Whale, F. J. Davis, A. Gilbert, G. R. Mitchell, *J. Mater. Chem.* **1997**, *7*, 625-630; b) W. R. Brode, J. H. Gould, G. M. Wyman, *J. Am. Chem. Soc*. **1952**, *74*, 4641-4646.
63. A. Ciesielski, S. Lena, S. Masiero, G. P. Spada, P. Samorì, *Angew. Chem. Int. Ed.* **2010**, *49*, 1963 –1966. Highlight on: *Nature* **2010**, *463*, 852.
64. J. W. Steed, D. R. Turner, K. J. Wallace *Core Concepts in Supramolecular Chemistry and Nanochemistry*, Wiley & Sons, Ltd, Chichester, UK, **2007**.
65. T. Muraoka, K. Kinbara and T. Aida, *J. Am. Chem. Soc*., **2006**, *128*, 11600–11605.
66. I. Tomatsu, A. Hashidzume and A. Harada, *Macromolecules*, **2005**, *38*, 5223–5227.
67. P. Bortolus and S. Monti, *J. Phys. Chem*., **1987**, *91*, 5046–5050.
68. B. J. B. Folmer and E. Cavini, *Chem. Commun*., **1998**, 1847–1848.
69. I. Tomatsu, A. Hashidzume and A. Harada, *J. Am. Chem. Soc*., **2006**, *128*, 2226–2227.
70. a) A. Harada, *Journal of Polymer Science: Part A: Polymer Chemistry* **2006**, *44*, 5113–5119; b) A. Harada, Y. Takashima and H. Yamaguchi, *Chem. Soc. Rev*., **2009**, *38*, 875–882.
71. (a) K. Takeo, K. Uemura, H. Mitoh, *J. Carbohydr. Chem*. **1988**, *7*, 293; (b) K. Takeo, H. Mitoh, K. Uemura, *Carbohydr. Res.* **1989**, *187*, 203; (c) P. Fiigedi, *Carbohydr. Res*. **1989**, *192*, 366; (d) T. J. Michalski, A. Kendler, M. L. Bender, *J. Incl. Phenom*. **1983**, *1*, 125; (e) R. L. Wife, D. E. Reed, D. P. Leworthy, D. M. Barnett, P. D. Regan, H. C. Volger, *Advances in Inclusion Science, Proceedings of the 1st International Symposium on Cyclodextrins*; J. Szejtli, Ed.; Akademiai Kiado: Budapest, **1982**; 301.
72. M. J. Pregel, E. Buncel, *Can. J. Chem.* **1991**, *69*, 130.

73. A. W. Coleman, P. Zhang, H. Parrot-Lopez, C.-C. Ling, M. Miocque, L. Mascrier, *Tetrahedron Lett.* **1991**, *32*, 3997.
74. T. Muraoka, K. Kinbara Y. Kobayashi and T. Aida, *J. Am Chem. Soc.*, **2003**, *125*, 5612–5613.
75. Y. Norikane and N. Tamaoki, *Org. Lett.*, **2004**, *6*, 2595–2598.

Chapter 5. Experimental Part

5.1 General

All reactions were carried out under magnetic or mechanical stirring. Reactions requiring anhydrous conditions were carried out in oven-dried glassware under dry argon atmosphere. For TLC analyses, Baker IB2-F silica gel plates were used. Column chromatography was performed on Aldrich silica gel 230-400 mesh. Reagents and solvents, including dry solvents, were purchased from Aldrich, Fluka or Alfa Aesar.

Melting points were determined using open glass capillaries and are uncorrected.

NMR spectra were recorded with Varian (Gemini 200, Inova 300, Mercury 600 MHz) and Bruker (Avance 400 MHz) instruments; decoupled ^{13}C NMR spectra were usually recorded. To assign carbons, DEPT spectra (multiplicity 1.5) were recorded. All NMR spectra were referenced relative to residual solvent peaks. Electrospray (ES) ionization mass spectra were obtained with a Micromass ZMD 4000. High resolution mass spectra (electronic impact) were recorded with a Thermo Finnigan MAT 95 XP spectrometer. CD spectra were recorded on a JASCO J-710 Spectropolarimeter (cell path length = 0.1 cm). EPR spectra were recorded on a Bruker ELEXSYS-500 instrument.

5.2 Synthetic Procedures

Below it is reported the synthetic strategy to obtain compounds described in the previous Chapters of this thesis. NMR characterization (in particular ^{13}C spectra) of derivatives (and their intermediate compounds) currently under investigation is not yet completed.

5.2.1 Chapter 2

- ***Derivative* 28a: *Synthetic procedure***

Spectrum reported in Figure 5.1 was obtained after addition of 2.6 eq of phenylhydrazine: reduction of the nytroxyl units to hydroxylamino groups allows the improvement of the spectral resolution (on the use of phenylhydrazine for reducing nitroxide moiety to the corresponding hydroxylamine, see reference 1).

3',5'-di-*O*-(2,2,6,6-Tetramethyl-1-oxylpiperidine-4-carbonyl)-2'-deoxyguanosine (28a)

2,4,6-Triisopropylbenzenesulfonyl chloride (446 mg, 1.47 mmol) was added to a solution of 4-Carboxy-2,2,6,6-tetramethylpiperidine-1-oxyl (309 mg, 1.54 mmol) in anhydrous acetonitrile (10 mL) and redistilled triethylamine (0.467 mL, 3.37 mmol) at 0 °C. The resulting solution was stirred for two hours then allowed to reach r.t. and stirred for additional 20 minutes. 2'-deoxyguanosine (200 mg, 0.7 mmol) (dried over P_2O_5 under vacuum for 2 h at 55 °C) and a catalytic amount of DMAP were then added and the mixture was stirred under argon overnight. After evaporation of the solvent *in vacuo*, dichloromethane (20 ml) was added and the organic layer was washed 3 times with saturated $NaHCO_3$ solution (30 mL). The organic layer was dried over Na_2SO_4 and concentrated *in vacuo*. The crude material was purified by flash column chromatography on silica gel (eluent: dichloromethane/methanol 98:2). The isolated product was precipitated from acetonitrile-diethyl ether to afford 133 mg (30 % yield) of the title compound as a pale pink solid. ^{1}H-NMR spectrum, obtained after addition of 2.6 eq of phenylhydrazine, is reported below. MS(ES): m/z 631.3 (MH^+), 654.3 (MNa^+); Anal. Calcd. for $C_{30}H_{45}N_7O_8$: C, 57.04; H, 7.18; N, 15.52; Found: C, 57.14; H, 7.16; N, 15.52.

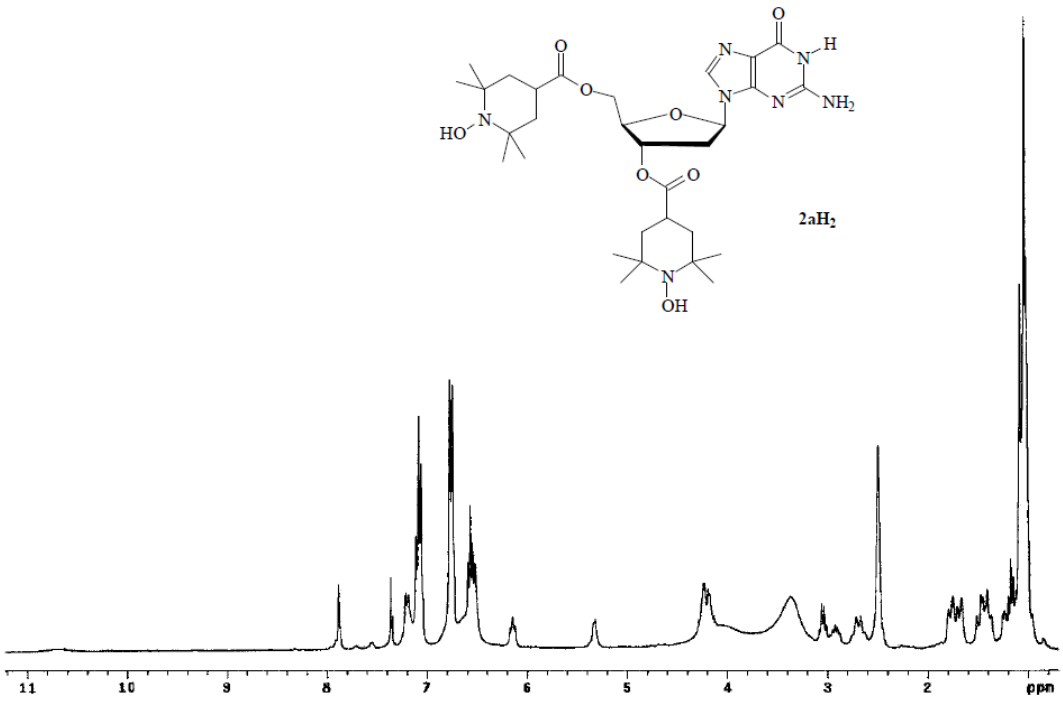

Figure 5.1. ^{1}H-NMR (300 MHz DMSO-d_6) of **28aH$_2$** (after addition of 2.6 equivalents of phenylhydrazine to the NMR tube containing biradical **28a**).

- ***Derivative* 28b: *Synthetic procedure***

3,3,5,5-Tetramethyl-4-oxocyclohexanecarboxylic acid (28c)

To a stirred suspension of 0.704 g (17.6 mmol) of sodium hydride dispersion (60 % in mineral oil) in 5 mL of dimethoxyethane (DME) at 0 °C under Argon was added dropwise a solution of 4-oxocyclohexanecarboxylic acid (500 mg, 3.52 mmol) in 1.5 mL of DME. Stirring was continued for 30' then a solution of CH_3I (1.09 mL, 17.6 mmol) in 5 mL of DME was added dropwise. Stirring was continued overnight at 0 °C. Another portion of NaH (0.14 g, 3.52 mmol) was added, followed after 30' by the addition of neat CH_3I (0.44 mL, 7.04 mmol). The mixture was left under stirring at 0 °C for 24 h, then a further portion of NaH (0.42 g, 10.6 mmol) was added, followed after 30' by the addition of neat CH_3I (0.66 mL, 10.6 mmol). Stirring was continued overnight at 0 °C. GCMS analysis showed at that point that the reaction was complete. The crude was then poured into 100 mL of ethyl ether. The resulting precipitate was filtered and transferred into water (50 mL). The mixture was acidified by addition of 10 mL of 1 N HCl and extracted with ethyl ether (3x50 mL). The organic phase was dried over $MgSO_4$ and the solvent was removed *in vacuo*. The resulting solid (570 mg) was crystallized from petroleum ether/methanol (ratio 10/1, 55 mL), affording the title compound as a white solid (544 mg, 78 %). M.p. 155-157 °C; ^{1}H-NMR (200 MHz, $CDCl_3$): δ 1.13 (s, 6H), 1.22 (s, 6H), 1.86-1.95 (m, 2H), 2.00-2.10 (m; 2H), 3.03 (tt, J=12.2 Hz, J=3.9 Hz, 1H) ppm; ^{13}C-NMR (50 MHz, $CDCl_3$): δ 27.57 (CH_3), 27.63 (CH_3), 35.38 (CH), 41.80 (CH_2), 43.82 (C), 180.95 (C), 218.37 (C) ppm; MS(EI): 198 (M^+), 142, 114, 70.

3',5'-di-*O*-(3,3,5,5-Tetramethyl-4-oxocyclohexanecarbonyl)-2'-deoxyguanosine (28b)

2,4,6-Triisopropylbenzenesulfonyl chloride (174 mg, 0.57 mmol) was added to a solution of 3,3,5,5-Tetramethyl-4-oxocyclohexanecarboxylic acid (120 mg, 0.6 mmol) in anhydrous acetonitrile (4 mL) and redistilled triethylamine (0.190 mL, 1.37 mmol) at 0 °C. The resulting solution was stirred for two hours then allowed to reach r.t. and stirred for additional 20 minutes. 2'-deoxyguanosine (78 mg, 0.27 mmol) (dried over P_2O_5 under vacuum for 2h at 55 °C) and a catalytic amount of DMAP were then added and the mixture was stirred under argon overnight. After evaporation of the solvent *in vacuo*, the crude material was purified by flash column chromatography on silica gel (eluent: dichloromethane/methanol 95:5). The isolated product was precipitated from acetonitrile-diethyl ether to afford 68 mg (40 % yield) of the title compound as a white solid.

^{1}H-NMR (600 MHz, CD_2Cl_2): δ MHz: 1.06 (s, 3H), 1.07 (s, 3H), 1.12 (s, 6H), 1.16 (s, 3H), 1.17 (s, 3H), 1.22 (s, 6H), 1.79-1.90 (m, 4H), 1.94-2.00 (m, 2H), 2.01-2.06 (m, 2H), 2.59-2.64 (m, 1H), 2.94-3.10 (m, 3H), 4.35-4.42 (m, m, 2H), 4.49-4.52 (m, 1H), 5.45-5.48 (m, 1H), 6.27 (dd, J=8.1 Hz, J=6.2 Hz, 1H), 6.50 (bs, 2H), 7.76 (s, 1H), 12.06 (bs, 1H) ppm; ^{13}C-NMR (150 MHz, CD_2Cl_2): δ 27.96 (CH_3), 28.00 (CH_3), 36.05 (CH), 36.09 (CH), 37.50 (CH_2), 42.44 (CH_2), 42.52 (CH_2), 44.25 (C), 44.29 (C), 64.63 (CH_2), 75.31 (CH), 83.26 (CH), 85.36 (CH), 118.16 (C), 136.33 (CH), 151.87 (C), 154.35 (C), 159.50 (C), 175.05 (C), 175.40 (C), 218.42 (C), 218.59 (C) ppm; MS(ES): m/z 650.4 (MNa^+); Anal. Calcd for $C_{32}H_{45}N_5O_8$: C, 61.23; H, 7.23; N, 11.16; Found: C, 61.14; H, 7.24; N, 11.14.

NOESY spectrum of [28b]$_8$•K$^+$•Pic$^-$

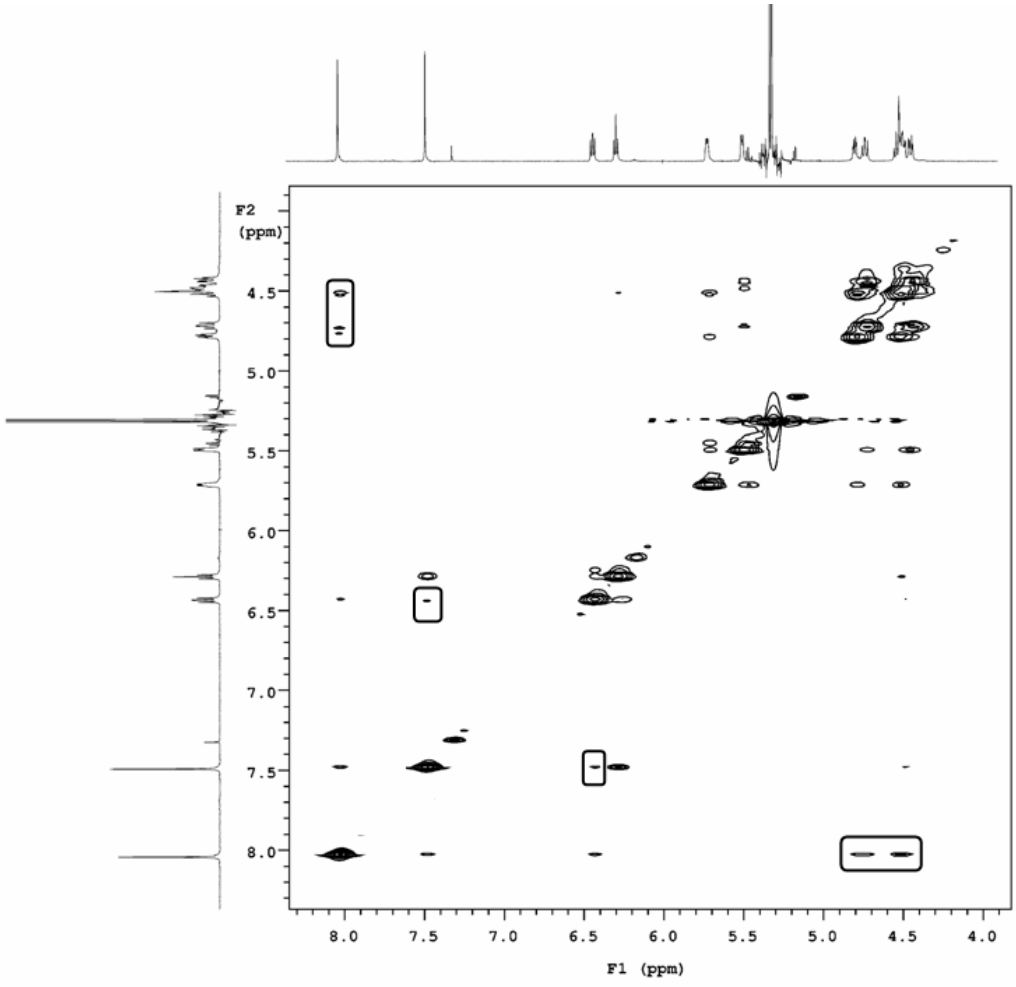

Figure 5.2. Portion of the NOESY spectrum of [**28b**]$_8$•K$^+$•Pic$^-$ in CD_2Cl_2 (600 MHz, r.t., mixing time 150 ms).

- ***Derivative* 29: *Synthetic procedure***

Compound **29a** was prepared according to a modified literature method.[2] Derivative **29c** was carried out according to previously described synthetic procedures (starting from compound **29b**: see reference 3; starting from guanosine: see reference 4).

2-*N*-Formamidine-guanosine (29a)

N,*N*-dimethylformamide dimethyl acetal (0.715 g, 0.797 mL, 6 mmol) was added to a suspension of guanosine (100 mg, 0.35 mmol) in anhydrous DMF (5 mL) . The reaction mixture was stirred under argon at r.t. for 20 h., then the solvent was removed *in vacuo* to give a yellow gum. The product was triturated with methanol and precipitated with diethyl ether to yield **29a** (107 mg, 90 %) as a white solid. ESI-MS: *m/z* (%): 339 (100) [**29a**-H]$^+$. ^{1}H NMR: see Figure 5.3. Elemental analysis: Calcd. (%) for $C_{13}H_{18}O_5N_6$: C 46.15, H 5.36, N 24.84; Found C 45.50, H 5.50, N 24.55.

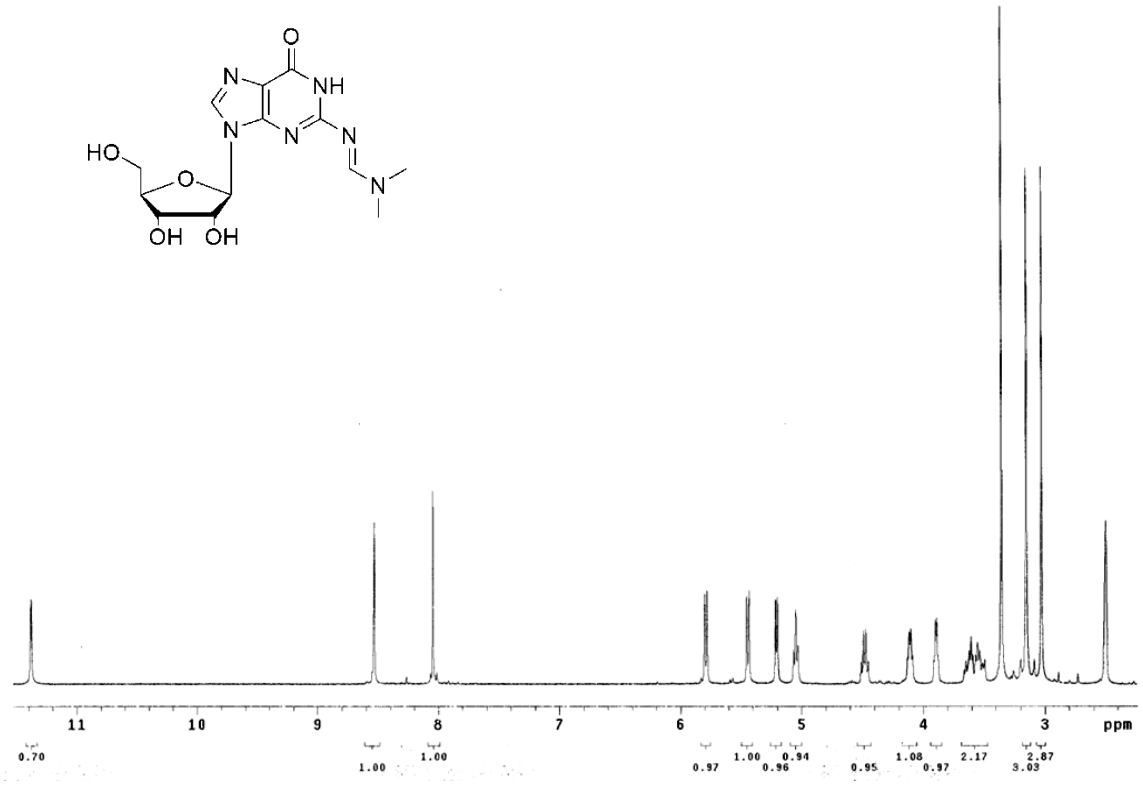

Figure 5.3. ^{1}H-NMR (300 MHz DMSO-d_6) of derivative **29a**.

5'-*O*-(*tert*-butyldimethylsilyl)-2-*N*-Formamidine-guanosine (29b)

Redistilled TEA (250 μL) and tBDMSi-Cl (247 mg, 1.64 mmol) were added to a solution of **29a** (505 mg, 1.49 mmol) in anhydrous DMF (13 mL). The reaction mixture was stirred under argon at r.t. overnight. Then redistilled TEA (0.5 eq.) and tBDMSi-Cl (0.5 eq.) were added to the solution every 8 h until di-*O*-silylated product appeared on TLC. The solvent was removed *in vacuo*, the crude material dissolved with CH_2Cl_2 (30 mL) and the organic layer was washed with H_2O (15 mL), 0.01 N HCl (15 mL), saturated $NaHCO_3$ (15 mL) and brine (15 mL). The organic layer was dried over Na_2SO_4 and concentrated *in vacuo* to give a yellow gum. The crude product was dissolved in CH_2Cl_2 and precipitated with diethyl ether to afford **29b** (540 mg, 80 %) as a white solid. ESI-MS: *m/z* (%): 453 (100) [**29b**-H]$^+$. ^{1}H NMR: see Figure 5.4. Elemental analysis: Calcd. (%) for $C_{19}H_{32}O_5N_6Si$: C 50.42, H 7.13, N 18.57; Found C 51.50, H 6.85, N 17.95.

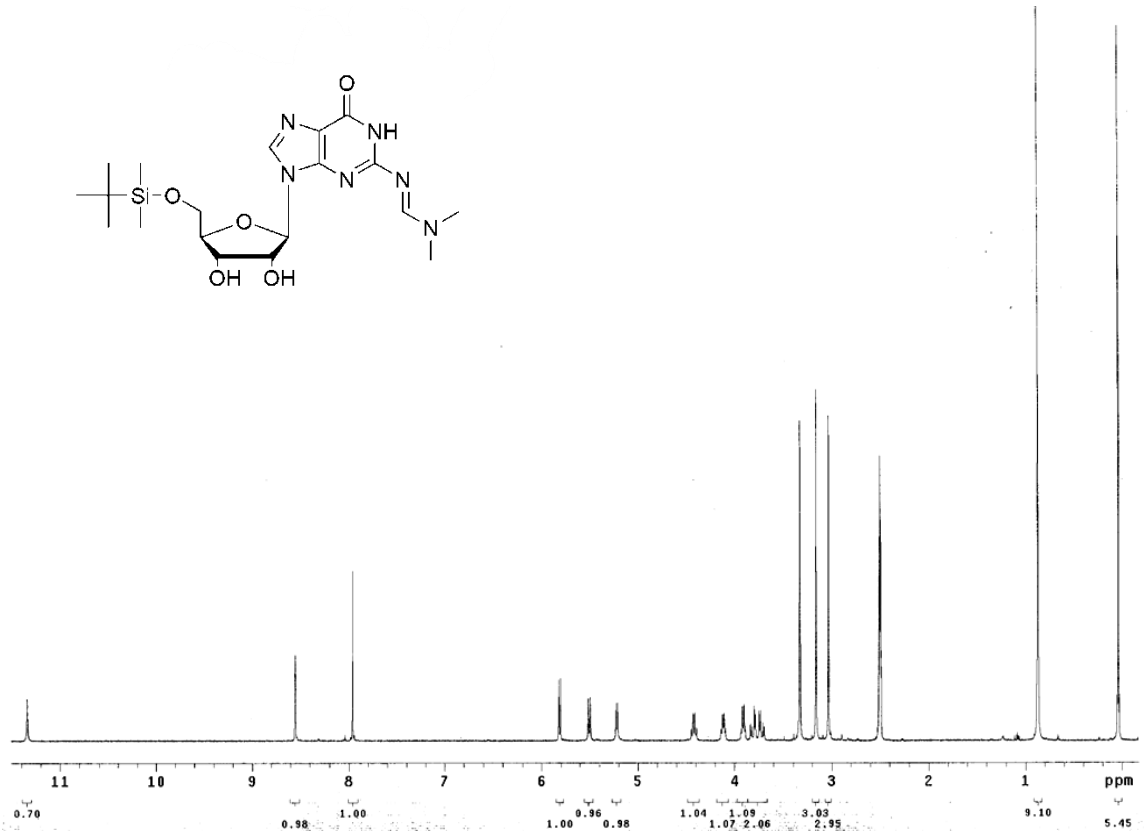

Figure 5.4. ^{1}H-NMR (300 MHz DMSO-d_6) of derivative **29b**.

5'-*O*-(*tert*-butyldimethylsilyl)-guanosine (29c)

29b (488 mg, 1,08 mmol) was treated with pyridine (2.1 mL) containing concentrated ammonia (0.42 mL) to give a solution that was stirred at 25 °C overnight. Concentrated ammonia (0.42 mL) was then added to the suspension and the reaction mixture was stirred until TLC indicated the reaction was completed. The resulting suspension was poured into vigorously stirred water to form colorless precipitates, which were collected by filtration and dried *in vacuo* to yield **29c** (430 mg, 100 %) as a white solid. ESI-MS: *m/z* (%): 398 (100) [**29c**-H]$^+$. ^{1}H NMR: see Figure 5.5. Elemental analysis: Calcd. (%) for $C_{16}H_{27}O_5N_5Si$: C 48.34, H 6.85, N 17.62; Found C 48.50, H 6.40, N 16.95.

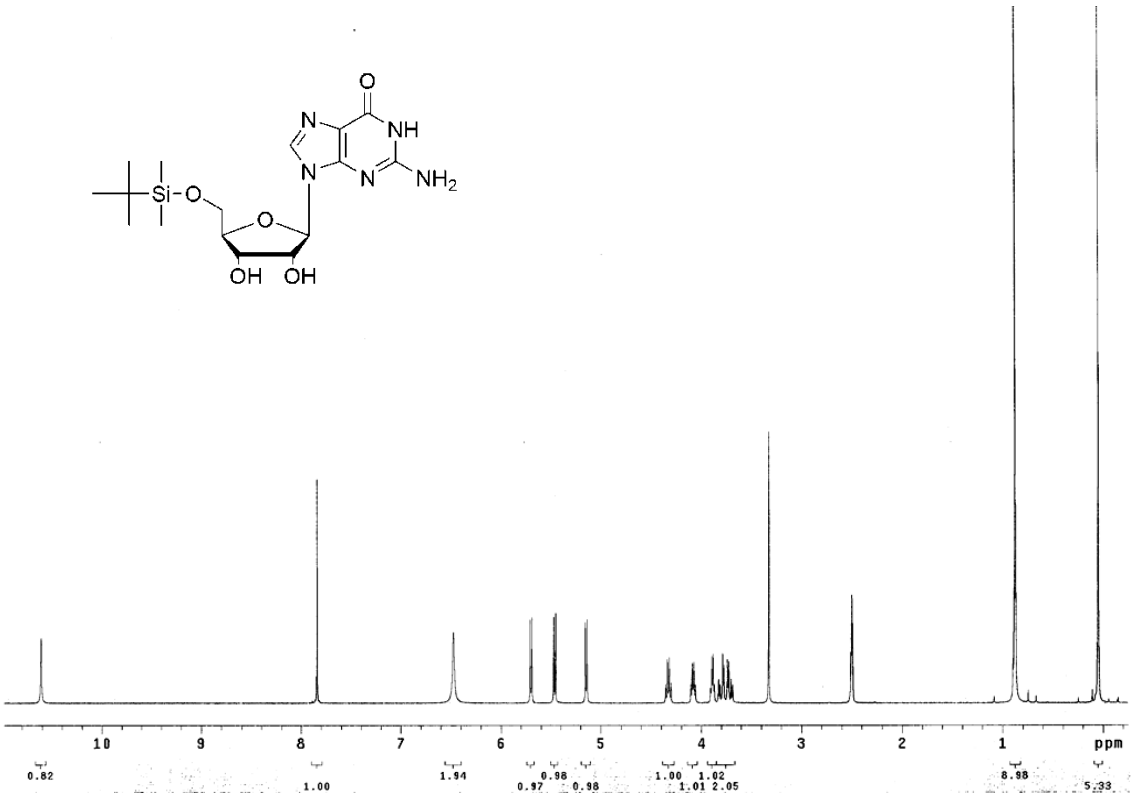

Figure 5.5. ^{1}H-NMR (300 MHz DMSO-d_6) of derivative **29c**.

Starting from guanosine

To a solution of guanosine (100 mg, 0.353 mmol) in anhydrous DMSO (0.71 mL) was added tBDMSi-Cl (59 mg, 0.388 mmol) and imidazole (53 mg, 0.77 mmol) . After the reaction mixture stirred under argon at r.t. for 20 h., the solution was poured into

water (10 ml) to form a colorless precipitate which was collected by filtration. The crude material was dissolved with CH_2Cl_2 (30 mL) and precipitated with diethyl ether to afford **29c** (112 mg, 80 %) as a white solid. All the spectroscopic data are in agreement with previous ones.

5'-*O*-(*tert*-butyldimethylsilyl)-2',3'-di-*O*-decanoyl-guanosine (29d)

Decanoyl anhydride (786 μL) and a catalytic amount of DMAP were added to a suspension of **29c** (385 mg, 0.97 mmol) in anhydrous acetonitrile (14 mL) and redistilled triethylamine (323 μL). The reaction mixture was stirred at r.t. under argon overnight. After evaporation of the solvent *in vacuo*, the crude material was purified by twice flash column chromatography on silica gel. To remove decanoyl acid it was flowed through the column dichloromethane/acetone 9:1 as eluent (compound can be visualized by spraying the plates with a solution of $KMnO_4$) and then dichloromethane/methanol 9:1 to obtain the desire product. Desilylation on the 5'-hydroxyl group can occur. The solvent was concentrated *in vacuo* to yield **29d** (478 mg, 70 %) as a white, pale yellow oil. ESI-MS: *m/z* (%): 706 (100) [**29d**-H]$^+$. ^{1}H NMR: see Figure 5.6. Elemental analysis: Calcd. (%) for $C_{36}H_{63}O_7N_5Si$: C 61.24, H 8.99, N 9.92; Found C 62.00, H 8.60, N 9.45.

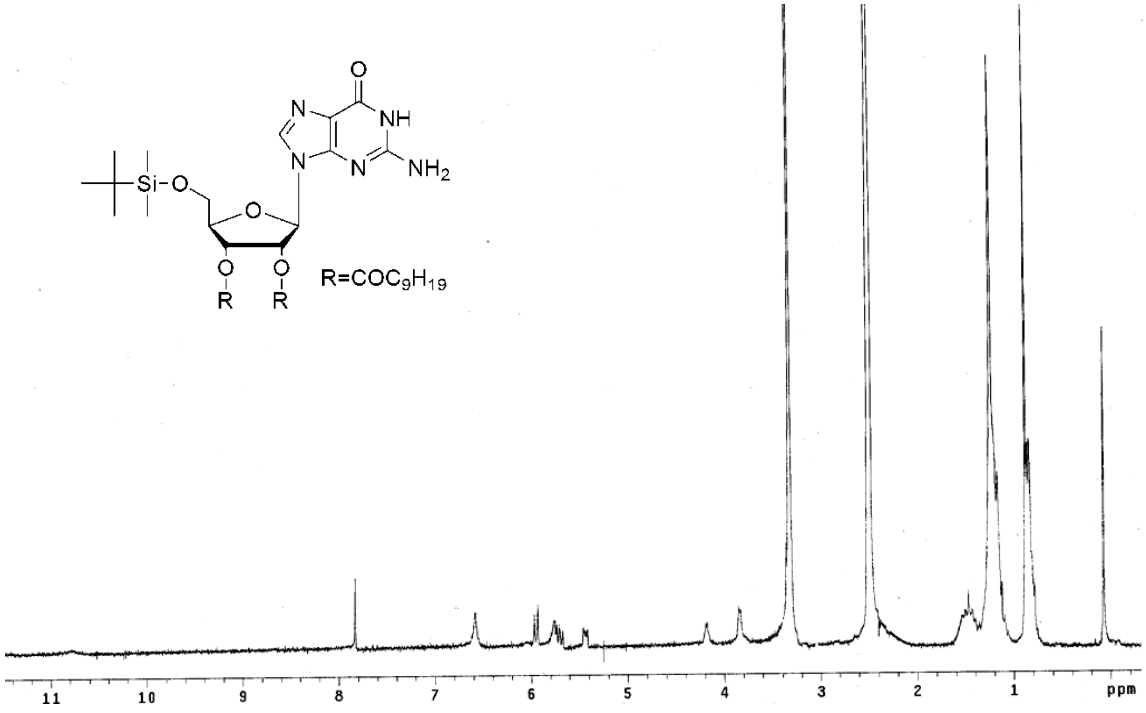

Figure 5.6. ^{1}H-NMR (200 MHz DMSO-d_6) of derivative **29d** after a first purification step. No integration due to the low spectral resolution.

5'-*OH*-2',3'-di-*O*-decanoyl-guanosine (29e)

Tetrabutylammonium fluoride (397 mg) and 2 drops of water were added to a solution of **29d** (684 mg, 0.97 mmol) in THF (10 mL). The solution was stirred at r.t. for 15 h. after which time TLC indicated the reaction was completed. After evaporation of the solvent *in vacuo*, the crude material was purified by flash column chromatography on silica gel using dichloromethane/methanol 9:1 as eluent. Hydrolysis on the 2' or 3'-hydroxyl group can occur during elution. The isolated product was precipitated from petroleum ether-acetonitrile to afford **29e** (516 mg, 90 %) as a colorless white powder. ESI-MS: *m/z* (%): 592 (100) [**29e**-H]$^+$. ^{1}H NMR: see Figure 5.7. Elemental analysis: Calcd. (%) for $C_{30}H_{49}O_7N_5$: C 60.89, H 8.35, N 11.84; Found C 61.00, H 8.25, N 11.45.

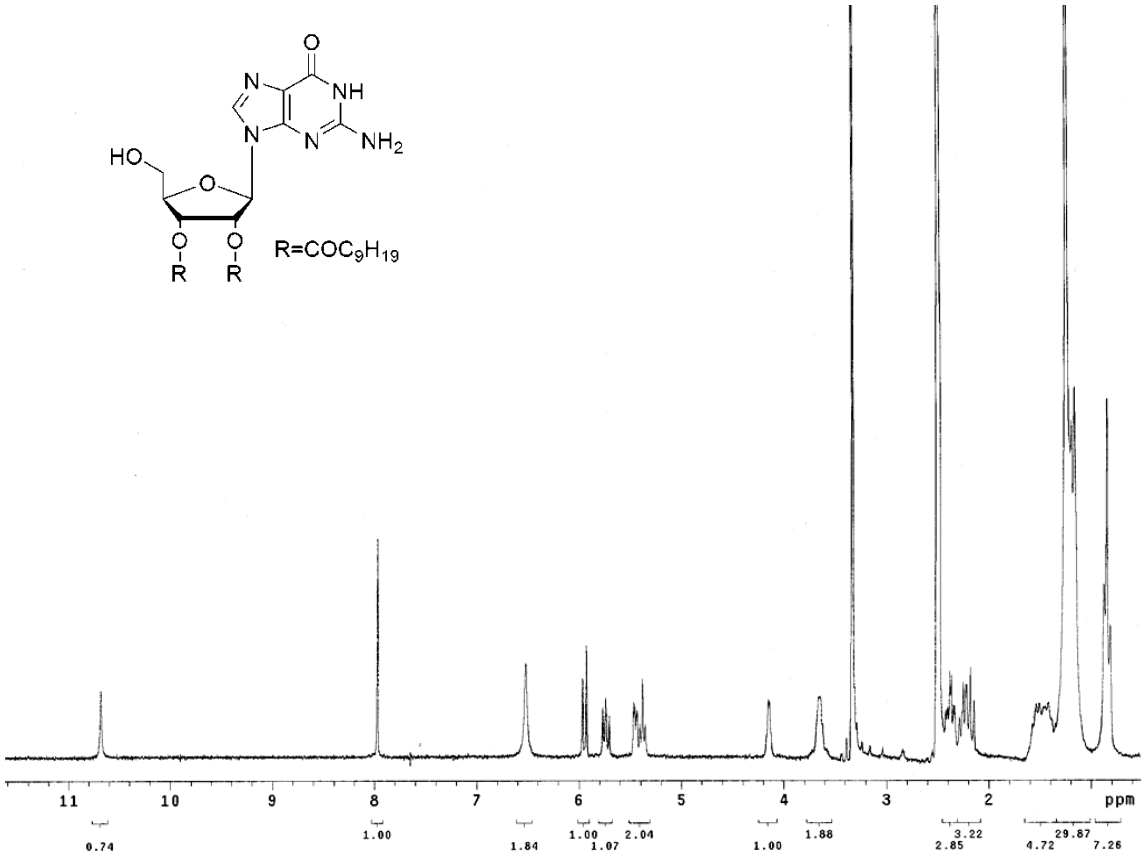

Figure 5.7. ^{1}H-NMR (300 MHz DMSO-d_6) of derivative **29e**.

5'-*O*-(2,2,6,6-Tetramethyl-1-oxylpiperidine-4-carbonyl)-2',3'-di-*O*-decanoyl guanosine (29)

2,4,6-Triisopropylbenzenesulfonyl chloride (446 mg, 1.47 mmol) was added to a solution of 4-Carboxy-2,2,6,6-tetramethylpiperidine-1-oxyl (309 mg, 1.54 mmol) in anhydrous acetonitrile (10 mL) and redistilled triethylamine (0.467 mL, 3.37 mmol) at 0 °C. The resulting solution was stirred for two hours then allowed to reach r.t. and stirred for additional 20 minutes. **29e** (414 mg, 0.7 mmol) and a catalytic amount of DMAP were then added and the mixture was stirred under argon overnight. After evaporation of the solvent *in vacuo*, dichloromethane (20 ml) was added and the organic layer was washed 3 times with saturated $NaHCO_3$ solution (30 mL). The organic layer was dried over Na_2SO_4 and concentrated *in vacuo*. The crude material was purified by flash column chromatography on silica gel (eluent: dichloromethane/methanol 98:2) to afford (216 mg, 40 %) as a pale pink solid. ESI-MS: *m/z* (%): 775 (100) [**29**-H]$^+$, see Figure 5.8. ^{1}H NMR: not reported. Low spectral resolution due to the nytroxyl unit. Elemental analysis: Calcd. (%) for $C_{40}H_{65}O_9N_6$: C 62.07, H 8.46, N 10.86; Found C 61.50, H 8.60, N 10.35.

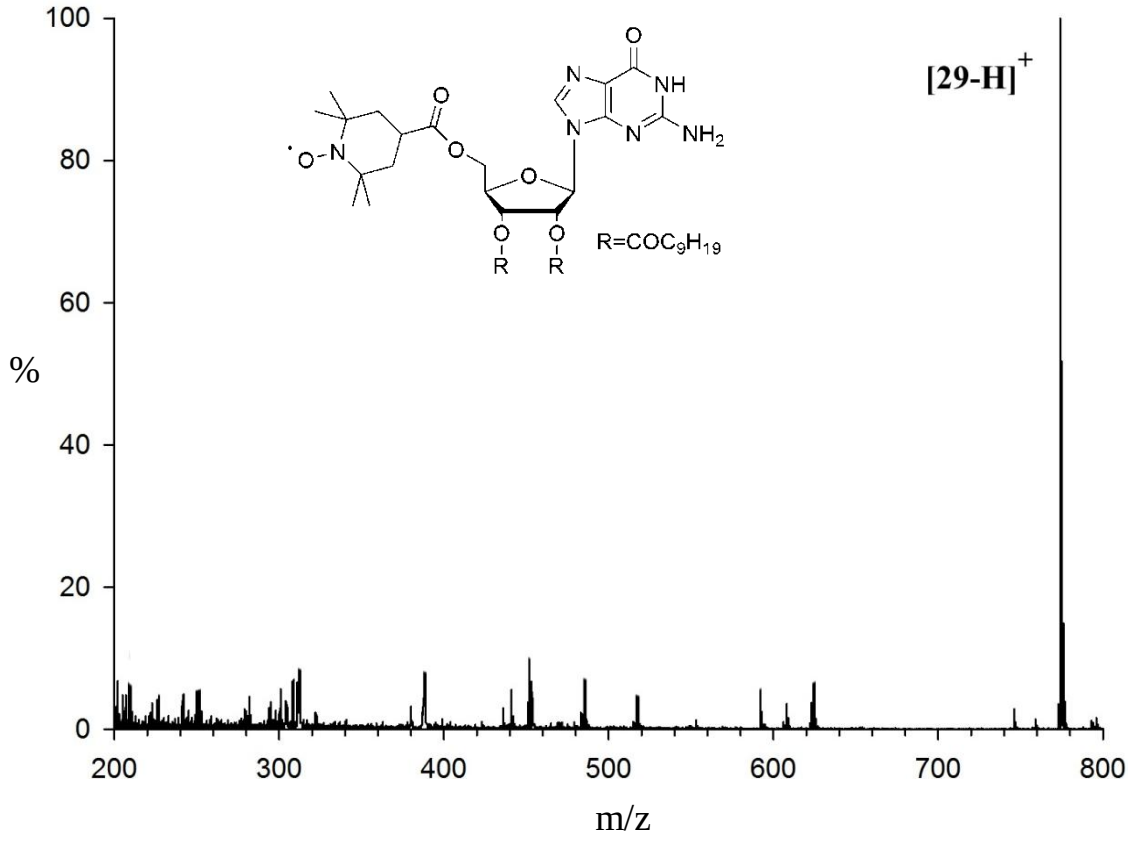

Figure 5.8. ESI-MS spectrum of the open-shell derivative **29**.

5.2.2 Chapter 4

- ***Derivative E*-42: *Synthetic procedure***

8-Bromo-2'-deoxyguanosine (**42a**) was prepared according to a previously described synthetic procedure,[5] and all the spectroscopic data are in agreement with published data. Suzuki-Miyaura cross-coupling reaction was performed following the methodology published by the Shaughnessy group.[6]

(*E*)-8-styryl-2'-deoxyguanosine (*E*-42b)

A degassed mixture of H_2O/acetonitrile (ratio 2/1, 21 mL) was added to a flask containing 8-bromo-2'-deoxyguanosine (**42a**) (690 mg, 2.0 mmol), (*E*)-2-phenylvinylboronic acid (385 mg, 2.6 mmol), Na_2CO_3 (425 mg, 4.0 mmol), triphenylphosphine-3,3',3''-trisulfonic acid trisodium salt (77 mg, 0.135 mmol) and $Pd(OAc)_2$ (12 mg, 0.054 mmol). The mixture was heated overnight at 80 °C under Argon, then cooled to room temperature, poured in to 50 mL of H_2O and neutralized with 10 % HCl. The precipitate formed was filtrated and dried *in vacuo* to give the title compound as a yellow powder (1.5 mmol, 75 % yield). ESI-MS: *m/z* (%): 368.1 (100) [***E*-42b**-H]$^-$. NMR spectra: see Figure 5.9. Elemental analysis: Calcd. (%) for $C_{18}H_{19}N_5O_4$: C 58.53, H 5.18, N 18.96; Found: C 58.56, H 5.19, N 18.93.

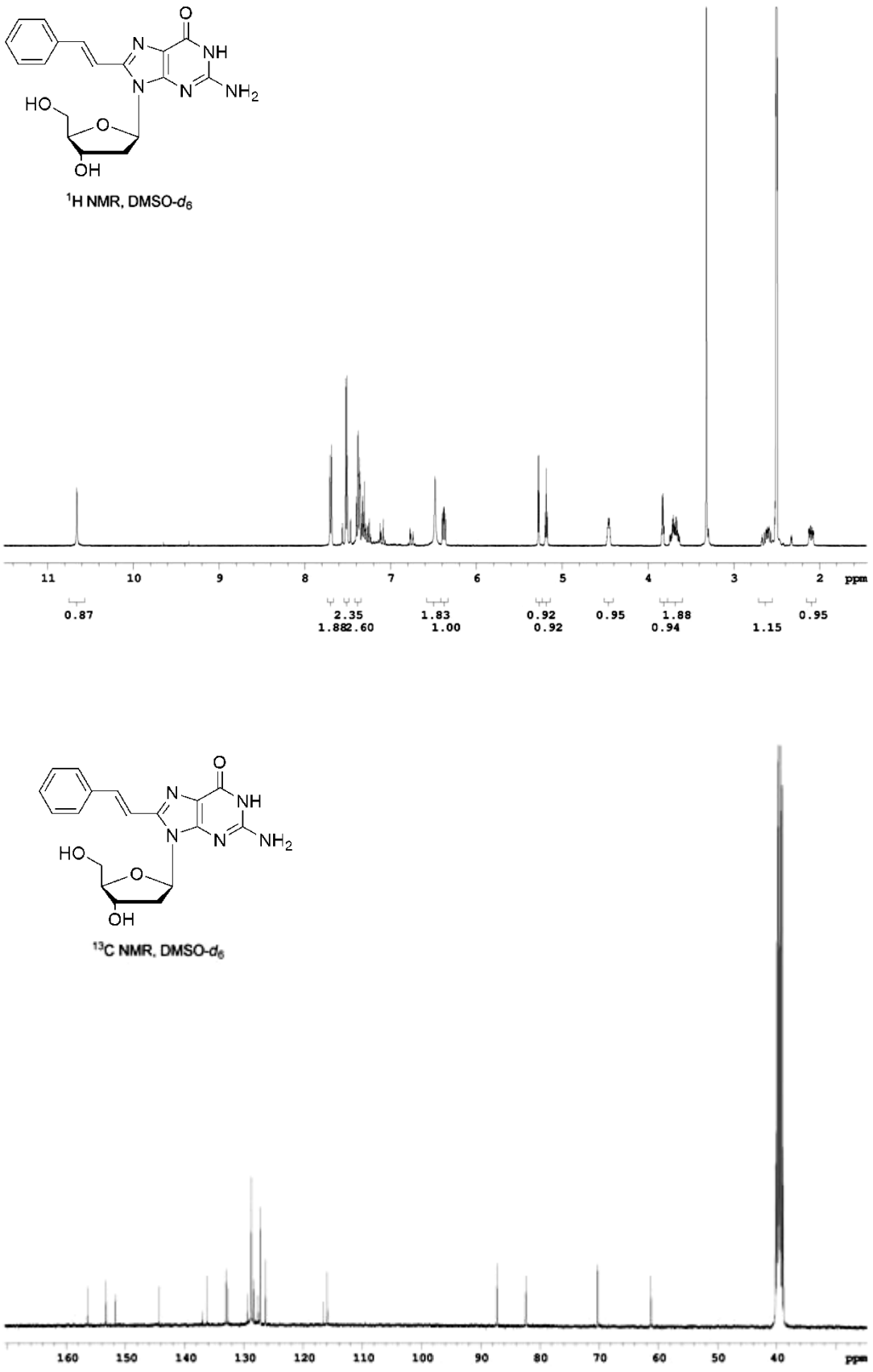

Figure 5.9. ^{1}H NMR (600 MHz, DMSO-d_6) and ^{13}C NMR (400 MHz, DMSO-d_6) spectra of derivative ***E*-42b**.

3', 5'-*O*-diacetyl-(*E*)-8-styryl-guanosine (*E*-42)

(*E*)-8-styryl-2'-deoxyguanosine (***E*-42b**) (370 mg, 1.0 mmol) was dried over P_2O_5 *in vacuo* for 2 h at 50 °C and then added to anhydrous DMF (4 mL). Redistilled Et_3N (0.36 mL, 2.6 mmol), acetic anhydride (0.23 mL, 2.4 mmol) and a catalytic amount of DMAP were added, and the resulting solution was stirred overnight at r.t. The crude, after evaporation *in vacuo* of the solvent, was applied to a silica gel column and eluted with a mixture of dichloromethane-methanol (96:4). The product was obtained as a yellow solid (360 mg, 80 % yield). ESI-MS: *m/z* (%): 452.2 (100) [***E*-42**-H]$^-$. NMR spectra: see Figures 5.10-5.11. Elemental analysis: Calcd. (%) for $C_{22}H_{23}N_5O_6$: C 58.27, H 5.11, N 15.44; Found: C 58.10, H 5.12, N 15.40.

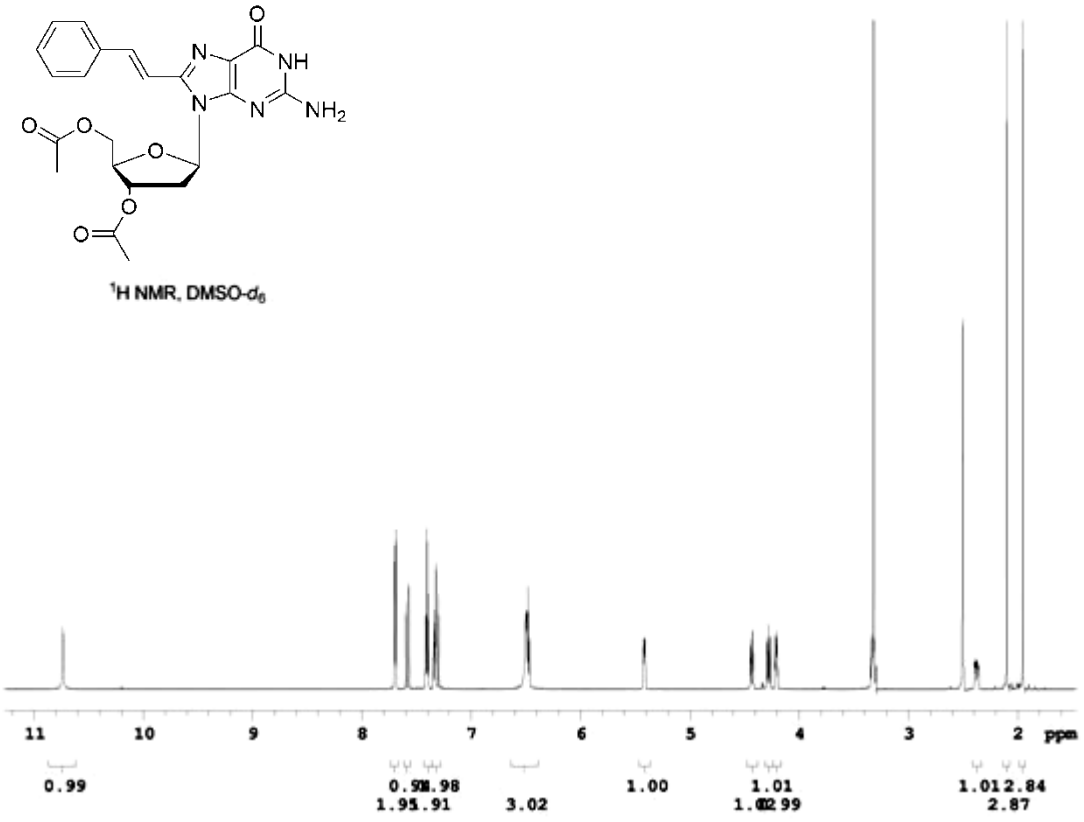

Figure 5.10. ^{1}H NMR (600 MHz, DMSO-d_6) of derivative ***E*-42**.

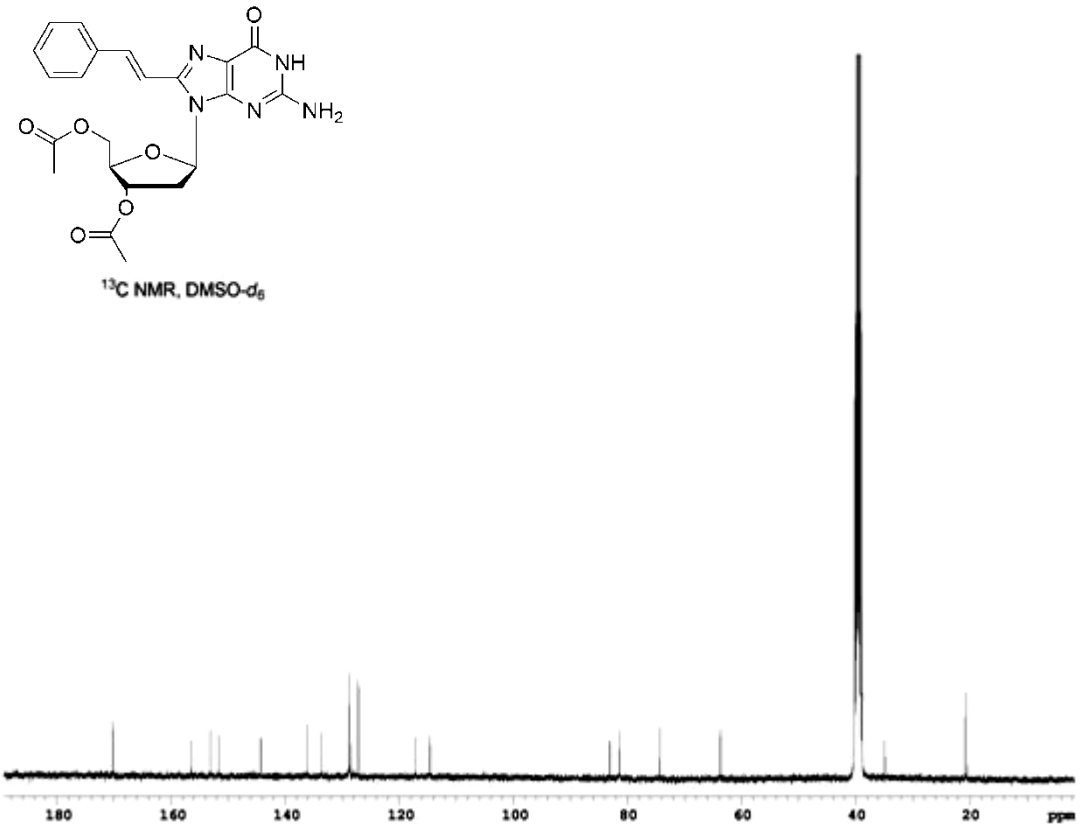

Figure 5.11. ^{13}C NMR (400 MHz, DMSO-d_6) of derivative ***E*-42**.

- ***Derivative E*-44: *Synthetic procedure***

9-octadecylguanine (**43**) was prepared according to a previously described synthetic procedure.[7] The preparation of **44a** was carried out according to a previously described synthetic procedure.[8] Suzuki–Miyaura cross-coupling of **44a** and (***E***)-2-phenylvinylboronic acid was performed following the methodology published by the Ogasawara group.[9]

9-Octadecyl-8-bromoguanine (44a)

To a stirred mixture of 9-Octadecylguanine (**43**) (173 mg, 0.43 mmol) in glacial acetic acid (1 mL), heated to 50 °C, was added bromine (23 μL, 0.43 mmol), and the reaction mixture was allowed to stand 3-5 h at 50 °C under stirring. The reaction mixture was then poured into 10-20 mL of ice-water with stirring and allowed to stand at room temperature for a few hours. The precipitate was filtered, washed with water and dried. The crude product was recrystallized from methanol to give **44a** (207 mg, 100 % yield)

as a white solid. ESI-MS: *m/z* (%): 482.2 (100) 484.2 (98) [**44a**-H]$^+$. ^{1}H NMR: see Figure 5.12. Elemental analysis: Calcd. (%) for $C_{23}H_{40}BrN_5O$: C 57.25, H 8.36, N 14.51; Found: C 57.10, H 8.37, N 14.54.

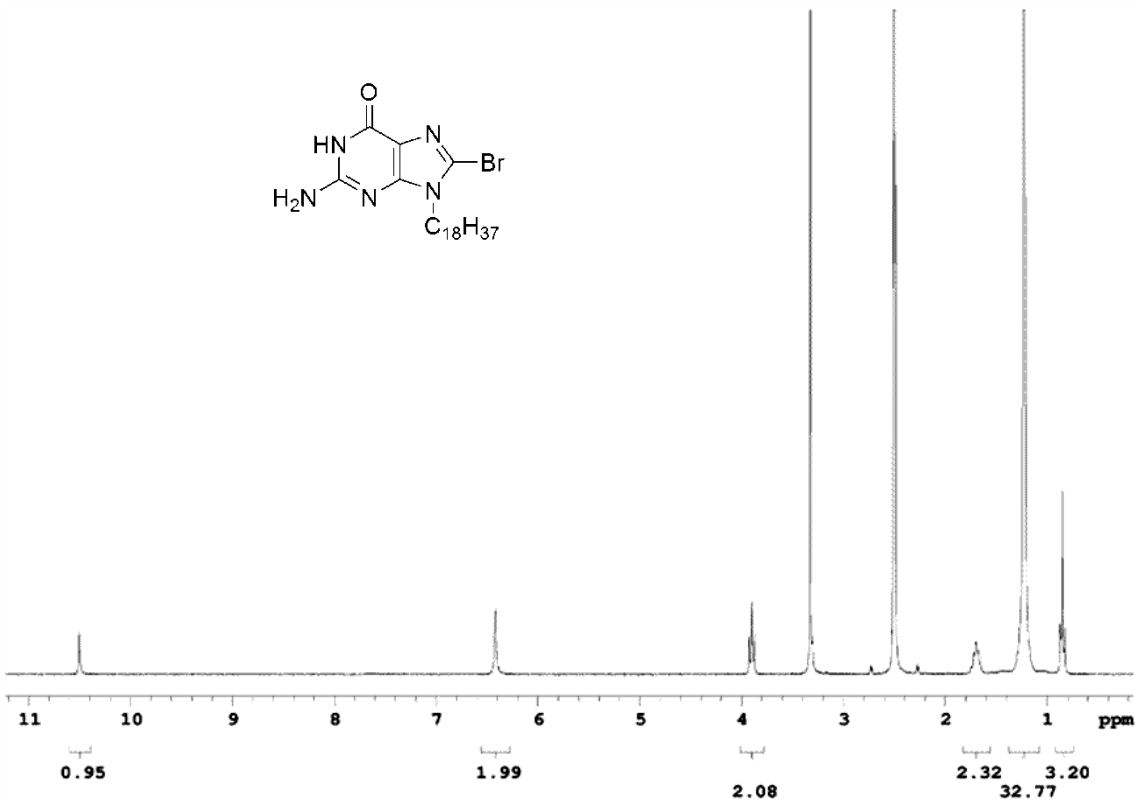

Figure 5.12. ^{1}H NMR (600 MHz, DMSO-d_6) of derivative **44a**.

9-Octadecyl-8-styrylguanine (*E*-44)

A mixture of DMF (15 mL) was added to a flask containing **44a** (200 mg, 0.41 mmol), (***E***)-2-phenylvinylboronic acid (74 mg, 0.5 mmol), Et_3N (228 μL, 1.64 mmol) under nitrogen. The mixture was stirred for 5 min at room temperature. To the solution was added $Pd(PPh_3)_4$ (22.73 mg, 0.02 mmol) and the mixture was stirred for 16 h at 110 °C. The resulting mixture was concentrated *in vacuo* and purified by silica gel chromatography (ethyl acetate/methanol 99:1). The product was recrystallized from methanol to give ***E*-44** (42 mg, 20 % yield) as a pale yellow solid. ESI-MS: *m/z* (%): 506 (100) [***E*-44**-H]$^+$. ^{1}H NMR: see Figure 5.13. Elemental analysis: Calcd. (%) for $C_{31}H_{47}N_5O$: C 73.62, H 9.37, N 13.85; Found: C 73.52, H 9.40, N 13.80.

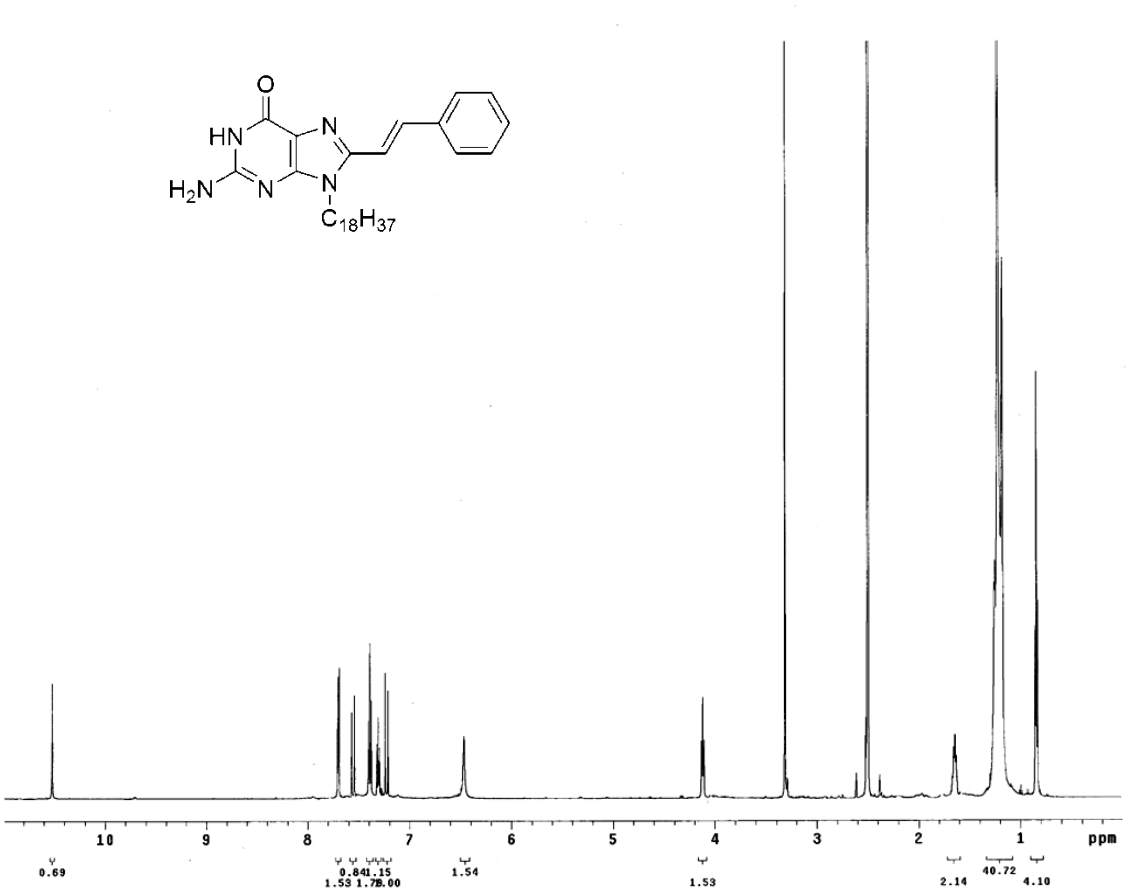

Figure 5.13. ^{1}H NMR (600 MHz, DMSO-d_6) of derivative ***E*-44**.

- ***Derivative* 45: *Synthetic procedure***

2'-3'-Isopropylideneguanosine (**45a**) was prepared according to a previously described synthetic procedure.[10] 2-*N*-octyl-2',3'-*O*-isopropylideneguanosine (**45b**) was carried out according to a previously described synthetic procedure.[11]

2'-3'-Isopropylideneguanosine (45a)

To a suspension of guanosine (1 g, 3.53 mmol) in 60 mL of acetone was added 70 % perchloric acid (0.41 mL, 4.75 mmol). After 70 minutes, concentrated ammonium hydroxide (0.67 mL, 4.98 mmol) was added to the reaction mixture and cooled down with ice-water bath. Water (60 mL) was added and the solution was concentrated under reduce pressure until the formation of a white precipitate. The solid was then filtered out and dried over vacuum to afford **45a** (0.95 g, 83.2 %). ESI-MS: *m/z* (%): 324.3 (100) [**45a**-H]$^{+}$. ^{1}H-NMR spectrum: see Figure 5.14. Elemental analysis: Calcd. (%) for $C_{13}H_{17}N_5O_5$: C 48.29, H 5.30, N 21.66; Found: C 48.15, H 5.35, N 21.60.

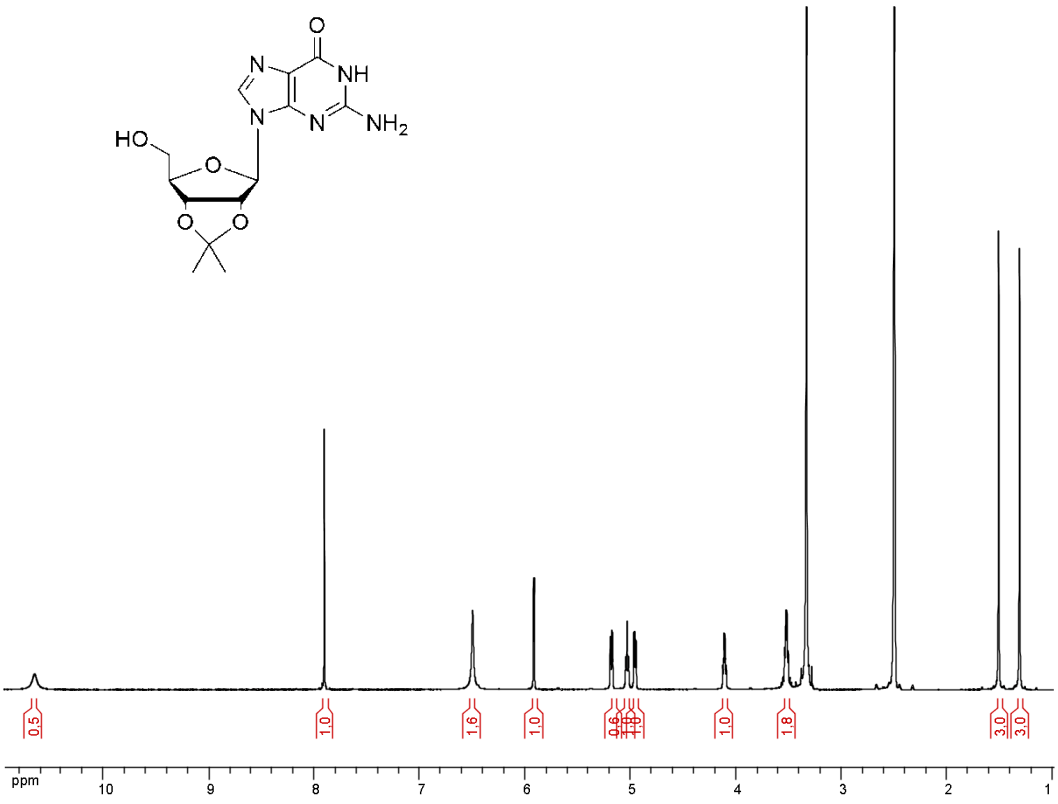

Figure 5.14. ^{1}H NMR (400 MHz, DMSO-d_6) of derivative **45a**.

2-*N*-octyl-2',3'-*O*-isopropylideneguanosine (45b)

To a solution of **45a** (100 mg, 0.31 mmol) and octanal (186 μL, 1.19 mmol) in MeOH (12 mL) was added sodium cyanoborohydride (112 mg, 1.78 mmol). The reaction mixture was stirred at 50 °C under nitrogen for 5 days. After removal of the solvent, 8 mL of H_2O was added and pH was adjusted to 7.0. After extraction with CH_2Cl_2, the organic layer was washed with saturated $NaHCO_3$, 0.1 N HCl and water. Following evaporation of the solvent, the resulting brown solid was purified by flash chromatography (6 % MeOH in CH_2Cl_2) to afford **45b** (55 mg, 41 %) as a white solid. ESI-MS: *m/z* (%): 436.3 (100) [**45b**-H]$^{+}$. ^{1}H-NMR spectrum: see Figure 5.15. Elemental analysis: Calcd. (%) for $C_{21}H_{33}N_5O_5$: C 57.91, H 7.64, N 16.08; Found: C 57.80, H 7.60, N 16.02.

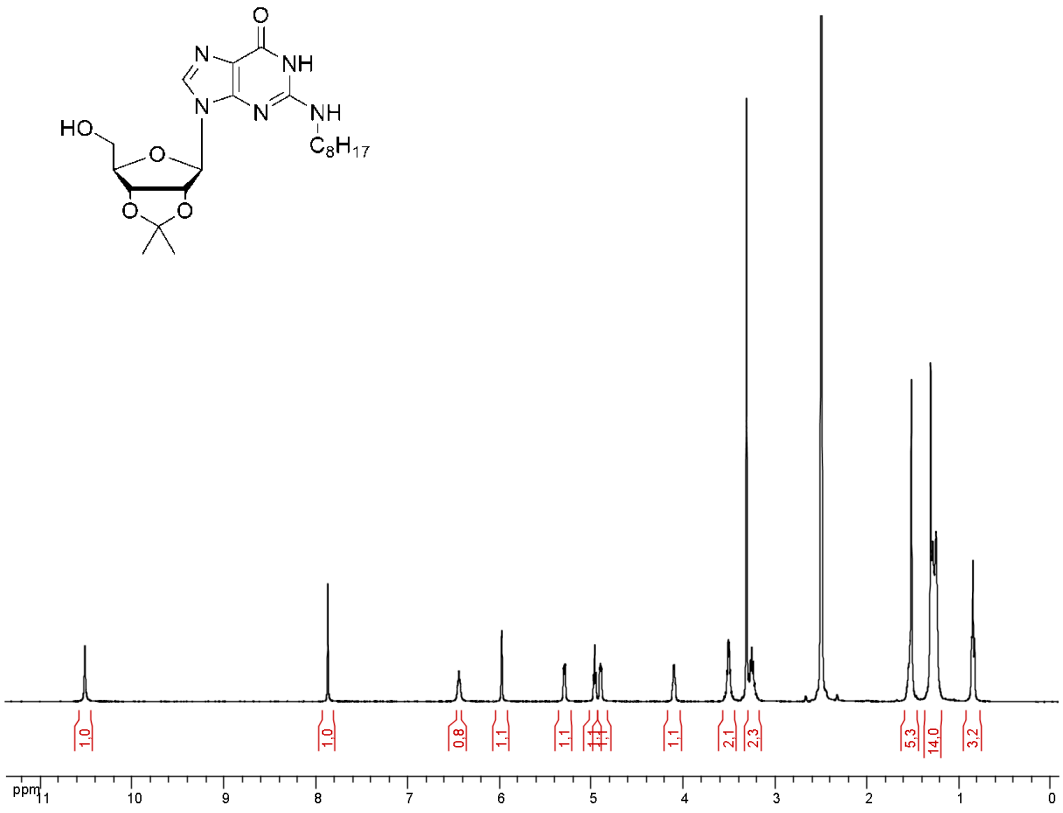

Figure 5.15. ^{1}H NMR (400 MHz, DMSO-d_6) of derivative **45b**.

Bis{4-[5'',5''-*O*-(2'-*N*-octyl-2'',3''-*O*-isopropylideneguanosine)]phenyl carboxylate}diazene (45)

4-Metylbenzenesulfonyl chloride (35 mg, 0.19 mmol) was added to a solution of azobenzene-4,4'-dicarboxylic acid (25 mg, 0.092 mmol) in anhydrous DMF (4 mL) and redistilled triethylamine (57 µL, 0.4 mmol) at 0 °C. The resulting solution was stirred for two hours then allowed to reach r.t. and stirred for additional 20 minutes. **45b** (88 mg, 0.204 mmol) and a catalytic amount of DMAP were then added and the mixture was stirred under argon overnight. After evaporation of the solvent *in vacuo*, dichloromethane (20 ml) was added and the organic layer was washed 3 times with saturated $NaHCO_3$ solution (30 mL). The organic layer was dried over Na_2SO_4 and concentrated *in vacuo*. The crude material was purified by flash column chromatography on silica gel (eluent: chloroform/methanol 99:1) to yield **45** (65 mg, 30 %) as a pale orange solid. ESI-MS: *m/z* (%): 1106.2 (100) [**45**-H]$^{+}$. ^{1}H-NMR spectrum: see Figure 5.16. Elemental analysis: Calcd. (%) for $C_{56}H_{72}N_{12}O_{12}$: C 60.86, H 6.57, N 15.21; Found: C 60.50, H 6.60, N 15.16.

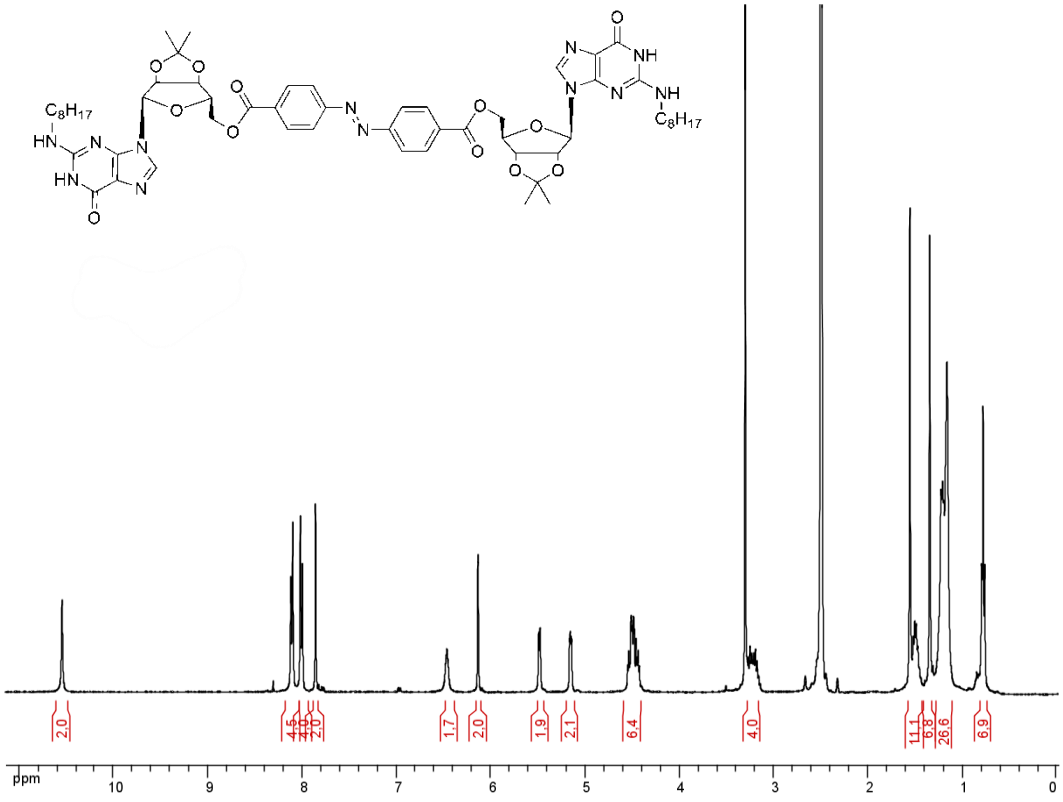

Figure 5.16. ^{1}H NMR (400 MHz, DMSO-d_6) of derivative **45**.

- ***Derivatives* 47-48: *Synthetic procedure***

Derivative **47a** was prepared according to a modified literature method.[12] The preparation of compound **47b** was carried out according to a previously described synthetic procedure.[13] Derivative **47d** was prepared according to a modified literature method.[14] Finally, the synthetic procedure, or its modification, described in reference 15 was followed to carry out derivatives **47-48**. Synthesis of 4-[4-(Dimethylamino)phenylazo]benzoic acid and 4-(phenylazo)benzoic acid are not reported; these derivatives were easily prepared following well-know literature methods.

Compounds were visualized by spraying the plates with a solution of 10 % sulfuric acid containing 1 % cerium sulfate and 1.5 % molybdic acid, followed by heating.

Hexakis(6-*O*-*tert*-butyldimethylsilyl)-α-CD (47a)

To dried α-cyclodextrin (2.88 g, 95 °C, 0.05 mmHg, 18 h) in DMF/Pyridine (ratio 7.5/1, 34 mL) was added, at 0 °C, *tert*-butyldimethylsilyl chloride (2.84 g, 6.35 equiv.) in dry DMF (7 mL). After stirring for 24 h at room temperature, the reaction mixture was poured into ice/water (350 mL) and stirred for 15 min. The resulting precipitate was filtered off, washed with ice-cold water, and dissolved in Et_2O (70 mL). The solution was washed with 5 % aqueous HCl solution (3 x 50 mL), saturated aqueous $NaHCO_3$ solution (50 mL), and saturated brine (50 mL). Finally, the solution was dried (anhydrous Na_2SO_4), filtered, and concentrated. The crude product (5.2 g) was purified by flash chromatography using Et_2O/EtOH (11/1) to afford **47a** (3.175 g, 65 %) as a white solid. All the spectroscopic data are in agreement with published data: M.p.: 331 °C (decomp), [see reference 16: 323 ± 326 °C, (decomp)]; ESI-MS: *m/z* (%): 1658 (100) [**47a**-H]$^+$. ^{1}H NMR (400 MHz, $CDCl_3$): δ= 4.88 (d, 6H; H-1), 4.01 (t, 6H; H-3), 3.91 (dd, 6H; H-6), 3.84 (d, 6H; H-6), 3.75 (d, 6H; H-5), 3.64 (dd, 6H; H-2), 3.59 (t, 6H; H-4), 0.89 (s, 54H; CH_3-C), 0.03 (s, 36H; CH_3-Si); ^{13}C NMR (100 MHz, $CDCl_3$): δ= 101.39 (C-1), 81.40, 74.45, 73.04, and 72.19 (C-2, C-3, C-4, C-5), 61.95 (C-6), 25.97 (CH_3-C), 18.42 (CH_3-C), -5.19 (CH_3-Si). Elemental analysis: Calcd. (%) for $C_{72}H_{144}O_{30}Si_6$: Calcd C 52.15, H 8.75; Found: C 52.39, H 8.53

Mono(2-*O*-tosyl)hexakis(6-*O*-*tert*-butyldimethylsilyl)-α-CD (47b)

To dried compound **47a** (3.44 g, 80 °C, 0.05 mmHg, 6 h) dissolved in dry THF (170 mL) was added a dispersion of NaH (75 mg, 1.5 equiv, 60 % in mineral oil). The solution was stirred for at least 17 h at room temperature and 1 h at reflux temperature. To this refluxing solution was added tosyl-chloride (396 mg, 1 equiv). After 1 h, TLC [Et_2O/MeOH (15/1)] showed the formation of two major new products. The reaction mixture was concentrated *in vacuo*, the product was dissolved in dichloromethane (200 mL), and the solution washed with water/brine (100 mL, 50:50, v/v), and dried ($MgSO_4$). The crude product was purified by flash chromatography using Et_2O/MeOH (15/1) to afford **47b** (940 mg, 25 %) as a white solid. All the spectroscopic data are in agreement with published data: M.p.: 218.5 °C (decomp); ESI-MS: *m/z* (%): 1812 (100) [**47b**-H]$^+$. ^{1}H NMR (400 MHz, $CDCl_3$:CD_3OD, 10:1, v/v): δ= 7.89 (d, 2H; Ar-H), 7.31 (d, 2H; Ar-H), 5.11, 4.91, 4.86, 4.81, 4.76 (5 × d, total 6H; H-1), 4.13-3.90 and 3.76-3.49 (4 × m, 35H; H-2, H-3, H-4, H-5, H-6), 3.32 (dd, 1H), 2.43 (s, 3H; Ar-CH_3), 0.88 (s, 54H; C-

CH_3), 0.04 (s, 36H; Si-CH_3); ^{13}C NMR (100 MHz, $CDCl_3$:CD_3OD, 10:1, v/v): δ= 145.42 and 132.03 (C-Ar), 129.51, 129.05 (CH-Ar), 102.95-101.36 and 99.32 (C-1), 81.62-80.03, 73.46-71.91, 69.32 (C-2, C-3, C-4, C-5), 62.11-61.94 (C-6), 25.96 (CH_3-Ar), 21.71 (CH_3-C), 18.43 and 18.29 (CH_3-C), -5.07 and -5.20 (CH_3-Si). Elemental analysis: Calcd. (%) for $C_{79}H_{150}O_{32}Si_6S$: C 52.35, H 8.34, S 1.77; Found C 52.34, H 8.30, S 1.63.

Mono(2^A,3^A-anhydro)hexakis(6-*O*-*tert*-butyldimethylsilyl)-α-CD (47c)

A suspension of NaH (44 mg, 60 % in mineral oil) in THF/EtOH (ratio 2/1, 60 mL) was heated at 85 °C and stirred for 20 minutes. Dry compound **47b** was added (1.19 g, 80 °C, 0.05 mmHg, overnight) and the reaction mixture had been stirred overnight at 85 °C. Then, the mixture was concentrated *in vacuo*, the residue dissolved in ethyl acetate (50 mL), and the solution washed with water (25 mL), 5 % $NaHCO_3$ (10 mL), brine (15 mL), dried ($MgSO_4$) and concentrated to dryness. The crude product was purified by flash chromatography using EtOAc/EtOH/H_2O (10/0.4/0.2) to afford **47c** (0.483 g, 45 %) as a white solid. ESI-MS: *m/z* (%): 1640 (100) [**47c**-H]$^+$. Elemental analysis: Calcd. (%) for $C_{72}H_{142}O_{29}Si_6$: C 52.72, H 8.73; Found C 52.44, H 8.85.

Mono(3-amino-3-deoxy)hexakis(6-*O*-*tert*-butyldimethylsilyl)-α-CD (47d)

To epoxide **47c** (400 mg, 0.244 mmol) dissolved in ethanol (43 mL) was added concentrated ammonia (37 mL). The reaction mixture was kept at 60 °C for 3 days in a closed carius tube. The reaction mixture was cooled down with ice-water bath, filtered out and the solid was washed with water. The crude reaction product was purified by flash chromatography using EtOAc/EtOH/H_2O (10/1/0.5) to afford **47d** (202 mg, 50 %) as a white solid. All the spectroscopic data are in agreement with published data: ESI-MS: *m/z* (%): 1657 (100) [**47d**-H]$^+$. ^1H NMR (400 MHz, $CDCl_3$:CD_3OD, 2:1, v/v): δ= 4.77 and 4.73 (2br.s, 5H; H-1), 4.52 (d, $^3J(H,H)$= 6 Hz, 1H; H^A-1), 4.05-3.23 and 3.03 (4 × m; H-2, H-3, H-4, H-5, H-6, CD_3OH), 0.75 (s, 54H; C-CH_3), -0.05 (m, 36H; CH_3-Si); ^{13}C NMR (100 MHz, $CDCl_3$:CD_3OD, 2:1, v/v): δ= 104.98, 102.70, 102.50, 101.89, and 100.85 (C-1), 81.05-71.61 (C-2, C-3, C-4, C-5) 62.37-61.33 (C-6), 52.09 (C-NH_2), 25.65-25.54 (CH_3-C), 18.02-17.87 (CH_3-C), -5.44- -5.84 (CH_3-Si). Elemental analysis: Calcd. (%) for $C_{72}H_{145}O_{29}Si_6N$: C 52.18, H 8.82, N 0.85; Found C 51.36, H 8.74, N 0.80.

***N*-mono[(3-amino-3-deoxy)hexakis(6-*O*-*tert*-butyldimethylsilyl)-α-CD]-4''-Dimethyl-aminophenyl-4'-azobenzamide (47e)**

2,4,6-Triisopropylbenzenesulfonyl chloride (12 mg, 0.04 mmol) was added to a solution of 4-[4-(Dimethylamino)phenylazo]benzoic acid (12 mg, 0.044 mmol) in anhydrous THF (5 mL) and redistilled triethylamine (15 μL, 0.11 mmol) at 0 °C. The resulting solution was stirred for two hours then allowed to reach r.t. and stirred for additional 20 minutes. Compound **47d** (73 mg, 0.044 mmol) (dried over P_2O_5 under vacuum for 2h at 55 °C) and a catalytic amount of DMAP were then added and the mixture was stirred under argon overnight. After evaporation of the solvent *in vacuo*, dichloromethane (20 ml) was added and the organic layer was washed 3 times with saturated $NaHCO_3$ solution (30 mL). The organic layer was dried over Na_2SO_4 and concentrated *in vacuo*. The crude material was purified by flash column chromatography on silica gel (eluent: chloroform/methanol 96:4) to afford **47e** (20 mg, 24 %) as a pale orange solid. ESI-MS: *m/z* (%): 1909 (100) [**47e**-H]$^+$. ^{1}H NMR: see Figure 5.17. Elemental analysis: Calcd. (%) for $C_{87}H_{158}O_{30}N_4Si_6$: C 54.75, H 8.34, N 2.94; Found C 55.10, H 8.10, N 2.55.

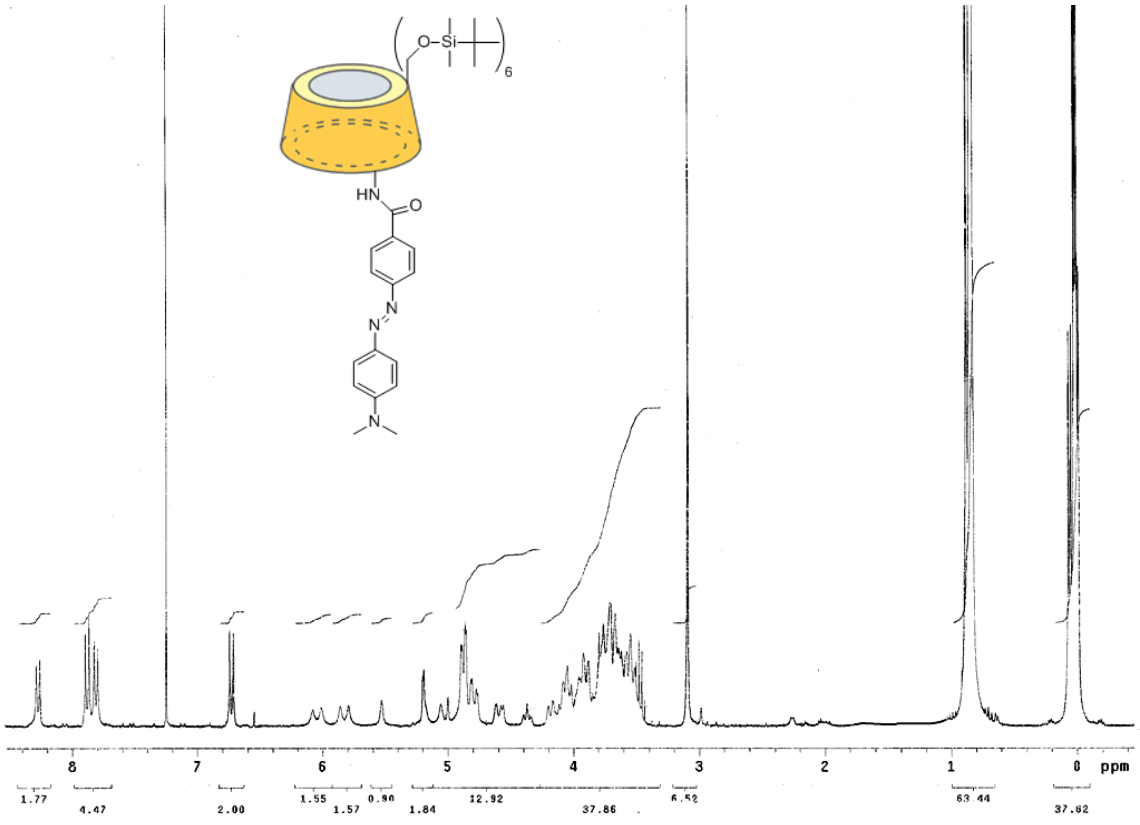

Figure 5.17. ^{1}H NMR (400 MHz, $CDCl_3$) of derivative **47e**.

_N_-mono[(3-amino-3-deoxy)-α-CD]-4''-Dimethylaminophenyl-4'-azobenzamide (47)

TBDMS-protected derivative **47e** (11 mg, 0.0057 mmol) was dissolved in trifluoroacetic acid (3 mL). The solution was stirred at room temperature for 10 min. The solvent was removed *in vacuo*. Methanol was added and evaporated *in vacuo* for azeotropic removal of any residual trifluoroacetic acid. The residue was dissolved in water and washed three times with diethyl ether. After freeze-drying, compound **47** was obtained as a pale orange solid in 100 % yield (7 mg). ESI-MS: *m/z* (%): 1223 (100) [**47**-H]$^+$. Elemental analysis: Calcd. (%) for $C_{51}H_{74}O_{30}N_4$: C 50.08, H 6.10, N 4.58; Found C 51.10, H 5.74, N 4.30.

2-*O*-mono[hexakis(6-*O*-*tert*-butyldimethylsilyl)-α-CD]-4'-phenylazobenzoate (48a)

2,4,6-Triisopropylbenzenesulfonyl chloride (42 mg, 0.114 mmol) was added to a solution of 4-(phenylazo)benzoic acid (33 mg, 0.144 mmol) in anhydrous THF (10 mL) and redistilled triethylamine (100 μL) at 0 °C. The resulting solution was stirred for two hours then allowed to reach r.t. and stirred for additional 20 minutes. Compound **47a** (200 mg, 0.12 mmol) (dried over P_2O_5 under vacuum for 2h at 55 °C) and a catalytic amount of DMAP were then added and the mixture was stirred under argon overnight. After evaporation of the solvent *in vacuo*, chloroform (40 ml) was added and the organic layer was washed with water (20 mL) and 5 % $NaHCO_3$ solution (20 mL). The organic layer was dried over Na_2SO_4 and concentrated *in vacuo*. The crude material was purified by flash column chromatography on silica gel (eluent: dichloromethane/methanol 95:5) to afford **48a** (96 mg, 43 %) as a pale orange solid. ESI-MS: *m/z* (%): 1867 (100) [**48a**-H]$^+$. ^{1}H NMR: see Figure 5.18. Elemental analysis: Calcd. (%) for $C_{85}H_{152}O_{31}N_2Si_6$: C 54.69, H 8.21, N 1.50; Found C 54.00, H 8.10, N 1.20.

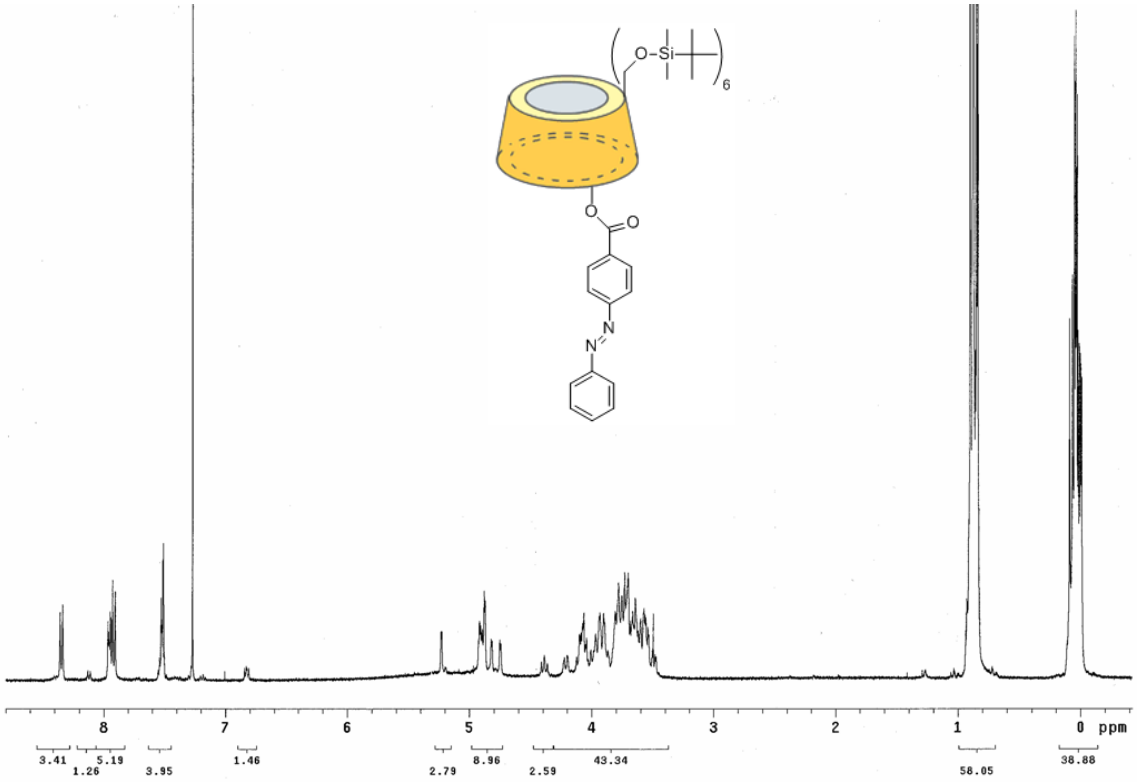

Figure 5.18. ^{1}H NMR (400 MHz, $CDCl_3$) of derivative **48a**.

2-*O*-mono-α-CD-4'-phenylazobenzoate (48)

To TBDMS-protected derivative **48a** (52 mg, 0.028 mmol) dissolved in MeOH/CH_2Cl_2 (ratio 5/1, 6 mL) was added trifluoroacetic acid (1.2 mL). The solution was stirred at room temperature for 3 days. The solvent was removed *in vacuo*. Methanol was added and evaporated *in vacuo* for azeotropic removal of any residual trifluoroacetic acid. The residue was dissolved in water and washed three times with diethyl ether. After freeze-drying, compound **48** was obtained as a pale orange solid in 100 % yield (33 mg). ESI-MS: *m/z* (%): 1181 (100) [**48**-H]$^{+}$. Elemental analysis: Calcd. (%) for $C_{49}H_{68}O_{31}N_2$: C 49.83, H 5.80, N 2.37; Found C 50.40, H 6.04, N 2.10.

5.3 Experimental Details

Here we report experimental details concerning derivatives **28a**-**28b** (Chapter 2) and static light scattering technique (Chapter 3).

5.3.1 Chapter 2

28a/28b: Sample preparation for ESR and CD measurements

A solution of **28a** (2 mL, 8 mM) or **28b** (2 mL, 14 mM) in CH_2Cl_2 or CD_2Cl_2 was stirred for 20 h at room temperature in the presence of crystalline potassium picrate (*ca.* 3 mg). After centrifugation, the yellow organic phase was collected and dilute if applicable for CD/UV and ESR or NMR measurements. 1 mL of the collected organic solution of **28a** (after KPic extraction) was added with the relevant amount of solid [2.2.2] cryptand **25** (1.5 mg) for ESR and CD measurements.

UV/Vis spectroscopic determination of the 28a/K^+ ratio in solution

100 μL of the dichloromethane solution (8 mM) of **28a**-KPic complex were transferred with a microsyringe into a 1 mL flask and diluted to the mark with the competing solvent acetonitrile. A CD/UV spectrum was recorded in order to verify complete disaggregation. The amount of picrate was determined from the absorbance at 375 nm assuming $\varepsilon = 16900\ cm^{-1}M^{-1}$.[17]

Molecular Dynamic Calculation Details for Self-Assembled Hexadecanitroxide

Final potential and kinetic energy = 2921.76 2197.91 kJ/mol
Average potential energy = 3007.92 kJ/mol
Average kinetic energy = 2237.00 kJ/mol (*Av temperature* = 298.9 deg K)
Average total energy = 5244.93 kJ/mol (*Std dev* = 110.28 kJ/mol)
Average potential energy <H> *scaled to* 300.0 deg K = 3015.82 kJ/mol
Av stretch 852.92 kJ/mol; *Av bend* 1308.06 kJ/mol
Av torsion 904.07 kJ/mol; *Av van der Waals* 157.68 kJ/mol
Av electrostatic -206.90 kJ/mol
Average distances between the O *atoms of nitroxide units*
Atom Pair: 43 312 Average distance = 10.0060 Angstroms

Atom Pair: 103 311 Average distance = 9.5110 Angstroms
Atom Pair: 163 310 Average distance = 10.6408 Angstroms
Atom Pair: 221 309 Average distance = 9.0773 Angstroms
Atom Pair: 309 524 Average distance = 9.9723 Angstroms
Atom Pair: 404 163 Average distance = 7.3944 Angstroms
Atom Pair: 404 310 Average distance = 10.4321 Angstroms
Atom Pair: 464 43 Average distance = 6.9918 Angstroms
Atom Pair: 464 312 Average distance = 11.0466 Angstroms
Atom Pair: 524 221 Average distance = 6.1691 Angstroms
Atom Pair: 582 103 Average distance = 6.5115 Angstroms
Atom Pair: 582 311 Average distance = 10.6413 Angstroms
Atom Pair: 670 671 Average distance = 7.1191 Angstroms
Atom Pair: 670 672 Average distance = 7.1035 Angstroms
Atom Pair: 670 673 Average distance = 10.2654 Angstroms
Atom Pair: 673 671 Average distance = 8.0136 Angstroms
Atom Pair: 673 672 Average distance = 7.3254 Angstroms

5.3.2 Chapter 3

Static Light Scattering

The light scattering experiments were carried out with an in-house apparatus[18] equipped with (i) a red He-Ne laser of wavelength λ_0 = 632.8 nm in vacuum, (ii) a discrete-angle goniometer acting within the range from 20° to 155°, (iii) a Hamamatzu type photomultiplier as detector, (iv) a photo-counting device, and (v) a toluene matching bath. The vertical polarization of the incident beam with respect to the scattering plane has been used. The analyzer, arranged between the measuring cell and the photomultiplier, could assume both the vertical and the horizontal orientations. The first position allows measurement of the isotropic V_V scattering while the second was applied in the study of the depolarized H_V scattering intensity.[19] The excess of light scattering intensity $V_V(q) = V_{Vsolution} - V_{Vsolvent}$ was measured as a function of scattering vector $q = \frac{4\pi n}{\lambda_0} \sin\frac{\theta}{2}$ with an accuracy of 1 % (θ the scattering angle, n the solvent refractive

index). The values of Raleigh excess scattering intensity $R(q)$ were obtained through the calibration of $V_V(q)$ with a benzene standard. The intensities $V_V(q)$, after normalization of the raw data, may be written R_V for the vertically polarized scattering light or R_H for the horizontally scattering light through an analyzer.

Using the following formula for stray light Rv:

$$R_V = K * C_{polym} * M * P(q) * S(q) \qquad 1.$$

where P(q) is the form factor and S(q) the long range interference from distant scatterers. Where for dilute solution S(q) ~1 and K is the optical factor for the system including the refractive index increment of the polymer as follow,

where $K_V = K_{\text{V benzene}}\left(\frac{dn}{dc}\right)^2$ is the optical contrast calibrated with benzene standard (the suffix give the polarization of incident beam and stray light).

The calibration of the spectrometer were made by evaluating the optical constant K_V or $K_{V,V}$ as follow:

$$K_V = \frac{4\pi^2 n_{ref}^2}{R_{V,ref} N_A \lambda_0^4} \qquad 2.$$

N_A Avogadro Number

λ_0 The wavelength in vacuum

n_{ref} The benzene refractive index

$R_{V,ref}$ the benzene Raleigh ratio for vertically polarized incident light

The chloroform refractive index and the average refractive index increment of the assembly for dG **1** to $CHCl_3$ are equal to n = 1.4459 and $dn/dc = 0.0769$ ml/g respectively.

The chloroform refractive index and the average refractive index increment of the assembly for G **30** to $CHCl_3$ are equal to n = 1.4459 and $dn/dc = 0.0830$ ml/g respectively.

According to Stockmayer, Casassa and Yamakawa[20] the ratio $\frac{Kc}{R_{vv}}$ may be read

versus q^2 as $$\frac{Kc}{R_{vv}} = \frac{1}{M_w P(q)}(1 + A_2 M_w c)^2 \qquad 3.$$

where R_{vv} is the normalized scattering intensity from vertically incident beam analyzed vertically, A_2 is the second virial coefficient, P(q) is the form-factor.

Equation 2 give the following using the formalism of Debye and Zimm[21]

$$\frac{KCp}{\Delta R_{VV}} = M_W^{-1} P^{-1}(q^2) + 2A_2 C \qquad 4.$$

The inverse of the form factor $P^{-1}(q^2)$ lead, after a MacLaurin transform at low q vector, to equation 5.

Here we get $< R_G^2 >_Z$ the second moment of the mass distribution which is the z average mean radius of giration as follow

$$\frac{KCp}{\Delta R} = M_W^{-1}(1 + \frac{q^2 < R^2 >_Z}{3} + ..) + 2A_2 C \qquad 5.$$

For extrapolation at $q^2 \to 0$ and $c \to 0$ equation 4 lead to the determination of the molecular mass and the second virial coefficient A_2. When the thermodynamical forces applied on the coil equilibrate we can write $A_2 = 0$. This athermal condition for binary mixture allow the determination of the apparent molecular mass $M_{W,\,app}$ for each concentration :

$$\frac{KCp}{\Delta R} = M_{w,app}^{-1}(1 + \frac{q^2 < R_Z{}^2 >}{3}) \pm ... \qquad 6.$$

Equation 6 contains all information on the shape and the conformation of the isolated polymer in solution. The determination of the radius of gyration is only valid in the guinier range qR<1 where the architectures of the polymers are barely distinguishable.

The plot of equation 5 versus $k'q^2 + k''C_p$, called Zimm-plot allows a simultaneous extrapolation to q=0 and C=0, which yields $M_W^{-1}(g \cdot mol^{-1})$ as the ordinate

intercept and $<R_G^2>_z^{1/2}$ as the initial slope of equation 6 and the second viral coefficient A_2 from equation 5.

Measurements of each sample have been carried out after various dilutions with precise volume of clarified solvent obtained by filtration through millipore filters size 0.45 µm. All the samples are directly processed in the measurements vial to avoid dust pollution.

References

1. Mezzina, E.; Fanì, M.; Ferroni, F.; Franchi, P.; Menna, M.; Lucarini, M. *J. Org. Chem*. **2006**, *71*, 3773–3777.
2. Seela, F.; Frohlich, T., *Helv. Chim. Acta*, **1994**, *77*, 399.
3. Y. Hayakawa and M. Kataoka, *J. Am. Chem. Soc.*, **1998**, *120*, 12395.
4. K. K. Ogilvie, A. F. Schifman, C. L. Penney, *Can. J. Chem.*, **1979**, *57*, 2230.
5. L. C. J. Gillet, O. D. Schärer, *Org. Lett*. **2002**, *4*, 4205-4208.
6. E. C. Western, J. R. Daft, E. M. Johnson, P. M. Gannett, K. H. Shaughnessy, *J. Org. Chem*. **2003**, *68*, 6767-6774.
7. A. Ciesielski, S. Lena, S. Masiero, G. P. Spada, P. Samorì, *Angew. Chem. Int. Ed.* **2010**, *49*, 1963 –1966.
8. M. A. Michael, H. B. Cottam, D. F. Smee, R. K. Robins and G. D. Kini *J. Med. Chem.* **1993**, *36*, 3431-3436.
9. S. Ogasawara, I. Saito, M. Maeda *Tetrahedron Letters* **2008**, *49*, 2479–2482.
10. B. Zhang, Z. Cui, L. Sun, *Org. Lett.* **2001**, *3*, 275-278.
11. Sako, M.; Kawada, H.; Hirota, K. *J. Org. Chem*. **1999**, *64*, 5719.
12. M. J. Pregel, E. Buncel, *Can. J. Chem*. **1991**, *69***,** 130.
13. F. Venema, H. F. M. Nelissen, P. Berthault, N. Birlirakis, A. E. Rowan, M. C. Feiters, R. J. M. Nolte, *Chem. Eur. J*. **1998**, *4*, 2237.
14. E. van Dienst, B. H. M. Snellink, I. von Piekartz, M. H. B. Grote Gamey, F. Venema, M. C. Feiters , R. J. M. Nolte, J. F. J. Engbersen, D. N. Reinhoudt, *J. Org. Chem.* **1995**, *60*, 6537.
15. A. Mulder, A. Juković, F. W. B. van Leeuwen, H. Kooijman, A. L. Spek, J. Huskens, D. N. Reinhoudt, *Chem. Eur. J*. **2004**, *10*, 1114-1123.
16. K. Takeo, K. Uemura, H. Mitoh, *J. Carbohydr. Chem*. **1988**, *7*, 293.
17. Moore et al, *J. Am. Chem. Soc.*, **1977**, *99*, 6398.
18. A. Libeyre, D. Sarazin, J. François, *J. Polym. Bull*. **1981**, *4*, 53.
19. G. G. Fuller, *Optical Rheometry of Complex Fluids: Theory and Practice of Optical Rheometry,* Oxford Univ. Press, Oxford, 1995.
20. Hiromi Yamakawa, "*Modern theory of polymer solutions*", Harper and Row, New-York, 1971.
21. P. Debye, *Phys. Coll. Chem*. **1947** , *51*, 18; B. H. Zimm, *J. Chem. Phys.* **1948**, *16*, 1093.